



**EFFECT OF GYPSUM ON THE HYDRO-MECHANICAL
CHARACTERISTICS OF PARTIALLY SATURATED
SANDY SOIL**


KHALID IBRAHIM AHMED

Geoenvironmental Research Centre
Cardiff School of Engineering
Cardiff University

Thesis submitted in candidature for the degree of Doctor of Philosophy
at
Cardiff University
September 2013

DECLARATION

This work has not been submitted in substance for any other degree or award at this or any other university or place of learning, nor is being submitted concurrently in candidature for any degree or other award.

Signed  (Khalid Ibrahim Ahmed)

Date 04 / 09/2013

STATEMENT 1

This thesis is being submitted in partial fulfilment of the requirements for the degree of Doctor of Philosophy (PhD).

Signed  (Khalid Ibrahim Ahmed)

Date 04 / 09/2013

STATEMENT 2

This thesis is the result of my own independent work/investigation, except where otherwise stated. Other sources are acknowledged by explicit references. The views expressed are my own.

Signed  (Khalid Ibrahim Ahmed)

Date 04 / 09/2013

STATEMENT 3

I hereby give consent for my thesis, if accepted, to be available for photocopying and for inter-library and for the title and summary to be made available to outside organisations.

Signed  (Khalid Ibrahim Ahmed)

Date 04 / 09/2013

ABSTRACT

Gypsum rich soils are of wide occurrence in the Middle East. They cover large areas of Iraq. Gypsum is one of the moderately soluble salts that can have significant effect on the engineering properties of soils. The effect of gypsum content and the stress state on the main hydraulic functions, volume change, shear strength and deformation characteristics of unsaturated silty clayey sand were experimentally examined. Statically compacted specimens of synthetic sand-gypsum mixtures were used. A new stress controllable pressure plate device was developed. The modified device was used to establish simultaneously both the stress-dependent soil-water characteristic curves (SD-SWCCs) and the stress-dependent hydraulic conductivity functions (SD-HCFs) during drying and wetting paths.

The test results revealed that the parameters of the drying SWCC such as the water holding capacity, the air-entry suction, the air-entry water content, and the residual suction are clearly increased with increasing gypsum content. Same effect of gypsum was noticed on the wetting SWCC parameters. A clear decrease in saturated water content, desorption rate, absorption rate, and water holding capacity with increasing the applied net normal stress was noticed. Transient outflow methods were used to measure the SD-HCFs. An increase in the SD-HCFs with increasing gypsum content was found. Clear hysteresis effects on $k(\psi)$ and minor hysteresis on $k(w)$ were noticed. It was found that the outflow methods can be applicable between the air-entry suction and residual suction only.

Direct shear tests were carried out on saturated and unsaturated specimens. The unsaturated specimens were air-dried and tested under constant water content conditions. Matric suction values were evaluated by incorporating the SD-SWCC test results. The friction angle related to matric suction (ϕ^b), the effective stress parameter (χ), and the suction stress (σ_s') were found clearly decrease with increasing gypsum content and with increasing the net normal stress level. However, test results of saturated specimens revealed that the effective shear strength parameters (ϕ' , c') are noticeably increased with increasing gypsum content in the soil mixture.

ACKNOWLEDGMENTS

In the Name of Allah, the All- Merciful, the All-Compassionate.

The praise is due to Allah, the All-Powerful, the All-Knowing, the All-Wise and the Compassionate for giving me the strength, health, patience and perseverance to complete this work in its best.

I would like to express my sincere gratitude to my senior supervisor Prof. Hywel Thomas and the co-supervisors Dr. Snehasis Tripathy and Dr. Talib Mahdi for all continuous support, motivation and invaluable academic guidance. Special thanks are extended to the examination panel, Prof. Chris Clayton, Prof. David Barrow, and Dr. Steve Rees for their worth comments, guidance and careful review of this thesis.

I would like to especially thank the Embassy of the Republic of Iraq / Cultural attaché for financial support during my study. My gratitude is also extended to all Professors of the University of Baghdad / College of Engineering for teaching me the principles of engineering through (1978-1986).

Great thanks also to the Geotechnical technician Mr. Len Czekaj and all the technical staff in Cardiff School of Engineering for their assistance in the lab. My special thanks also extended to all academic staff especially Dr. Michael Harbottle for his annual reviews of my research. I would like to express my gratitude also to all admin staff in the research office and the Geoenvironmental research centre especially Mrs Pauline Welsh, Mrs Chris Lee, Mrs Jeanette Whyte, Mrs Aderyn Reid. My sincere thanks also extended to my colleagues and friends in the Geoenvironmental Research Centre and other School Departments for their friendship and kindness.

Finally, and most of all, I would like to express my deepest gratitude and appreciation to my wife and my children Dhuha, Ibrahim and Ahmed for their help, sacrifices, and patience during my studies.

TABLE OF CONTENTS

<i>DECLARATION</i>	<i>ii</i>
<i>ABSTRACT</i>	<i>iii</i>
<i>ACKNOWLEDGMENTS</i>	<i>iv</i>
<i>TABLE OF CONTENTS</i>	<i>v</i>
<i>LIST OF TABLES</i>	<i>xi</i>
<i>LIST OF FIGURES</i>	<i>xiii</i>
 <i>1: INTRODUCTION</i>	 <i>1</i>
1.1. General background	1
1.2. Objectives and scope of the research	4
1.3. Thesis organization	7
 <i>2: LITERATURE REVIEW</i>	 <i>9</i>
2.1. Introduction	9
2.2. Gypsiferous soils	10
2.2.1. Gypsum properties	11
2.2.2. Effect of gypsum on soil behaviour	13
2.2.3. Effect of soaking on mechanical properties of gypsiferous soils	15
2.3. Unsaturated soil state	16
2.3.1. State variables and material variables	16
2.3.2. Stress state variables	17
2.3.2.1. The variable effective stress state single approach	18
2.3.2.2. The two independent stress state variable approach	19
2.3.2.3. The true effective stress state variable approach	20
2.3.3. Total head as a state variable	22
2.4. Soil suction and soil-water characteristic curve	23
2.4.1. Soil suction and potential energy	23
2.4.2. Components of soil suction	25
2.4.3. Overview of soil suction measurement techniques	26
2.4.4. Chilled mirror hygrometer	28
2.4.5. Suction controlling techniques	29
2.4.6. Axis translation techniques	31
2.4.6.1. Pressure plate extractor	32

2.4.6.2. Tempe pressure cells	34
2.4.6.3. Volumetric pressure plate extractor	36
2.4.6.4. Stress-controllable volumetric pressure plate	38
2.4.7. Soil-water characteristic curve	41
2.4.8. Hysteresis of soil-water characteristic curve	44
2.4.9. Influence of stress state on SWCCs	47
2.4.10. Influence of compaction water content on soil structure	50
2.5. Unsaturated hydraulic conductivity	51
2.5.1. Basic definitions	51
2.5.2. Overview of measuring methods of unsaturated conductivity	51
2.5.3. One-dimensional transient flow governing equation	53
2.5.4. Outflow methods	54
2.5.4.1. The multistep method	55
2.5.4.2. The one-step method	56
2.5.5. Ceramic disc impedance	58
2.6. Shear strength and failure criteria	59
2.6.1. The extended Mohr-Coulomb criterion	60
2.6.2. Single stress state Mohr-Coulomb criterion	62
2.6.3. True effective stress failure criterion	64
2.6.4. Shear strength prediction using constitutive models	66
3: MATERIALS, EQUIPMENT AND METHODOLOGY	68
3.1. Introduction	68
3.2. Materials and samples preparation	69
3.3. Soil classification parameters	70
3.4. Experimental programme	73
3.4.1. Compaction tests	73
3.4.2. Consolidation tests	74
3.4.3. Soil-water characteristic tests	76
3.4.3.1. Testing device	77
3.4.3.2. Specimen preparation	77
3.4.3.3. Testing procedure and calculations	78
3.4.4. Chilled mirror hygrometer tests	81
3.4.4.1. Testing device	81

3.4.4.2. Specimen preparation and testing procedure	82
3.4.4.3. Representation of test results	83
3.4.5. Soil shrinkage characteristic tests	83
3.4.5.1. Testing procedure for SCCs	84
3.4.5.2. Calculations of CLOD tests	86
3.4.5.3. Mathematical modelling of SCCs	87
3.4.6. Stress-dependent soil-water characteristic tests	88
3.4.7. Stress dependent-unsaturated hydraulic conductivity function tests	89
3.4.8. Direct shear tests on saturated specimens	90
3.4.8.1. Overview	90
3.4.8.2. Direct shear testing device	91
3.4.8.3. Device calibration	92
3.4.8.4. Specimens preparation	94
3.4.8.5. Testing procedure and calculations	95
3.4.8.6. Stresses and strains	96
3.4.9. Direct shear tests on unsaturated specimens	98
3.4.9.1. Overview	98
3.4.9.2. Experimental programme	99
3.4.9.3. Specimens preparation	101
3.4.9.4. Device adjustment	102
3.4.9.5. Testing procedure for unsaturated soil specimens	105
3.4.9.6. Calculations of unsaturated shear strength functions	106

4: MODIFIED DEVICE FOR MEASURING TWO STRESS DEPENDENT- UNSATURATED HYDRAULIC FUNCTIONS

4.1. Introduction	109
4.2. The modified stress controllable pressure plate device	110
4.2.1. Background	110
4.2.2. Uses and features of the modified device	110
4.2.3. Design and construction details	111
4.2.3.1. The base plate of the cell	113
4.2.3.2. The cell ring	114
4.2.3.3. The dual grooved spacers	115
4.2.3.4. The pneumatic compartment cap	117

4.2.3.5. The cell assemblage	118
4.2.3.6. The pressurized air panel	118
4.2.4. Specimen preparation and testing procedures	120
4.2.4.1. Specimen compaction and saturation	120
4.2.4.2. Testing procedure for SD-SWCCs determination	121
4.2.4.3. Testing procedure for SD-HCF determination	122
4.2.4.4. Diffused air removal	123
4.3. Testing programme	124
4.3.1. SD-SWCCs tests	125
4.3.2. SD-HCFs tests	126
4.4. Calculations	126
4.4.1. Calculations of SD-SWCCs	126
4.4.2. Calculations of SD-HCFs	128
4.5. Summary	132
5: RESULTS AND DISCUSSION OF BASIC TESTS	134
5.1. Introduction	134
5.2. Effect of gypsum content on compaction characteristics	134
5.3. Effect of gypsum content on compressibility characteristics	139
5.4. Soil-water characteristics	143
5.4.1. Same specimen approach-SWCC tests	144
5.4.2. Separate specimens approach-SWCC tests	145
5.4.3. Effect of gypsum content on SWCC parameters	146
5.4.4. Matric suction-volumetric water content relationships	148
5.4.5. Applied suction and volume change	149
5.5. Water content-total suction relationships	152
5.6. Shrinkage characteristics	155
5.7. Concluding remarks	158
6: STRESS-DEPENDENT SOIL-WATER CHARACTERISTICS	160
6.1. Introduction	160
6.2. Test results preview	161
6.3. Effects of gypsum content on the SD-SWCCs parameters	169
6.3.1. Effects of gypsum content on SD-SWCCs-water content parameters	169

6.3.2. Effects of gypsum content on the SD-SWCCs-suction parameters	170
6.3.3. Effects of gypsum content on the slope of the SD-SWCC	171
6.3.4. Effects of gypsum content on hysteresis phenomenon	172
6.3.5. Effect of gypsum content on suction-water content equalization time	173
6.4. Effects of net normal stress on SD-SWCCs parameters	174
6.4.1. Effect of net normal stress on initial water content of SD-SWCC	174
6.4.2. Effect of net normal stress on characteristic zones of SD-SWCC	175
6.4.3. Effects of net normal stress on SD-SWCCs characteristic points	176
6.4.4. Effect of net normal stress on the slope of SD-SWCCs	176
6.4.5. Effect of net normal stress on hysteresis phenomenon	176
6.5. Mathematical modelling of SD-SWCCs	177
6.6. Comparison of SWCCs obtained from different equipment	180
6.7. Combined SWCCs of different sand-gypsum mixtures	184
6.8. Summary and concluding remarks	188
 7: STRESS DEPENDENT-UNSATURATED HYDRAULIC CONDUCTIVITY FUNCTIONS	 189
7.1. Introduction	189
7.2. Effect of gypsum content on SD-HCFs	189
7.2.1. Hydraulic conductivity-matric suction relationships	190
7.2.2. Hydraulic conductivity-gravimetric water content relationships	196
7.3. Comparison of Doering's approach with Gardner's approach	201
7.4. Effect of net normal stress on SD-HCFs	204
7.4.1. Hydraulic conductivity-matric suction relationships	204
7.4.2. Hydraulic conductivity-gravimetric water content relationships	208
7.5. Summary and concluding remarks	211
 8: SHEAR STRENGTH AND DEFORMATION CHARACTERISTICS	 213
8.1. Introduction	213
8.2. Results of direct shear tests on saturated specimens	213
8.2.1. Stress-strain characteristics	214
8.2.2. Effect of gypsum content on saturated shear strength	220
8.2.3. Mohr-Coulomb failure envelopes and shear strength parameters	221
8.3. Results of direct shear tests on unsaturated specimens	223

8.3.1. Shear strength-water content relationships	224
8.3.2. Failure envelopes in plane of net normal stress-shear stress	226
8.3.3. Apparent cohesion and friction angle versus water content	230
8.3.4. Failure envelopes in plane of matric suction-shear stress	231
8.3.5. Effect of gypsum content on ϕ_b and χ	236
8.3.6. Prediction of unsaturated failure envelopes	239
8.3.7. Suction stress characteristic curves	242
8.3.8. Shear strength failure envelopes in terms of intergranular effective stress	247
8.4. Concluding remarks	249
<i>9: CONCLUSIONS AND RECOMMENDATIONS</i>	251
9.1. Conclusions from conventional, standard tests	252
9.2. Conclusions from developed-stress dependent-hydraulic tests	254
9.3. Conclusions from shear strength tests	257
9.4. Recommendations for future works	259
<i>REFERENCES</i>	262
<i>APPENDIX: A</i>	278
<i>APPENDIX: B</i>	279

LIST OF TABLES

Table 2.1. Summary of common laboratory and field techniques for measuring soil suction (modified from Lu and Likos, 2004).	27
Table 2.2. Summary of common laboratory techniques of controlling soil suction.	30
Table 3.1. Index properties of the prepared samples.	71
Table 3.2. The framework of direct shear tests on unsaturated specimens.	100
Table 3.3. Normal loads result from different degrees of head screw tightness.	103
Table 4.1. Initial conditions for specimens statically compacted from different sand-gypsum mixtures.	126
Table 5.1. Compaction characteristics of the sandy soil with different gypsum additives (standard Proctor tests).	135
Table 5.2. Fittings parameters and statistical indices of SWCCs of different sand-gypsum mixtures, carried out via commercial pressure plate by using separate approach.	146
Table 5.3. SWCC parameters for different sand-gypsum mixtures.	147
Table 5.4. Fitting parameters of the SCCs of different sand-gypsum mixtures found from separate specimens-SWCC tests, implemented by using the commercial pressure plate.	151
Table 5.5. Fitting parameters of the SCCs of different sand-gypsum mixtures determined from CLOD tests.	157
Table 6.1. SWCCs parameters for specimens having different gypsum contents tested under different loading conditions.	168
Table 6.2. Initial gravimetric water contents of the SD-SWCCs of different sand-gypsum mixtures.	175
Table 6.3. The fitting parameters and the coefficient of determination (R^2) for specimens having five different gypsum contents, tested under four different net normal stress levels.	178
Table 6.4. Comparison of SWCCs parameters obtained by using the modified stress controllable pressure plate device and those obtained from the commercial pressure plate.	182
Table 6.5. Residual suction and residual water content for different sand-gypsum mixtures defined from the combined SWCCs in comparison to those found from the single SWCCs.	188
Table 8.1. Lateral displacement corresponding to maximum shear stress under different normal stress levels for different sand-gypsum mixtures.	217
Table A.1. Fitting parameters and statistical indices of different SWCCs found by using the commercial pressure plate (using the same specimens throughout the whole tests).	278
Table A. 2. Fitting parameters and statistical indices of different combined SWCCs after the joining of the dew point potentiometer results with that of the	

modified stress controllable pressure plate device for specimens tested under 0 kPa net normal stress.	278
Table B.1. Peak shear strength of saturated sand-gypsum mixtures having different gypsum contents by weight.	284
Table B.2. Peak shear strength parameters of saturated sand-gypsum mixtures having different gypsum contents by weight.	284

LIST OF FIGURES

Figure 2.1. Chilled-mirror dew point hygrometer, (A) a photograph of WP4-C model device and (B) schematic diagram of the chilled mirror technique (Lu and Likos, 2004).	29
Figure 2.2. Pressure plate extractor, (a) photograph and (b) cross-sectional drawing (Soilmoisture Equipment Corp, 2008).	33
Figure 2.3. Tempe pressure cell, (a) photograph of disassembled cell, (b) cross sectional view of the cell (Soilmoisture Equipment Corp., 2008).	35
Figure 2.4. Schematic drawing showing the setup of the volumetric pressure plate extractor with hysteresis attachments (Soilmoisture Equipment Corp., 2008).	37
Figure 2.5. Stress-controllable volumetric pressure plate extractor developed by Ng and Pang (2000), (a) a photograph of different components and the cell assemblage, (b) schematic drawing of the experimental setup.	40
Figure 2.6. A photograph showing Fredlund SWCC device (GCTS Testing Systems).	41
Figure 2.7. Typical soil-water characteristic curve (modified from Perez-Ruiz, 2009).	42
Figure 2.8. Typical presentation of soil-water characteristic curves showing initial drying curve, main drying curve, main wetting curve and scanning curves (modified from Pham et al., 2003).	45
Figure 2.9. Effect of stress state on soil-water characteristic curves for, (a) specimens compacted dry of optimum water contents, (b) specimens compacted wet of optimum water contents (Vanapalli et al., 1998).	48
Figure 2.10. Effect of stress state on soil-water characteristic curves (Ng and Ping, 2000).	49
Figure 3.1. Grain-size distribution of gypsum at different soaking periods (Hydrometer tests).	72
Figure 3.2. Particle size distribution curves of sandy soil, gypsum, and the synthetic samples.	73
Figure 3.3. Schematic drawing of static compaction mould for specimens used for consolidation tests.	75
Figure 3.4. Photographs showing (a) compaction mould components, (b) compaction setup for specimens used for SWCC tests.	78
Figure 3.5. Photograph of the general set-up of the direct shear device.	92
Figure 3.6. Calibration lines of horizontal displacement transducer during forward, backward, and second forward movement.	93
Figure 3.7. Shear box component with the compaction ram used in static compaction.	94
Figure 3.8. A schematic diagram showing the corrected cross-sectional sheared area in a circular shear box.	97
Figure 3.9. A schematic diagram showing the normal pressure pneumatic system of the direct shear device.	102

Figure 4.1. A photograph of experimental setup of the modified device.	112
Figure 4.2. A photograph of disassembled modified cell.	112
Figure 4.3. Mechanical drawings of the base plate of the modified cell.	113
Figure 4.4. A photograph showing the base plate of the modified cell, (A) with the ceramic disc, (B) before installing the ceramic disc.	114
Figure 4.5. The mechanical drawings of the grooved spacers used with the modified stress controllable pressure plate cell.	116
Figure 4.6. Isometric assemblage of the basic components of the modified cell.	116
Figure 4.7. Mechanical drawings of the pneumatic compartment cap of the modified cell.	117
Figure 4.8. Schematic section of modified stress controllable pressure plate cell.	118
Figure 4.9. A photograph of disassembled and assembled manometer cell.	119
Figure 4.10. The mechanical drawings of compaction mould compatible with specimen ring of the modified device.	120
Figure 4.11. A photograph showing; (a) the compaction mould components, (b) the compaction setup.	121
Figure 4.12. Elapsed time versus $\ln ((V_f - V_t)/V_f)$ for calculating the hydraulic diffusivity according to Gardner (1956)'s approach.	132
Figure 5.1. Standard compaction curves for different sand-gypsum mixtures.	135
Figure 5.2. Maximum dry density and optimum water content for the soil with different percentages of gypsum.	136
Figure 5.3. Void ratio-water content curves for different sand-gypsum mixtures.	138
Figure 5.4. Minimum void ratio, minimum porosity, and the corresponding degree of saturation for different sand-gypsum mixtures.	138
Figure 5.5. Loading and unloading void ratio-log effective stress curves for different sand-gypsum mixtures.	140
Figure 5.6. Compression index (C_c) versus mean effective stress curves for different sand-gypsum mixtures.	141
Figure 5.7. Rebound index (C_r) versus mean effective stress for different sand-gypsum mixtures.	141
Figure 5.8. Compression index vs. initial void ratio for different sand-gypsum mixtures.	143
Figure 5.9. SWCCs of different sand-gypsum mixtures carried out by using commercial pressure plate according to ASTM D 6836-02 (same specimen approach).	144
Figure 5.10. The drying SWCCs of different sand-gypsum mixtures carried out by using commercial pressure plate according to ASTM D 6836-02 (separate specimen approach).	146
Figure 5.11. Matric suction-volumetric water content curves of different sand-gypsum mixtures found from the pressure plate tests on separate specimens by using the wax method.	149

Figure 5.12. Void ratio-matric suction curves of different sand-gypsum mixtures based on pressure plate tests on separate specimens with volume measurements by using the wax method.	149
Figure 5.13. Void ratio-gravimetric water content curves of different sand-gypsum mixtures found from the pressure plate tests on separate specimens in conjunction with volume determination using the wax method.	150
Figure 5.14. Gravimetric water content-total suction relationships of different sand-gypsum mixtures determined by using chilled mirror hygrometer.	152
Figure 5.15. Effect of gypsum content on osmotic suction of the sandy soil used.	154
Figure 5.16. Parameters of total suction SWCCs for different sand-gypsum mixtures (based on Figure 5.14).	154
Figure 5.17. Shrinkage characteristic curves for different sand-gypsum mixtures determined from CLOD tests.	156
Figure 6.1. Effect of gypsum content on the drying and the wetting SWCCs of specimens tested under 0 kPa by using the modified stress controllable pressure plate device.	161
Figure 6.2. The drying and the wetting SD-SWCCs of the sandy soil having 0% gypsum content.	162
Figure 6.3. The drying and the wetting SD-SWCCs of the sandy soil having 20% gypsum content.	162
Figure 6.4. The drying and the wetting SD-SWCCs of the sandy soil having 40% gypsum content.	163
Figure 6.5. The drying and the wetting SD-SWCCs of the sandy soil having 65% gypsum content.	163
Figure 6.6. The drying and the wetting SD-SWCCs of the sandy soil having 80% gypsum content.	164
Figure 6.7. Air-entry, air-expulsion, water-entry, and residual suction values of different sand-gypsum mixtures, tested under different net normal stress levels.	166
Figure 6.8. Air-entry, air-expulsion, water-entry, and residual water contents of different sand-gypsum mixtures tested under different net normal stress levels.	167
Figure 6.9. Effect of gypsum content on the water holding capacity of the sandy soil under different net normal stress levels.	170
Figure 6.10. Effect of gypsum content on the slope of SD-SWCC of the sandy soil under different loading condition.	172
Figure 6.11. Time required for matric suction-water content equalization versus applied matric suction during the drying and the wetting processes for different sand-gypsum mixtures tested under 0 kPa net normal stress level.	174
Figure 6.12. The relationship between the fitting parameter "a", Fredlund and Xing (1994)'s model, and the air-entry/air-expulsion suction values for	

various sand-gypsum mixtures that tested under different net normal stress levels.	179
Figure 6.13. The relationship between the fitting parameter "m", Fredlund and Xing (1994)'s model, and the residual suction value for various sand-gypsum mixtures that tested under different net normal stress levels.	180
Figure 6.14. Comparison of the SWCCs established from the modified stress controllable pressure plate device with that established by using the commercial pressure plate.	181
Figure 6.15. Comparison of the drying SD-SWCCs established from the modified stress controllable pressure plate device for the silty clayey sand with published matric suction measurements on poorly graded silty sand using null-type technique (Tripathy et al., 2012).	183
Figure 6.16. Combined SWCCs for different sand-gypsum mixtures, (A) 0%, (B) 20%, (C) 40%, (D) 65%, and (E) 80% gypsum content.	186
Figure 7.1. The drying and the wetting hydraulic conductivity functions in terms of matric suction, according to Doering's approach, for different sand-gypsum mixtures, tested under net normal stress levels of (A) 0, (B) 100, (C) 200, and (D) 400 kPa.	192
Figure 7.2. Measured drying and wetting stress dependent $k(\psi)$ s at (a) 4 kPa, (b) 39 kPa, (c) 78 kPa net normal stress levels for a compacted decomposed silty clay using the instantaneous profile method (Ng and Leung, 2012).	195
Figure 7.3. The drying and the wetting hydraulic conductivity functions in terms of gravimetric water content, according to Doering's approach, for different sand-gypsum mixtures, tested under net normal stress of (A) 0, (B) 100, (C) 200, and (D) 400 kPa.	198
Figure 7.4. The hydraulic conductivity functions in terms of volumetric water content, at average net normal stresses of 4 kPa, 39 kPa, and 78 kPa for a compacted decomposed silty clay using the instantaneous profile method (Ng and Leung, 2012).	199
Figure 7.5. A comparison between hydraulic conductivity functions found according to Doering's approach and that found according to Gardner's approach for different sand-gypsum mixtures tested under 100 kPa net normal stress, (A) during drying process, (B) during wetting process.	202
Figure 7.6. The drying and the wetting hydraulic conductivity functions in terms of matric suction, according to Gardner's approach, tested under different levels of net normal stress for sand-gypsum mixtures having (A) 0% , (B) 20%, (C) 40%, (D) 65%, and (E) 80% gypsum content by weight.	206
Figure 7.7. The drying and the wetting stress dependent-hydraulic conductivity functions in terms of gravimetric water content, according to Gardner's approach for sand-gypsum mixtures having (A) 0% , (B) 20%, (C) 40%, (D) 65%, and (E) 80% gypsum content by weight.	211
Figure 8.1. Stress-deformation characteristic curves for different sand-gypsum mixtures tested under normal stress of 100 kPa, (A) Shear stress versus lateral displacement, and (B) Vertical deformation versus lateral displacement.	215

Figure 8.2. Stress-deformation characteristic curves for different sand-gypsum mixtures tested under normal stress of 400 kPa, (A) Shear stress versus lateral displacement, and (B) Vertical deformation versus lateral displacement.	216
Figure 8.3. Effect of gypsum content on initial shear stiffness of specimens tested under different normal stress levels.	219
Figure 8.4. Effect of gypsum content on peak/maximum shear stress for specimens tested under different normal stress levels.	220
Figure 8. 5. Mohr-Coulomb failure envelopes of different sand-gypsum mixtures.	222
Figure 8.6. Effect of gypsum content on saturated shear strength parameters.	223
Figure 8.7. Peak or maximum shear stress vs. water content at four levels of net normal stress for sand-gypsum mixtures having (A) 20%, (B) 40%, (C) 80% gypsum content by weight.	225
Figure 8.8. Shear strength failure envelopes at different water contents (different matric suctions) for sand-gypsum mixtures having (A) 0%, (B) 20%, (C) 40%, (D) 65%, and (E) 80% gypsum content by weight.	229
Figure 8.9. Apparent cohesion and apparent friction angle versus gravimetric water content for different sand-gypsum mixtures.	230
Figure 8.10. Shear strength failure envelopes with respect to matric suction under four constant net normal stress levels for sand-gypsum mixtures having (A) 0%, (B) 20%, (C) 40%, (D) 65%, and (E) 80% gypsum content by weight.	234
Figure 8.11. Effect of gypsum content on matric suction friction angle (ϕ_b) under four levels of net normal stress, (A) For matric suction range of 0 to 130 kPa, (B) Matric suction at residual zone.	238
Figure 8.12. Effect of gypsum content on effective stress parameter (χ), under four levels of net normal stress, for matric suction range of 0 to 130 kPa.	239
Figure 8.13. Comparison of Rassam and Cook (2002)'s predictive function with the experimental shear strength envelopes, at different levels of net normal stress, for unsaturated sand-gypsum specimens having (A) 0%, (B) 40%, and (C) 65% gypsum content by weight.	241
Figure 8.14. SSCCs in terms of water content (According to the approach of Lu and Likos, 2006) for sand-gypsum mixtures having (A) 0%, and (B) 80% gypsum content by weight, at different levels of net normal stress.	243
Figure 8. 15. SSCCs in terms of matric suction (According to the approach of Lu and Likos, 2006) for sand-gypsum mixtures having (A) 0%, and (B) 80% gypsum content by weight, at different levels of net normal stress.	245
Figure 8.16. SSCCs in terms of water content (According to the approach of Ning Lu, 2006) for different sand-gypsum mixtures at net normal stress level of (A) 200 kPa, and (B) 400 kPa.	247
Figure 8.17. Shear strength failure envelopes in terms of intergranular effective stress for different sand-gypsum mixtures.	249

Figure B.1. Stress-deformation characteristic curves for different sand-gypsum mixtures tested under normal stress of 200 kPa, (A) Shear stress versus lateral displacement, (B) Vertical deformation versus lateral displacement.	279
Figure B.2. Peak or maximum shear stress vs. water content under four levels of net normal stress for sand-gypsum mixtures having (A) 0%, and (B) 65% gypsum content by weight.	280
Figure B.3. Comparison of Rassam and Cook (2002)'s predictive function with the experimental shear strength envelopes, at different levels of net normal stress, for unsaturated sand-gypsum specimens having (A) 20%, and (B) 80% gypsum content by weight.	281
Figure B.4. SSCCs in terms of water content (According to the approach of Lu and Likos, 2006) for sand-gypsum mixtures having (A) 20%, (B) 40%, and (C) 65% gypsum content by weight, at different levels of net normal stress.	283
Figure B.5. SSCCs in terms of matric suction (According to the approach of Ning Lu, 2006) for different sand-gypsum mixtures at net normal stress level of (A) 200 kPa, and (B) 400 kPa.	284

CHAPTER ONE

INTRODUCTION

1.1. General background

Gypsum (calcium sulphate dehydrate) is one of the moderately soluble salts that can have a detrimental effect on pavements, buildings and earth structures. Gypsum dissolves with water and produces caverns and/or progressive settlements, accelerating seepage flows and the accompanying deterioration of foundations (Subhi 1987; Razouki et al. 1994). Furthermore, the presence of gypsum salts as a part of soil solid phase or dissolved within the pore fluid may cause significant effect on the engineering properties of the soil. This effect depends essentially on the amount and type of gypsum, and on the environmental circumstances under which the soil is used.

Gypsiferous soils are widespread in the Middle East especially in regions peripheral to the Red sea and Arabian Gulf. They cover large areas of Iraq which may be extended to 20% of the total Iraq's area (FAO, 1990). The province of Al-Anbar, the largest province in Iraq, contains large areas of gypsiferous soils. Gypsum could be found there at various depths or at ground surface depending on the environmental conditions and the geological history of the region. As in the other regions of Iraq, there are three main forms of gypsum deposit in Al-Anbar province; mixed through soil layers, small lumps or patches distributed in soil layers, and gypsum crystals at or near ground surface as a result of ground water evaporation (Barzanji,1973). In such hot dry regions, evaporation exceeds precipitation so that, natural soils and aggregates may contain varying quantities of soluble salts especially at superficial layers. The area under investigation in this study is the district of Al-Fallujah in Al-Anbar province. This district receives an average precipitation of 200

mm between November and May while the annual potential evaporation exceeds 2000 mm. During the last 10 years, the maximum temperature reached 51°C and the minimum went down to - 5 °C. Temperatures above 47 °C in summers and below 0 °C in winters are common.

Gypsiferous soils have been studied in the past within the classical framework of soil mechanics that is related to saturated condition. As such, they are characterised as collapsible, problematic soils that suffer large settlement and have significant loss of strength under long term flooding. However, in arid and semi-arid areas where gypsiferous soils are found, the top soil layers are mostly in unsaturated state (Fredlund & Rahardjo, 1993; Murray & Sivakumar, 2010). Studies on gypsiferous soils within unsaturated zone, where the impact of gypsum presence on the soil characteristics and usability of such soils may be largely different, are quite rare. Thus, in hot desserts, when gypsiferous soils are mostly dry or unsaturated, gypsum may acts as a cementing agent between soil particles leading to a clear increase in soil cohesion. On the other hand, in wet regions, the dissolution of gypsum due to rainwater percolation or the fluctuation of water table may result in softening of these soils and serious damage to the structures founded on such soils may occur.

Nevertheless, it may be rare to find an integrated study in literature where both the mechanical and hydraulic characteristics were examined together to understand the interaction of these characteristics on each other and to realize comprehensively the behaviour of unsaturated gypsiferous soils.

Classical soil mechanics has developed in temperate areas of the world, and as such has concentrated on the fully saturated soils, whereas in many situations engineering problems are related to soil layers that lie at or near the surface which may be partly saturated, with a pore water suction (Fredlund & Rahardjo, 1993; Murray & Sivakumar, 2010). The case of unsaturated soil represents the general encountered case for many geotechnical problems. However, comparing with saturated condition, the behaviour of unsaturated soil is more difficult to investigate due to the complex thermodynamics correlations for soil phases, but it is often less critical.

Two key functions are usually used to characterize the hydraulic behaviour of unsaturated soils; the soil-water characteristic curve (SWCC) and the unsaturated hydraulic conductivity function (HCF). The relationship between water content and soil suction is referred to as the SWCC, which quantifies the energy required to remove water from soil pores during a drying or a wetting process. The HCF quantifies the soil's change in impedance to water flow as it becomes unsaturated. The hydraulic conductivity of an unsaturated soil is mostly related to the volume of water in the pore spaces because the presence of air restricts the available pathways for water flow. Knowledge of the SWCC and HCF is essential in analysing numerous geotechnical problems, such as transient and steady seepage in unsaturated embankment, contaminant transport and remediation in unsaturated zone, water balance at the interface of soil and atmosphere, and the net recharge rate to the ground water.

Water flow and retention characteristics may be directly affected by the average pore size distribution in the soil matrix, which in turn could be influenced by the physical state and the state of stress in the soil. Thus, it is essential to mimic the physical and stress conditions of the field when the hydraulic functions, SWCC and HCF, have to be evaluated for a particular soil at the laboratory. From this point of view, special attention in this study has been given to study the stress-dependent soil-water characteristic curves (SD-SWCCs) and the stress-dependent hydraulic conductivity functions (SD-HCFs) for unsaturated gypsum rich sandy soils.

The mechanical behaviour of a particular soil is intrinsically linked to the hydraulic characteristics of that soil. Volume change, shear strength and shear deformation characteristics are directly affected by the changes in the pore-air and pore-water pressures which can be associated with the flow of water through soil, or that generated from the application of an external load, such as an engineering structure. More specifically, matric suction variations associated with environmental changes can have significant effects on the strength and deformation characteristics of unsaturated soils. These characteristics are influenced by drying and wetting cycles, loading and unloading, as well as the time.

Many geotechnical problems, such as bearing capacity for shallow foundations, slope stability and land sliding under changing climatic conditions, lateral earth pressure and stability of retaining structures, excavation and borehole stability are related to the unsaturated shear strength evaluation of the particular soil. Problems such as consolidation and settlement, collapsing soil, swelling and shrinkage of soil can be related to the deformation characteristics of the soil. Thus, predicting shear strength and shear deformations of unsaturated soil represents the cornerstone in analysis numerous engineering problems.

Shear strength can be defined as the maximum shear stress the soil is capable to sustain along a failure plane under a given external and/or internal stress state. Shear strength of unsaturated soils can be directly quantified through unsaturated shear strength tests, in which matric suction is mostly controlled by axis-translation technique. These tests are time consuming and require extensive laboratory facilities, which are costly.

The shear strength of unsaturated soil can be described in terms of different combinations of stress state variables. Thus, there are three main criteria to describe the shear strength. These are the single stress-state variable criterion (Bishop, 1959), the two stress-state variable criterion (Fredlund and Morgenstern, 1977), and the true effective stress concept introduced by Lu and Likos (2006). In this research, the experimental results were analysed according to each of these criteria and an evaluation for different shear strength parameters, for different sand-gypsum mixtures under various loading conditions, were carried out.

In fact, a better understanding of the hydraulic and mechanical behaviour with the associated environmental circumstances leads to use a gypsiferous soil in a reasonable way and this makes the cost to be minimum. Hence, a more adequate use of gypsiferous soils could have major impact on the economy and development potential of the countries where these soils are spread.

1.2. Objectives and scope of the research

The primary objective of this research was to experimentally examine the behaviour and characteristics of a sandy soil taken from Al-Fallujah district / Iraq

with different gypsum additives, under various loading conditions, toward understanding the impact of gypsum content on the main hydraulic functions, volume change, shear strength and deformation characteristics of unsaturated sandy soils. This was accomplished by conducting an extensive laboratory testing programme using the sandy soil with different gypsum additives. These mixtures were prepared artificially since it is quite seldom in nature to find exactly the same soil with different gypsum contents. Furthermore, natural gypsiferous soils usually contain some other salts which may affect the behaviour of gypsum salts. Thus, to eliminate the effect of such salts and to control any interaction on soil properties, synthetic soil samples were considered in this work.

The experimental programme includes three main parts. The first part comprises of some conventional standard tests. The effect of gypsum content on the specific gravity, liquid limit, plastic limit, shrinkage limit, grain-size distribution curve, compaction behaviour, consolidation characteristics, soil-water characteristic curve, and the shrinkage characteristic curve have been investigated in the first part.

The second and the third parts of the experimental programme represent the core of this research. A detailed investigation of the drying and the wetting stress-dependent soil-water characteristic curves (SD-SWCCs) and the stress dependent-unsaturated hydraulic conductivity functions (SD-HCFs) for different sand-gypsum mixtures were included in the second part. The first aim behind this investigation was to evaluate the effect of net normal stress level on these hydraulic functions. To achieve this aim, a new stress controllable pressure plate device has been developed. The new device is used to measure simultaneously both the SD-SWCC and the SD-HCF during drying and wetting processes with high efficiency and repeatability. A single soil specimen is used to obtain these functions with any number of data points without dismantling the device.

A further aim of the second experimental part was the promotion of using experimentally-derived hydraulic characteristics in geotechnical applications. Accordingly, the goals behind the development of the new stress controllable pressure plate device were to facilitate the measuring of the two fundamental hydraulic functions, under different loading conditions, within a reasonable time, and

to present plain procedures allowing simple interpretation of the measured experimental data.

Shear strength and deformation characteristics of saturated and unsaturated sand-gypsum mixtures having different gypsum contents were included in the third part of the experimental programme. The common experimental procedures for determining the shear strength of unsaturated soils are time consuming and costly. Thus, one of the main objectives of the third experimental part was to develop a simple procedure to determine the shear strength of unsaturated soils by using conventional direct shear device that is used for determining the shear strength of saturated soils. Constant water content direct shear tests on initially air-dried specimens were carried out. The matric suctions of the tested specimens were correlated by using the SD-SWCC test results. The possibility of measuring the soil-water characteristic curve under net normal stress levels identical to those used in direct shear tests enhances the reliability in estimating the matric suction to be incorporated with the direct shear test results of air-dried specimens. This facility makes the direct shear testing approach that uses moisture controlled specimens instead of matric suction controlled specimens to be more reliable and applicable.

Considering the main criteria of describing the shear strength of unsaturated soils, the second main objective of the shear strength tests was to find the effect of gypsum content, and the effect of the applied net normal stress level on each of the following:

- (1) The contribution of matric suction to shear strength (τ_s).
- (2) Matric suction failure envelopes.
- (3) The internal friction angle related to matric suction (ϕ^b).
- (4) The effective stress parameter (χ).
- (5) The suction stress function.
- (6) The shear stress-shear displacement behaviour.
- (7) The vertical deformation-shear displacement behaviour.
- (8) The initial shear stiffness.
- (9) The saturated shear strength parameters (c' and ϕ').

As a third objective of the shear strength tests was to verify the validity of Rassam and Cook (2002)'s semi-empirical predictive model by using the obtained shear strength test results. This model was originally proposed to predict the failure envelopes of unsaturated silty sand soil.

1.3. Thesis organization

This work includes eight chapters; the literature review chapter, two chapters introduce the applied methodology, three chapters present the results and discussion, in addition to the introduction and conclusion chapters.

Chapter 2 begins with a brief review of the basic properties of gypsum and some of relevant studies on saturated gypsiferous soils. The core of this chapter is focused on the basic topics of unsaturated soil mechanics. The concepts of water retention and flow characteristics in addition to the relevant stress state and volumetric state variables that used for unsaturated soil behaviour representation are reviewed. Special attention is given to the common techniques of measuring and controlling soil suction with a detailed discussion of the axis translation technique. The outflow transient techniques for measuring the unsaturated hydraulic conductivity are reviewed, as well. Finally, the most common criteria for describing the shear strength of unsaturated soils and their limitations are discussed.

Chapter 3 explains the importance and significance of materials selection to suit the research objectives, and the classification properties of the used materials (gypsum and the sandy soil). The preparation of sand-gypsum mixtures and their resulting index properties are presented. Different parts of the experimental programme are addressed with particular details for different series of tests including the details of the used devices, calibrations and adjustments, specimen preparation, test procedures and calculations.

Chapter 4 introduces a newly modified stress controllable pressure plate device for measuring simultaneously the stress-dependent soil-water characteristic curves (SD-SWCCs) and the stress-dependent hydraulic conductivity functions (SD-HCFs). The significant device features, design and construction details, specimen preparation, testing procedures and calculations are described in detail. This chapter

presents also the experimental programme which has been carried out on various sand-gypsum mixtures under different loading conditions.

Chapter 5 presents results analysis and discussion for six series of standard conventional tests. These tests include a series of standard compaction tests, a series of one-dimensional consolidation tests, a series of shrinkage characteristics tests (CLOD tests), and three series of soil-water characteristic curve tests. The effect of gypsum content on some important parameters related to these tests are discussed and defined.

Chapter 6 and Chapter 7 include analysis and discussion of test results of the SD-SWCC and SD-HCF during both drying and wetting processes, under the influence of different net normal stress levels, for five sand-gypsum mixtures by using the modified stress controllable pressure plate device. The effect of gypsum content and the influence of net normal stress level on the relevant hydraulic parameters are addressed.

Chapter 8 presents the shear strength and deformation characteristics for various sand-gypsum mixtures at saturated and unsaturated conditions. In total, results of 32 tests on saturated specimens and 120 tests on unsaturated specimens are presented. The influence of gypsum content and the effect of water content on the saturated and unsaturated shear strength parameters are brought out. The stress-deformation behaviour that includes the shear stress-horizontal shear displacement and vertical displacement-horizontal displacement relationships are presented, as well.

Chapter 9 summarizes the conclusions and recommendations derived from this work and the recommendations for future works.

CHAPTER TWO

LITERATURE REVIEW

2.1. Introduction

Numerous studies can be found in literature on gypsiferous soils within the classical approach that is related to the saturated condition. Studies on gypsiferous soils in an unsaturated state approach are quite rare. In addition, there are a very few studies available in the literature where both the mechanical and flow characteristics were examined in an integrated manner to better understand the engineering behaviour of unsaturated soils.

This chapter begins with a brief review of the basic properties of gypsum and some of relevant studies on saturated gypsiferous soils. The core topics in this chapter are focused on describing the fundamental concepts of unsaturated soils, the most important unsaturated characteristic functions, and the common techniques of measuring and controlling soil suction with a detailed discussion of the axis translation techniques which are more related to the present study. These topics are intended to provide a suitable background to develop a new device for establishing two important characteristic functions for unsaturated soils, such as the soil-water characteristic curve and the unsaturated hydraulic conductivity function. Furthermore, the outflow transient techniques for measuring the unsaturated hydraulic conductivity are reviewed. In the last section, the most common modelling and prediction methods for shear strength of unsaturated soils and their limitations are discussed.

2.2. Gypsiferous soils

Gypsiferous soils are known as problematic soils from engineering point of view. The problems may be related to the collapsibility of such soils, progressive settlements, accelerating seepage of water through soil, and strength reduction. Gypsum ($\text{CaSO}_4 \cdot 2\text{H}_2\text{O}$) is considered as one of the fairly soluble salts that can have a detrimental effect on pavements, buildings and earth structures.

Gypsiferous soils cover approximately one million km^2 worldwide (Verheye and Boyadgiev, 1997). These soils are of wide occurrence in the Middle East, especially in areas peripheral to the Arabian Gulf and Red Sea (Blight, 1976; Fookes, 1976, 1978; Fookes and French, 1977; Tomlinson, 1978). They cover large parts of the national territory of Iraq which may be extended up to 20% of the total area of Iraq, i.e., 9% of the World's gypsiferous soils are found in Iraq (FAO, 1990). The main characteristic of Iraqi soils in the vicinity of Baghdad is gypsum content of 0-80%. For that reason a special attention was given to study the behaviour of such soils.

Gypsum is commonly encountered in soil formations of semi-arid and arid regions where precipitation is not enough to leach it from the soil profile. Gypsum accumulations usually occur either by evaporation of mineralized fluctuated groundwater or by the precipitation within the groundwater itself, and it is mostly found interbedded with limestone and dolomite (Blight, 1976).

The presence of gypsum in a soil largely influences the physical and mechanical properties of the soil. This influence depends mainly on the amount and type of gypsum present in the soil, the environmental circumstances under which the soil is used, and the type of engineering problem under consideration (Razouki and El-Janabi, 1999; Razouki and Kuttah, 2004; Fattah et al., 2008). The noticeable amount of gypsum that causes serious change in soil properties can be one of the interesting points for many researchers. The Iraqi Standard Specification published by the State Corporation of Roads and Bridges (SCRB, 2003) considers salty or gypsiferous soil containing more than 10% of total soluble salts to be unsuitable when used in the top 50 cm of embankments. This value of 10% may be increased up to 20% in areas of low rainfall (less than 100 mm/year).

Gypsiferous soils are usually characterized as collapsible soils, decreasing strength upon wetting, and dissolving in flowing water. However, such soils are reliable for construction under dry weather and even under short term inundation, but become problematic, collapsible, and suffer large settlement under long term flooding with water (Al-Saoudi et al., 2001; Al-Mufty, 1997).

In natural depositions, gypsiferous soils are found in relatively low density, low water content, and mostly possess high apparent cohesion. Upon wetting, gypsiferous soils show large reduction in void ratio under low level of stress that may be close to the usual overburden pressure (Al-Nouri and Saleam, 1994). In contrast to the consolidation settlement where the reduction in void ratio results from time dependent pore-water drainage, the collapse settlement in such soils takes short time and it may coincide with intake of water.

Collapse is defined as the decrease in the height of a confined soil following wetting at a constant applied vertical stress (ASTM D 5333-03). A collapsible soil may withstand relatively large applied vertical stress with small settlement at low water content, but this soil will exhibit large settlement after wetting with no additional increase in stress. According to the ASTM D 5333-03, collapse is quantified by two terms, the first term is referred to as "collapse potential" which represents the magnitude of collapse at any level of normal stress and it can be determined by following the double oedometer approach. The second term is so called "collapse index" which represents the magnitude of collapse under 200 kPa normal stress, and this can be evaluated by doing a single collapse test. The addition of water to gypsiferous soils causes a significant reduction in the bonding stresses at the intergranular contacts that contribute in the shear strength, and thus leading to volume reduction in the soil mass.

2.2.1. Gypsum properties

The word gypsum is derived from the Greek word gypsos. Gypsum is calcium sulphate dihydrate ($\text{CaSO}_4 \cdot 2\text{H}_2\text{O}$). Gypsum contains 32.6% calcium oxide (CaO), 46.5% sulphur trioxide (SO_3) and 20.9% combined water (H_2O), Klein and Hurlbut (1985). Upon heating gypsum can be transformed into Bassanite ($\text{CaSO}_4 \cdot \frac{1}{2}\text{H}_2\text{O}$) and

then to anhydrite (CaSO_4). The dehydration starts at 40°C and reaches a level corresponding to the semi-hydrate (Bassanite) at 70°C . At about 95°C the remaining $\frac{1}{2}\text{H}_2\text{O}$ molecule in bassanite is lost, and the structure transforms to that of anhydrite (CaSO_4).

Dehydration of gypsum is associated with a volume decrease of up to 38% (Zanbak and Arthur, 1986), which may lead to excessive settlement of the overlying structures. Conversely, upon wetting the transformation of anhydrite to gypsum is accompanied with a volume increase up to 62% (Blatt et al., 1980) and this creates a swell pressure and floor heave in tunnels and massive rock uplift in dams (Brune, 1965).

Azam et al. (1998) examined the swell pressure of the three different phases of calcium sulphate. The results show that the swell pressure for gypsum, bassanite, anhydrite are 330, 1400, and 1660 kPa respectively, compared to 3200 kPa for a highly expansive clay tested in the same investigation. The initial void ratios for gypsum, bassanite, and anhydrite were 0.28, 0.50 and 0.61 respectively, compared to 0.79 for the expansive clay.

In its typical form, gypsum is colourless or white but if impurities are present then it may be red, brown or orange. Gypsum is a soft crystal with hardness, on Mohs scale, rating of 2 and particle density of approximately 2.3 (Blyth, 1971). Anhydrite is relatively hard crystal with a hardness rating of 3.5 and particle density of approximately 2.9 (Blyth, 1971).

Gypsum particles have no negative charges and consequently have no cation exchange capacity. This property causes the cohesive forces between gypsum particles to be low, and this in turn reflects on the overall gypsiferous soil cohesion with a degree depends on gypsum percentage.

Gypsum is considered a moderately soluble salt (Shihab et al., 2002). It dissolves in water into calcium ions and sulphate ions. Its solubility is 2.6 g/l in pure water at 25°C and a pressure of 1 atmosphere (Barazanji, 1973). As a comparison, sodium chloride has a solubility of 360 g/l in the same conditions. Beside the

temperature and the pressure, there are many other factors affect the degree of solubility of gypsum. Among these are: the kinds and concentrations of other existent salts, the velocity of the flowing water, and the specific surface of gypsum particles (Barazanji, 1973).

The presence of salts such as calcium bicarbonate ($\text{Ca}(\text{HCO}_3)_2$) and sodium sulphate (Na_2SO_4) in soil decreases the solubility of gypsum, while the presence of other salts such as sodium chloride (NaCl) and magnesium chloride (MgCl_2) increases the solubility. However, the existence of some less soluble salts in soil such as barium chloride (BaCl_2), potassium oxalate ($\text{K}_2\text{C}_2\text{O}_4$), ammonium oxalate ($\text{C}_2\text{H}_8\text{N}_2\text{O}_4$), ammonium carbonate ($(\text{NH}_4)_2\text{CO}_3$), and ammonium phosphate ($(\text{NH}_4)_3\text{PO}_4$) may greatly reduce the gypsum solubility by coating gypsum molecules and isolate them from water (Al-Kaissy and Naji, 1985; Younan, 1986; Al-Janabi, 1990).

2.2.2. Effect of gypsum on soil behaviour

Through the classical framework of soil mechanics, some studies on the behaviour of saturated gypsiferous soils may be found in literature. The majority of those studies were conducted using samples from natural gypsiferous soil depositions which mostly contain some other soluble salts beside gypsum which may interfere the effect of gypsum on soil behaviour. Investigations carried out on silty clay gypsiferous soil from Baghdad show that the increase of gypsum content decreases both the liquid limit and the plasticity index of that soil (Subhi, 1987; Al-Heeti, 1990). Tests on highly expansive clay, from Eastern province of Saudi Arabia, show that the liquid limit and the plastic limit decrease, whereas the shrinkage limit increases with an increase in the amount of both gypsum and anhydrite in clay (Azam et al., 1998).

The effect of gypsum on compaction characteristics of granular gypsiferous soil was examined by Kattab (1986). The results show that the increase of gypsum up to 15% by weight causes a gradual increase in the maximum dry density associated with a decrease in the optimum water content. Conversely, when the gypsum content increases more than 15% by weight, the maximum dry density starts to decrease

associated with an increase in the optimum water content. Similar trend can be noticed from results of Al-Dilaimy (1989) on clayey gypsiferous soils but the defined percentage of gypsum was 5% instead of 15%. This variation can be attributed to the difference in the pore-size distribution of the granular soil from that of the clayey soil.

Laboratory tests carried out by Razouki et al. (2008) to study the compaction behaviour of fine-grained gypsiferous soil show that the compaction curve of the tested soil has double peaks showing two maximum dry densities and two optimum water content. They referred to the maximum dry density at the lower optimum water content (OWC) as the "dry maximum dry density" and to that at the high OWC as the "wet maximum dry density".

The compressibility characteristics of gypsiferous silty soil were examined using conventional oedometer (Al-Aithawi, 1990; Al-Heeti, 1990). The results show that the soil tested exhibits low compressibility and the primary consolidation ended in a relatively short duration and a secondary consolidation was noticed.

The influence of gypsum on shear strength parameters of a sandy soil and a clayey soil were examined by Seleam (1988) and Al-Qaissy (1989), respectively. Results illustrate that the increase of gypsum in sandy soil causes both the angle of internal friction and the effective cohesion to increase for a gypsum content of 25% up to 80%. However, for cohesive soil, the cohesion decreases and the angle of internal friction increases as the gypsum content increases. This behaviour may be attributed to the fact that the cohesion between gypsum particles and clay particles is less than that between the particles of cohesive soil itself, whereas the increase in the angle of internal friction is because the friction between gypsum and soil particles is greater than that between soil particles itself.

Barzanji (1984) investigated the infiltration rate characteristics of gypsiferous soils in north of Iraq. It was reported that for the same soil texture and the same initial water content, the infiltration rate increases as the gypsum content increases.

2.2.3. Effect of soaking on mechanical properties of gypsiferous soils

Some investigations have been carried out to study the effect of long-term soaking on the California Bearing Ratio (CBR) and on the shear strength parameters of some Iraqi gypsiferous soils that have different textures and different gypsum contents. Razouki and El-Janabi (1999) used well graded silty sand gypsiferous soil containing 64% gypsum. The results reveal a sharp decrease in CBR with the increasing of soaking period, especially within the first week. Thereafter, the loss in CBR took place at a smaller rate and it approaches a constant value after about six months. The decrease in CBR may be attributed to the leaching of gypsum with increasing soaking period. Similar behaviour are shown for gypsiferous silty sand containing 28% gypsum (Razouki and Ibrahim, 2007), high plasticity clay containing 34% gypsum (Razouki and Kuttah, 2006), and low plasticity clay soil containing 33% gypsum (Razouki et al., 2007).

To investigate the effect of soaking period on shear strength parameters, a series of unconsolidated undrained triaxial tests were carried out on low plasticity clay soil with a gypsum content of 33 % (Razouki et al., 2007), and another series of direct shear test on sandy lean clay containing 33% gypsum (Razouki et al., 2008). Both studies showed a significant drop in cohesion and angle of internal friction with an increase in soaking period. The reduction in shear strength parameters upon soaking is similar to the reduction of CBR with soaking, and this may be attributed to the effect of water on the bonding forces between particles and the dissolution of gypsum particles from the contact areas between particles.

To improve the strength characteristics of gypsiferous soils, the CBR test results of Razouki and Ibrahim (2007) show a significant improvement on CBR value can be achieved by increasing the compaction effort. Soil specimens made under low compaction effort were affected more by soaking than those made under high compaction effort. Similar to that, results of Razouki et al. (2007) reveal that the increase of compaction effort from standard to modified Proctor causes a significant increase in the shear strength parameters of the soil tested and this phenomenon is more pronounced for soaked conditions. This behaviour may be attributed to the effect of compaction on the permeability of soil specimens. As the compaction effort increases, the permeability of the specimens decreases, owing to an increase in

density and corresponding decrease in void spaces. Thus, the increase in compaction effort causes a reduction in the dissolution process of gypsum.

2.3. Unsaturated soil state

The general field of soil mechanics can be categorized into that part dealing with saturated soils and another part dealing with unsaturated soils. An unsaturated soil has more than two phases, and the pore-water pressure is always negative as compared to the pore-air pressure. Unsaturated soils have commonly been viewed as a three-phase system (Lambe and Whitman, 1979). However a fourth independent phase has been introduced by Fredlund and Morgenstern (1977). This phase is the air-water interface or what is called the contractile skin. Therefore, dealing with unsaturated soils requires not only the principles of mechanics and hydraulics as stated by Terzaghi (1943) in his definition to the classical soil mechanics, but it needs also the application of thermodynamics principles that describe the equilibrium among gas-liquid-solid phases, the transition of matter from one phase to another, and the desorption or adsorption of one phase of matter onto or from an adjacent phase of different matter (Fredlund and Rahardjo, 1993; Lu and Likos, 2004).

2.3.1. State variables and material variables

To describe different soil phenomena and to predict their occurrences and behaviour, a number of state variables, material variables, and governing laws are required. State variables are those that are required to describe the state of the system for the phenomenon at hand and they do not have to have the same physical units (Lu, 2008). Material variables (soil parameters) are those properties that depend on the soil type, and they are usually varied from one soil to another soil and/or from one state to another state.

It may be convenient in soil mechanics to differentiate between stress state variables, deformation state variables, and flow state variables. Common stress state variables are the total stress, pore pressure, effective stress, net stress, suction stress, shear stress, and the principle stresses (Lu and Likos, 2004). Commonly used deformation state variables are the strain and the void ratio. Widely used flow state

variables are the degree of saturation, gravimetric or volumetric water content, and the total hydraulic head (Lu and Likos, 2004).

Material variables may be also categorized as classification parameters, mechanical parameters, and hydraulic parameters. Widely known classification parameters of a soil are the grain-size distribution, the consistency limits, and the specific gravity of soil solids. The most pronounced mechanical parameters of a soil are the angle of internal friction, the soil cohesion, and the compressibility indices. The two key hydraulic properties for an unsaturated soil are the soil-water characteristic function which shows the soil water content as a function to the soil suction, and the unsaturated hydraulic conductivity function which is the permeability of soil as a function to the water content or matric suction (Fredlund and Rahardjo, 1993; Benson and Gribb, 1997).

2.3.2. Stress state variables

Stress state variables are the constitutive variables used in describing the mechanical behaviour of a soil mass. The volume change and the shear strength behaviour can be formulated in terms of the state of stress in the soil. The number of stress state variables required to describe the state of stress in a soil mass depends primarily upon the number of phases of the soil under consideration (Fredlund and Rahardjo, 1993). In consequence, the state of stress in unsaturated soil is fundamentally different from that in saturated soil.

The effective stress, which was defined by Terzaghi (1923) as the difference between the total stress and the pore-water pressure, is considered a fundamental state variable for describing the state of stress in saturated soil (Clyton et al., 1995). Terzaghi's effective stress equation, which is shown below, forms the fundamental basis for studying the saturated soil mechanics.

$$\sigma' = \sigma - u_w \quad 2.1$$

where σ' is the effective stress, σ is the total stress, and u_w is the pore-water pressure. All mechanical aspects of a saturated soil, the volume change and the shear strength characteristics are governed by the single-valued effective stress. Physically,

effective stress describes the stress acting on the soil skeleton and propagating through it, i.e., the stress acting at the partial-partial contacts.

For unsaturated soil, the physical meaning of the effective stress remains the same. However, when the soil is saturated and the pore-water pressure is positive, the effect of the water pressure is to reduce the effective stress (Terzaghi, 1943), whereas in case of unsaturated soil, the pore-water pressure is negative, and thus creating tensile forces acting to increase the effective stress and pull the soil grains together.

Furthermore, pore pressure in saturated soil is a neutral stress, meaning it is isotropic and invariant in direction, and acting on the entire surface of the soil grains, and thus having no shear component (Noor et al., 2008; Lu and Likos, 2004). Therefore, the state of stresses that control the engineering behaviour may be well defined from a boundary level perspective (Terzaghi, 1943; Clayton et al., 1995). However, pore pressure is no longer be a neutral stress in unsaturated soil medium, and it is disintegrating to three forms: air pressure acting on the dry or hydrated portions of the soil grain surfaces; water pressure acting on the wetted portions of the soil grain surfaces through a menisci formed near the grain contacts; and surface tension acting along the air-water interfaces (Lu and Likos, 2006). Therefore, the system is no longer being an equivalent continuum medium and difficulties arise in describing the state of stress. There are three main approaches used to describe the state of stress in unsaturated soils, these approaches are discussed in the following subsections.

2.3.2.1. The variable effective stress state single approach

The resultant interparticle stress in unsaturated soil was described in variety of extended forms of Terzaghi (1923)'s effective stress equation. Those forms were modified to take into account the effect of the negative pore-water pressure (Croney et al., 1958; Bishop, 1959; Aitchison, 1961; Jennings, 1961; Richards, 1966). Among those, Bishop's single-valued effective stress equation which has gained widespread reference:

$$\sigma' = (\sigma - u_a) + \chi (u_a - u_w) \quad 2.2$$

where σ' is the effective interparticle stress, σ is the total stress, u_a is the pore-air pressure, u_w is the pore-water pressure, and χ is a soil parameter that vary with the degree of saturation or matric suction and it is referred to as the "effective stress parameter" . The term $(\sigma - u_a)$ represents the net normal stress applied to the soil mass, the term $(u_a - u_w)$ is called "matric suction", and the product $\chi(u_a - u_w)$ is referred to as the "suction stress" which represents the part of interparticle stress due to the suction. The magnitude of χ parameter is unity for a saturated soil and zero for a dry soil. In both these extreme cases, Bishop's effective stress equation reduces to the classical Terzaghi's effective stress equation.

The nature of χ , its determination by experimental techniques, and its mathematical representation will be discussed later in Section 2.6. The χ parameter appears to be difficult to evaluate and seems to have different magnitudes for different problems and different magnitudes for different types of soil (Bishop and Blight, 1963; Burland, 1965; Blight, 1965; Lu and William, 2006). Morgenstern (1979) found that the χ parameter when determined for volume change process has different value from that determined for shear strength, and that is also true for all other proposed extended forms of the effective stress equation which use a soil parameter to describe the stress state. For that reason and due to difficulties associated with the experimental or theoretical determination of the effective stress parameter, the general applicability of the effective stress approach for unsaturated soil mechanics have been limited in practice and continues to be a subject of debate (Lu and Likos, 2004).

2.3.2.2. The two independent stress state variable approach

Coleman (1962) suggested the use of net normal stress $(\sigma - u_a)$ and matric suction $(u_a - u_w)$ as independent stress state variables to describe stress-strain relations for unsaturated soil. Bishop and Blight (1963) mentioned some advantages of using net normal stress and matric suction as stress state variables. In other words, there has been a tendency to separate Bishop's effective stress equation into two independent stress state variables and the need of incorporation a soil parameter in the stress state description no longer exists.

Fredlund and Morgenstern (1977) concluded that any two of three possible normal stress variables: $(\sigma - u_a)$, $(\sigma - u_w)$, $(u_a - u_w)$, may be used to describe the stress state of unsaturated soil. These combinations are: net normal stress and matric suction, effective stress and matric suction, net normal stress and effective stress. These stress state variables were used then to formulate constitutive equations that describe the mechanical behaviour, volume change and shear strength of unsaturated soil.

Like the single variable effective stress state approach, the use of two independent stress state variables needs to associate some material variables that reflect the effect of desaturation on mechanical properties (such as ϕ^b which reflects the increase in shear strength with respect to matric suction). As with the χ parameter, experimental and conceptual difficulties exist with determining these material variables and there are uncertainties in their uniqueness over a wide range of saturation. These reasons have limited the practical applicability of the two independent stress state variable approach as well (Khalili and Khabbaz, 1998; Nuth and Laloui, 2008; Lu et al., 2010).

Moreover, Lu (2008) clarified that matric suction is not a stress variable but it can be considered as a stress state variable, and then the direct usage of it in any stress-based model is mechanically erroneous. In other words, matric suction is by nature a variable controlled by state variables such as temperature and soil water content and it would be inconsistent to consider it as an independent state variable. Also he pointed out that there is an interdependency or coupling between matric suction and the net normal stress if both of them are concurrently used to describe the state of stress.

2.3.2.3. The true effective stress state variable approach

Based on a micromechanical interparticle force consideration and following the classical concept of effective stress, Lu and Likos (2006) introduced the concept of "suction stress" as a characteristic function of the soil-water system. Suction stress characteristic curve (SSCC) is defined as the function of suction stress to degree of saturation, water content, or matric suction. In this regard, they distinguished three

types of intergranular forces which are: (1) active skeletal forces transmitted through the soil grains; (2) active local forces concentrated at or near the interparticle contacts; (3) passive local forces at or near the interparticle contacts to counterbalance the active skeletal and local forces. The first and third types of forces are often sufficient to be considered in saturated soils, while considering the three types of forces becomes necessary in unsaturated soil condition.

From a microscopic view, the second type of force may disintegrate to several intergranular forces acting within the vicinity of the grain contacts which are: (1) physicochemical forces that include van der Waals attractive forces (resulting from electromagnetic field interaction between adjacent atoms of approaching surfaces), and electrical double-layer repulsive forces which are due to charge deficiency within the soil solid crystalline lattice; (2) cementation forces between particles result from covalent or ionic bonds formed between the cementing agent and soil particles; (3) surface tension forces at the air-water interfaces; (4) the forces arising from negative pore-water pressure. It was proposed that these four types of forces can be conceptually lumped into a macroscopic stress referred to as suction stress (Lu and Likos, 2006; Oh et al., 2012).

Together with net normal stress, suction stress is considered completely defines the effective stress (intergranular stress) in unsaturated soil or what is herein referred to as "the true effective stress" as shown:

$$\sigma'' = (\sigma - u_a) - \sigma'_s + \sigma_{co} \quad 2.3$$

where σ'' is the true effective stress, $(\sigma - u_a)$ is the net normal stress, σ'_s is the suction stress which is a characteristic function of the soil-water system that referred to as suction stress characteristic curve, σ_{co} is the apparent tensile stress at the saturated state which can be estimated as $(\sigma_{co} = c'/\tan \phi')$ with c' being the effective saturated cohesion and ϕ' the effective friction angle. Lu and Likos (2006) considered the suction stress as a positive term and its representation in the effective stress equation was with a positive sign. Later on some researchers considered a negative sign to the suction stress and its representation in the effective stress equation was a negative term also (Oh et al., 2012).

The suction stress characteristic curve (SSCC) can be found directly through the modified shear strength tests that employ the axis translation technique to control matric suction. The SSCC, however, may be described as a function to the water content or degree of saturation and then it can be determined by means of conventional shear strength tests using water controlled specimens rather than suction-controlled specimens. The conventional tests are significantly simpler than the modified tests, beside that, the describing of SSCC as a function to the water content facilitates the strength monitoring of the unsaturated soils in the field since measuring the field water content is much faster and easier than measuring matric suction.

2.3.3. Total head as a state variable

The driving potential for the flow of water may be described by using the total hydraulic head as a flow state variable, which represents the total energy per unit weight of water at a certain point. The hydraulic head has primary three components of energy, namely the gravitational head or elevation head, the pressure head, and the velocity head as shown by Bernoulli's equation below.

$$h_t = z + \frac{u_w}{\gamma_w} + \frac{v_w^2}{2g} \quad 2.4$$

where h_t is the total hydraulic head, z is the elevation above an arbitrarily chosen datum, u_w is the pore-water pressure, γ_w is the weight density of water, v_w is the water flow velocity, and g is the gravitational acceleration.

The velocity head in a soil is negligible and the total head can be sufficiently represented by the summation of the elevation head and the pressure head.

$$h_t = z + \frac{u_w}{\gamma_w} \quad 2.5$$

The total head concept is generally applicable to both saturated and unsaturated soil conditions (Fredlund and Rahardjo 1993; Lu and Likos, 2004). However, the major difference is that the pressure head governed by the pore-water pressure is positive in saturated soil and negative in unsaturated soil. The negative pore-water pressure is mostly expressed in terms of matric suction ($u_a - u_w$) which has a positive sign in an unsaturated soil. Thus the total head can be expressed as:

$$h_t = h_g + h_m \quad 2.6$$

where h_g is the gravitational head ($h_g = z$), and h_m is the matric suction head which can be expressed as:

$$h_m = - \frac{u_a - u_w}{\gamma_w} \quad 2.7$$

In isothermal flow systems, water flows from a point of high total head to a point of low total head, regardless of whether the pore-water pressures are positive or negative, i.e. water flows in the direction of a decreasing hydraulic head or what is called "the hydraulic head gradient". In some applications, water may flow under the influence of an osmotic gradient and then the osmotic suction has sometimes been included as a component in the total head equation for flow. However, it is superior to deal with the osmotic suction gradient as the driving potential for the osmotic diffusion process and to analyze the bulk flow of water separately from the diffusion process since two different and independent mechanisms are involved (Corey and Klute, 1985; Corey and Kemper, 1961).

2.4. Soil suction and soil-water characteristic curve

Water retention in unsaturated soil zones is of fundamental importance to geotechnical engineers and soil scientists, and this is primarily characterised through the soil-water characteristic curve (SWCC) which represents the soil suction (matric or total) as a function to the water content (gravimetric or volumetric) or degree of saturation. The soil-water characteristic curve is also referred to as the soil-water retention curve, the soil-water release curve, and the capillary pressure curve (ASTM D 6836-02). The SWCC is an essential tool in evaluating the shear strength and the volume change characteristics of unsaturated soils. Furthermore, the hydraulic conductivity of unsaturated soils is usually estimated by using the SWCC and the saturated hydraulic conductivity (Fredlund and Rahardjo, 1993; Lu and Likos, 2004).

2.4.1. Soil suction and potential energy

The concept of soil suction was developed in the early 1900s in relation to the soil-water-plant system (Buckingham, 1907; Gardner and Widtsoe, 1921; Richards, 1928). In the middle of the last century, soil suction was introduced in explaining the

mechanical behaviour of unsaturated soils and some other engineering problems (Croney et al., 1950).

From a thermodynamic view, soil suction quantifies the drop in the potential energy of soil pore-water (the free energy state of soil water) relative to a reference potential of free pure water (Richards, 1965) through the following relationship:

$$E = \frac{RT}{\omega_v} \ln(RH) = \frac{RT}{\omega_v} \ln\left(\frac{u_v}{u_{v0}}\right) \quad 2.8$$

where E is the free energy per unit mass of soil pore-water comparing to that of free pure water (J/kg), R is the universal gas constant (J/mol.K), T is the absolute temperature in Kelvin (K), ω_v is the molecular mass of water vapour (kg/mol), u_v is the vapour pressure in equilibrium with soil pore-water (kPa), u_{v0} is the saturated vapour pressure in equilibrium with free pure water at the same temperature (kPa), and RH is the relative humidity which can be defined as the ratio of the absolute humidity in equilibrium with soil solution to the absolute humidity in equilibrium with free pure water at the same temperature (Pan et al., 2010; Lu and Likos, 2004; ASTM D 6836-02; Fredlund and Rahardjo, 1993).

The potential of soil pore-water in Equation 2.8 is expressed as energy per unit mass (J/kg). In addition, the potential of soil pore-water can be expressed as an energy per unit volume, a pressure potential (i.e., J/m³ = N.m/m³ = N/m² = Pa), or as energy per unit weight, a head energy (i.e., J/N = N.m/N = m). Conversation from energy per unit mass to pressure potential or head potential may be achieved by considering the following relations:

$$\psi = -\rho_w \cdot E \quad 2.9$$

$$h_m = \frac{E}{g} \quad 2.10$$

$$h_m = -\frac{\psi}{g \cdot \rho_w} \quad 2.11$$

where ψ is the soil suction (Pa), ρ_w is water density (kg/m^3), E is the potential (J/kg), h_m is matric suction head potential (m), and g is gravitational acceleration (m/s^2). As mentioned above the reference potential is the free pure water, and thus the energy potential or the matric suction head potential will have a negative sign in reference to the free pure water.

2.4.2. Components of soil suction

The free energy state of soil pore-water is defined in Equation 2.8 considering the change from a reference condition of free pure water, and thus will be a negative value. The physical and physicochemical mechanisms responsible for decreasing the potential of the pore-water relative to this reference state include capillary effects, short-range adsorption effects, and osmotic effects (Pan et al., 2010; Lu and Likos, 2004; Fredlund and Rahardjo, 1993).

Capillary effects, which include the curvature of the air-water interface and the associated negative pore-water pressure, are the dominant mechanisms at relatively high values of water content which are corresponding to low values of suction. The capillary effects are governed primarily by the particle and pore structure and pore-size distribution (Lu and Likos, 2006).

Short-range adsorption effects, which result mainly from electrical and van der Waals force fields, are the dominant mechanisms at relatively low values of water content which are corresponding to high values of suction, where pore-water is primarily in the form of adsorbed films on particle surfaces. The short-range adsorption effects are governed by surface area of the soil particles and the surface charge intensity of the soil mineral (Bolt 1956; Lambe 1960).

Osmotic effects result from dissolved solutes in the pore-water which reduce the potential of the pore-water to a degree depends on the type and concentration of the solute (Murray & Sivakumar, 2010; Lu and Likos, 2004; Fredlund and Rahardjo, 1993). Suction arising from the combined effects of capillary and short-range adsorption is usually grouped under the general term "matric suction" while suction arising from the effects of dissolved solutes is known as "osmotic suction". The

algebraic sum of the matric and osmotic component is referred to as "total suction" (Fredlund and Rahardjo, 1993). Suction components are usually altered with environmental changes. In most geotechnical problems the osmotic suction changes are generally less significant than matric suction changes (Fredlund & Rahardjo, 1993; Murray & Sivakumar, 2010).

Considering the definition of soil suction in Equation 2.8, matric suction can be defined by considering the vapour pressure in equilibrium with soil pore-water, relative to vapour pressure in equilibrium with a free solution identical in composition to the soil water. Similarly, osmotic suction can be defined by considering the vapour pressure in equilibrium with free solution identical in composition with the soil water, relative to the vapour pressure in equilibrium with free pure water (Fredlund and Rahardjo, 1993; ASTM D 6836-02).

2.4.3. Overview of soil suction measurement techniques

Conventional techniques for measuring soil suction and corresponding soil-water characteristic curves include tensiometers, null-type pressure plates, psychrometers, and porous sensors techniques. In general these techniques can be categorized as field or laboratory methods. Laboratory methods can be categorized by the measured component of suction (matric or total), and differentiated as either a direct or indirect measurement. In direct techniques, the equilibrium state of soil-water system is measured directly without involving an external medium as an absorbent for moisture equalization such as filter papers, gypsum block conductivity sensors, and other porous materials.

Tensiometers and null-type pressure plates are used for direct measurement of matric suction, whereas the psychrometers and porous sensors (filter papers and electrical/thermal conductivity sensors) fall in the category of indirect measurements. Standard tensiometers are used to measure suction values limited by the capacity of water to sustain high negative pressure without cavitation. Theoretically, this value is 100 kPa, but due to presence of some impurities, dissolved gases, and air bubbles in water, the practical limit is about 70 to 80 kPa. Later on some improvements have been made to the tensiometer technique to measure matric suction up to 1500 kPa

(Ridley & Burland, 1993; Guan and Fredlund, 1997; Tarantino and Mongiovi, 2003; Toker, 2002). Null-type pressure plate method utilizes the axis translation technique to extend the range of direct measurement of matric suction up to 1500 kPa without the problem of water cavitation (Fredlund, 1989; Tripathy et al., 2005; Tripathy et al., 2012; Vanapalli et al., 2008; Leong et al., 2009). These techniques were well reviewed by many researchers such as Ridley & Wray (1995), Pan et al. (2010), Rahardjo and Leong (2006), Lu and Likos (2004), Guan (1996), Fredlund and Rahardjo (1993). Table 2.1 summarizes several common suction measurement techniques in terms of direct or indirect, suction component, approximate measurement range, and the applicability in laboratory or field.

Table 2.1. Summary of common laboratory and field techniques for measuring soil suction (modified from Lu and Likos, 2004).

Suction component measured	Technique	Measurement range (kPa)	Laboratory / Field	Direct / Indirect measuring
Matric suction	Tensiometers	0 - 100	Laboratory and field	Direct
	Null-type axis translation apparatus	0 - 1500	Laboratory	Direct
	Contact filter paper	Entire range	Laboratory and field	Indirect
	Electrical / thermal conductivity sensors	0 - 400	Laboratory and field	Indirect
Total suction	Psychrometers	100 - 8000	Laboratory and field	Indirect
	Chilled-mirror hygrometers	500 - 450,000	Laboratory	Indirect
	Noncontact filter paper	1000 - 500,000	Laboratory and field	Indirect

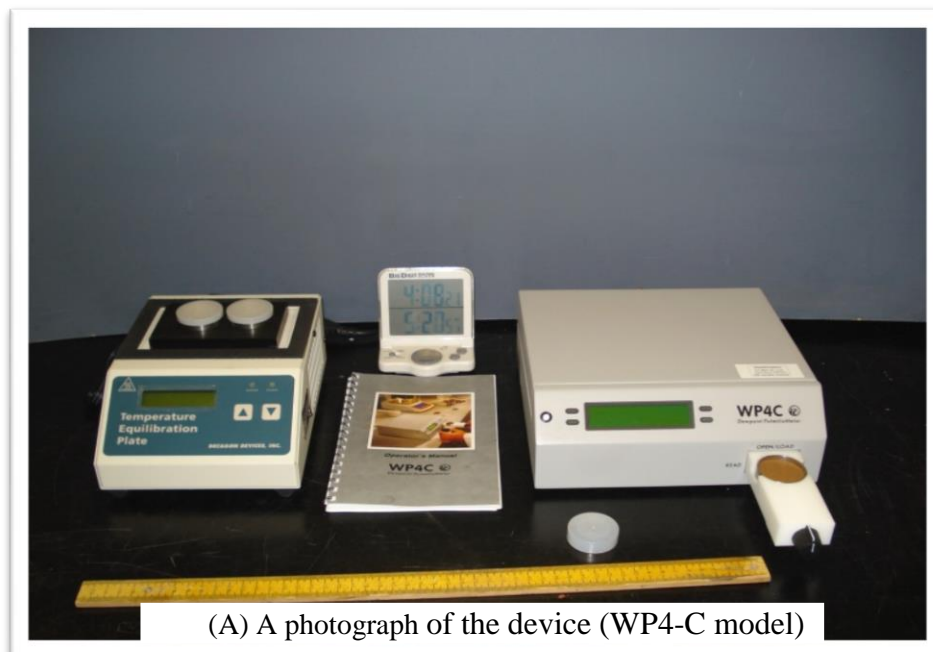
The measurement of total suction is usually carried out by placing a soil specimen in a closed isothermal chamber, then the relative humidity in the head space of the chamber is measured by means of psychrometer after the temperature and vapour pressure between the specimen and the head space are allowed to come to equilibrium. The relative humidity of the head space is related to the soil suction by using Kelvin's law, which applies here to the total suction because all of the mechanisms (dissolved solutes, hydration effects, and capillary effects) that act to reduce the potential of the pore-water are accounted for.

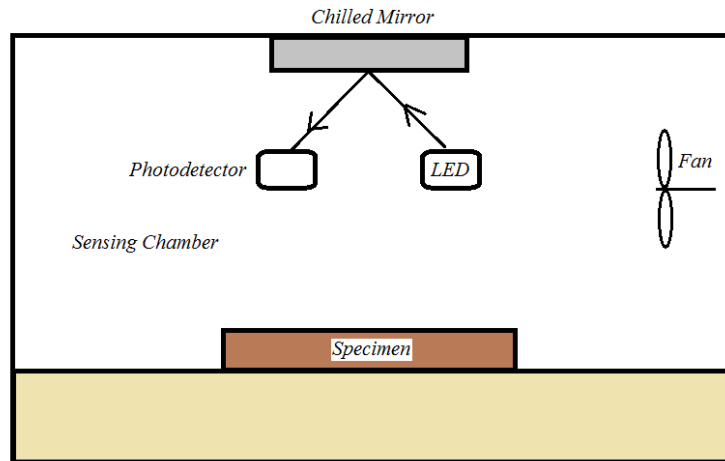
There are several types of psychrometers used to measure the relative humidity such as thermocouple psychrometers, hygrometers, thermistor psychrometers, and transistor psychrometers (Harrison & Blight, 2000; Sivakumar, 2005). The common types of hygrometers include dew-point hygrometers and water-vapour adsorptive type hygrometers. A chilled-mirror dew-point hygrometer was used in this study to

find the SWCC in terms of total suction for different sand-gypsum mixtures. Therefore, this type will be reviewed in more detail in the following section.

2.4.4. Chilled mirror hygrometer

The operating principle of this technique includes measuring the dew-point of water vapour in equilibrium with soil specimen by a miniature cooled mirror located above the specimen in a closed chamber as displayed in the schematic diagram shown in Figure 2.1. The mirror is constructed from a material with good thermal conductivity such as silver or copper, and properly coated with an inert metal such as iridium, rubidium, nickel, or gold to prevent tarnishing and oxidation. The mirror is cooled by an attached Peltier thermoelectric unit until it reaches the dew-point of the ambient water vapour in the closed chamber. When this point of temperature has been reached, condensation will begin to form on the mirror surface. The mirror is illuminated with a regulated LED (Light Emitting Diode), and the light reflected by the mirror is received by a photodiode. When water vapour condenses on the mirror, the light received by the photodiode is reduced due to scattering.





(B) Schematic diagram

Figure 2.1. Chilled-mirror dew point hygrometer, (A) a photograph of WP4-C model device and (B) schematic diagram of the chilled mirror technique (Lu and Likos, 2004).

The cooling power applied to the Peltier thermoelectric unit is adjusted by a microprocessor circuit, so that the rate of condensation and evaporation of water molecules and the mass of water on the mirror is kept constant. In this condition the temperature of the mirror which is measured usually by a platinum resistance thermometer is equal to the dew point temperature of the ambient water vapour in equilibrium with the soil specimen. The dew-point temperature can then be related to the ambient relative humidity and corresponding total suction through Kelvin's law (Yankee Environmental Systems, 2006; Lu and Likos, 2004; Gee et al., 1992).

The measuring range of this technique is relatively wide, ranging from around 3% relative humidity (about 450 MPa suction) to 99.9 % relative humidity (0.10 MPa suction). This technique is commonly employed to find the soil suction corresponding to relatively low water content, i.e., suction values greater than 1000 kPa. Under such conditions of dryness, the osmotic component of the total suction is generally small, and the matric suction and total suction are comparable. Thus, this technique can be used in conjunction with an axis-translation technique to establish the entire SWCC (ASTM D 6836-02).

2.4.5. Suction controlling techniques

Unlike suction measurement techniques that rely on measurements of suction for specimens of controlled water content, suction controlling techniques rely on

measurement of water content for specimens of controlled suction in a temperature and humidity controlled laboratory environment. Suction controlling techniques were primarily developed for determining the soil-water characteristic curves. As well as, suction controlling could be considered as the corner stone in implementation of unsaturated shear strength, compressibility, and hydraulic conductivity tests.

Suction controlling techniques may be categorized as those that control matric suction and those that control total suction which are also referred to as humidity control techniques. Isopiestic humidity control is one of the traditional methods for controlling total suction, while the hanging column, the centrifuge, and the axis translation techniques are the most well-known methods for controlling matric suction (Lu and Likos, 2004; ASTM D 6836-02; Fredlund and Rahardjo, 1993), see Table 2.2.

Table 2.2. Summary of common laboratory techniques of controlling soil suction.

Suction component	Technique	Controlling range
Matric suction	Hanging column	0 - 80
	Centrifuge	0 - 120
	Axis translation techniques	0 - 1500
Total suction	Isopiestic humidity control	0 - 400

The hanging column technique is one of the standard methods for determining the soil-water characteristic curve (SWCC) in terms of matric suction (ASTM D 6836-02). Due to water cavitation, the matric suction application range in this method is limited from 0 to 80 kPa, so it is suitable to define the SWCC for coarse grained soils. This method may be used also for other soils to provide a detailed description of the initial part of SWCCs near saturation and to define accurately the suction required to introduce air into the pores of a saturated soil that is referred to as the air-entry suction (ψ_a).

To control the matric suction over a range far greater than the cavitation limit of water under negative pressure, axis translation techniques are the most popular standard methods for determining the SWCC at matric suction levels up to 1500 kPa where almost all of the soil moisture movement takes place especially in sandy and silty soils (Lins et al., 2009; Chen et al., 2007; Wildenschild et al., 2001; Fredlund et

al., 2011). In addition, the axis-translation technique is commonly used to apply the required matric suction in volume change, shear strength, hydraulic conductivity testing of an unsaturated soils (Gan and Fredlund, 1988; Wheeler and Sivakumar, 1995). Unlike the hanging column method, in axis translation techniques the pore-water pressure is maintained mostly at atmospheric pressure and the pore-air pressure is raised to apply the suction via the axis translation principle. Different types of pressure plates using the axis translation principle are discussed in the following section.

2.4.6. Axis translation techniques

Axis translation is the application of matric suction to a soil by controlling the pore-air pressure, u_a , and the pore-water pressure, u_w , so that the difference between the pore-air pressure and the pore-water pressure equals to the desired matric suction (ASTM D 6836-02). This can be achieved by using a high air-entry ceramic plate or cellulose membrane that separates the air phase from the water phase while maintaining a good continuity between both these phases and the soil-water-air system (Murray & Sivakumar, 2010).

The axis translation technique simply translates the origin of reference for the pore-water pressure from atmospheric value to a positive value equal to the air pressure in the chamber, and accordingly the water pressure in the measuring system does not be highly negative, and then the problem of cavitation is avoided. This technique was first proposed by Hilf (1956) and then applied by many researchers in developing different types of pressure plates for controlling matric suction and establishing the SWCCs. In the present study, this technique has been used to develop a new stress controllable pressure plate device.

There are different types of pressure plate devices having different features, specifications, and arrangements. In all these types, mostly saturated soil specimens are placed in contact with a water saturated ceramic plate placed in a closed chamber. Matric suction is applied by raising incrementally the air pressure in the chamber while maintaining water pressure at the soil plate interface at atmospheric pressure. Pore-water pressure in the soil core will be raised with the same magnitude of the air

pressure increment, and this causes water to flow from the specimen until the equilibrium water content corresponding to the applied suction is reached.

Depending on the type of the pressure plate, the equilibrium water content is then determined either by considering the initial water content of the specimen and measuring the volume/weight of the expelled water, or by measuring the water content gravimetrically by weighing the specimen after removal from the chamber. Several increments of matric suction are applied, and several equilibrium water contents are measured to construct the SWCC (ASTM D 6836-02; Lins et al., 2009; Lins, 2009; Lu and Likos, 2004; Fredlund and Rahardjo, 1993; Fredlund et al., 2011).

In general, the pressure plate technique is suitable to control/measure matric suction corresponding to intermediate water content values. Uncertainties in the continuity of the air phase have arisen near saturated conditions, and some uncertainties in the continuity of the water phase may take place near dry conditions (Bocking and Fredlund, 1980). Bittelli and Flury (2009) also showed that at low water potentials, when matric suction is greater than 200 kPa in case of a silty loam soil, the SWCC determined by using pressure plates has water content values higher than those obtaining by using the dew point meter method at the same water potentials.

Standard pressure plate devices and some non standard ones, which are relevant in some features to the new developed device, will be discussed in detailed in the following subsections.

2.4.6.1. Pressure plate extractor

The pressure plate extractor is one of the standard methods used widely in determining the SWCC, in terms of matric suction, in the range of 0 to 1500 kPa (ASTM D 6836-02). The primary components of the system are a steel pressure chamber and a saturated high air-entry ceramic porous plate as shown in Figure 2.2. The ceramic plate is covered on one side by a neoprene diaphragm sealed to the edges of the plate. An internal screen between the plate the diaphragm provides a passage for the flow of water. This passage is vented to the atmosphere through an

outflow tube located on the top of the plate. Thus, the water pressure in this reservoir is separated from the air pressure in the chamber via the air-water interfaces that arch the saturated pores of the ceramic plate. Ceramic plates are commercially available with air-entry values of 1, 3, 5, and 15 bars.

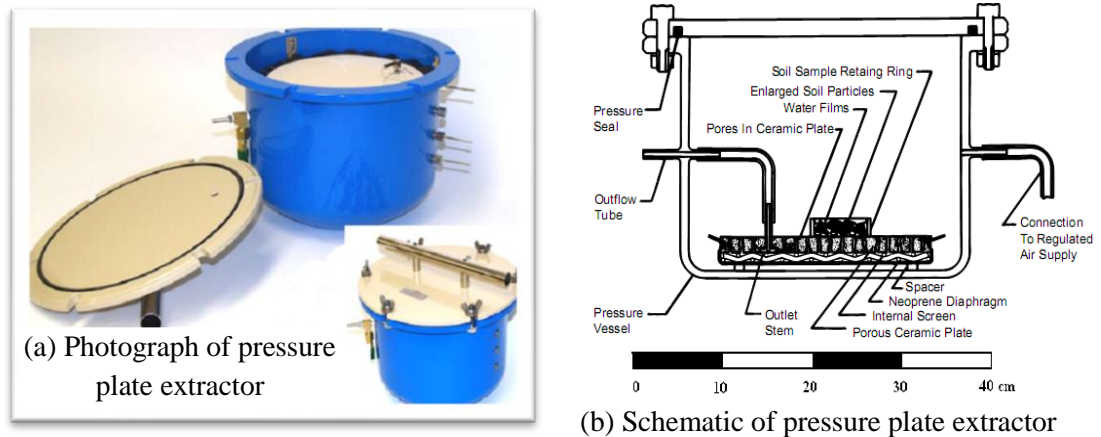


Figure 2.2. Pressure plate extractor, (a) photograph and (b) cross-sectional drawing (Soilmoisture Equipment Corp, 2008).

Soil specimens are prepared inside retaining rings of appropriate dimensions according to the ASTM D 6836-02 and then placed on the top of the saturated ceramic plate. Specimens are initially saturated by inundation while they are in contact with the ceramic plate. As in all types of axis translation pressure plates, air pressure in the chamber is raised to some level to apply the desired suction while pore-water is allowed to flow from the specimen until the equilibrium water content corresponding to the applied suction is reached.

Water content of one or more of the specimens is measured gravimetrically by weighing the specimens after removal from the extractor, and thus generating one point on the soil-water characteristic curve. Several equilibriums are established at successive increments of matric suction to generate additional points on the SWCC using the other specimens. Alternatively, the same specimens may be used throughout the test for different levels of matric suction. In this case, the specimens must be removed quickly from the pressure plate and weighed and then placed back on the ceramic plate as soon as possible (ASTM D 6836-02).

In fact, re-establishing hydraulic contact between the specimen and the ceramic plate may be difficult when the specimen has been desaturated. For this reason, the use of separate specimens for each suction increment is preferable and those specimens should be prepared so that they are as identical as possible.

The weakness point of this type of pressure plate is the accumulation of the diffused air through and below the ceramic plate especially when the test runs for a relatively long time, and this problem greatly affects the continuity of the water phase. On the other hand, this type of pressure plates does not have a flushing system to remove the air bubbles throughout the test.

2.4.6.2. Tempe pressure cells

Tempe pressure cells provide a simple method to determine soil-water characteristic curve over a range of matric suction from 0 to 100 kPa. Figure 2.3 shows a photograph of a standard disassembled cell and a cross sectional view. The cell consists primarily of a top and a base plexiglass cap, a brass cylinder, and a porous ceramic disc. A single soil specimen is prepared inside the brass cylinder and then the specimen is placed on the top of the saturated ceramic disc. After saturating the soil specimen while it is in contact with the ceramic disc, the cell is assembled and the air pressure inside the cell is raised to apply the desired increment of matric suction.

When the equilibrium water content of the soil specimen is reached, the air bubbles below the ceramic disc has to be removed first and then the entire apparatus is weighed to find the amount of water mass lost due to pore-water drainage. The weighing process may then be repeated at successive water content equilibrium points corresponding to successive increments of matric suction and the differences in weight from one soil suction value to another are found. Once the highest desired level of matric suction is attained, the cell is disassembled and the final water content of the specimen is determined gravimetrically. Water content values corresponding to the preceding increments of matric suction may be back-calculated by considering the final water content in conjunction with the incremental differences in the weight. From these pairs of data, the soil characteristic curve can be constructed (Fredlund and Rahardjo, 1993; Lu and Likos, 2004; SoilMoisture Corp., 2008).

The flushing of air bubbles below the ceramic disc is done by using a syringe to inject water through the unventilated drainage tube. Holding the cell upside down and some tilting of the cell with repeated shots of water are usually required to remove the air bubbles, and this may affect the water phase continuity of the specimen with the saturated ceramic disc. Furthermore, by this manner the air bubbles cannot be removed easily, since there is no water circulation, and that is may be one of the weakness points of the Tempe cell.

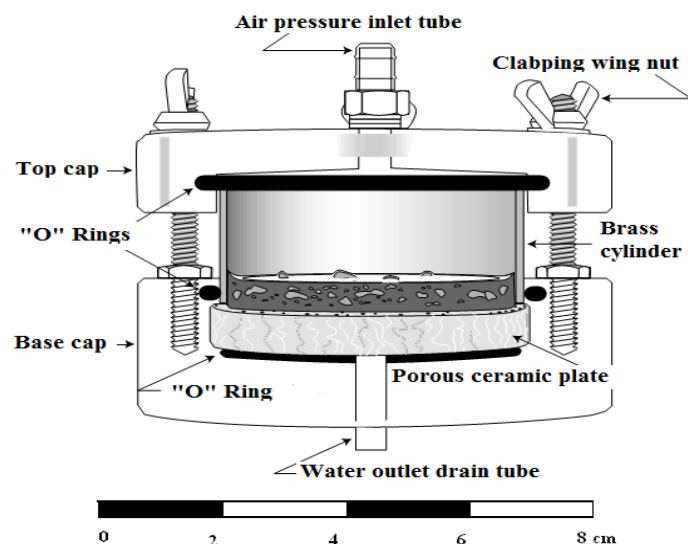
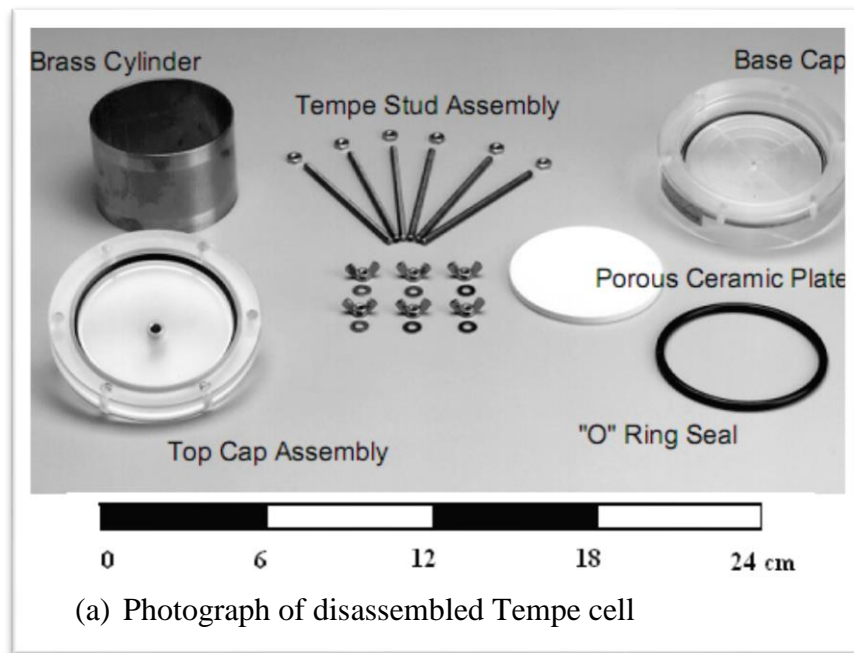


Figure 2.3. Tempe pressure cell, (a) photograph of disassembled cell, (b) cross sectional view of the cell (Soilmoisture Equipment Corp., 2008).

2.4.6.3. Volumetric pressure plate extractor

The volumetric pressure plate extractor can be applied to measure the SWCCs associated with both drying and wetting processes in a range of matric suction from 0 to 200 kPa. For this purpose some hysteresis attachments are connected with the extractor. When the hysteresis attachments are used, the volume of water expelled at each increasing increment in matric suction can be retained and measured. When the applied matric suction values are subsequently reduced, the volume of water returns to the soil specimen can also be measured. Knowing the final water content of the soil specimen corresponding to the last matric suction and the water volume changes between successive matric suctions, water contents corresponding to each value of matric suction can be back calculated and then both the drying and the wetting SWCCs are constructed.

The device consists primarily of a base plate equipped with a 200 kPa air-entry ceramic disc, a cylinder, and a top plate. The base has five machined symmetrical grooves, for inflow/outflow of water, connected to two outlet tubes on opposite sides of the base plate. The design of the grooves in such away provides a good manner for circulating water and removing the diffused air bubbles.

Figure 2.4 shows the setup of the extractor with its hysteresis attachments. The hysteresis attachments consist of a heater block, vapour saturator, air trap, ballast tube, and burette. The heater block is mounted on the top plate to prevent moisture from condensing on the inside walls of the extractor by rising slightly the wall's temperature in comparing to the ambient environment. However, this condensation can be avoided by conducting the test in a temperature-controlled room without the need of this heater. The vapour saturator is used to completely saturate incoming air to the extractor so that there will be no drying effect to the specimen tested and no error is introduced to the water volume measurement. The air trap is attached to collect air that may diffuse through the high air-entry disc. The ballast glass tube serves as a horizontal storage for water flowing in or out of the soil specimen and to maintain the same hydraulic water head during extraction or imbibition processes. The burette is used to store or supply water and to indicate the volume of water removed or added to the soil specimen (Soilmoisture Equipment Corp., 2008; Fredlund and Rahardjo, 2003; ASTM D 6836-02; Ng and Menzies, 2007).

The test procedure is started, as with the other pressure plate methods, by preparing the soil specimen inside a retaining ring, then placing and saturating it above the saturated ceramic disc. Connections are made to the various hysteresis attachments and then water is added through the burette to fill various connecting tubes and the air trap up to the level marks. Air bubbles underneath the ceramic disc should be flushed before starting the test and before taking each reading to the volume of water in the burette, and this is accomplished by running a roller over the connecting tube as shown in Figure 2.4. Running the roller forces the water to circulate from the air trap through the grooves in the base of the extractor to the air trap again, and thus pumping action forces out air bubbles to accumulate in the air trap.

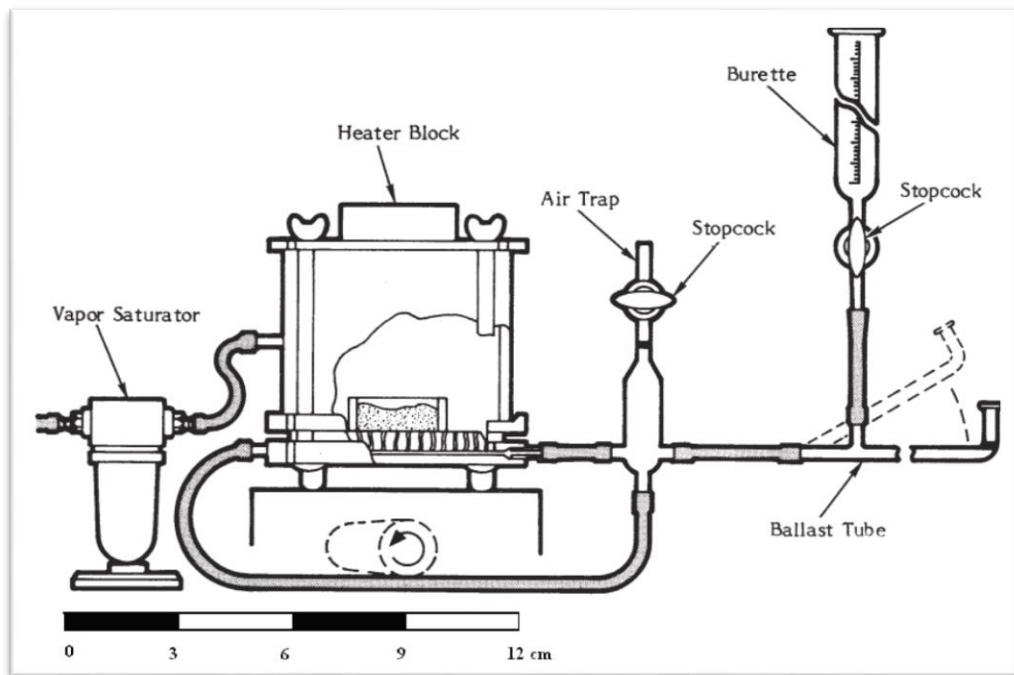


Figure 2.4. Schematic drawing showing the setup of the volumetric pressure plate extractor with hysteresis attachments (Soilmoisture Equipment Corp., 2008).

When the flushing is completed, water is adjusted again to the level mark of the air trap by opening the stopcock at the top of the air trap and applying a small vacuum to the outlet stem of the air trap. Water level in the horizontal ballast tube should be adjusted also up to its level mark, and this is achieved by slightly opening the stopcock at the end of the burette until the water level reaches the mark. However, the level of the horizontal ballast tube must be at the same level with the ceramic disc-soil specimen interface.

On the completion of the above adjustments, the reading of the water volume in the burette is taken, and then the first increment of matric suction is applied and hence the pore-water starts to flow to the ballast tube. At equilibrium when the flow is ceased, the flushing process is repeated and the water levels in the air trap and in the ballast tube have to be adjusted again to the level marks before taking the reading of the accumulated water volume in the burette. These procedures are repeated for successive increments in matric suction to complete the drying SWCC.

Upon completion the drying process, the test can be continued with the wetting process by successive decrements in matric suction, and this causes water to flow back from the ballast tube to the soil specimen. Water required for the backflow is supplied to the ballast tube by opening the burette's stopcock. At the end of the run after the latest equilibrium value has been established, the water content of the whole specimen is determined gravimetrically, and the water content values corresponding to different equilibrium points are back calculated by considering the changes in the burette readings between successive values of matric suction. Therefore, the drying and the wetting SWCCs can be constructed.

The weakness of the volumetric pressure plate technique may be the evaporation of water from the open ends of the burette and the ballast tube especially in long run tests. This evaporation affects significantly the accuracy of water content determination at different equalization points if it is not taken into consideration. The second point is the water circulation from and to the air trap, to remove air bubbles, by rolling on the connecting tube. This process needs the tube to be soft enough, whereas on the other hand, this tube has to be rigid enough and has a constant section so that the system may be considered stable dimensionally. Even though these conflicting requirements are satisfied, the rolling process and the adjustment of water up to level marks is not straight forward and needs many trials to be accurately satisfied.

2.4.6.4. Stress-controllable volumetric pressure plate

Ng and Pang (2000) modified the commercial volumetric pressure plate by adding a loading piston through the top plate. The desired net normal stress may be

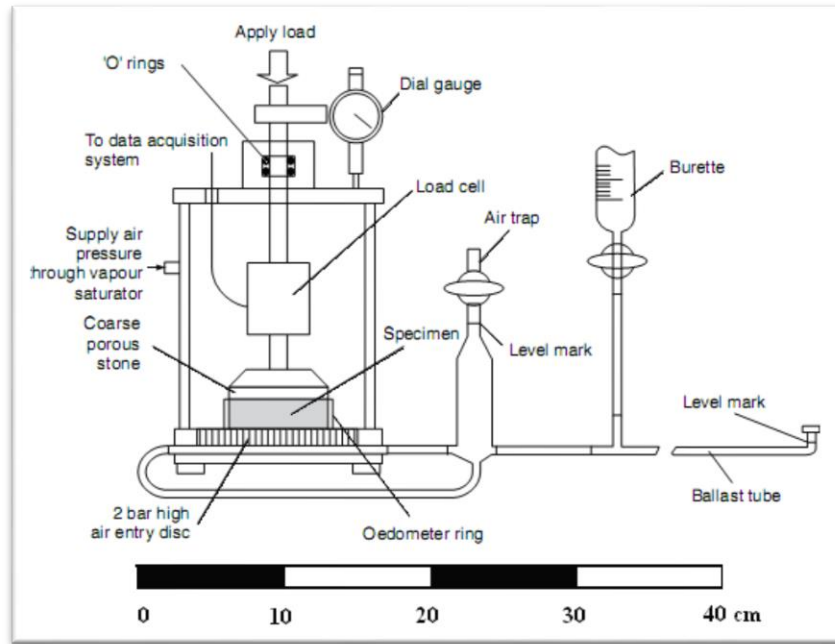
applied to the soil specimen and the stress-dependent soil-water characteristic curves (SD-SWCCs) in both drying and wetting processes can be measured.

Figure 2.5 shows the components and the experimental setup of the modified volumetric pressure plate extractor. Dead weights via the loading piston are used to apply the desired net normal stress to the soil specimen prepared inside an oedometer ring. O-rings are used around the loading piston at the top plate opening to keep the air tightness inside the cell. To eliminate the error of the frictional forces between the piston and the O-rings, a load cell is provided near the end of the piston to measure the actual applied load on the soil specimen.

The test procedure and the calculations are similar to that associated with the use of the commercial volumetric pressure plate that explained in the previous section except the application of the desired net normal stress. The matric suction range that can be applied in this modified cell is the same as for the commercial volumetric pressure plate extractor which is up to 200 kPa. However, the problem of evaporation from the burette and the ballast tube, and the impracticability of air bubbles flushing which are emerged with the use of the traditional pressure plate are still outstanding here in the modified cell.



(a) A photograph of the modified volumetric pressure plate



(b) Schematic drawing of the experimental setup

Figure 2.5. Stress-controllable volumetric pressure plate extractor developed by Ng and Pang (2000), (a) a photograph of different components and the cell assemblage, (b) schematic drawing of the experimental setup.

To extend the range of the applied matric suction, and to ease the flushing of the air bubbles, another modified cell was suggested by Padilla et al. (2005) and commercially produced by GCTS Testing Systems. It was referred to as Fredlund SWCC Device. The cell is made from stainless steel and the matric suction can be applied up to 1500 kPa. Vertical loads up to 10 kN can be applied using a loading frame. Figure 2.6 shows a photograph of the commercially produced device which in fact has slight differences from that modified by Ng and Ping (2000).

In Fredlund SWCC device, water released or absorbed from the specimen is measured using two graduated burettes. By using these burettes, air bubbles can be flushed by applying a slight air pressure on the top end of one burette and force water to flow through the grooves underneath the ceramic disc to the other burette. The flow of water is then alternated from the second burette to the first one, and so on, until all the air bubbles are removed. This method of flushing is easier than that followed in the traditional volumetric pressure plate extractor, but the height of water in the burettes have to be taken into consideration when matric suction has to be calculated.



Figure 2.6. A photograph showing Fredlund SWCC device (GCTS Testing Systems).

2.4.7. Soil-water characteristic curve

The soil-water characteristic curve (SWCC) is a fundamental relationship in unsaturated soil mechanics. The SWCC reflects the engineering behaviour of unsaturated soils such as the hydraulic conductivity, the shear strength, and the volume change. In general terms, the SWCC describes the relationship between soil suction (matric or total) and soil gravimetric water content or volumetric water content or degree of saturation (ASTM D 6836-02).

The SWCC describes the thermodynamic potential of the soil pore-water relative to that of free pure water as a function to the soil water content (Fredlund and Rahardjo, 1993; Lu and Likos, 2004). At relatively low water contents, the pore-water potential is relatively low compared with free pure water and the pore-water here is mainly in the form of thin films on the particle surfaces. This state is referred to as adsorption regime where suction is governed by an adsorption property which is related to the surface area of the soil particles, the surface charge density of the soil mineral, and the type and valency of any adsorbed exchangeable cations (Lu and Likos, 2004).

At relatively high water contents, the potential of pore-water is relatively high and its difference from the potential of free pure water decreases, thus the soil suction is relatively low. Here, the capillary mechanism starts to govern the retention of pore-water which is controlled by the particle and pore structure and pore size distribution. This stage is designated as a capillary regime (McQueen and Miller, 1974). Eventually, when the potential of the pore-water is equal to the potential of free pure water, the soil suction is equal to zero and the degree of saturation approaches unity. A typical SWCC is shown in Figure 2.7. The curve adopts an S-shape when the soil suction is plotted on logarithmic scale.

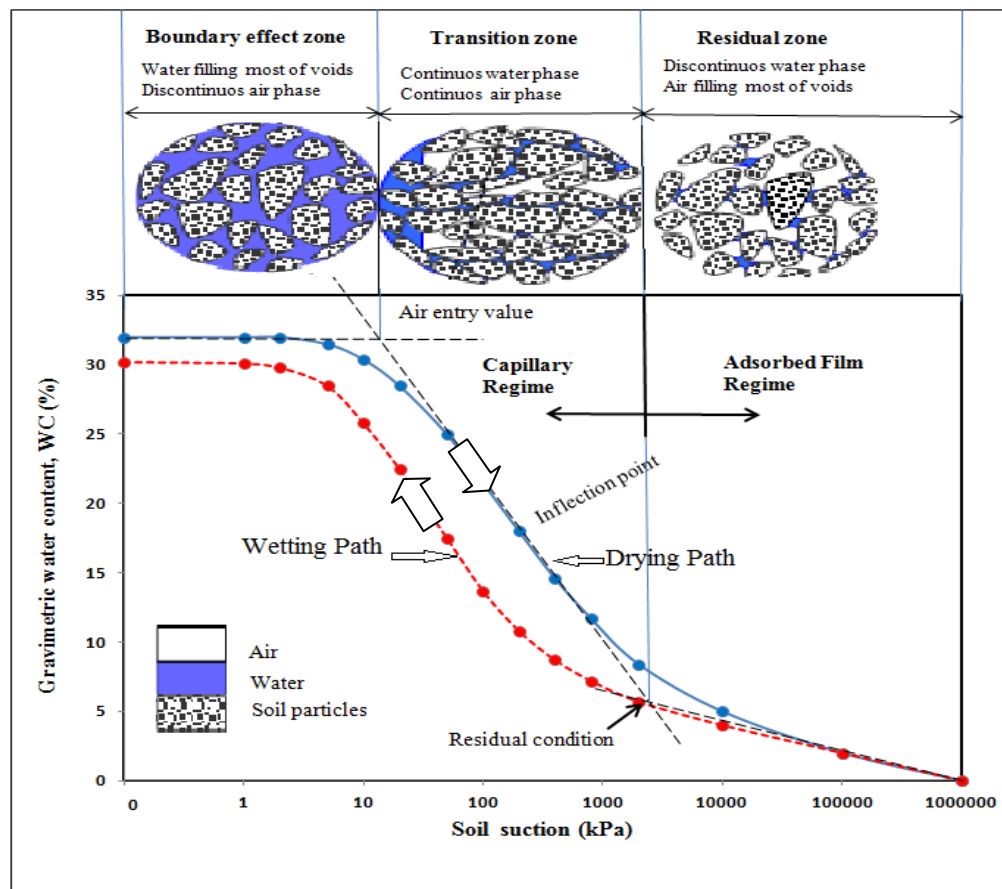


Figure 2.7. Typical soil-water characteristic curve (modified from Perez-Ruiz, 2009).

One parameter of interest on the SWCC is the "air-entry value". This value represents the suction value needed to cause water to be drawn from the largest pore space within the soil system and air starts to occupy these voids (Brooks and Corey, 1964; Fredlund and Rahardjo, 1993; Vanapalli et al., 1999; ASTM D 6836-02; Lins, 2009; Lins et al., 2009; Fredlund et al., 2011). Referring to Figure 2.7, the air-entry value can be defined graphically by extending the constant slope segment, which

passes through the inflection point, of the SWCC to intersect the extending line of the saturation segment (Vanapalli et al., 1999; Fredlund et al., 2011). The corresponding value of suction for the intersection point is taken as the air-entry suction for that soil. In general, the value of air-entry suction depends on the size of the largest pores, and thus the grain-size and grain-size distribution of the particle matrix. The finer the grain-size, the finer the pore-size, and the higher the air-entry suction is.

Based on the S-shape of the SWCC (Figure 2.7), Vanapalli (1994) identified three zones of desaturation: the boundary effect zone, the transition zone, and the residual zone. In the boundary effect zone, soil pores are filled in water with the possibility of some isolated air pockets in existence or the presence of air in a dissolved form in that pore-water. As the applied suction increases, water sustains more tension and starts to release slightly until the air-entry value is reached. The air-entry point indicates the beginning of the so called transition zone.

In the transition zone, the pore-water remains in a continuous phase governed by the capillary mechanism, and the air pockets start to form a continuous air phase. With the increasing of the applied suction, water is drained quicker causing soil to dry rapidly and producing a reduction in the continuity of the water phase. Ultimately, at the end of the transition zone, the increasing in suction causes relatively small decrease in soil water content, and this indicates the beginning of the so called residual zone. At the residual zone, the water phase starts to be discontinuous due to the low soil water content and water removing become more difficult with the increasing of soil suction, however, the air phase is continuous in this phase (Vanapalli et al., 1999).

The point at which the residual zone is started is referred to as the "residual point". This point may be obtained on the intersection of the tangent line to the SWCC at the inflection point and the extended line of the final segment of the curve, which is governed by the highly adsorption mechanism, as shown in Figure 2.7 (Vanapalli et al., 1999). The values of water content and suction corresponding to the residual point are designated as "residual water content" and "residual suction",

respectively. However, when the residual point is not clearly defined, a residual suction of 1500 kPa may be taken as a recommended value (van Genuchten, 1980).

The general shape of the SWCC usually reflects the influence of material properties including pore size distribution, grain-size distribution, density, clay content, mineralogy, and organic material content (Fredlund and Rahardjo, 1993; Vanapalli et al., 1999; Lu and Likos, 2004; Ng and Menzies, 2007; Lins, 2009). For sandy soils, the residual segment of the SWCC is mostly has an asymptotic trend to the suction axis since the amount of water adsorbed under surface hydration mechanism (adsorption mechanism) is very little, and this is due to the relatively very small specific surface and surface charge properties. The capillary mechanism dominates over the majority of the unsaturated water content range of sandy soils.

The mean slope of SWCC at the capillary regime is governed mainly by the pore size distribution of the material. Soils with a relatively narrow pore size distribution have relatively wide water content domain corresponding to narrow range of suction, i.e. steep SWCC slope (Yang et al., 2004). Due to a relatively large pore throats formed between and among sand particles, relatively low air-entry suction is encountered in sandy soils.

In contrast to sandy soils, a greater amount of pore-water is required for surface hydration with the high suction regime in fine-grained soils such as clays. Clay particles mostly have charged surfaces and relatively very high specific surface area. Expansive clayey soils may sustain extremely high suction over a wide range of water content, i.e., the residual part of SWCC is extended over a relatively wide range in water content. As well as, the air-entry suction of clayey soils is much greater than that of sandy soils since it is controlled by relatively very small pores. Silty soils have an intermediate trend between sand and clay trends (Lu and Likos, 2004; Ng and Menzies, 2007).

2.4.8. Hysteresis of soil-water characteristic curve

There is no unique relationship between soil suction and water content for a given soil. Soil undergoing drying process such as evaporation or gravity drainage usually tends to retain a greater amount of water than that under wetting process such

as infiltration or capillary rise for the same magnitude of suction (Maqsoud et al., 2004; Tami et al., 2004). Since the soil-water characteristic curve (SWCC) depends largely on the hydraulic loading path, the differentiation between wetting characteristic curves and drying characteristic curves is normally required to account for the significant hysteresis impact on the flow characteristic, the strength characteristic, and the deformation behaviour of unsaturated soil systems (Fredlund and Rahardjo, 1993; Lu and Likos, 2004; Ng and Pang, 2000).

The relationship between water content and suction is typically presented by the existence of an initial drying (desorption) curve, main drying curve, and main wetting (adsorption) curve as well as an infinite number of scanning curves laying inside the main drying-wetting loop (Pham et al., 2003; Lins et al., 2009; Fredlund et al., 2011) as shown in Figure 2.8. The initial drying curve results from the drying process of an initially saturated soil specimen. The wetting of an initially dry specimen results the main wetting curve. When the specimen is dried again, the resulting curve is the main drying curve. The main hysteresis loop defined by the main drying curve and the main wetting curve, both of these curves are reversible which can occur in numerous cycles while the initial drying curve is irreversible.

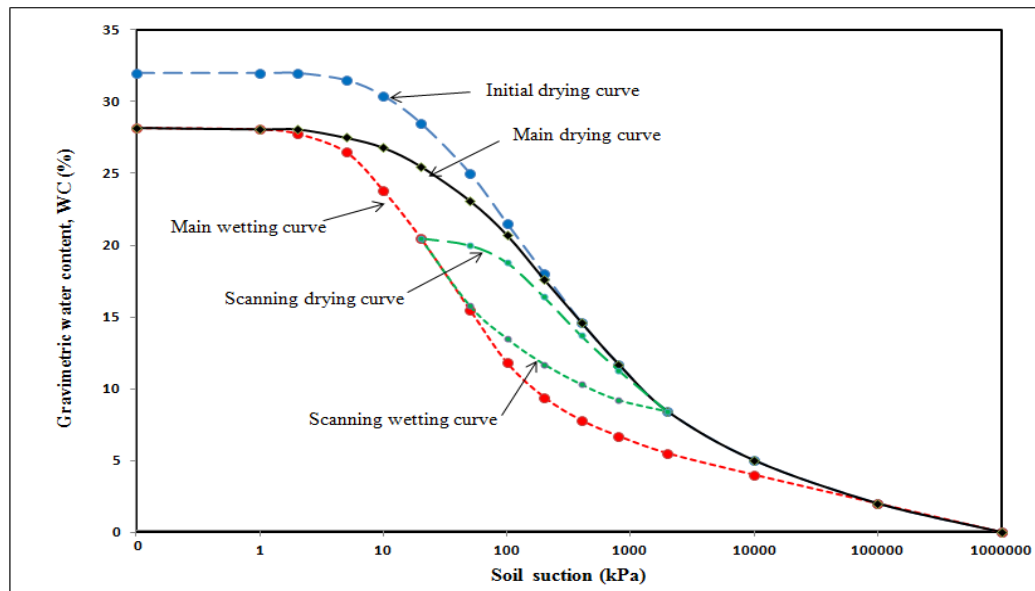


Figure 2.8. Typical presentation of soil-water characteristic curves showing initial drying curve, main drying curve, main wetting curve and scanning curves (modified from Pham et al., 2003).

It can be noticed from Figure 2.8 that the breadth of the hysteresis loop across the entire SWCC is most pronounced in the transition zone when water retention is governed by the capillary mechanism, while it is less pronounced at the residual zone when pore-water retention falls under the adsorption mechanism. Figure 2.8 also shows that full saturation on the wetting path may not be possible due to the entrapment of occluded air bubbles (Yang et al., 2004). Furthermore, there is a probable redistribution of the pore system and the closed pores during the drying and wetting cycle (Lins, 2009).

The phenomenon of hysteresis was first noticed by Haines (1930) and then reported and analysed by many researchers such as Topp and Miller (1966), Topp (1969), Topp (1971a), Poulovassilis (1970), Pavlakis and Barden (1972), Mualem (1984b), Simunek et al. (1999), Ebrahimi-Birang et al. (2007), Lins et al. (2009) Lins (2009), Bonder and Miguel (2011), and Fredlund et al. (2011). Hysteretic behaviour has been attributed to several mechanisms. The most important of these mechanisms are:

- (1) The non-homogenous pore-size distribution often referred to as the ink-bottle effect (Haines 1930; Miller and Miller, 1988). The drainage of water during a drying process is controlled by the small interconnecting pore throats, while the imbibition of water during a wetting process is governed by the comparatively large pore bodies.
- (2) The contact angle hysteresis also referred to as the rain drop effect (Bear, 1972). This angle is visualized as the angle between the tangent of the air-water interface and the tangent of the water-solid interface. This angle is relatively large during the wetting phase and comparatively small during the drying phase.
- (3) Entrapped air, which refers to the formation of occluded air bubbles in dead-end pores during wetting.
- (4) Different alteration of pore fabric during drying and wetting processes for fine grained soils.

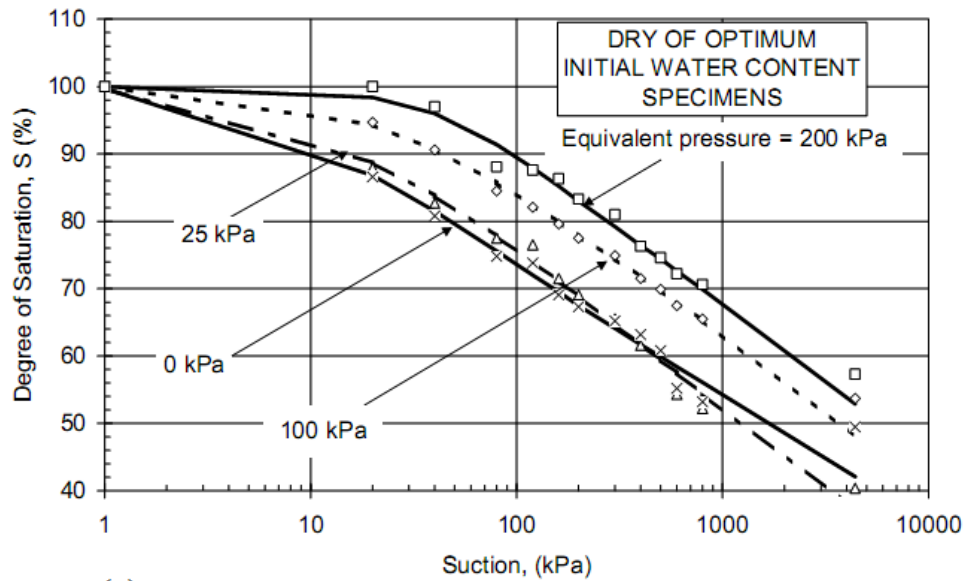
The first and second mechanisms are likely to be the most important for relatively coarse grained soil, such as the sandy soil under consideration in this research.

2.4.9. Influence of stress state on SWCCs

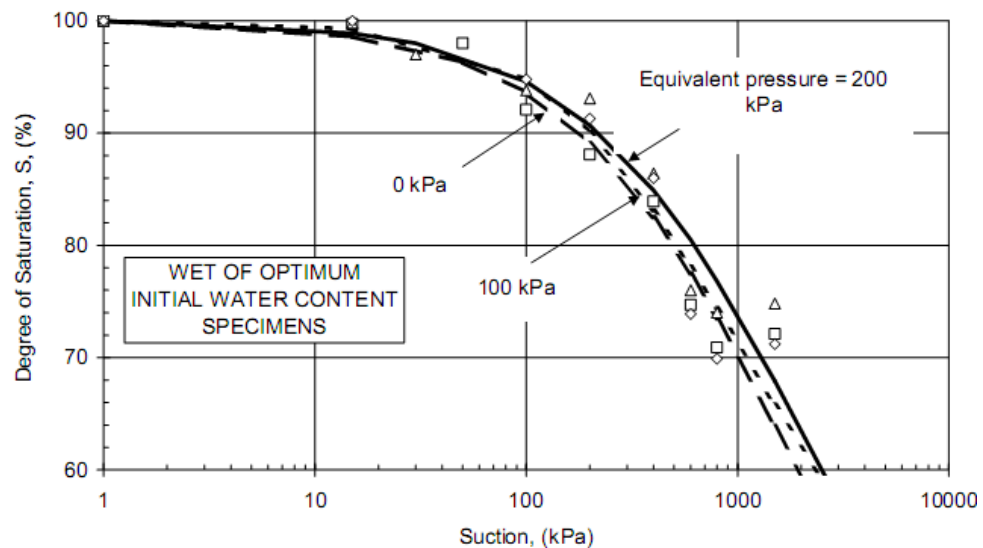
It is theoretically recognized that the stress state can influence the average pore size distribution in the soil specimen and then influence the SWCC (Fredlund and Rahardjo, 1993). Thus, it is so important to simulate the physical state and the stress state conditions of the field when the SWCC has to be determined for a certain soil in the laboratory.

A few experimental studies have been carried out to examine the effect of stress state on the SWCC. Among those, Vanapalli et al. (1998) who studied the influence of the total stress state on the SWCC of a compacted fine-grained soil at three different compaction water contents representing dry of optimum, optimum, and wet of optimum conditions. The concept of equivalent pressure had been used to represent different stress state. The soil specimens were first loaded and then unloaded using a conventional consolidation apparatus to create a known stress history or stress state in the specimens. In other words, specimens were prepared at different initial void ratios to simulate the effects of different normal stress levels which were proposed to be encountered. To estimate the amount of stress equivalent to a prepared void ratio, both the loading and the unloading void ratio versus stress relationships, determined by using conventional oedometer, had been required. Subsequently, the SWCCs of the preloaded specimens were determined using a traditional pressure plate apparatus, in which the change of degree of saturation due to the variation of soil suction was measured under almost zero-applied net normal stress.

Vanapalli et al. (1998) noted that at any particular value of suction, specimens subjected to higher equivalent pressures had higher degrees of saturation, higher air-entry values, and lower desorption rate. In addition, he noted that the effect of stress state on SWCC was more pronounced for specimens compacted with initial water contents dry of optimum while it was not significant for specimens compacted at initial water contents wet of optimum, see Figure 2.9.



(a)



(b)

Figure 2.9. Effect of stress state on soil-water characteristic curves for, (a) specimens compacted dry of optimum water contents, (b) specimens compacted wet of optimum water contents (Vanapalli et al., 1998).

To examine the effect of net normal stress directly by applying the desired pressure, Ng and Pang (2000) modified a stress-controllable volumetric pressure plate extractor. They studied the influence of net normal stress level on the SWCC of an undisturbed completely decomposed volcanic soil (CDV). The results are shown in Figure 2.10 which reveal good agreement to that found by Vanapalli et al., 1998 (Figure 2.9). It was concluded that soil specimens loaded to higher net normal stress exhibit lower initial volumetric water contents. With the increasing of matric suction,

the volumetric water content of all specimens showed decrease but at different rates. The higher the applied net normal stress on the specimen, the lower the rate of reduction in volumetric water content.

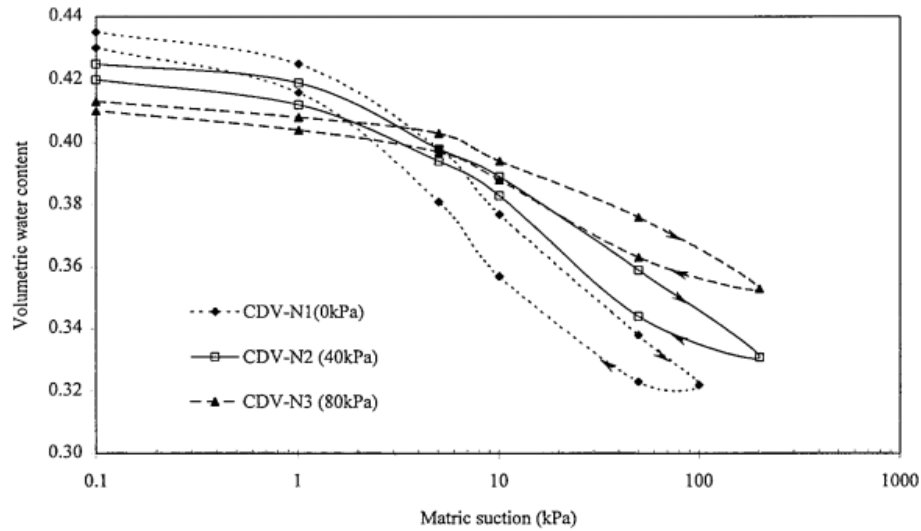


Figure 2.10. Effect of stress state on soil-water characteristic curves (Ng and Ping, 2000).

Ng and Pang (2000) also noticed a consistent trend for all soil specimens to have larger air-entry value when they were subjected to a higher stress. This is probably related to the presence of a smaller average pore sizes distribution in soil specimens under higher load. Furthermore, it was noticed that during the wetting process, the volumetric water content increased more rapidly for specimens subjected to smaller net normal stresses and returned back to a position lower than the original one for all the three tested specimens. The size of the hysteresis loops seemed to be independent of the range of the net normal stresses considered. This hysteresis was attributed mainly to the smaller contact angles at the receding soil-water interface during drying as compared to the advancing soil-water interface during wetting. However, other researchers indicated that higher net normal stress causes the size of the hysteresis loop becomes smaller while the shape of SWCC is not strongly influenced (Zhou, 2008; Sharma, 1998).

Confining stress and deviator stress have also a noticeable effect on the SWCC. Similar to net normal stress, Thu et al. (2007) showed that the air-entry value increased with increasing net confining stress for compacted silt specimens, while the slopes of the drying and the wetting SWCCs do not appear to depend on the net

confining stress. On the other hand, Tse (2007) pointed out that the increasing in stress level causes a reduction in desorption rate, absorption rate, hysteresis loop size and amount of air entrapment. Tse (2007) also reported that under the same net mean stress but at a higher stress ratio, specimens tend to show higher water retention ability and lesser hysteretic responses.

In fact, the increasing of any type of external pressure on a soil specimen causes the void ratio to be smaller. Direct examination of the effect of initial void ratio on SWCC demonstrated that the smaller the initial void ratio (i.e. the denser the soil) leads to higher air-entry value, higher residual degree of saturation, and the hysteresis loops tend to move to higher suctions on the degree of saturation -suction plot (Kawai et al., 2000; Jotisankasa, 2005; Lins et al., 2009).

Alonso et al. (1987) and Sivakumar et al. (2006) showed that unsaturated soil may either swell or collapse upon wetting, as a function of the applied stress. If the confining stress is sufficiently low the soil will swell due to wetting, and if it is high, the soil will collapse. Nevertheless, the soil may experience a reversal volumetric behaviour upon wetting, i.e., initial swelling followed by collapse. Matyas and Radharkrishna (1968) have pointed out that a reduction in interparticle stress and a reduction in the rigidity of the soil mass can be happened upon soil wetting and the decrease in suction associated with.

2.4.10. Influence of compaction water content on soil structure

Soil specimens compacted at water content representing the dry and the wet of the optimum water content will have different soil structure and pore-size distribution (Gens et al., 1995; Vanapalli et al., 1999). Compaction of soil specimens at the dry side of optimum water content produces a flocculated structure with relatively large connected pore spaces. In contrast, the compaction of the specimens at the wet of optimum produces a dispersed structure with mostly small disconnected pore spaces (Cui and Delage, 1996). The boundary between these two conditions (dry and wet of optimum) is the optimum water content (Tarantino and Tombolato, 2005).

2.5. Unsaturated hydraulic conductivity

The unsaturated hydraulic conductivity is one of the primary soil parameters required when performing seepage analysis for unsaturated soil systems, such as the analysis of landslides due to rainfall infiltration, modelling contaminant migration, and the modelling of flow and volume change in collapsing soils, compacted soils, and expansive clays (Paul Simms, 2003; Benson and Gribb, 1997).

2.5.1. Basic definitions

The unsaturated hydraulic conductivity function of soil ($K(\theta)$), also termed as unsaturated water coefficient of permeability, is defined as the relationship between the hydraulic conductivity and the water content or the soil suction (Lu and Likos, 2004; Fredlund et al., 1994; Leong and Rahardjo, 1997). The hydraulic conductivity is defined as the discharge velocity of fluid through a porous medium under influence of a hydraulic gradient equal to unity (Fredlund et al., 1994). The unsaturated hydraulic conductivity depends on soil variables describing the pore structure (e.g., void ratio or porosity), the pore fluid properties (e.g., density and viscosity), and the relative amount of pore fluid in the system (e.g., degree of saturation or gravimetric/volumetric water content), Lu and Likos (2004), Fredlund et al. (1994). The unsteady state flow of water in porous media may be described in terms of hydraulic diffusivity, $D(\theta)$, which is defined as the ratio of the hydraulic conductivity to the specific moisture capacity and it is usually written as a function of volumetric water content as follows (Lu and Likos, 2004):

$$D(\theta) = \frac{K(\theta)}{C(\theta)} \quad 2.12$$

where the specific moisture capacity $C(\theta)$ is the slope of the relation between matric suction head (h_m) and the volumetric water content (θ):

$$C(\theta) = \frac{\Delta\theta}{\Delta h_m} \quad 2.13$$

2.5.2. Overview of measuring methods of unsaturated conductivity

Methods for measuring unsaturated hydraulic conductivity may be categorized to field or laboratory methods and both of these may be classified as steady or

unsteady state with time. These methods differ in accuracy, complicity, cost, and time required to complete the test. However, there are many indirect methods to calculate the unsaturated hydraulic conductivity from other characteristics such as the soil-water characteristic curve, particle-size distribution curve, saturated hydraulic conductivity, and the volume-mass parameters (Brooks and Corey, 1964; Mualem, 1976; van Genuchten, 1980; Fredlund et al., 1994; Leong and Rahardjo, 1997).

Field methods are typically much more expensive than laboratory methods, but field measurements should be more representative of the field condition, and are recommended when the best possible estimate of the unsaturated hydraulic conductivity is needed. The common field methods for measuring unsaturated hydraulic conductivity are the infiltration tests and the instantaneous profile methods which are used for surficial soil applications (Hillel et al., 1972; Hillel and Gardner, 1970), while the cone penetrometer methods can be applied for deeper soil layers (Gribb, 1996; Leonard et al., 1996).

There are a number of laboratory methods available for measuring the hydraulic conductivity of unsaturated soil. Good reviews of these methods have been published by Klute (1972), Dirksen (1991), Stephens (1994), and Benson and Gribb (1997). Among the laboratory methods are the steady state methods that yield more accurate measurements of hydraulic conductivity comparing with the unsteady state methods. In the steady state methods, the flux, gradient, and the water content of the soil are constant with time, while each of these parameters varies with time for unsteady-state or transient techniques (Fredlund and Rahardjo 1993; Klute, 1972; Lu and Likos, 2004; Benson and Gribb 1997; Vanapalli et al., 2007).

The steady-state methods are performed by applying constant boundary conditions to a soil specimen. Assuming the validity of Darcy's law, the hydraulic conductivity corresponding to the applied matric suction is computed after the steady-state conditions are achieved (i.e. the hydraulic gradient, the flow rate, and the water content reach constant values).

Most of the steady state methods are similar to those used to measure saturated hydraulic conductivity. Thus, they can be classified to constant head methods

(constant suction gradient) or constant flow rate methods. In constant flow rate methods, measurements are made for matric suction, while the measurements are made for the flow rate in the constant suction gradient tests. The constant head technique is more common because a variable head results variations in pore-water pressure that produce changes in water content and correspondingly the hydraulic conductivity of the soil specimen.

The steady state methods have few ambiguities and the state of stress (net normal stress and matric suction) can be carefully controlled or varied to reflect the field condition and to simulate the overburden pressure. Besides that, the analysis used to calculate the hydraulic conductivity is simple and directly follows Darcy's law without any assumptions. However, steady state methods are costly, tedious, need long time to be conducted, and require careful attention because low flow rates need to be measured accurately. Thus, alternative laboratory methods may be necessary. The common alternative methods are the unsteady state tests such as the instantaneous profile methods and the transient outflow methods.

Unsteady methods are generally less tedious to conduct and need less time for testing. However, the analysis of unsteady data is often more complicated and has more problems than the analysis of steady methods. In transient methods, water content, matric suction, and the flow rate are variant with time. The calculation of hydraulic conductivity always depends on some analytical solutions of the transient flow governing equation (Richard's equation). Otherwise, Darcy's law may be applied over time steps during which conditions are assumed to be approximately steady.

2.5.3. One-dimensional transient flow governing equation

In unsaturated soils, water is held in pore spaces by adhesive and cohesive forces which are the result of adsorption and surface tension (Fleming, J. B., 2001; Fredlund and Rahardjo, 1993; Lu and Likos, 2004). The potential energy, which represents the stored energy gained from position or internal condition, is the primary important quantum that controls the direction and magnitude of water flow in soils. It is mostly described in terms of total suction or total head as illustrated in Section 2.3.3.

According to the principles of energy conservation, water flows from a point of higher potential to a point of lower potential. In unsaturated soils those potential differences are usually results from wetting or drying processes and then both the water content and the matric potential at any point within the flow system may be a function of time. This flow regime is called transient or time dependent which is different from the steady state flow systems where water flows at a constant rate with respect to time and both matric potential and water content are invariant.

The governing equation for one dimensional transient flow (unsteady flow) in soil can be derived by applying the continuity equation, or what is called the principle of mass conservation, and considering Darcy's equation (Richards, 1931). This can be written as:

$$\frac{\partial}{\partial z} \left[k_z(h_m) \left(\frac{\partial h_m}{\partial z} + 1 \right) \right] = \frac{\partial \theta}{\partial t} \quad 2.14$$

where z is the vertical spatial variable, $k_z(h_m)$ is the unsaturated hydraulic conductivity as a function to matric suction, h_m is the matric suction head, θ is the volumetric water content, and t is the time.

2.5.4. Outflow methods

Outflow methods are unsteady methods using transient laboratory techniques that mostly allow simultaneous determination of the hydraulic conductivity and the soil-water characteristic curve. They need less time as compared to the steady-state methods and provide better control on mass than other unsteady methods. An important advantage of the outflow methods is that they are conducted using conventional axis-translation equipment which are used for determining the soil-water characteristic curve such as hanging column, pressure plate extractors, or Tempe cell systems. These methods consist of monitoring the time-dependent flow rate of pore-water from specimens subjected to an applied increment or series of applied increments in matric suction.

The outflow methods may be classified into four types: the multistep method, the one-step method, the multistep direct method, and the multistep continuous outflow method. The first two methods are conducted using conventional axis-

translation equipment, while the multistep direct method and the multistep continuous method are conducted using axis translation equipment provided with some tensiometers. The tensiometers are used to find the hydraulic gradient profile through the specimen tested, and then the hydraulic conductivity function is calculated directly by assuming the validity of Darcy's law over a small time steps. The multistep method and the one step method were applied in the current study and therefore they are discussed in detail in the flowing sections.

2.5.4.1. The multistep method

The original outflow method is the multistep method which was first developed by Gardner (1956). This method involves subjecting a soil specimen to a series of incremental steps in matric suction and measuring the time-dependent outflow rate and the total outflow volume for each step. In the original method the specimens were placed on a traditional pressure plate extractor during the soil-water characteristic curve determination test. The outflow water was measured by attaching a burette to the outflow port at the bottom of the pressure plate.

To linearize the general form of the governing transient flow equation, Gardner made the following six assumptions:

1. The hydraulic conductivity or the hydraulic diffusivity of the specimen remains constant over the applied suction increment.
2. Suction is linearly related to water content over the suction increment.
3. The high air-entry ceramic disc has no impedance to the pore-water outflow.
4. Flow is one-dimensional.
5. The gravitational head is negligible.
6. The specimen is homogenous and rigid.

Considering these assumption, the governing diffusion equation may be transformed to:

$$D_z \cdot \frac{\partial^2 \psi}{\partial z^2} = \frac{\partial \psi}{\partial t} \quad 2.15$$

where ψ is the soil suction, z is the spatial variable in the direction of the flow which is equal to zero at the bottom of the specimen and equal to L at the top of the

specimen (Binson and Gribb 1997). Applying the top and the bottom boundary conditions, the pore-water pressure equal to the atmospheric at the bottom and the hydraulic head gradient ($\partial h / \partial z$) equal to zero at the top of the specimen, Gardner (1956) solved the above transient diffusion equation by using Fourier series. Neglecting all terms of the series except the first, the following expression for cumulative outflow has been formed:

$$\ln \left(\frac{V_f - V_t}{V_f} \right) = \ln \left(\frac{8}{\pi^2} \right) - \left(\frac{D \cdot \pi^2}{4 L^2} \right) \cdot t \quad 2.16$$

where V_f is the total volume of water accumulated for the applied suction increment and V_t is the outflow volume during elapsed time t . A plot of $\ln (V_f - V_t / V_f)$ versus t has an intercept $\ln (8 / \pi^2)$ and a slope of $- (D \cdot \pi^2 / 4 L^2)$. The hydraulic diffusivity is determined by knowing the slope and then the hydraulic conductivity is calculated by using Equation 2.12. The calculated $K(\theta)$ value is considered to be corresponding to the average water content during the specified matric suction increment, which is taken as $\psi_o + \Delta\psi / 2$. Where ψ_o is the matric suction before the applying of suction increment $\Delta\psi$ (Benson and Gribb, 1997).

The main advantages of the multistep method are (i) the tests yield the unsaturated hydraulic conductivity function as well as the soil-water characteristic curve, (ii) the tests are conducted with less time and less complicated equipment, as compared to the steady-state methods (Benson and Gribb, 1997), and (iii) the mass is accounted carefully than the other unsteady methods.

On the other hand, the primary disadvantages of the multistep method are (i) the plate impedance may be significant especially for soils have high hydraulic conductivity, (ii) the outflow volume rate is often small and difficult to measure accurately, (iii) the air bubbles beneath the ceramic disc and in the outflow line can cause remarkable error, and (iv) the evaporation from the burette causes an under estimation to the outflow volume.

2.5.4.2. The one-step method

This method consists of applying one large step in matric suction and monitors the outflow rate for a broad range in water content. Gardner (1962) has shown that

for certain boundary conditions, diffusivity can be calculated from instantaneous outflow rate, water content, and the geometry of the tested soil specimen.

Contributions to the development of the one-step outflow method have included those of Doering (1965), Gupta et al. (1974), Passioura (1976), Valiatzas et al. (1988), and others. The experimental procedures used by the above researchers were approximately the same but the methods used to analyse the outflow data were different depending on the assumptions used to solve the general diffusion equation and the initial and boundary conditions which had been considered.

The time required to complete a one-step outflow test is much less than that required when conducting the multistep outflow method. However, the one-step method does not yield the soil-water characteristic curve simultaneously. Therefore, to establish the unsaturated hydraulic conductivity function, the SWCC has to be determined independently. Moreover, when the applied step in matric suction is too large, the initial hydraulic gradient is large and varies dramatically throughout the test and consequently the state of stress will change significantly during the test which can cause notable error in results especially in compressible soils.

Among the common approaches for analysis the one-step outflow data is the solution of Doering (1965) which is distinguished by its simplicity and that was led to its widespread popularity. Doering uses Gardner's solution, Equation 2.16, without the need of assuming a constant diffusivity throughout the whole matric suction step and then the solution reduces to:

$$D(\theta) = - \frac{4L^2}{\pi^2(\theta_t - \theta_f)} \cdot \frac{d\theta}{dt} \quad 2.17$$

where $D(\theta)$ is the hydraulic diffusivity as a function of water content, θ_t is the volumetric water content at time t , θ_f is the volumetric water content at equilibrium, and L is the thickness of the specimen. The derivative $(d\theta/dt)$ is approximated by considering a series of time steps and computed as $(\Delta\theta/\Delta t)$ for each step, then the diffusivity is computed according to the average water content of each step.

The implicit assumptions of Doering's method are that the impedance of the high air-entry ceramic disc is neglected and the diffusivity is constant throughout the whole specimen thickness at any given time.

As a comparison between the unsaturated hydraulic conductivity measured with the one-step and the other methods, Stephens (1989) found a good agreement between Doering's one-step method and the field instantaneous profile method when he conducted a series of tests on fluvial sand. As well as, Doering (1965) reported that the results obtained from the one-step method is nearly similar to those obtained from the multi-step method and the constant flux steady-state method when he conducted tests on five soils ranging from clay to silty sand.

2.5.5. Ceramic disc impedance

One of the key differences of the saturated hydraulic conductivity tests and the unsaturated hydraulic conductivity tests is the high air-entry ceramic disc which is used when testing unsaturated soils. Not only in hydraulic conductivity tests but in most tests related to unsaturated soils, the ceramic discs play the main role in conducting the tests precisely. Ceramic discs are much less permeable than porous stones used in saturated hydraulic conductivity testing, and this impedance can be important and should be taken into consideration especially when a relatively high permeable soil has to be tested.

Benson and Gribb (1997) recommended that the head loss through the ceramic disc should be accounted for if the saturated hydraulic conductivity of the ceramic disc is less than an order of magnitude higher than the hydraulic conductivity of the soil at water content at which it is tested.

The flow of water in the transient outflow methods may be categorized into three stages (Green et al., 1998). The first stage starts with the beginning of the test where the saturated permeability of the ceramic disc controls the flow, so that the cumulative outflow volume is linearly proportional to the time. The second stage starts when the water content of the bottom layer, which is in contact with the ceramic disc, reaches to equalization according to the applied matric suction after a short time from the start of the test. At this stage, the flow rate decreases as the soil

permeability starts to control the flow and the ceramic disc impedance becomes negligible as the test progresses. During the second stage, the core soil specimen behaves as a semi-infinite column, and the accumulated outflow volume is a linear function of the second root of elapsed time (\sqrt{t}). When this linear relation ceases, stage three of the outflow starts and the boundary condition at the top end of the soil specimen begins to influence the flow. At this stage, the water content over most of the soil column may be assumed uniform.

The main conclusion which can be drawn from Green et al. (1998)'s classification is that the ceramic disc impedance has to be taken into consideration when analysing the outflow data. Especially when the multistep outflow method (Gardner, 1956) and the one-step outflow method (Doering, 1965) are followed in the analysis. That is because both these methods were derived by including the first and the second stages of the transient flow.

To avoid the influence of ceramic disc impedance, Klute and Dirksen (1986) suggested the direct measurement of the hydraulic gradient within the specimen by using two tensiometers provided that the pore-water pressure is greater than minus 80 kPa. However, the head loss through the ceramic disc can be calculated directly by applying Darcy's law as follows:

$$\Delta H_c = \frac{Q}{A} \times \frac{L_c}{K_c} \quad 2.18$$

where ΔH_c is the head loss through the ceramic disc, Q is the flow rate through the system, L_c is thickness of the ceramic disc, K_c is saturated coefficient of permeability of the ceramic disc, A is the cross sectional area of the ceramic disc.

2.6. Shear strength and failure criteria

Measuring, modelling, and predicting the shear strength of soil represent the corner stone in analysing numerous engineering problems such as bearing capacity, slope stability, lateral earth pressure, pavement design, and foundation design. The shear strength of soil, whether saturated or unsaturated, may be defined as the maximum shear stress the soil is capable of sustaining along the failure plane under a given external and/or internal stress state. There are three main approaches to

evaluate the stress state in unsaturated soil; the single stress-state variable approach proposed by Bishop (1959), the two stress-state variable approach proposed by Fredlund and Morgenstern (1977), and the true effective stress concept introduced by Lu and Likos (2006). Referring to these approaches, different failure criteria and different models have been formulated to describe the shear strength behaviour of unsaturated soil (Bishop, 1960; Graecen, 1960; Fredlund et al., 1978; Lamborn, 1986; Peterson 1988; Peterson, 1990; Fredlund et al., 1996; Vanapalli et al., 1996; Rassam and Williams, 1999; Sun et al., 2000; Rassam and Freeman, 2002; Toll and Ong 2003; Khalili et al., 2004; Tarantino 2007; Sheng et al., 2008). The shear strength criteria relevant to the current study are reviewed in this section.

In saturated soil, shear strength is commonly described using Mohr-Coulomb failure criterion as follows:

$$\tau_f = c' + (\sigma - u_w)_f \tan \phi' \quad 2.19$$

where τ_f is the shear stress on the failure plane at failure, c' is the effective cohesion, $(\sigma - u_w)_f$ is the effective normal stress on the failure plane at failure, and ϕ' is the effective angle of internal friction.

In unsaturated soil, however, there is an internal stress acting locally on soil grains that results specifically from partial saturation of the soil and it is independent of external loading or overburden pressure. This stress originates from the combined effects of negative pore-water pressure and surface tension (Lu and Likos, 2006). The effect of this additional internal loading on the shear strength may be captured by incorporating the matric suction into the Mohr-Coulomb failure criterion in one of the following approaches.

2.6.1. The extended Mohr-Coulomb criterion

Considering the two stress-state variable approach, which was explained in Section 2.3.2.2, Fredlund et al. (1978) formulated an extended M-C criterion to describe the shear strength behaviour of unsaturated soil by introducing an additional parameter, ϕ^b , to capture the increase in shear strength with increasing matric

suction. The resulting failure envelope is a plane in the space of net normal stress, matric suction, and shear stress and may be written as:

$$\tau_f = c' + (\sigma - u_a)_f \tan \phi' + (u_a - u_w)_f \tan \phi^b \quad 2.20$$

where τ_f is the shear stress on the failure plane at failure, c' is the effective cohesion, $(\sigma - u_a)_f$ is the net normal stress on the failure plane at failure, ϕ' is the angle of internal friction related to the net normal stress, $(u_a - u_w)_f$ is the matric suction at failure, and ϕ^b is an internal friction angle related to matric suction which shows the rate of increase in shear strength relative to matric suction. This friction angle, ϕ^b , was originally assumed to be constant and this leads to describe a planer surface envelope in a three dimensional space. It was later demonstrated from increased experimental evidence that ϕ^b is a highly nonlinear function with respect to matric suction and the failure envelope becomes a curved surface (Escario and Saez, 1986; Fredlund et al., 1987; Gan et al., 1988; Drumright, 1989; Escario et al., 1989; Vanapalli et al., 1996).

There is a clear relationship between the nonlinear nature of the shear strength envelope with respect to the increasing of matric suction and the soil-water characteristic curve. Within the capillary saturated zone of the SWCC and prior to the air-entry suction, the soil pores remain essentially saturated, the shear strength envelope is approximately linear, and ϕ^b is effectively equal to the angle of internal friction ϕ' . Beyond the air-entry suction within the transition zone, a clear nonlinearity in ϕ^b starts and increases towards the residual regime. As drainage of pore-water continues, changes in the geometries of interparticle pore-water menisci take place. These changes reduce the resultant interparticle forces that contribute to the effective stress on the soil skeleton and ultimately contribute to the shear strength (Fredlund and Rahardjo, 1993; Fredlund et al., 1987). In other words, the reduction in the volume of pore-water within this zone effectively reduces the contribution of matric suction in increasing the shear strength. Referring to the strong correspondence of this nonlinearity with the SWCC, Fredlund et al. (1987) suggest that the problem may be handled by dividing the failure envelope into several linear segments with varying ϕ^b angles by imitating the approximated linear segments of the SWCC.

It can be concluded that it is more logical to conceptualize the reduction in the rate of contribution of matric suction to the shear strength as a result to the reduction in the mobilization of matric suction to the effective interparticle stress, rather than a reduction in friction coefficient which is represented by $\tan \phi^b$. Physically, it may be inconsistent to visualize the friction angle as a variable related to the soil water content. On the other hand, it is more logical to have one friction angle with respect to different kinds of stress whether it is an internal or external.

2.6.2. Single stress state Mohr-Coulomb criterion

The single stress state variable approach proposed by Bishop (1959) may be useful to highlight the influence of degree of saturation on the contribution of matric suction to the shear strength. In this approach, Terzaghi's effective stress was extended to join both two independent state variables, net normal stress and matric suction, by introducing one material variable referred to as "effective stress parameter χ ". Using his extended effective stress concept and applying the conventional Mohr-Coulomb criterion, Bishop (1960) suggested the following failure envelope equation:

$$\tau_f = c' + [(\sigma - u_a)_f + \chi_f(u_a - u_w)_f] \tan \phi' \quad 2.21$$

where τ_f is shear strength and c' and ϕ' are the effective cohesion and effective friction angle, respectively. The effective stress parameter χ is a function to the degree of saturation or matric suction. This parameter reflects the contribution of matric suction to the effective stress. The parameter χ equals to 1.0 when the condition is saturated and zero when dry. This parameter can be evaluated directly from typical direct shear tests (Lu and Likos, 2004). When the net normal stress is controlled, matric suction is measured or controlled, effective cohesion and friction angle are predetermined from saturated tests, the unsaturated shear strength is measured, the effective stress parameter can be calculated by rearranging Equation 2.21 as follows:

$$\chi = \frac{\tau_f - c' - (\sigma - u_a)_f \tan \phi'}{(u_a - u_w)_f \tan \phi'} \quad 2.22$$

Based on best fit to experimental results, many mathematical representations of χ have been proposed. Bishop (1959) proposed a nonlinear form of χ as a function to degree of saturation:

$$\chi = S^k = \left(\frac{\theta}{\theta_s}\right)^k \quad 2.23$$

where S is the degree of saturation, θ is the volumetric water content, θ_s is the saturated volumetric water content, and k is a fitting parameter.

Later on, Khalili and Khabbaz (1998) formalized χ as a function to the normalized matric suction:

$$\chi = \begin{cases} \left[\frac{(u_a - u_w)}{(u_a - u_w)_a}\right]^{-0.55} & \text{for } (u_a - u_w) > (u_a - u_w)_a \\ 1 & \text{for } (u_a - u_w) < (u_a - u_w)_a \end{cases} \quad 2.24$$

where $(u_a - u_w)_a$ is the air-entry suction for drying process and it is the air-expulsion suction for wetting process.

Vanapalli et al. (1996) proposed another form to predict χ and its validity was examined later (Vanapalli and Fredlund, 2000) and showed good fit with the experimental shear strength results of Escario et al. (1989). This form can be written as:

$$\chi = \frac{S - S_r}{1 - S_r} = \frac{\theta - \theta_r}{\theta_s - \theta_r} \quad 2.25$$

where S_r is the residual degree of saturation, and θ_r is the residual volumetric water content.

Comparing the extended Mohr-Coulomb criterion (Equation 2.20) with Bishop's effective stress concept (Equation 2.21), it can be noticed that both these approaches are physically different but mathematically the same. Subtraction one equation from another lead to:

$$\chi = \frac{\tan \phi^b}{\tan \phi'} \quad 2.26$$

Accordingly, the extended Mohr-Coulomb criterion may be written in terms of χ and the saturated angle of friction. Until now, the effectiveness, validity, and practicality of the preceding two different approaches for describing the shear strength of unsaturated soil remain a matter of debate in literature.

2.6.3. True effective stress failure criterion

To avoid the uncertainties and ambiguities in the theoretical formulation and experimental determination of ϕ^b and χ , Lu and Likos (2004) suggested the use of suction stress concept without considering independently the variables that define it (the matric suction and χ). Mohr-Coulomb criterion incorporating Bishops effective stress can be re-written as:

$$\tau_f = c' + (\sigma - u_a)_f \tan \phi' + \chi_f(u_a - u_w)_f \tan \phi' \quad 2.27$$

$$\tau_f = c' + (\sigma - u_a)_f \tan \phi' - \sigma'_s \tan \phi' \quad 2.28$$

$$\sigma'_s = -\chi_f(u_a - u_w)_f \quad 2.29$$

where σ'_s is the suction stress which is physically resulting from local interparticle forces. These forces are the resultant of three components which are: the increase in physicochemical forces due to desaturation in reference to the saturated condition; attractive forces arising from surface tension at air–water interfaces; and attractive forces arising from typically negative pore-water pressure. In saturated soils the effects of physicochemical forces, which indeed exist, have conventionally been captured by the saturated effective cohesion term, c' , in Mohr-Coulomb criterion.

The representation of Equation 2.28 in three dimensional space of shear stress, net normal stress, and suction stress shows that the failure surface remains planner regardless to the desaturation process. This feature makes it possible to represent the complete failure surface in the net normal stress-shear stress plane by plotting constant matric suction lines, leading to a series of parallel lines with different values of matric suction.

Hence, experimentally, if a series of conventional direct shear tests is carried out for specimens prepared at different water contents, a series of parallel failure envelopes corresponding to different water contents can be constructed by drawing lines parallel to the saturated failure envelope and passing through the state of stress at failure for each test (Lu and Likos, 2004). Therefore, the suction stress as a function to water content can be determined. In other words, suction stress for a specimen at given water content can be back calculated using Equation 2. 28. Thus, the suction stress characteristic curve (SSCC) can be found by conducting shear strength tests for water-controlled specimens rather than suction-controlled specimens. Using this approach, it can be circumvented about the necessity to determine the matric suction or the effective stress parameter χ since the most relevance variable is neither matric suction nor χ but the product of the two which is identified as suction stress.

Furthermore, Lu and Likos (2006) introduced the use of "true effective stress" concept to represent the failure envelope. True effective stress includes three components which are: intergranular bonding stress that provides cohesion in saturated soil, net normal stress, and suction stress. The representation of failure envelope for saturated or unsaturated soil in the true effective stress-shear stress plane results a unique line passing through the origin regardless the degree of saturation. Applying the classical Mohr-Coulomb failure criterion in conjunction with true effective stress concept results:

$$\tau_f = \sigma'' \tan \phi' \quad 2. 30$$

$$\sigma'' = (\sigma - u_a) - \sigma'_s + \sigma_{co} \quad 2. 31$$

$$\sigma_{co} = c' / \tan \phi' \quad 2. 32$$

where τ_f is the shear stress on failure plane at failure, σ'' is the true effective stress, $(\sigma - u_a)$ is the net normal stress, σ'_s is the suction stress, σ_{co} is the tensile strength of soil at saturation, c' and ϕ' are the saturated cohesion and friction angle, respectively.

2.6.4. Shear strength prediction using constitutive models

Different formulations have been proposed in recent years to predict the unsaturated shear strength based on some parameters that obtained from common tests. The majority of those methods use the soil-water characteristic curve and the saturated shear strength parameters to evaluate the unsaturated shear strength. As described in Section 2.6.2, most of these formulations are for evaluating the parameter χ in Bishop's failure envelope equation.

Rassam and Williams (1999) used a three-dimensional, nonlinear regression analysis and proposed a power-additive function to describe the shear strength of unsaturated soils. The proposed function incorporates the effect of normal stress on the contribution of matric suction to the shear strength as shown below:

$$\tau_f = c' + \sigma \tan \phi' + \left[\psi \tan \phi' - (\psi - \psi_a)^\beta (\gamma + \lambda \sigma) \right] \quad 2.33$$

where τ_f is the shear strength, σ is the net normal stress, c' and ϕ' are the saturated shear strength parameters, ψ is the matric suction, ψ_a is the air-entry suction, and β , γ , λ are fitting parameters. It may be noticed from Equation 2.33 that the fourth term represents the decrease in the contribution of matric suction to the shear strength due to the desaturation, which is coupled to the net normal stress. It is of interest here to notice that Equation 2.33 expresses the effect of increasing net normal stress on decreasing the contribution of matric suction to the shear strength of soil.

Later on, Rassam and Cook (2002) considered constant values of net normal stress in two-dimensional plane of shear strength versus matric suction and rearranged Equation 2.33 as follows:

$$\tau_s = \tau - (c' + \sigma \tan \phi') = \psi \tan \phi' - \alpha (\psi - \psi_a)^\beta \quad 2.34$$

where τ_s is the contribution of matric suction to the shear strength, τ is the total shear strength, $(c' + \sigma \tan \phi')$ is the saturated shear strength, and α replaces the expression $(\gamma + \lambda \sigma)$ for Equation 2.33. Since the net normal stress is considered a constant, then it is important to notice that the fitting parameters α and β in Equation 2.34 will be relevant to the net normal stress under which the unsaturated shear strength is evaluated.

To quantify the fitting parameters α and β , Rassam and Cook (2002) considered two boundary conditions. The first is $\phi^b = 0$ at residual suction, and the second is the contribution of matric suction to the shear strength at residual suction is equal to τ_{sr} , which should be experimentally evaluated. Solving Equation 2.34 by considering these boundary conditions results:

$$\beta = \frac{\tan\phi'(\psi_r - \psi_a)}{\psi_r \tan\phi' - \tau_{sr}} \quad 2.35$$

$$\alpha = \frac{\psi_r \tan\phi' - \tau_{sr}}{(\psi_r - \psi_a)^\beta} \quad 2.36$$

The values of residual suction ψ_r and air-entry suction ψ_a are evaluated from a predetermined soil-water characteristic curve. Rassam and Cook (2002) recommended that the SWCC has to be carried out on specimen which is pre-consolidated under the same value of net normal stress used to evaluate the unsaturated shear strength. Also the saturated angle of internal friction has to be known, and then the only unsaturated test which is needed to be carried out is the shear strength at residual suction in order to find τ_{sr} .

CHAPTER THREE

MATERIALS, EQUIPMENT AND METHODOLOGY

3.1. Introduction

To evaluate the influence of gypsum content on the engineering properties of a sandy soil, which has been taken from Al-Fallujah district / Iraq, an extensive laboratory programme was designed. Synthetic soil mixtures from the sandy soil with different gypsum additives were considered. The classification properties of the sandy soil and hydrated gypsum are presented in this chapter. The preparation of sand-gypsum mixtures and their resulting index properties are presented. These properties include the particle density, grain-size distribution, and the consistency limits.

The experimental programme contains both hydraulic and mechanical tests. These tests are, compaction tests, consolidation tests, soil-water characteristic curve tests, soil shrinkage characteristic tests, stress-dependent soil-water characteristic curve (SD-SWCC) tests, stress dependent-hydraulic conductivity function (SD-HCF) tests, and shear strength tests on both saturated and unsaturated soil specimens. These tests were carried out in an environment controlled room, since most of unsaturated soil characteristics are clearly sensitive to the temperature and humidity variations. The room temperature was controlled at 20-22°C and the humidity at 40-50%.

The details of the devices used, the preparation of the specimens, test procedures and calculations, and the testing programme for each test series are presented in this chapter. The calibrations and adjustment of the direct shear device used for testing stiff unsaturated soil specimens are presented. The details of the modified device

used for establishing the SD-SWCCs and the SD-HCFs, the related testing procedures, and the experimental programme are presented in detail in Chapter 4.

3.2. Materials and samples preparation

To study the effect of gypsum content on the hydro-mechanical properties of gypsiferous sandy soils, a sandy soil from Al-Fallujah district / Al-Anbar province / Iraq was taken. Synthetic soil samples were prepared from the sandy soil with different additives of hydrated gypsum since it could not be possible to find natural soil samples having the same host soil with different gypsum contents. Furthermore, natural gypsiferous soil depositions predominantly contain some other soluble salts beside gypsum which may alter the effect of gypsum on soil behaviour. Eight synthetic soil samples were considered by adding eight different percentages of gypsum to the sandy soil. These percentages are 0%, 10%, 20%, 30%, 40%, 50%, 65%, and 80% by dry weight.

As in the most regions, soils at the district of Al-Fallujah have inherently spatial variability in both horizontal and vertical directions, in addition to time variability of the solutes distribution within soil profile during precipitation or evaporation. Thus, the soils vary from coarse-grained soil to fine-grained soil, but in general the predominant soil might be silty sands (SM) to sandy clay (CL). To obtain a reprehensive soil sample with low cost, the composite sampling method (Mason, 1992) was adopted. Thus, relatively homogenized sample made up of a number of increments or subsamples was collected. The subsamples were taken by considering the concept of random or probabilistic selection. In this concept, each subsample point within the area had an equal probability of being selected, and every particle within the subsample had an equal chance of being selected. To increase the homogeneity and reduce the variability in each subsample, stratified sampling manner was used. Each subsample was taken from a single stratum, where the stratum is expected to be uniform in character.

At the laboratory, the shipped soil sample was mixed thoroughly to reduce the variance of distribution and segregation which might be occurred during shipping. To control the segregation and grouping error occur during implementation of the

experimental programme, the shipped sample was divided to many parts (nearly 1kg weight each) and each part was stored in a small plastic container. For each individual test, the sand-gypsum mixture required to prepare the test specimen was mixed separately by mixing predefined weights of the sandy soil and the hydrated gypsum in small can. A special care was given to this process to ensure a good distribution of gypsum particles through the mixture with minimum segregation effects.

Gypsum, dihydrate calcium sulphate $\text{CaSO}_4 \cdot 2\text{H}_2\text{O}$, was prepared by using gypsum plaster or as widely known as plaster of Paris, $\text{CaSO}_4 \cdot \frac{1}{2}\text{H}_2\text{O}$. Plaster particles were completely dispersed in water to produce uniform, homogenous slurry. A soaking period of five minutes enabled gypsum particles to be completely wetted. Further mixing of plaster slurry was continued throughout the setting stage until the casting strength was completely lost. Additional water was added to the slurry to avoid any possible bonds and to ensure a complete hydration to gypsum particles. The mixture was then air dried for three days before being used to prepare the required mixtures.

3.3. Soil classification parameters

The index properties of the soil used, gypsum, and the soil-gypsum mixtures were determined following the British Standard (BS 1377-2, 1990). These tests include determination of the particle density, the particle size distribution including wet sieving and hydrometer tests, the liquid limit, and the plastic limit. The shrinkage limit tests were carried out by using the wax method (ASTM D 4943-08). The properties of the sandy soil, gypsum, and seven sand-gypsum mixtures are presented in Table 3.1.

The particle density tests were carried out by using the small pycnometer method which is the preferable method for soils consisting of clay, silt and sand-sized particles. For the sandy soil the specimens were oven dried at 105 °C before the test as stated in BS Standard, while gypsum specimens were oven dried at 45 °C to avoid any change in particle density due to loss of water of hydration. Instead of

distilled water, white spirit was used in the determination of gypsum particle density to avoid the dissolution of gypsum particles (BS 1377-2, 1990).

Table 3.1. Index properties of the prepared samples.

Properties	Values							
	Gypsum content (%)							
	0	10	20	30	40	50	65	80
Particle density (Mg/m^3)	2.65	2.62	2.59	2.56	2.52	2.49	2.44	2.39
D60 (mm)	0.092	0.087	0.082	0.076	0.070	0.056	0.040	0.027
D30 (mm)	0.050	0.036	0.021	0.018	0.015	0.015	0.016	0.015
D10 (mm)	0.000	0.001	0.001	0.002	0.003	0.008	0.013	0.013
Coefficient of uniformity, Cu	114	87	70	30	18	7	3	2
Coefficient of curvature, Cc	33.5	14.9	4.7	1.7	0.8	0.5	0.5	0.6
Liquid Limit (%)	22.4	21.7	20.9	20.6	23.5	29.0	30.2	37.1
Plastic Limit (%)	16.5	15.5	14.8	14.5	16.0	20.0	21.0	27.1
Shrinkage Limit (%)	13.0	11.5	10.7	10.5	12.5	16.0	17.6	22.5

As an alternative method for determining gypsum particle density, saturated water with gypsum salt was suggested, in this study, to be used instead of white spirit. When the water is pre-saturated with gypsum salt, it will be unable to dissolve gypsum any more during the particle density test. Following this method, gypsum particle density were determined and then compared to that found by using white spirit. Very good agreement was found with a difference not exceeding 0.005 Mg/m^3 .

The particle density was found to be 2.65 Mg/m^3 for the sandy soil and 2.33 Mg/m^3 for gypsum. Based on these densities, the mean particle density for samples having different gypsum contents was calculated.

Combined wet sieving and hydrometer tests were carried out on both the sandy soil and the hydrated gypsum. To account for any heterogeneity in the sandy soil and reduce the distribution and segregation error that may be induced by gravity during storage or handling, the sieve and hydrometer analysis were carried out twice during the experimental programme and the average grain-size distribution curve was taken. The hydrometer test on gypsum was repeated four times at different soaking period in water with the presence of the dispersant agent in order to examine if there is any change in particle size due to gypsum dissolution. Soaking periods of 1, 4, 7, and 14 days were considered. Figure 3.1 shows the hydrometer grain-size distribution curves

of gypsum at different soaking periods. These curves demonstrate that gypsum particle sizes can be considered stable with different soaking periods as long as the same suspension was examined. That is related to the fact that gypsum has limited solubility in water which is around 2.6 g/l only (Barazanji, 1973), and this number can be considered insignificant comparing with the mass of gypsum solids used in a sedimentation test which is around 50 g in one litre suspension.

The combined grain-size distribution curves (wet sieving and hydrometer analysis) for the sandy soil and the gypsum are presented in Figure 3.2. The grain-size distribution curves of different sand-gypsum mixtures were calculated depending on the distribution curves of their constituents and the mixing percentages. These curves are presented between the grain-size curves of the sand and gypsum that form the boundary curves.

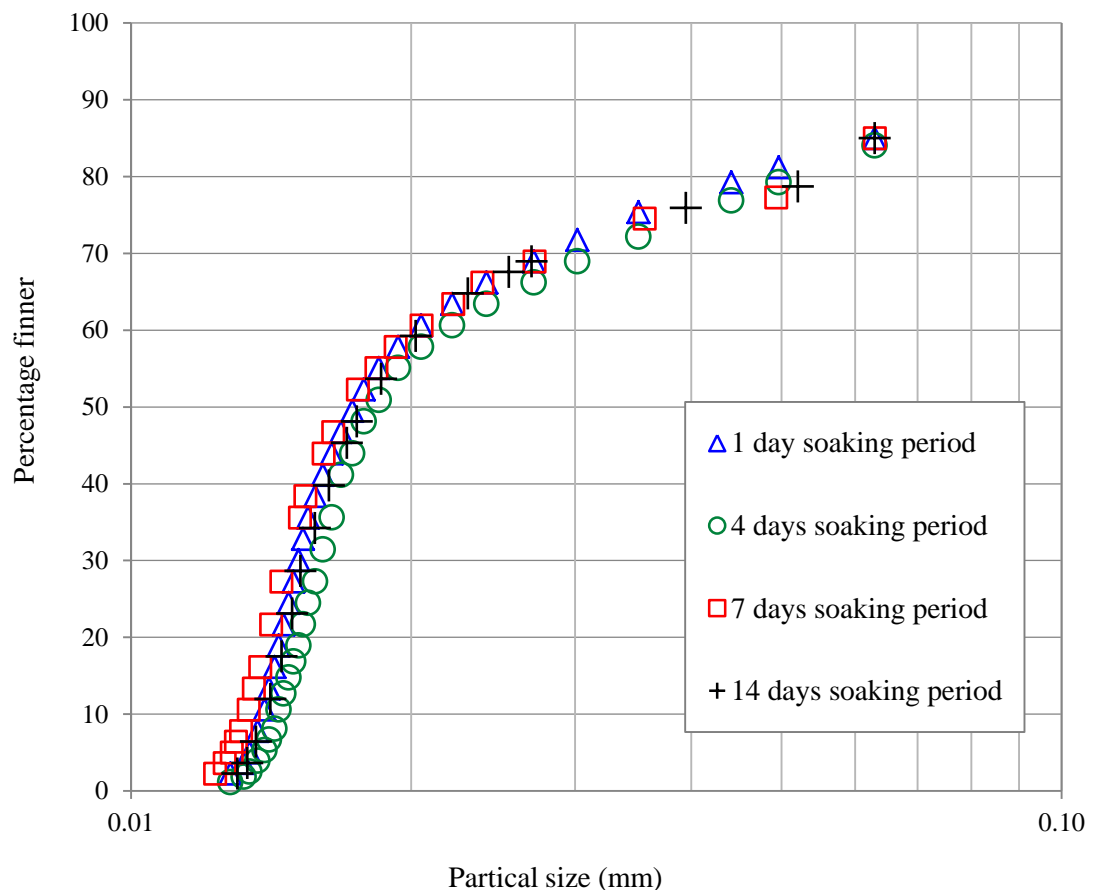


Figure 3.1. Grain-size distribution of gypsum at different soaking periods (Hydrometer tests).

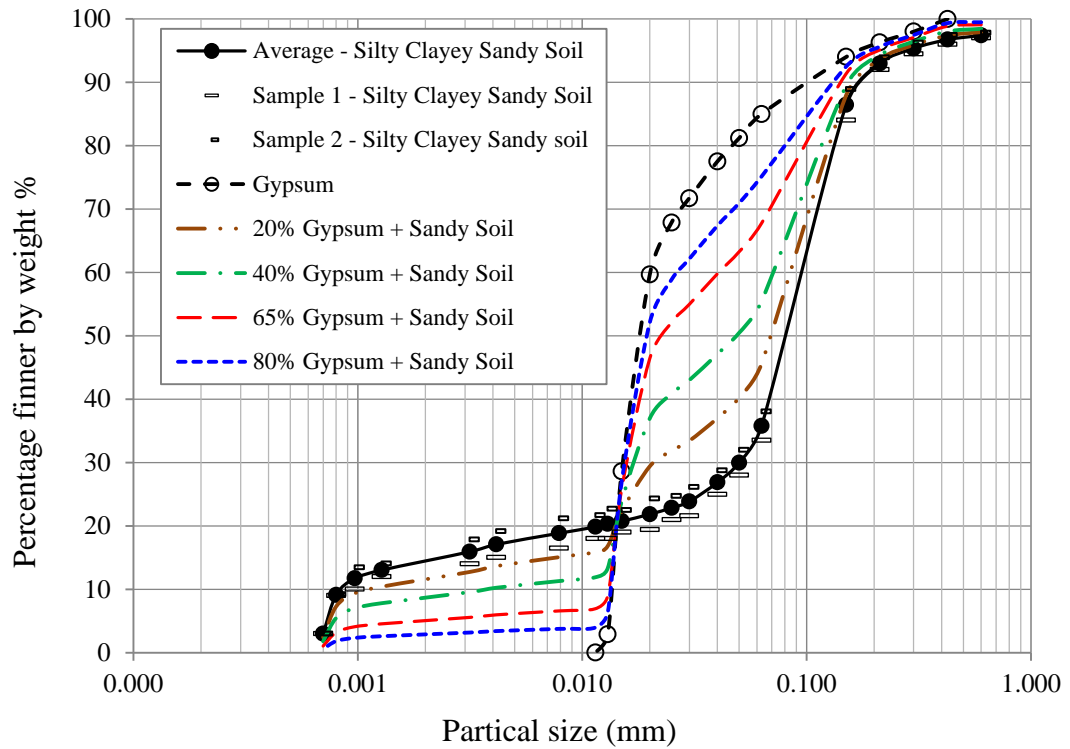


Figure 3.2. Particle size distribution curves of sandy soil, gypsum, and the synthetic samples.

The sandy soil contains 64% fine sand of particles size between 0.150 and 0.063 mm, 22% silt, and 12% clay. It is classified as silty clayey sand according to Unified Classification System and designated as SC-SM (ASTM D 2487-06). On the other hand, gypsum has a very uniform particles size with 60% between 0.010 and 0.020 mm. This uniformity has a clear effect on the grain-size distribution parameters of the prepared samples with a degree depends on the added gypsum percentage as shown in Table 3.1.

3.4. Experimental programme

This section describes the details of the implemented experimental programme. The details of the equipment used, the preparation of soil specimens, the testing procedure and calculations, and the testing programme for each test series are presented.

3.4.1. Compaction tests

Soil compaction is the process by which soil particles are forced to pack more closely together through a reduction in the air voids by using mechanical means

(Terzaghi and Peck, 1960; BS 1377-4-1990). The compaction characteristics of eight sand-gypsum mixtures were determined following the procedures described in clause 3 of the British Standard (BS 1377-4-1990). These mixtures had 0, 10, 20, 30, 40, 50, 65, and 80% gypsum content by weight. The objective of these tests is to evaluate the effect of gypsum content on the optimum water content and the corresponding maximum dry density of the tested soil. Standard Proctor effort of 600 kN.m/m³ was considered, in which 27 blows were applied from a 2.5 kg rammer falling through a height of 300 mm to compact the soil in three layers into a one litre compaction mould. A motorized apparatus was used with a metal rammer having 50 mm diameter circular face.

Gypsum is considered susceptible to crushing during compaction since gypsum particle is a soft crystal with a hardness rating of 2 (Blyth, 1971). This causing gypsum particles to reduce in size by the action of the 2.5 kg rammer. Therefore, the characteristics of the material may progressively change after each compaction attempt. To overcome that, separate batches of soil mixture at different moisture contents, each for compacting once only, were prepared to perform the compaction test. Water content increments of 1% were considered with smaller increments of water around the expected optimum water content to increase the accuracy of the test. The determination of water contents was carried out by following the British Standard (BS 1377-1-1990) with drying in a fan-assisted oven maintained at a temperature not exceeding 50 °C to keep gypsum hydrated water and prevent phase transform. The porosity and void ratio corresponding to the maximum dry density for different sand-gypsum mixtures were determined by using the volume-mass relationships.

3.4.2. Consolidation tests

One-dimensional consolidation tests were carried out on five saturated sand-gypsum mixtures in accordance with clause 3 of BS 1377-5:1990. These mixtures had gypsum contents of 0, 20, 40, 65, and 80% by weight. The primary objective of these tests was to find the effect of gypsum content on compressibility parameters such as the compression index (C_c) and the rebound index (C_r). As a secondary objective, the determined compression index could be used in conjunction with the

stress-dependent soil-water characteristic curve tests to evaluate the volume changes resulting from the application of net normal stress.

Consolidation apparatus of fixed ring type was used. The inside diameter and height of the ring were 70 and 20mm, respectively. Specimens were prepared inside the cell ring by static compaction to specified thickness of 8.41 mm, predetermined dry density, and predetermined compaction water content using a compaction mould designed specially to be compatible with the cell ring. A schematic drawing showing the components of the compaction mould and their assembling is shown in Figure 3.3. The inner surface of the ring was coated with silicone grease to minimize wall friction with the soil specimen. A loading frame machine was used to apply the required static load with a constant displacement rate of 0.2 mm/min. The specimens were compacted at their optimum water content to reach a dry density equal to 90% of the maximum dry density obtained from the standard Proctor test for the particular soil sample.

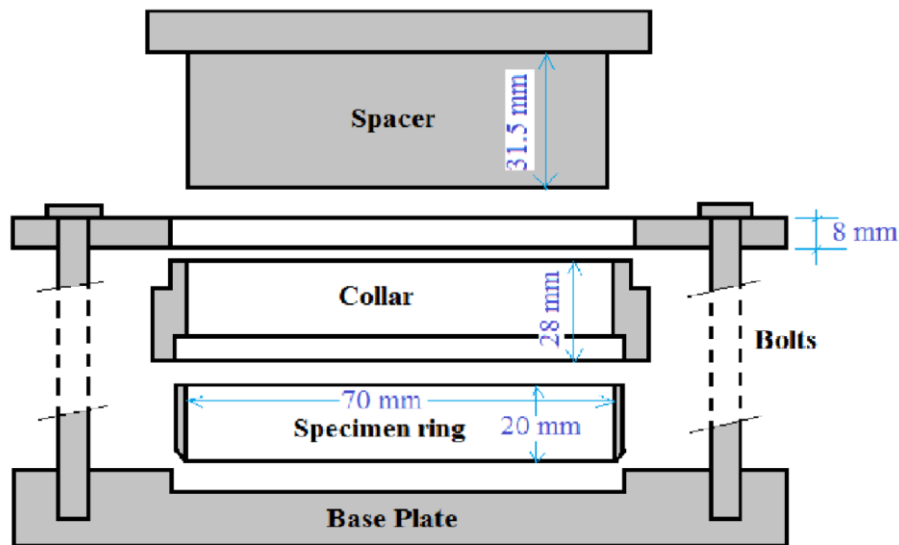


Figure 3.3. Schematic drawing of static compaction mould for specimens used for consolidation tests.

As usual the test starts by loading the soil specimen axially in consequent increments of applied stress (Clayton et al., 1995). Each increment was kept constant until the primary consolidation has ceased. During loading the decrease in height of the specimen was monitored at suitable intervals. When the desired maximum

loading has been reached, the load was released from the specimen through a successive decrements and the increase in height of the specimen was monitored periodically. A loading range of 8 kPa to 800 kPa with a load increment ratio equal to one, and load increment duration of 24 hours were considered. The loading was removed in decrements similar in values and durations to that of the applied increments.

By knowing the initial parameters (dry mass, specific gravity, volume, thickness) of the specimens and considering the changes in specimen thickness through successive pressure increments or decrements, the compressibility parameters for the tested specimens were determined by using the basic definitions as follows:

$$C_c = \frac{\Delta e}{\log\left(\frac{\sigma_2}{\sigma_1}\right)} \quad 3.1$$

$$C_r = \frac{\Delta e}{\log\left(\frac{\sigma_1}{\sigma_2}\right)} \quad 3.2$$

where C_c is the compression index, C_r is the recompression index, Δe is the change in void ratio due to the applied pressure increment or decrement, and σ_1, σ_2 are the applied pressures. The consolidation tests results are presented and discussed in detail in Chapter 5.

3.4.3. Soil-water characteristic tests

The soil-water characteristic curve (SWCC) describes the relationship between soil suction (matric or total) and soil water content (gravimetric, volumetric, or degree of saturation). In this section, determination of the drying SWCC in terms of matric suction and gravimetric water content is described. Six sand-gypsum mixtures with a gypsum content of 0, 10, 20, 30, 40, and 50% by weight were tested. The experimental programme was included two series of tests. In the first series, each specimen was used throughout the complete test under different applied suction increments to establish many points on the SWCC, whereas in the second series, separate specimens were used for each suction increment. The details of the experimental procedure for these tests are described in the following sections.

3.4.3.1. Testing device

Pressure plate extractor produced by Soil Moisture Equipment Corporation was used to determine the SWCCs for various sand-gypsum mixtures by following the ASTM D 6836-02. In this method, different suctions are applied to soil specimen and the corresponding water contents are measured gravimetrically. Suctions were applied via the axis-translation principle, in which the pore water pressure is maintained at nearly atmospheric, and the pore air pressure is raised to apply the suction.

A laboratory compressed air supply line was used. The regulation of the applied air pressure has remarkable effect on the accuracy of the equilibrium water content value of the soil specimen tested. To provide high accuracy on the applied air pressure, double pressure regulation was utilized. Low pressure regulator in series with a "Nullmatic" type regulator were used. The Nullmatic regulator continuously exhausts a certain amount of air, but it provides a good accuracy on pressure regulation. Bourdon gage was used to measure the applied air pressure, as well as, water manometer was connected in series with the bourdon gage to measure the small air pressure values.

3.4.3.2. Specimen preparation

To establish the SWCCs for any sand-gypsum mixture, a predefined weight of the mixture with a predefined amount of water were mixed and kept in a small air-tight container in a temperature controlled room to allow for water to distribute uniformly for at least one day. Stainless-steel specimen rings, 45 mm inside diameter and 10 mm height, were used to retain the test specimens. The inner surfaces of the specimen rings were lubricated with technical grade silicon grease. The specimens were statically compacted to a specified thickness of 7.6 mm, predetermined dry density, and predetermined compaction water content by using a compaction mould designed specially to fit with the specimen rings used. The components of the compaction mould and their assembly are shown in Figure 3.4. A loading frame was used to apply the required static load with a constant displacement rate of 0.2 mm/min.



Figure 3.4. Photographs showing (a) compaction mould components, (b) compaction setup for specimens used for SWCC tests.

3.4.3.3. Testing procedure and calculations

The prepared soil specimens with their retaining rings were placed over filter papers on pre-saturated porous ceramic disc for saturation. Duplicate soil specimens were used. This was done by allowing an excess of water to stand on the surface of the ceramic disc for 24 hours. Non-cohesive specimens generally required to be within the retaining rings during the saturation process in order to avoid dislodging from the retaining ring. After the completion of the saturation, the gravimetric water contents for these specimens were measured by using the duplicate ones. Then, the specimens were surcharged each by 500 g weight to ensure good hydraulic contact, and the air pressure was raised to apply the first increment of matric suction, which was 4 kPa. This increment caused water to flow from the specimens until the equilibrium water contents corresponding to the applied suction were reached.

By considering the transient outflow methods, reviewed in Chapter 2, it can be concluded that the time required to reach equilibrium varies according to the square of the specimen height. Thus, in this study, small specimen height was used so that the time required to reach equilibrium was reasonable. After the equilibrium was established, the specimens with their retaining rings were removed quickly from the extractor and weighed immediately and then kept in an air-tight container.

Meanwhile, the ceramic disc was re-saturated with water by leaving an excess water to stand on its surface for approximately 2 hours under an applied air pressure of 100 kPa. This process allows the air bubbles beneath the ceramic disc to be flushed out due to the continuous saturated water flow throughout the ceramic disc.

Upon completion of the re-saturation process, a thin film of water was left on the ceramic plate surface and then the specimens were placed back and twisted approximately 45° to ensure good hydraulic contact. Successive matric suctions were applied and several equilibrium points were established to construct the soil-water characteristic curve for each of the specimens tested. Matric suction values of 4, 10, 20, 50, 100, 200, and 400 kPa were applied. In this method, each soil specimen was used throughout the complete test and subjected to all suction increments to establish the SWCC. However, there were some concerns about the possibility of re-establishing hydraulic contact between the soil specimens and the ceramic disc after applying pre-defined matric suction increments and the corresponding dryness of the specimens.

Alternatively, second series of tests were carried out, in which separate specimens were used for each suction step, i.e., each specimen was subjected to one suction step only as per the ASTM D 6836-02. Thus, to establish SWCC of eight water content-matric suction points, sixteen identical specimens were prepared when duplicate specimens were used to establish each point of the SWCC. The duplicate specimens were placed once in the pressure plate extractor for saturation and then the pre-defined matric suction step was applied. When the equalization was reached, the duplicate specimens were removed from the pressure plate and weighed to determine the gravimetric water contents by considering their initial dry weights. Once the weights of the specimens were measured, the specimens were waxed and the total volume of each one was measured by using the wax method (ASTM D 4943-08). To establish another point on the SWCC, other duplicate specimens were used and the above procedures were repeated. The SWCC for each sand-gypsum mixture was established by considering the mean values of the duplicate specimens measurements. All specimens that used to define a soil-water characteristic curve for a certain soil mixture were prepared to be identical as far as possible.

The SWCCs for different sand-gypsum mixtures were determined by following the two different approaches mentioned above. In the first approach, the same specimens were used under different increments of matric suctions, while in the second approach new specimens were used for each step of suction. The use of separate specimens for each step of matric suction enabled measuring the total volume for each specimen after the equilibrium of water content and matric suction was reached. Knowing the specimen volume, the dry mass of the specimen, the gravimetric water content, therefore, the volumetric water content and the specimen void ratio corresponding to the equilibrium matric suction were calculated by using the mass-volume relationships. Consequently, the SWCCs in terms of the gravimetric water content, the SWCCs in terms of the volumetric water content, the void ratio-matric suction relationship, and the void ratio-gravimetric water content were established for each sand-gypsum mixture.

The SWCCs in terms of both gravimetric and volumetric water contents were best-fitted by using the mathematical model suggested by Fredlund and Xing (1994). This model takes the following form for representing the gravimetric water content as a function to the soil suction:

$$w(\psi) = F(\psi) \frac{w_s}{\{\ln[e + (\psi/a)^n]\}^m} \quad 3.3$$

where $w(\psi)$ is the gravimetric/volumetric water content at any soil suction, $F(\psi)$ is a correction function that extends the range of suctions beyond residual suction to zero water content condition, w_s is the saturated water content, and a , n , and m are fitting parameters related to the SWCC under consideration. The variable e is the base of the natural logarithm. The correction function, $F(\psi)$, can be written as follows:

$$F(\psi) = 1 - \frac{\ln(1 + \frac{\psi}{\psi_r})}{\ln[1 + (\frac{1000000}{\psi_r})]} \quad 3.4$$

where ψ is any soil suction and ψ_r is the residual soil suction. However, the correction function $F(\psi)$ may be taken equal to one at low suction values (Fredlund, et al., 2011).

The soil fitting parameters for all measured SWCCs and the corresponding coefficient of determination (R^2) were determined. However, each of air-entry suction (ψ_a), air-entry gravimetric water content (w_a), residual suction (ψ_r), and residual gravimetric water content (w_r) for each of the SWCCs were determined by using the graphical approach suggested by Vanapalli et al. (1994). The results of the first and second series of tests and all the corresponding parameters of SWCCs related to different sand-gypsum mixtures are presented and discussed in detail in Chapter 5.

3.4.4. Chilled mirror hygrometer tests

In this section, the determination of the SWCCs in terms of total suction is described. The entire SWCCs, from near saturation suction to around 300 MPa suction, were determined for five sand-gypsum mixtures of 0, 20, 40, 65, and 80% gypsum contents by weight. The main objective of these tests was to find the effect of gypsum content on the SWCC throughout the residual zone, more specifically in the range of suction values start beyond the maximum value achieved by using the axis-translation pressure plate to about 300 MPa. As a second objective, readings of total suction near saturation give an idea about osmotic suction values for different sand-gypsum mixtures. At saturation or at slightly above saturation, matric suction values were taken equal zero and the total suctions were considered as the osmotic suctions only.

3.4.4.1. Testing device

WP4C Dewpoint PotentialMeter produced by Decagon Devices, Inc. was used to determine the entire SWCCs for different sand-gypsum mixtures following the procedure laid out in the ASTM D 6836-02. The measured suction range of the device is from 0 to 300 MPa with an accuracy of ± 0.05 MPa at suction range from 0 to 5 MPa, and an accuracy of 1% at suction range from 5 to 300 MPa. The measuring time is about 10 to 15 min. for most soil specimens in precise mode. The device is calibrated before each use by using 0.5 molal potassium chloride (KCl) solution that has water potential = 2.22, ± 0.05 MPa.

3.4.4.2. Specimen preparation and testing procedure

For each sand-gypsum mixture, a specimen of 37.37 mm diameter and 5 mm thickness was prepared inside a stainless steel dish. A predefined weight of the soil mixture was statically compacted inside the dish at the optimum water content to 90% of the maximum dry density determined from standard Proctor test.

The specimen was, therefore, saturated by adding a defined weight of water and measuring the overall weight of the specimen with the dish. Filter paper was used above the specimen during saturation to keep it without disturbance. After saturation, the dish containing the specimen was sealed for at least 24 hours to allow for water to distribute uniformly. Then the total suction was measured by inserting the dish into the chilled mirror hygrometer. Once the total suction was measured, the weight of the specimen with the retaining dish was measured to the nearest 0.0001 g to calculate the gravimetric water content, and this establish one point on the SWCC.

To establish another point on the SWCC, the specimen was allowed to dry by exposure to the atmosphere until the next water content was achieved. This step was controlled by monitoring the overall weight of the specimen and the retaining dish periodically. After the specimen was dried to the next water content, the dish was sealed and allowed the specimen to equilibrate for 24 hours. After equilibration, the total suction and the weight of the specimen were measured as in the previous step. The procedure was repeated until the total suction values corresponding to the entire range of water content were measured.

After the final step of measuring the total suction was completed, the specimen was oven dried for 24 hours and the dry weight was measured. Considering the final dry weigh, back calculations to the gravimetric water contents at different steps were done and compared with water contents based on the initial dry weight of the soil to account for any loss of soil during the preparation of the specimen.

To get acceptable precision for total suction measurements at water contents near saturation when the readings are almost around the lower range of the device used, measurements were done corresponding to small water content increments. Furthermore, the WP4C Dewpoint PotentiaMeter was set up on the "continuous

mode" for suction readings corresponding to high water content values, as recommended in the user's manual. In such mode, the total suction of the specimen was measured continuously and the best representative suction readings were chosen.

3.4.4.3. Representation of test results

In chilled mirror hygrometer technique, the water content is controlled and the corresponding suction is measured. In other words, the independent variable is the water content, while the depended variable is the total suction. Thus, the water content was represented on the x-axis, and the total suction was represented on the y-axis. However, when the SWCC determined from pressure plates (low suction values) was combined with that determined from chilled mirror hygrometer (high suction values), the water content was represented as usual on the y-axis as a function to the soil suction which was represented on the x-axis. This representation mimics the presentations of other soil functions like the unsaturated hydraulic conductivity and the grain-size distribution curve.

3.4.5. Soil shrinkage characteristic tests

The changes in volume of a soil associated with changes in the water content are usually described by the soil shrinkage characteristic curve (SCC), McGarry and Malafant (1987). The shrinkage characteristic curve can be represented as either the void ratio versus water content or the specific volume (the inverse of dry density of a soil) versus water content (Haines, 1923). This curve is an important part of the constitutive behaviour of the soil and can be used in the determination of volume-mass property functions of unsaturated soils. The shrinkage curve can be used in conjunction with the soil-water characteristic curve to establish the relationship of void ratio versus soil suction.

As reviewed by many researchers, typical shrinkage curve may have an S-shape with two curvilinear parts at the ends and a linear portion at the middle (Tripathy et al., 2002; Bensallam et al., 2012). These three parts are corresponding to three stages of shrinkage which are the structural shrinkage, normal shrinkage, and the residual shrinkage, respectively (Haines, 1923). During the normal shrinkage, the reduction in the bulk volume of the soil is equal to the volume of water lost, while at the first and

third stages the decrease in bulk volume of the soil is less than the volume of the lost water. However, the structural shrinkage stage may not exist in many soil conditions and then the SSC will comprise the normal shrinkage stage represented by a saturated line and the residual stage represented by curvilinear segment (Fredlund et al., 2002).

CLOD test has been used to measure the SCC. The test has been first developed at the New Mexico Engineering Research Institute to predict heave under air field pavements (McKeen, 1981; McKeen and Hamberg, 1981). The procedure of this test is a modification of the coefficient of linear extensibility (COLE) test procedure which had been used by the Soil Survey Laboratory, U.S.D.A., since 1959 (Brasher et al., 1966).

To establish a shrinkage curve, unconfined soil clod is coated with a waterproof plastic resin and measurements of volume and weight are taken periodically while the clod is in the process of drying under laboratory humidity. The coating resin is permeable to water vapour, permitting a coated clod to gain or lose water, but practically impermeable to liquid water, as such permitting volume measurements by displacement of water. At the same time, the resin is flexible and that is mean the coating adheres to a cold and contracts or expands as the clod shrinks or swells. In this study the SCCs of different sand-gypsum mixtures were determined with the objective of determining the effect of gypsum content on the shrinkage characteristics of gypsiferous soils. As well as, the SCCs can be used to evaluate the volume changes associated with the applying of different levels of matric suction during the stress-dependent soil-water characteristic curve tests.

3.4.5.1. Testing procedure for SCCs

The test procedure for establishing the SCCs starts by preparing clods having gypsum contents of 0, 10, 20, 30, 40, 65, and 80% by dry weight. The clods were prepared by static compaction to form cylindrical specimen shape of 45 mm diameter and 7.6 mm height. The compaction mould shown in Figure 3.3 was used to compact the specimens at their optimum water content to 90% of the maximum dry density obtained from the standard compaction tests.

The compacted specimens with their rings were placed over a saturated ceramic plate for the saturation process. The saturation was done by allowing an excess of water to stand on the surface of the ceramic plate for 24 hours. Upon completion of the saturation process, the specimens were subjected to a matric suction ranging from 10 to 30 kPa in pressure plate device to bring them to a water content and then a consistency suitable to handle without dislodging or disturbing. The water content in which the soil specimen can be handled in an appropriate manner depends on the soil texture. Soil-mixtures with high gypsum content exhibited good consistency to deal with at relatively high water contents.

Therefore, the specimens were extracted from the retaining rings and their water contents were measured using duplicate specimens. Then, each clod was held by a thread, weighed, and briefly immersed in the resin without delay. The immersed clods were weighed again and then suspended from the thread and allowed to dry for 10 to 20 minutes. The type of resin used in this study was Polyvinyl Acetate glue emulsion, and its commercial mark was "UniBond WATERPROOF PVA". This type of resin was first suggested and used by Tadza (2011).

To measure the changes of the resin density during drying, an analogous of known weight and volume made up from plastic was immersed in the resin and suspended beside the coated soil clods. This analogous plastic piece was left to dry at the same time, same environment. Volume changes and weight changes for the soil clods and the coated plastic piece were measured periodically while clods were allowed to dry slowly under ambient laboratory conditions. Measurements were continued until the clods reached constant weights after about seven days. Then, the clods were dried in a fan-assisted oven maintained at a temperature not exceeding 50 °C, and the final volumes and weights were measured. Volumes of the clods were found by weighing each clod twice, once while it was suspended in air and another while it was suspended in water. By applying Archimedes rule, the difference between each of these pairs of weights is equal to the bulk volume of the coated clod times the mass density of water at laboratory temperature.

The volume and mass of the resin that coated the soil clod at any time were found by considering the following: (a) the initial resin mass of the soil clod which is

equal to the difference in the initial weight of the clod before and immediately after immersing in the resin. (b) the changes in resin density and mass with time, i.e., the volume and mass measurements of the coated plastic piece.

3.4.5.2. Calculations of CLOD tests

The water content-void ratio points of a shrinkage characteristic curve can be calculated by following the steps listed below:

- (1) The dry weight of the soil clod (W_d) can be calculated as follows:

$$W_d = \frac{W_1}{1 + w_i} \quad 3.5$$

where:

w_i : The initial water content of the soil clod determined from a duplicate soil specimen.

W_1 : The initial weight of the wet soil clod before coating with resin.

- (2) From the weight readings of the plastic specimen, the density of the resin (γ_r) at elapsed time, t , from the beginning of drying is:

$$\gamma_r = \frac{\gamma_w(W_{t3} - W_3)}{(W_{t3} - W_{t4}) - (W_3 - W_4)} \quad 3.6$$

where:

γ_w : The weight density of water at laboratory temperature.

W_3 : The weight of the plastic specimen, suspended in air.

W_4 : The weight of the plastic specimen, immersed in water.

W_{t3} : The weight of the resin coated-plastic specimen at elapsed time t , suspended in air.

W_{t4} : The weight of the resin coated-plastic specimen at elapsed time t , immersed in water.

- (3) The weight of the resin which is coated the soil clod (W_{rt}) at elapsed time t is calculated as follows:

$$W_{rt} = \frac{(W_2 - W_1)(W_{t3} - W_3)}{(W_5 - W_3)} \quad 3.7$$

where:

W_2 : The initial weight of the resin coated-soil clod, suspended in air.

W_5 : The initial weight of the resin coated-plastic specimen, suspended in air.

(4) The volume of the resin which is coated the soil clod (V_{r_t}) at elapsed time t is:

$$V_{r_t} = W_{r_t} / \gamma_{r_t} \quad 3.8$$

(5) The net weight of soil clod (W_{s_t}) at elapsed time t is:

$$W_{s_t} = W_{t1} - W_{r_t} \quad 3.9$$

(6) The net volume of soil clod (V_{s_t}) at elapsed time t is:

$$V_{s_t} = \frac{W_{t1} - W_{t2}}{\gamma_w} - V_{r_t} \quad 3.10$$

where:

W_{t1} : The weight of the resin coated-soil clod at elapsed time t , suspended in air.

W_{t2} : The weight of the resin coated-soil clod at elapsed time t , immersed in water.

(7) The water content (w_t) of the soil clod at elapsed time t is:

$$w_t = \frac{W_{s_t} - W_d}{W_d} \times 100\% \quad 3.11$$

(8) The void ratio (e) of the soil clod at elapsed time t is:

$$e = G_s \cdot \gamma_w \cdot \frac{V_{s_t}}{W_d} - 1 \quad 3.12$$

where G_s is the specific gravity of soil solids. Equations 3.6 to 3.12 are applied repeatedly for all periodic sets of weight readings that cover the full range of the measured shrinkage characteristic curve.

3.4.5.3. Mathematical modelling of SCCs

One of significant advantages of the CLOD test is that the volume changes are monitored along a gradually varying moisture change path, and this produces a smooth shrinkage curve for each sample. These data provide void ratio and water content at various points. To quantify the behaviour of soil shrinkage with different

gypsum content, the shrinkage curves were represented mathematically by using Fredlund et al. (2002)'s model. The mathematical representation of the SCCs and the corresponding SWCCs facilitates greatly the conjunction of these two functions when the void ratio versus soil suction relationships or the SWCCs in terms of volumetric water content were determined. Fredlund et al. (2002)'s equation could be written as follows:

$$e(w) = a \left[\frac{w^c}{b^c} + 1 \right]^{1/c} \quad 3.13$$

where $e(w)$ is the void ratio as a function to the water content, w , a is a fitting parameter represents the minimum void ratio obtained from the shrinkage of the soil, c is a fitting parameter represents the curvature of the shrinkage curve, b is a fitting parameter related to the slope of the tangent of the shrinkage curve. The slope of the line between void ratio and water content is equal to (a/b) and it is related to the initial volume-mass properties of the soil as follows:

$$\frac{a}{b} = \frac{G_s}{S} \quad 3.14$$

where G_s is the specific gravity of the soil solids, and S is the initial degree of saturation of the tested specimen. On the other hand, the slope of the void ratio versus water content curve at the normal phase of shrinkage is referred to as CLOD index, C_w , which expresses the volume compressibility with respect to water content.

$$C_w = \frac{\Delta e}{\Delta w} \quad 3.15$$

where Δe is the incremental change in void ratio corresponding to the incremental change in water content, Δw .

3.4.6. Stress-dependent soil-water characteristic tests

It has been well recognized that factors such as void ratio, soil structure, and stress state can influence the average pore size distribution in the soil specimen and then influence the SWCC (Fredlund and Rahardjo, 1993). Thus, it is preferable to simulate the stress state of the field when the SWCC has to be determined for a certain soil at the laboratory. Few experimental studies have been carried out to examine the effect of stress state on the SWCC. In this study, stress-dependent soil-water characteristic curves (SD-SWCCs) of silty clayey sand with different

percentages of gypsum were investigated under both drying and wetting paths. A new stress controllable pressure plate device was developed for this purpose.

The modified device was used to measure conveniently and efficiently the drying and the wetting SD-SWCCs. Continuous determination of specimen water content during the tests was accurately determined without dismantling the device by weighing the overall cell. This feature makes the device suitable to measure the unsaturated hydraulic conductivity function of the tested specimen simultaneously with the determination of the SD-SWCCs.

The testing programme was undertaken to establish the SD-SWCCs of five different sand-gypsum mixtures tested under five different levels of net normal stress, which were 0, 100, 200, 300, and 400 kPa. The design and construction details of the modified stress controllable pressure plate device, the detailed experimental programme, the preparation of the specimens, the testing procedure, and the calculations of these test results are presented in Chapter 4.

3.4.7. Stress dependent-unsaturated hydraulic conductivity function tests

The laboratory methods used for determining unsaturated hydraulic conductivity may be classified into steady-state and unsteady-state methods as reviewed in chapter two. In the steady state methods, the flux, the hydraulic gradient, and the water content of the soil are constant with time, while each of these parameters are varying with time for unsteady-state or transient techniques. Among the unsteady-state methods are the transient outflow methods that mostly depend on some analytical solutions to Richard (1931)'s equation which is the governing equation for the one-dimensional transient flow in homogenous soils (no change in hydraulic conductivity in the direction of flow).

The transient outflow methods may be categorized into four types, among those are the multistep method and the one step method. These methods are usually conducted on specimens under drying conditions using conventional axis-translation equipment without applying any surcharge loads. In these methods, the transient diffusion equation is usually solved for determining the hydraulic diffusivity function. Then, the hydraulic conductivity function is calculated by knowing the

specific moisture capacity which is defined from the soil-water characteristic curve when it is represented as a function of volumetric water content versus matric suction as a head.

In this study, the original multistep analysis approach by Gardner (1956) was used to analyse the results of the tests which were carried out by using the newly modified stress controllable pressure plate device. Furthermore, the one step approach by Doering (1965) was used as an alternative approach for the analysis of the results and a comparison between these two approaches was done. The tests were implemented in conjunction with the tests of SD-SWCCs determination in both the drying and the wetting processes under different applied net normal stress levels.

Five extensive series of stress dependent-hydraulic conductivity functions (SD-HCFs) were carried out on five sand-gypsum mixtures having gypsum contents of 10, 20, 40, 65, and 80%. These mixtures were tested at four different net normal stress levels (0, 100, 200, and 400 kPa). The unsaturated hydraulic conductivity functions were determined by monitoring the time-dependent decrease in weight of specimens subjected to series of applied increments of matric suction. Similarly, during the wetting process, the time-dependent increases in weight of specimens subjected to series of applied decrements of matric suction were monitored. The details of the experimental programme, preparation of specimens, testing device, testing procedures, and calculations are presented in Chapter 4.

As a reference value, the saturated hydraulic conductivity of the silty clayey sandy soil without gypsum additives was found by using a falling head permeameter according to BS 1377-5 (1990). The specimen was placed in the permeameter at its optimum water content and dry density of 1.8 Mg/m^3 . An average value of $4 \times 10^{-9} \text{ m/s}$ was found to represents the saturated hydraulic conductivity of the sandy soil without gypsum.

3.4.8. Direct shear tests on saturated specimens

3.4.8.1. Overview

The direct shear test is one of several methods available for measuring the shear strength of soils. In this test a soil specimen of square or circular cross section is

laterally restrained and sheared along a mechanically induced horizontal plane while subjected to a pressure applied normal to that plane. The shearing force can be applied either by increasing the force at a given rate and measuring the resulting displacement, or by applying displacement at a given rate and measuring the resulting force. The first method is called stress-controlled method while the second one is called strain-controlled method. As the strain is gradually increased the shearing resistance builds up until the peak stress is reached and failure begins. As the strain is further increased the resistance falls to a steady value known as steady state strength, and the arrangement of the soil particles comes up to a loose state (Lambe, 1951). The strain-controlled method was adopted in this study and the shearing resistance was measured at regular intervals of displacement. The peak shear strength was considered in calculating the shear strength parameters by using Mohr-Coulomb failure criterion.

The experimental programme was designed to examine the effect of gypsum content on the saturated shear strength parameters of the sandy soil. These parameters are the effective angle of shearing resistance and the effective cohesion. Eight sand-gypsum mixtures were tested having gypsum percentages of 0, 10, 20, 30, 40, 50, 65, and 80% by dry weight. Three identical specimens for each of the eight soil mixtures were tested under three different normal pressures (100, 200, 400 kPa). In total, more than 30 tests were carried out, from them 24 tests were adopted. Some tests were repeated due to experimental uncertainties or for test results conformation. All tests were performed under saturation condition.

3.4.8.2. Direct shear testing device

The designed experimental programme was performed using a Wykeham-Farrance, 27-WF2180, Automatic digital direct/residual shear machine. The machine is equipped with a microprocessor system that records and processes the measurements of shear force, axial pressure, vertical deformation, and horizontal displacement. The device incorporates a pneumatic closed loop system for the automatic application of the axial pressure by a high performance pressure regulator. An automatic management of the test was achieved by connecting the device to a PC through a serial port using ASCII protocol, HyperTerminal software. Three modes

for data acquisition (linear, exponential, and polynomial mode versus time) through different test stages were available. These modes are related to the pre-set time intervals for recording the test measurements, either for consolidation or shearing stage. Exponential mode was selected for recording consolidation data, and linear recording mode for shearing data. Figure 3.5 shows the general set-up of the direct shear device.

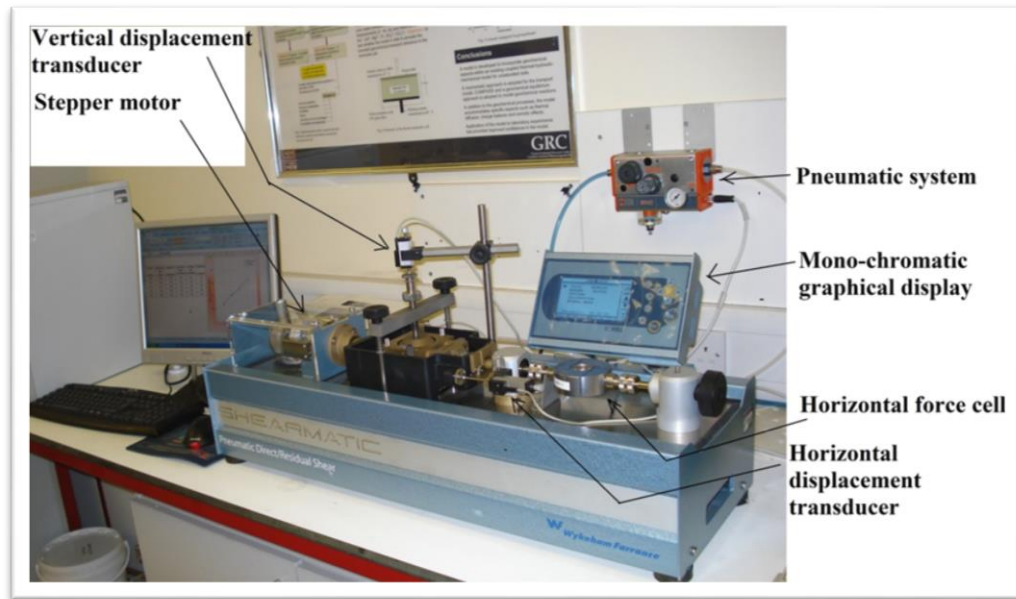


Figure 3.5. Photograph of the general set-up of the direct shear device.

Small shear box was used in this study with a circular cross section of 60 mm in diameter. The initial specimen height was 23.4 mm for all tests.

3.4.8.3. Device calibration

The machine is equipped with two displacement transducers (horizontal displacement and vertical deformation transducers) and two strain gauge transducers (load cell for lateral shear force measurement and pressure transducer measuring the axial pressure acting on the sample). Each of these transducers was calibrated by using reference micrometer for displacement calibration, and reference load cell for force calibration. It was possible for each transducer to make linear calibration with a single factor or polynomial calibration with several factors. The polynomial calibration is usually used to get high accuracy along the full range of the strain gauges measurements, especially in the range below 10% of full scale.

Each transducer was calibrated by applying a series of increments of displacement (or force) to it and these increments were measured by using well calibrated reference instrument. Two readings were obtained corresponding to each increment, a digital signal reading from the transducer under calibration and a physical reading from the reference instrument with physical units. These pairs of readings were taken to cover the full scale of the transducer under consideration. Upon completion that, a series of decrements of displacement (or force) were applied and another set of pairs of readings was gathered from the other direction of movement or loading. For each pair of readings, the calibration factor was calculated as the ratio of the physical reading to the digital signal reading. By comparing these factors, very slight differences were found between loading unloading paths or forward backward displacements. However, simple evaluation concerning the linearity of each transducer and the range in which the best calibration should be performed was done by plotting these pairs of data. Figure 3.6 shows an example for the calibration readings of the horizontal displacement transducer during forward, backward, and a second forward movement. It can be noticed from Figure 3.6 that the difference between the calibration factors during forward movements (average of 1.0903) and that during backward movement (1.0921) is only 0.165%, which can be considered insignificant.

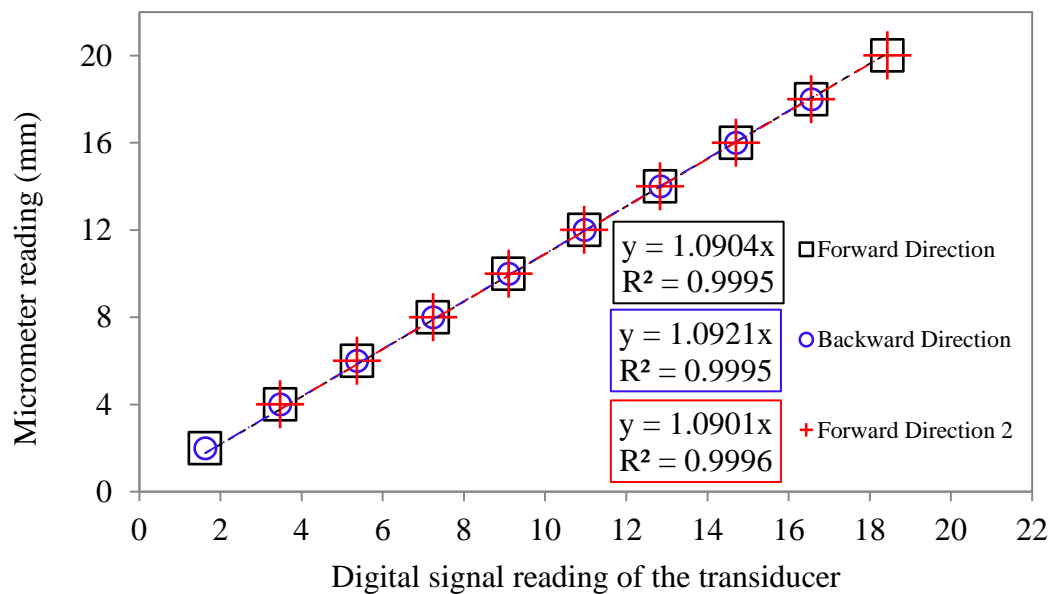


Figure 3.6. Calibration lines of horizontal displacement transducer during forward, backward, and second forward movement.

3.4.8.4. Specimens preparation

Three similar specimens were prepared for each sand-gypsum mixture to be tested under three different normal pressures of 100, 200, and 400 kPa. Firstly, the soil mixture was prepared by mixing predefined weights of dry sand and gypsum in a small plastic can. The mixture was mixed dry, then with water to be at the optimum water content, and kept for at least one day in air-tight container in a temperature controlled room to allow for water to distribute uniformly. Silicone grease was applied to the inside faces of the shear box and to the surfaces of contact between the two halves of the box. Then, the parts of the shear box were assembled and the entire soil mixture was poured from the container into the shear box. The soil specimen was compacted directly inside the shear box via static compaction method at the optimum water content to achieve a dry density equal to 90% of the maximum dry density obtained from the standard Proctor test. A compaction ram was machined to fit the shear box and to control the compacted specimen thickness to 23.4 mm for all tests performed. By this manner, the initial specimen parameters such as the bulk density and the void ratio could be defined by considering the volume-mass relationships. A loading frame machine was used to apply the required static load with a constant displacement rate of 0.2 mm/min. The components of the shear box and the compaction ram are shown in Figure 3.7.

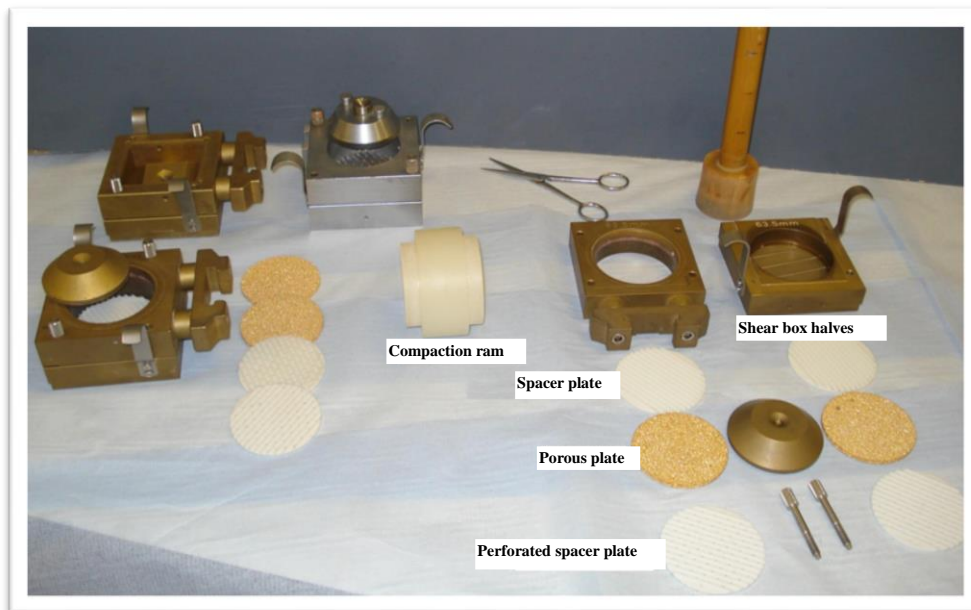


Figure 3.7. Shear box component with the compaction ram used in static compaction.

For curing and cohesive forces equalization, the compacted specimen with the shear box was warped by stretch polyethylene film and stored in a temperature and humidity controlled room for 48 hours prior to shearing. This period enables any excess pore pressures to dissipate as well.

3.4.8.5. Testing procedure and calculations

After preparing the soil specimens inside the shear box as described in the previous section, the specimens were tested in accordance with clause 4 of BS 1377-7:1990. In each test, the specimen was first saturated by flooding the direct shear carriage with de-aired distilled water. The soil specimen in the direct shear box was allowed to intake water for 24 hours under a nominal surcharge (loading cap, grooved perforated spacer, and porous plate). The specimen then was consolidated under the pre-decided vertical normal load until the primary consolidation was completed. Eight hours of consolidation were found to be satisfactory for all tested specimens.

On completion the consolidation stage and before starting the shearing process, the rate of shearing displacement had to be decided adequately. Rapid shear of a saturated soil may cause positive or negative pore water pressure to be built up depending on the density of the sheared soil. Loose soil tends to contract during shearing while dense soil tends to expands during shearing. Soil contraction is associated with an increase in pore water pressure if the soil is sheared more rapidly than its pore water can flow out. In contrary, soil expansion is associated with negative pore water pressure if the rate of shear is too rapid to permit the free inflow of water. Negative pore water pressure causes an increase in the effective intergranular stress while positive pore pressure reduces that. Therefore, rapid shear of a saturated soil may cause a decrease in the strength of a loose soil or an increase in the strength of a dense soil. Thus, the adequate rate of shearing displacement was very important to decide before starting the shearing process.

By using the consolidation readings, the square-root time versus vertical deformation was plotted, and the time required to reach 100% consolidation, t_{100} ,

was found. The minimum time to failure (t_f) was calculated in accordance with clause 4 of BS 1377-7:1990 as follows:

$$t_f = 12.7 t_{100} \quad 3.16$$

The horizontal shear displacement of the specimen at failure was estimated to be 10 mm. This value was divided by the calculated value of t_f to find the maximum rate of displacement to be applied during the shearing process. A rate of shearing displacement of 0.02 mm/min was adopted. This value was found to be satisfactory for all eight tested sand-gypsum mixtures. The adopted rate of shear displacement was slow enough to prevent development of pore pressures.

During the shearing process, the microprocessor of the device was set to record the shearing force, the horizontal displacement, the vertical deformation, and the elapsed time at regular intervals of horizontal displacement of 0.20 mm and continue to a full travel. A total horizontal displacement of 14 mm was decided to be the end of travel for the shear box. This value was found to be extended beyond the maximum shear point (peak shear stress) by appropriate distance for all tested specimens.

Upon completion the shearing process, the water was siphoned off from around the specimen and the specimen was allowed to stand for about 10 min to enable the free water to drain off. The vertical force was released then, and the specimen was extruded to measure the water content gravimetrically. Considering the final saturated water content and knowing the particle density of the tested soil, the final void ratio of the specimen at failure was calculated. By back calculation using the vertical deformation readings, the values of void ratio at all the test stages could be calculated and compared with the calculated values based on the initial specimen condition. The detailed results and discussion of the direct shear test on saturated specimens are presented in Chapter 7.

3.4.8.6. Stresses and strains

For each set of readings obtained corresponding to an increment in horizontal displacement during a shear test, the shear stress (τ) on the failure surface was

calculated by dividing the measured shear force by the corrected cross sectional area of the sheared specimen. The sheared area between the two specimen halves reduces with the progress of shearing process as shown in Figure 3.8.

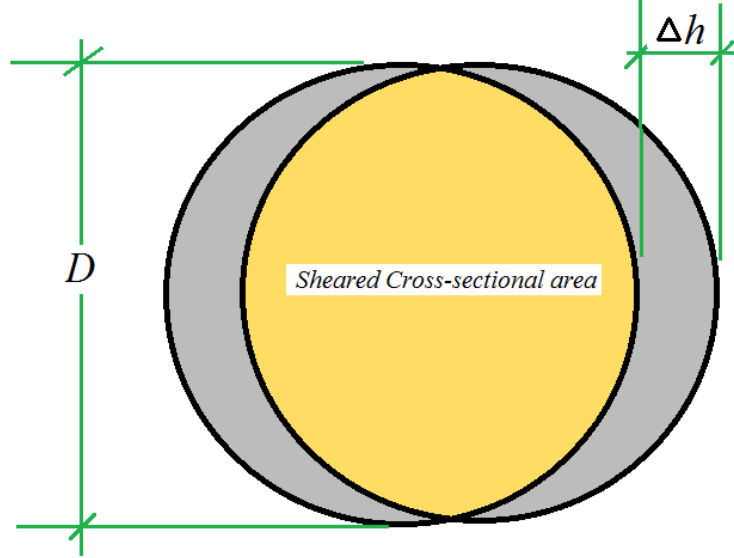


Figure 3.8. A schematic diagram showing the corrected cross-sectional sheared area in a circular shear box.

The corrected cross sectional area (A_c) could be calculated as follows:

$$A_c = \frac{D^2}{2} \cdot \left\{ \theta - \frac{\Delta h}{D} \cdot \sin \theta \right\} \quad 3.17$$

$$\theta = \cos^{-1} \left(\frac{\Delta h}{D} \right) \quad \text{in radians} \quad 3.18$$

The stress distribution across the specimen is complex, and thus the calculated value of shear stress represents an approximate mean value. The calculated shear stress as ordinates was plotted against horizontal displacement as abscissa, and then the value of the maximum or the peak shear stress and the corresponding horizontal displacement were defined.

To determine the effective angle of shearing resistance (ϕ') and the effective cohesion (c') for each sand-gypsum mixture, the maximum or the peak shear stress value was adopted as a failure criterion and then represented as ordinates against the corresponding normal stresses and best fitted by straight line. The angle of shearing

resistance was determined from the slope of the line and the apparent cohesion was determined from the intercept, both in terms of effective stress.

To determine the volume changes of the specimen during the shearing process, a graph of vertical deformation of the specimen as ordinates against horizontal displacement as abscissa was plotted for each tested specimen. Dense specimen usually dilates until failure occurs, however, when the shearing resistance drops, and after that a slight decrease in volume may occur. Loose specimen, on the other hand, compresses under the shearing action.

3.4.9. Direct shear tests on unsaturated specimens

3.4.9.1. Overview

In saturated soil, shear strength is commonly resulted from two components, the cohesion component and the frictional component that results from external loading (skeletal forces). The resultant shear strength could be described through Mohr-Coulomb failure criterion. In unsaturated soils, however, the shear strength has a third component beside the two components of the saturated soil. The third component results from an internal stress acting locally on soil grains that arises particularly from desaturation of the soil and it is independent of the external loading. This component can be captured by incorporating the soil matric suction in conjunction with a soil parameter (i.e., the effective stress parameter, χ , or the angle of shearing resistance related to matric suction, ϕ^b) as presented in Section 2.3.2.

The modified direct shear or triaxial shear equipment, which have the facilities to control the matric suction, are usually used to measure the shear strength of unsaturated soils (Escario, 1980; Ho et al., 1982; Gan et al., 1988; Vanapalli et al., 1996). These equipment are costly, time consuming, and need high skill and laboratory expertise. For those reasons, during the last decade, many researchers trended to use the conventional direct shear device to find the shear strength of unsaturated soil specimens through water content controlled conditions instead of suction controlled conditions (Lane et al., 2001; Vanapalli and Lane, 2002; Feuerharmel et al., 2006; Lu and Likos, 2006; Casini et al., 2011).

Conventional tests of water-controlled specimens are much easier and faster than suction-controlled specimens. Furthermore, the describing of shear strength as a function of water content makes it more preferable in practical applications, because the measuring of field water content is easier and faster than measuring soil suction.

Water-controlled specimen technique was adopted in this study to examine the effect of gypsum content and the effect of de-saturation on the shear strength of gypsiferous soils. To examine the reliability of this technique, the results of the direct shear tests, on unsaturated soil specimens with different initial degrees of saturation, were used in conjunction with the data obtained from the stress-dependent soil-water characteristic curve (SD-SWCC) tests. This enables the evaluation of shear strength as a function to the matric suction. The SD-SWCC data was represented as a mathematical equation in the shear strength function by using the reverse form of Fredlund and Xing (1994)'s mathematical model.

As an additional approach, the concept of suction stress (Lu and Likos, 2006) was adopted without considering independently the variables that define it (i.e., matric suction and χ). By using this concept, it was circumvented about the necessity of determining the matric suction or the effective stress parameter χ , since the most relevant variable to the shear strength is neither the matric suction nor χ but the product of the two which is identified as suction stress. This could be noticed clearly from the failure envelope equation suggested by Bishop (1960), Equation 2. 21.

Furthermore, the suction stress characteristic curves (SSCCs) in terms of water content were determined for different sand-gypsum mixtures by using the results of the direct shear tests. As well as, it is possible to find the SSCCs in terms of matric suction by incorporating the results of the stress-dependent soil-water characteristic curve tests.

3.4.9.2. Experimental programme

One of the primary objectives of this study was to determine the effect of gypsum content on the unsaturated shear strength function of gypsiferous soils. This objective was achieved by carrying out an extensive laboratory programme includes more than 150 direct shear tests on different unsaturated sand-gypsum mixtures.

These tests were carried out in conventional direct shear apparatus on soil specimens that were saturated and air-dried to pre-defined water contents. The specimens were consolidated and sheared under undrained conditions for the water phase while the air phase was allowed to be under atmospheric condition, i.e., the tests were carried out under constant water content conditions.

The experimental programme was designed to examine five different sand-gypsum mixtures having 0, 20, 40, 65, and 80% gypsum content by weight. Each soil mixture was tested at about six different water contents under four different net normal stresses (100, 200, 300, and 400 kPa). Thus, each series of tests on each sand-gypsum mixture was comprised about 24 tests. Some tests were repeated due to experimental uncertainties or for test results conformation. In total, more than 150 direct shear tests of statically compacted unsaturated specimens were carried out on the silty clayey sand with different percentages of gypsum content. Table 3.2 shows the framework of the experimental programme.

Table 3.2. The framework of direct shear tests on unsaturated specimens.

First series: Gypsum content = 0%							
Net normal stress (kPa)	Gravimetric water contents of tested specimens (%)						
100	15.2	9.8	7.7	6.9	6.1		
200	15.1	9.8	7.7	7.0	6.0		
300	15.5	9.9	7.7	7.0	6.0		
400	16.0	9.7	8.0	7.0	6.1		
Second series: Gypsum content = 20%							
100	15.5	10.9	9.3	8.2	7.4	6.7	
200	16.2	10.9	9.1	8.2	7.5	6.7	
300	16.4	10.9	9.1	8.1	7.5	6.7	
400	16.6	10.9	9.2	8.1	7.6	6.7	
Third series: Gypsum content = 40%							
100	16.5	12.7	10.8	9.4	7.8	6.7	
200	16.2	12.8	10.9	9.5	7.6	6.5	
300	16.3	12.7	10.8	9.6	7.7	6.6	
400	16.4	12.7	11.0	9.3	7.8	6.5	
Fourth series: Gypsum content = 65%							
100	19.3	13.4	9.0	8.2	7.4	6.7	5.6
200	19.3	13.3	9.1	8.2	7.2	6.7	5.8
300	19.0	13.4	9.0	8.2	7.2	6.6	5.8
400	18.6	13.2	9.1	8.2	7.2	6.5	5.5
Fifth series: Gypsum content = 80%							
100	23.6	11.8	8.9	7.5	6.6	5.6	
200	23.4	12.1	8.9	7.5	6.4	5.5	
300	23.1	11.7	8.8	7.5	6.5	5.6	
400	22.8	12.1	9.0	7.5	6.4	5.5	

The matric suction values of the air-dried specimens were determined by knowing the water content values and using the soil-water characteristic curve of the sand-gypsum mixture under consideration. For any test, the initial condition and the equalized matric suction of the water-controlled specimen are expected to alter during the consolidation stage firstly and then during the shearing stage. The alteration of matric suction during the consolidation stage, due to the effect of net normal stress, was defined accurately in this study by conducting a series of stress-dependent soil-water characteristic curve (SD-SWCC) tests for each sand-gypsum mixture. These tests were carried out under the same levels of net normal stress that used in the shearing tests. Furthermore, the same hydraulic loading path was considered, i.e., the water-controlled specimens for the direct shear tests were prepared under drying path which were analogous to those tested under the drying SD-SWCC. As well as, the compaction parameters of the prepared specimens for the direct shear tests were made identical as far as possible to those prepared for the SD-SWCCs tests.

The second alteration of matric suction may be happened during the shearing process. In this study, the results of the shear strength tests were analysed based on assumption that there were no changes in matric suction during the shearing process as long as the specimens were sheared under constant water content conditions at reasonably short period, not exceeding 28 min. However, the volume changes of the specimens during the shearing process were measured, and those measurements usually give an indication of the possible associated changes in the matric suction during the shearing process. The dilation of specimen during shearing process may be associated with an increase in matric suction, while the reduction in volume results a possible decrease in matric suction.

3.4.9.3. Specimens preparation

The soil specimens were statically compacted inside the shear box directly by following the same procedure adopted in compaction the specimens for the saturated tests (Section 3.4.8.4). All specimens were compacted to constant volume, constant thickness of 23.38 mm, at the optimum water content, to achieve a dry density equal to 90% of the maximum dry density obtained from the standard proctor test. The

specimens were saturated by placing them in a shallow pan flooded with distilled water while they were subjected to a vacuum of 20 kPa. A saturation period of 4 hours was found to be suitable. The saturated specimens were then subjected to different periods of air-drying to produce variation in water content from specimen to another and correspondingly variation in matric suction. The air dried soil specimens were then wrapped by stretch polyethylene film and stored in a temperature and humidity controlled environment for a minimum of 48 hours to attain equilibrium conditions with respect to water content and suction throughout the specimens. After that the specimens were consolidated and sheared as described below in Section 3.4.9.5.

3.4.9.4. Device adjustment

Like other conventional direct shear devices, the used device has been designed primarily to test saturated specimens or granular dry specimens, i.e., specimens at plastic state or low stiffness state. Figure 3.9 shows a schematic drawing of the pneumatic system which is integrated in the Wykeham-Farrance, 27-WF2180, direct shear machine to apply and control the desired normal pressure on the specimen automatically.

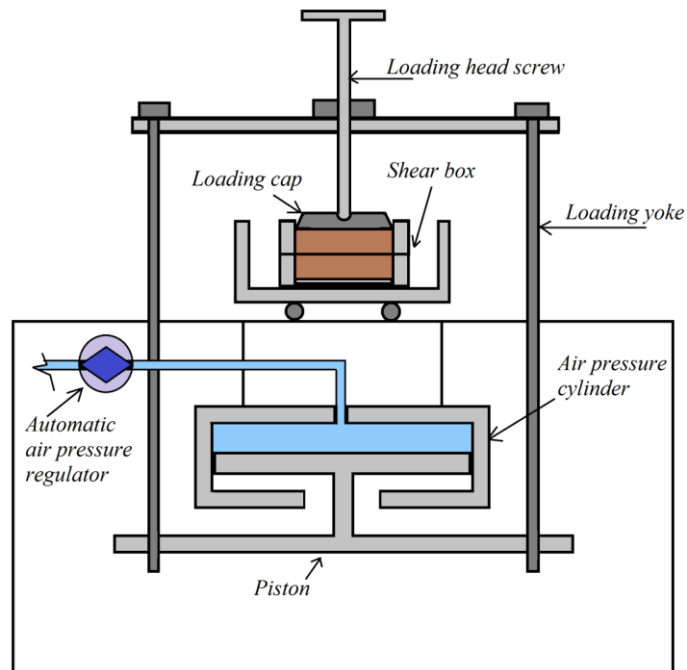


Figure 3.9. A schematic diagram showing the normal pressure pneumatic system of the direct shear device.

In typical tests, the loading head screw is gently turned to achieve good contact with the loading cap of the shear box. At this step, the piston inside the air pressure cylinder is at the top end of the cylinder, and any tightness in the head screw will result by an amount of normal load applied manually on the specimen, i.e., the system will act as a manual vice. This manual loading was evaluated by placing a load cell beneath the head screw and tightened it to different degrees as described in Table 3.3.

Table 3.3. Normal loads result from different degrees of head screw tightness.

Head screw status	Manual normal load (N)
Very loose	8
Loose	19
Lightly screwed	60
Gently screwed by two finger tips	90
Relatively tightened by two finger tips	316
Tightened by two finger tips	541

When a desired normal pressure is set up to a certain value and the test started, the compressed air will flow inside the air cylinder under the control of the automatic pressure regulator to match the preset pressure value. Thus, the piston will move downward to transfer the pressure to the specimen via the attached loading yoke. The vertical displacement of the piston is equal to the amount of the vertical consolidation of the specimen under the applied normal pressure, and this depends on the coefficient of compressibility of the specimen.

Upon completion of the consolidation stage and starting the shearing process, the specimen exhibits vertical dilation when the initial void ratio of the specimen is smaller than the critical void ratio. Consequently, the piston of the air pressure cylinder will move back upward with an amount equal to the vertical dilation of the specimen. Meanwhile, the applied normal pressure still has the same presetting value as long as the piston is not restricted and the air pressure inside the pneumatic cylinder is controlled by the automatic pressure regulator.

When the value of vertical dilation approaches the amount of consolidation of the specimen, which occurred through the first stage, the piston will return back to the top end of the pressure cylinder. Hence, the pneumatic loading yoke of the device

cannot move freely upward and some restriction on vertical dilation will be started. Consequently, any further dilation will be restricted and the automatic pressure regulator no longer be able to control the normal pressure at the desired value. In such a case, the loading yoke will act as a vice and this restriction will be associated with a built up of normal pressure which is proportional to the stiffness of the specimen.

In this study, most of the unsaturated gypsiferous specimens exhibited high stiffness especially when they were air dried to relatively low water contents. Most of these specimens showed dilation during shearing process with an amount proportional inversely with the applied net normal stress. Specimens sheared under 100 kPa net normal stress exhibited dilation more than those sheared under higher values of net normal stress, and this amount of dilation was mostly greater than the amount of compression during the consolidation stage. Thus, a remarkable restriction from the loading yoke was noticed on the dilation of these specimens during the shearing stage. Consequently, the built up normal pressure, conjugated to that restriction, was noticed mostly greater than the pneumatic pressure which is recorded and displayed by the microprocessor of the device. This matter was experimentally evaluated by installing a small load cell between the loading cap of the shear box and the loading head screw. Through this load cell, the actual normal force applied on the top of the specimen was measured and compared with the pneumatic system reading to evaluate the system reliability.

To overcome the restriction problem of the loading yoke in testing unsaturated stiff specimens, it was suggested in this study to leave a small gap between the loading head screw and the loading cap of the shear box. This gap was suggested to be equal or more than the anticipated dilation through the shearing stage. By following this adjustment, the readings of the inserted load cell were found to be exactly matching the readings of the pressure transducer which is originally installed into the device.

The introduced gap between the loading head screw and the loading cap causes an initial vertical transducer settlement which should be accounted for when the

vertical displacements have to be evaluated. To circumvent this, the following simple procedures were suggested:

- (i) The loading head screw is gently turned to ensure good contact with the loading cap.
- (ii) The vertical transducer is installed and adjusted to zero reading.
- (iii) After the setting of the vertical transducer, the head screw is turned counter clockwise to set the desired gap.
- (iv) The introduced gap is measured accurately by notice the readings of the vertical displacement transducer which will be in negative sign that indicates upward movement.
- (v) Once the consolidation stage is started, the initial transducer settlement will be counterbalanced by the negative reading of the transducer and the vertical displacement readings will start from zero and going on in positive.

The above steps ensure that the piston of the pneumatic air cylinder has enough space to move upward and downward throughout the test without restriction, since the piston starts movement from a midpoint neither from the top end of the cylinder.

3.4.9.5. Testing procedure for unsaturated soil specimens

After preparing the soil specimens inside the shear box at predetermined water contents as described in Sections 3.4.8.4 and 3.4.9.3, the specimens were tested in accordance with clause 4 of BS 1377-7:1990. Unlike the saturated specimens, unsaturated soil specimens were subjected to consolidation under the desired net normal stress for a period of 2 hours only. This period was found to be satisfactory for all unsaturated specimens tested, since longer period may alters the water content of the tested specimens significantly. The specimens were then sheared at a strain rate of 0.50 mm/min. This rate was adopted after some pilot tests had been carried out at different strain rates. The adopted rate of shear displacement was fast enough to keep the changes in matric suction during shearing process to a minimum and to consider that the soil specimens were sheared under undrained conditions. The assumption that there was no significant change in suction of the soil specimen during the shearing stage may be a reasonable assumption because the shearing of the specimen was completed over a short period (i.e., 28 minutes). Vanapalli et al.

(2000) used similar assumption for analysis of shear strength test results on a silty soil. However, the dilation of specimen during shearing may cause an increase in matric suction and vice versa the contraction of specimen may result in suction decrease.

Like the shearing tests of saturated specimens, a total horizontal displacement of 14 mm was decided to be the end of travel of the shear box for the unsaturated specimen tests. This value was found to be adequate to mobilize the maximum shear stress. During the shearing process, the shearing force, the horizontal displacement, the vertical deformation, and the elapsed time were recorded at regular intervals of horizontal displacement of 0.20 mm and continued to a full travel of 14 mm. Once the shearing process was completed, the net normal stress was released and the specimen was extruded to measure its water content. Furthermore, after preparing and air-drying the soil specimens inside the shear box, the water content of each specimen was monitored before testing and after that by weighing the whole specimen and the shear box. The changes in water contents of the specimens during preparing and testing stages were found very small and could be neglected.

3.4.9.6. Calculations of unsaturated shear strength functions

Similar to the saturated tests, the mean value of the shear stress on the shearing plane corresponding to each increment in lateral displacement was calculated by dividing the measured value of the shear force by the corresponding corrected cross sectional area of the shear box. Therefore, the shear stress versus horizontal displacement curve was plotted for each test and the shear strength was defined as the peak or maximum shear stress. For each test, a graph showing the vertical deformation of the specimen against the horizontal displacement was plotted, and the values of deformation and displacement corresponding to the peak shear stress were defined. The void ratio of the specimen at failure, the volumetric water content, and the degree of saturation can be calculated based on the initial condition of the specimen (total volume, dry mass, particles density), the measured water content at failure, and the vertical deformation at failure.

The matric suction values of the sheared soil specimens corresponding to different values of water content were evaluated from the stress-dependent soil-water

characteristic curves (SD-SWCCs) data. The SD-SWCCs were found for specimens identical to those used for shear strength tests. The SD-SWCCs were represented mathematically by using Fredlund and Xing (1994)'s model. The reverse form of this model, which describes the matric suction as a function to the gravimetric water content, was incorporated with the shear strength data to describe the shear strength as a function to matric suction. Fredlund and Xing (1994)'s reverse model can be written as follows:

$$\psi(w) = a \left[e^{\left(\frac{w_s}{w}\right)^{\frac{1}{m}}} - e \right]^{\frac{1}{n}} \quad 3.19$$

where $\psi(w)$ is the specimen matric suction as a function to gravimetric water content; w is the gravimetric water content; w_s is the saturated water content; and a , n , and m are fitting parameters related to the SD-SWCC under consideration. The character e is the base of the natural logarithm. However, the correction function $F(\psi)$ in Fredlund and Xing (1994)'s model was taken equal to one since the values of matric suction were relatively low.

The contribution of matric suction to the shear strength, τ_s , was calculated for each test as the peak shear stress at failure minus the saturated shear strength of that specimen. The values of the saturated shear strength for different sand-gypsum mixtures were measured and the values of the effective shear parameters (c' , ϕ') were determined as stated in Section 3.4.8 .

As reviewed in Section 2.3.2, there are three main approaches to evaluate the stress state and then the shear strength in unsaturated soils. These approaches are the single stress-state variable approach proposed by Bishop (1959), the two stress-state variable approach proposed by Fredlund and Morgenstern (1977), and the true effective stress concept introduced by Lu and Likos (2006). Referring to these three approaches and considering the values of the estimated matric suction (ψ) and its contribution to shear strength (τ_s), the internal friction angle related to matric suction (ϕ^b), the effective stress parameter (χ), the suction stress (σ'_s), and the true effective stress (σ'') were calculated as follows:

$$\tan \phi^b = \frac{\tau_s}{\psi} \quad 3.20$$

$$\chi = \frac{\tan \phi^b}{\tan \phi'} \quad 3.21$$

$$\sigma'_s = -\frac{\tau_s}{\tan \phi'} = -\chi \psi \quad 3.22$$

$$\sigma'' = \frac{\tau_f}{\tan \phi'} \quad \text{where} \quad \sigma'' = (\sigma - u_a) - \sigma'_s + \sigma_{co} \quad 3.23$$

$$\sigma_{co} = c' / \tan \phi' \quad 3.24$$

where τ_f is the bulk shear strength on failure plane at failure; $(\sigma - u_a)$ is the net normal stress; σ_{co} is the tensile strength of soil at saturation; c' and ϕ' are the saturated cohesion and friction angle, respectively.

Consequently, for each sand gypsum mixture, the following series of plots were constructed:

- (i) The failure envelopes in the plane of shear stress-net normal stress corresponding to different water contents or different matric suctions.
- (ii) The failure envelopes in the plane of shear stress-matric suction corresponding to different levels of applied net normal stress.
- (iii) The failure envelopes in the plane of shear stress-water content corresponding to different levels of applied net normal stress.
- (iv) The suction stress characteristic curves as a function to water content corresponding to different levels of applied net normal stress.

The detailed results of the shear strength tests carried out on unsaturated specimens and their discussion are presented in Chapter 8.

CHAPTER FOUR

MODIFIED DEVICE FOR MEASURING TWO STRESS DEPENDENT-UNSATURATED HYDRAULIC FUNCTIONS

4.1. Introduction

Water flow and retention in unsaturated soil zones is of fundamental importance to analyse many engineering problems. This is primarily characterised through the soil-water characteristic curve (SWCC) and the hydraulic conductivity function (HCF). Among the state parameters that influence these two key functions is the surcharge load. Thus, it is necessary to simulate the stress state of the field when the hydraulic characteristics have to be determined for a certain soil in the laboratory.

The primary objective of this chapter is to introduce a newly modified device for establishing the drying and the wetting stress-dependent soil-water characteristic curves (SD-SWCCs) simultaneously with the stress dependent-hydraulic conductivity functions (SD-HCFs), as well as, the scanning curves. This chapter also presents the experimental programme which was carried out by using the newly modified device. Laboratory tests were carried out on the silty clayey sand with different gypsum additives to examine the effect of gypsum content on the hydraulic characteristics under different loading conditions (different net normal stress levels and different matric suctions). As a second objective of these tests was to demonstrate the reliability and precision of the modified device in measuring the main hydraulic functions of unsaturated soils.

4.2. The modified stress controllable pressure plate device

4.2.1. Background

There are different types of pressure plate devices having different features, specifications, and arrangements. Among those that have some relevant features to the newly developed device are: (1) Tempe pressure cells which are used to determine the drying SWCC only, under zero net normal stress, over a range of matric suction from 0 to 100 kPa (Fredlund and Rahardjo, 1993; Lu and Likos, 2004; Yang et al., 2004; Soil Moisture Corp., 2008), (2) the volumetric pressure plate extractor which can be applied to establish the SWCCs associated with both drying and wetting processes in a range of matric suction from 0 to 200 kPa, without applying net normal stress (Soilmoisture Equipment Corp., 2008; Fredlund and Rahardjo, 1993; ASTM D 6836-02; Ng and Menzies, 2007), (3) the stress-controllable volumetric pressure plate which was developed by Ng and Pang (2000) to establish the stress-dependent soil-water characteristic curves (SD-SWCCs) in both drying and wetting processes over a range of matric suction from 0 to 200 kPa, and (4) Fredlund SWCC device that is used to measure the SD-SWCCs under both drying and wetting processes in a range of matric suction from 0 to 1500 kPa (Padilla et al., 2005).

The procedure adopted with the using of the above mentioned devices is to measure the water contents of the soil specimen at different matric suctions by monitoring the volume of expelled water/intake water from/into the soil specimen by using some hysteresis attachments. As an exception of that are the Tempe cells where the water content of the soil specimen is monitored periodically by weighing the entire apparatus to find the amount of water mass lost due to pore water drainage.

4.2.2. Uses and features of the modified device

The newly modified device consists primarily from stress controllable pressure plate cells connected to a pressurized air panel to apply the desired net normal stress and matric suction values. The device can be used to measure conveniently and efficiently the drying and the wetting hydraulic characteristic functions that include the SD-SWCCs and SD-HCFs at various vertical stress levels under K_0 condition. Thus, the field overburden pressure can be simulated to some extent. The desired

vertical stress is applied pneumatically inside the cell without the need to a loading frame machine, and this reduces greatly both the cost and the laboratory space required. Furthermore, the use of an internal pneumatic system to apply the required normal stress skips over the need of using O-rings around a loading shaft and the problems associated with that, like friction and possible leakage of pressurized air. Single soil specimen is used to obtain the drying and the wetting SD-SWCCs with any number of data points. The volume of diffused air can be measured and removed simply, quickly, and efficiently. A periodic determination of specimen water content during the test is readily and very accurately determined with an accuracy of 0.01% without dismantling the device during testing. The released or absorbed water from the specimen is measured by weighing the overall cell and monitoring the differences in consequent weights. Thus, there is no need to use volume indicator burettes to monitor the inflow or outflow volumes of water. Consequently, there is no evaporation problem from the retained water in the attached outflow/inflow system, such as that usually associated with the use of volumetric pressure plates, especially during long term tests.

The high accuracy with which water removal and uptake from or into the specimen can be measured make the device suitable to measure the unsaturated hydraulic conductivity function (HCF) of soils, in both drying and wetting paths, under different levels of net normal stress by following the transient multistep methods. The measurements of HCFs can be carried out in conjunction with the determination of SWCCs. Furthermore, the device has the flexibility to be used also to measure the matric suction of a soil specimen at certain water content by using null type technique. Water level in a simple outlet tube is monitored to detect and prevent water content change by varying the applied matric suction until approaching the soil matric suction.

4.2.3. Design and construction details

The device set up of a number of identical modified pressure plate cells connected to one air pressure panel. Thus, several soil specimens may be tested at the same time within a small laboratory space. A photograph of the device experimental

setup is shown in Figure 4.1 and a photograph of disassembled cell is shown in Figure 4.2.

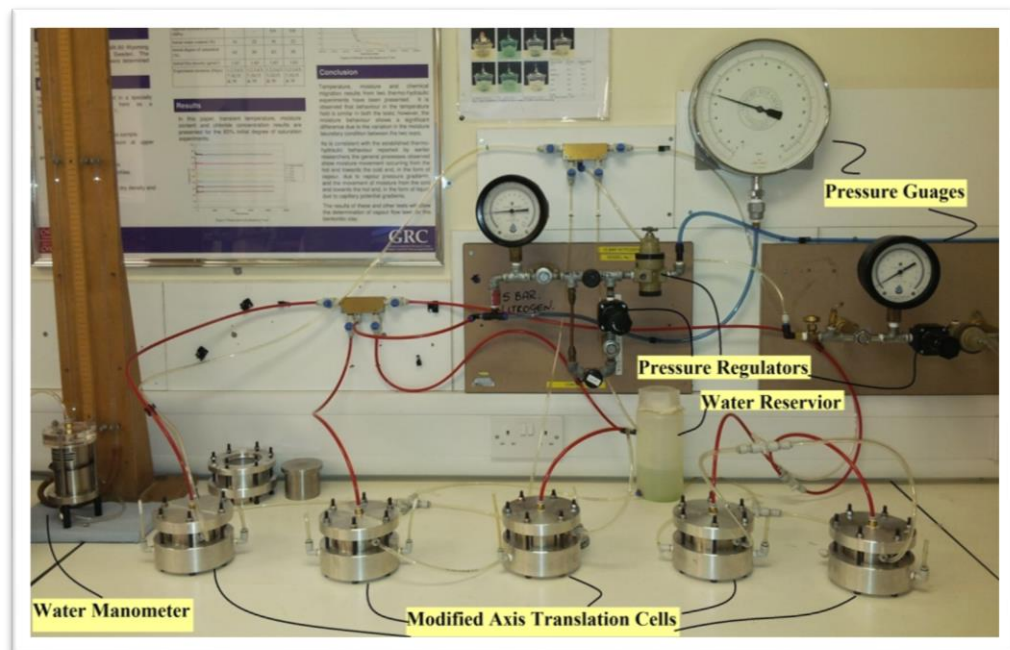


Figure 4.1. A photograph of experimental setup of the modified device.

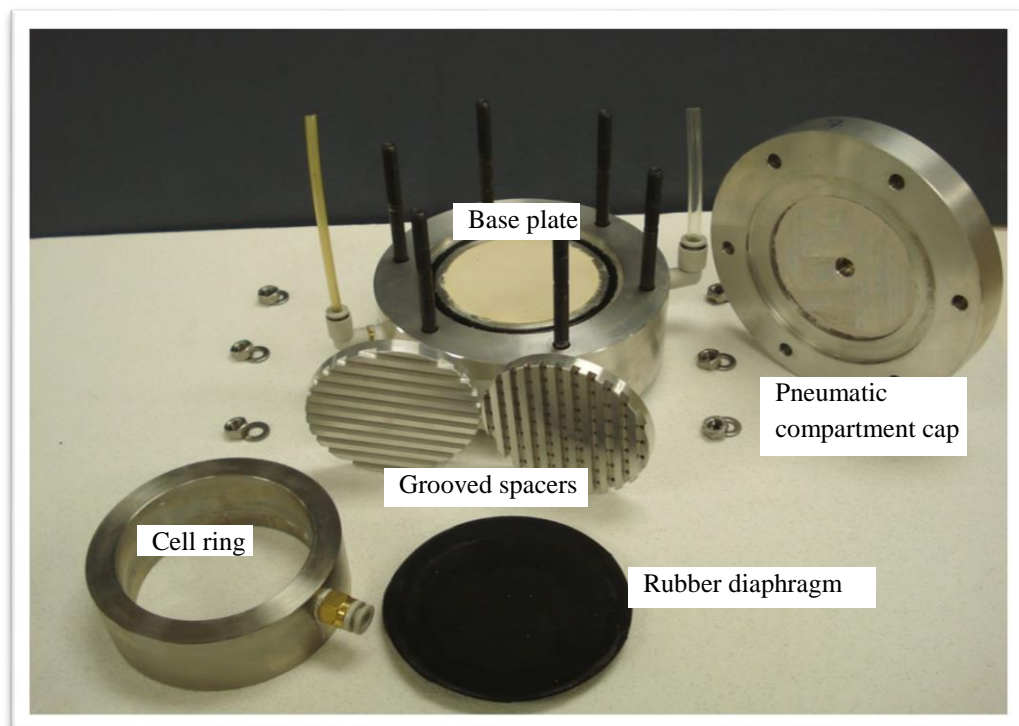


Figure 4.2. A photograph of disassembled modified cell.

The primary components of the modified cell are base plate with porous ceramic disc, cell ring, dual grooved spacers, and pneumatic compartment cap. All these components were machined from 7075 Aluminium alloy, that posses adequate strength and light weight, except the cell ring which was machined from stainless steel. The details of each of the primary components of the cell, the cell assemblage, and the pressurized air panel are presented in the following subsections.

4.2.3.1. The base plate of the cell

The base plate has an outer diameter of 127 mm and an overall thickness of 40 mm as shown through the mechanical drawings presented in Figure 4.3. It contains a recess of 10.9 mm in depth and a spiral grooved water reservoir in a circular area of 66.2 mm in diameter, see Figure 4.4.

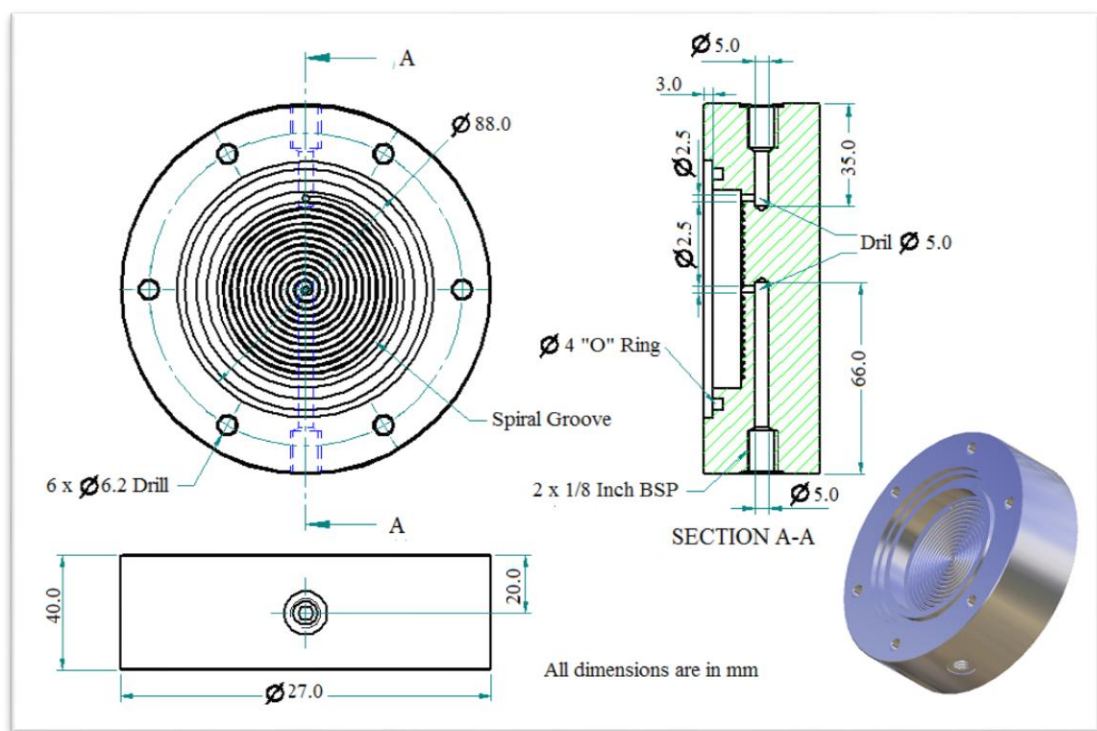


Figure 4.3. Mechanical drawings of the base plate of the modified cell.

The spiral groove has a semi-circular section of 3 mm wide and 2 mm in depth. A 5-bar ceramic disc, 66 mm in diameter and 11 mm in thickness, has been carefully ground and fitted into the recess so that there is a minimum space for entrapment of air. The fine space between the peripheral edge of the ceramic disc and the wall of the recess was filled carefully by epoxy with an attention to avoid any air voids

which may be formed while placing the epoxy as such voids would weaken the bond. The top surface of the ceramic disc was finished above the inner surrounded surface of the base plate by 0.1 mm.

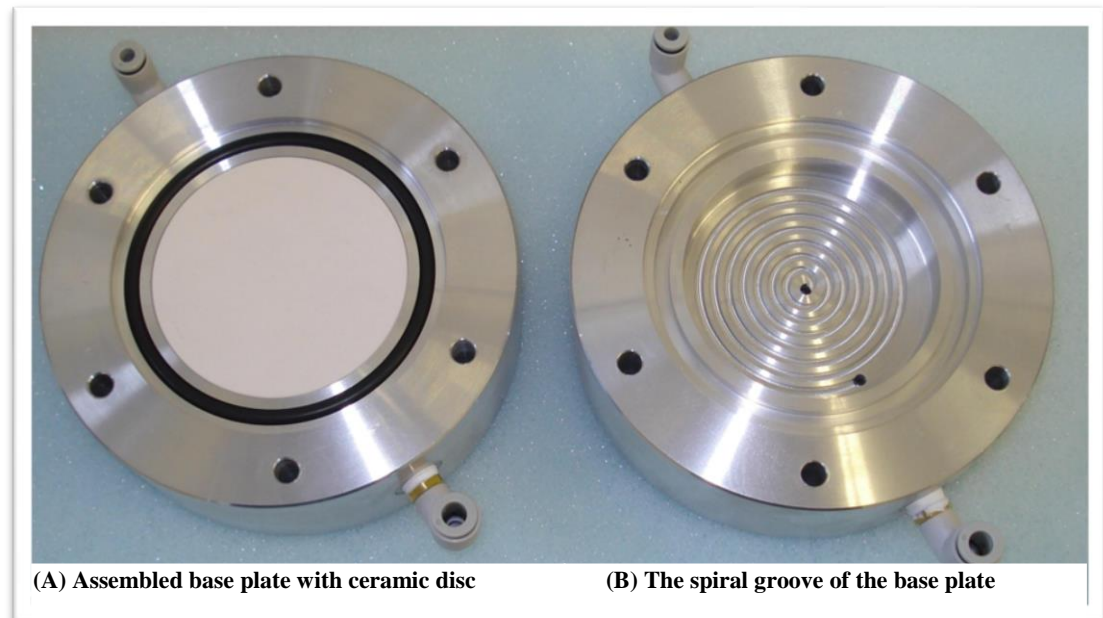


Figure 4.4. A photograph showing the base plate of the modified cell, (A) with the ceramic disc, (B) before installing the ceramic disc.

The spiral water channel makes the flushing of air bubbles so efficient since the flow of water is forced to move in one direction during flushing starting from the edge of the spiral and ending at the centre of the spiral and vice versa. The spiral design avoids the dead end water channels and this minimises the possibility of air bubbles entrapment. This spiral grooves provide a channel for the outflow/inflow of water from the extractor to two outlet tubes located on opposite sides of the base plate, or vice versa.

4.2.3.2. The cell ring

The cell ring has been designed to be the cell body as well as the soil specimen ring concurrently. It is firstly used as a part of a compaction mould to prepare the soil specimen inside it by static compaction, and then it is brought with the specimen to form the cell body. It has an inside diameter of 68 mm, wall thickness of 10 mm, and a height of 30 mm, see Figures 4.2 and 4.6. The height of the ring was designed to contain a soil specimen of 14 mm thickness and two grooved spacer discs of 8.5 mm

thickness each, so that the top surface of the spacers is finished above the edge of the ring by 1 mm. The ring has a side air inlet fitting to provide the soil specimen with the desired regulated air pressure. The base plate was designed in such a way that the specimen ring fits snugly into a recess of 3 mm depth and 88 mm in diameter. The specimen ring is sealed to the base plate by an "O" ring sits in a groove at the bottom of the recess, and it is sealed to the top cap when assembled by a flat rubber diaphragm that is primarily used for the purpose of applying the required normal stress pneumatically. The seals assure a reliable pressure seal requiring only gentle screwing of the clamping bolts.

In this design, the soil specimen covers the whole surface area of the ceramic disc, i.e., there is no exposed area of ceramic disc in contact directly to the pressurized air of the cell, which may have some effect on water phase continuity as indicated recently by some researches such as Leong et al.(2011) and Power et al. (2011). As well as, the soil specimen occupies the whole inside volume of the cell, and then there is no need to additional attachments such as vapour saturator to saturate the inflow air with the aim of preventing the soil from drying by evaporation.

4.2.3.3. The dual grooved spacers

The dual grooved spacers have been designed to provide two important functions. These functions are: to pass on and distribute the air pressure over the whole specimen surface area; and to transmit the total normal pressure from the pneumatic compartment to the soil specimen. These spacer discs were machined with a diameter of 67.5 mm and a thickness of 8.5 mm as shown through the mechanical drawings presented in Figure 4.5. They have rectangular section grooves of 3 x 3 mm, spaced on each other by 3 mm.

The spacers are placed above the soil specimen with the grooved surfaces face each other to form together a grid of air flow channels. The air inlet was positioned on the cell ring to be in front of the cross section of these channels. In such a way, the pressurized air could enter from the side inlet, distributed through the air channels, and percolated to the voids of the specimen through numerous openings (2

mm in diameter) dispersed on the bottom spacer which is in contact to the soil specimen. An isometric assemblage of the cell component is shown in Figure 4.6.

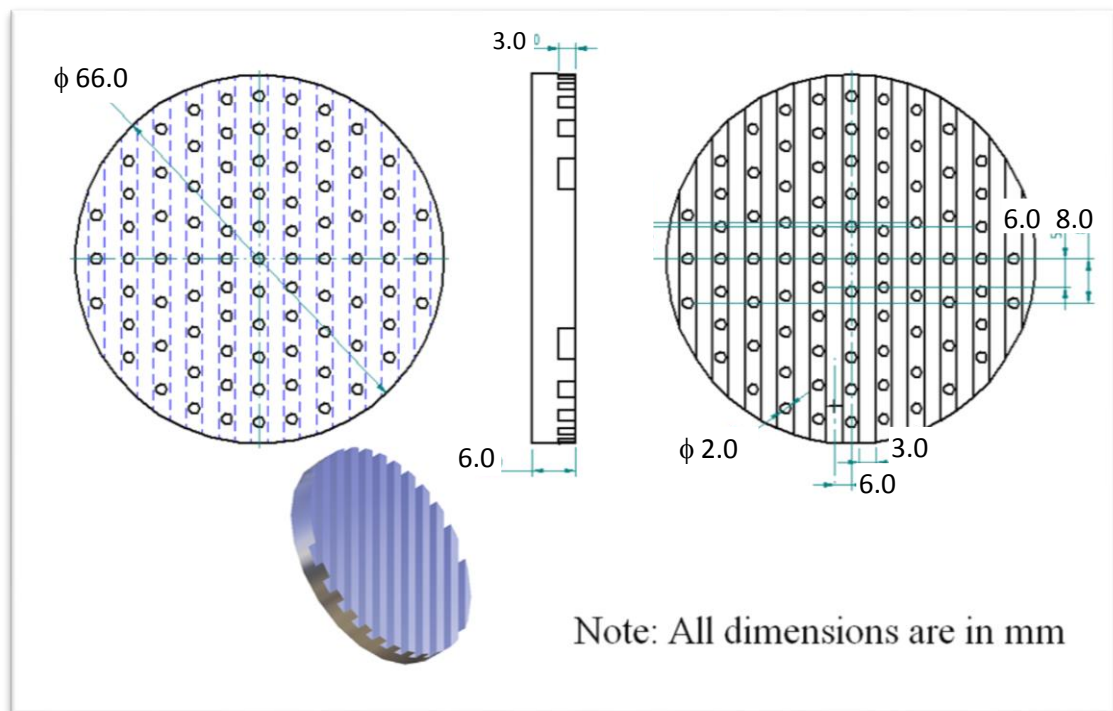


Figure 4.5. The mechanical drawings of the grooved spacers used with the modified stress controllable pressure plate cell.

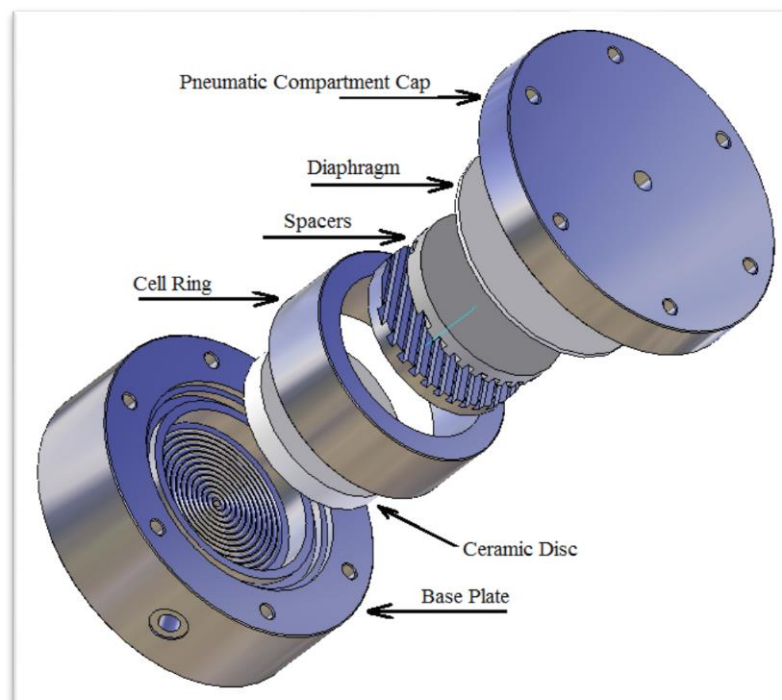


Figure 4.6. Isometric assemblage of the basic components of the modified cell.

4.2.3.4. The pneumatic compartment cap

The pneumatic compartment cap was designed to serve as the top cap for the pressure plate cell as well as to provide the desired normal pressure to the top of the dual spacers. It consists of two parts, a cap containing a small air compartment and a flexible rubber diaphragm. The outer diameter of the cap is 127 mm and the thickness is 18 mm as shown through the mechanical drawings in Figure 4.7. It has two concentric recesses of 3 mm depth each. The diameter of the outer recess is 88 mm while the inner one is 68 mm. The cap has an air inlet fitting in its centre to supply the pressurized air to the inner compartment, and then the pressure transfers through the flexible rubber diaphragm to the dual spacers, which in turn transfer the pressure to the soil specimen.

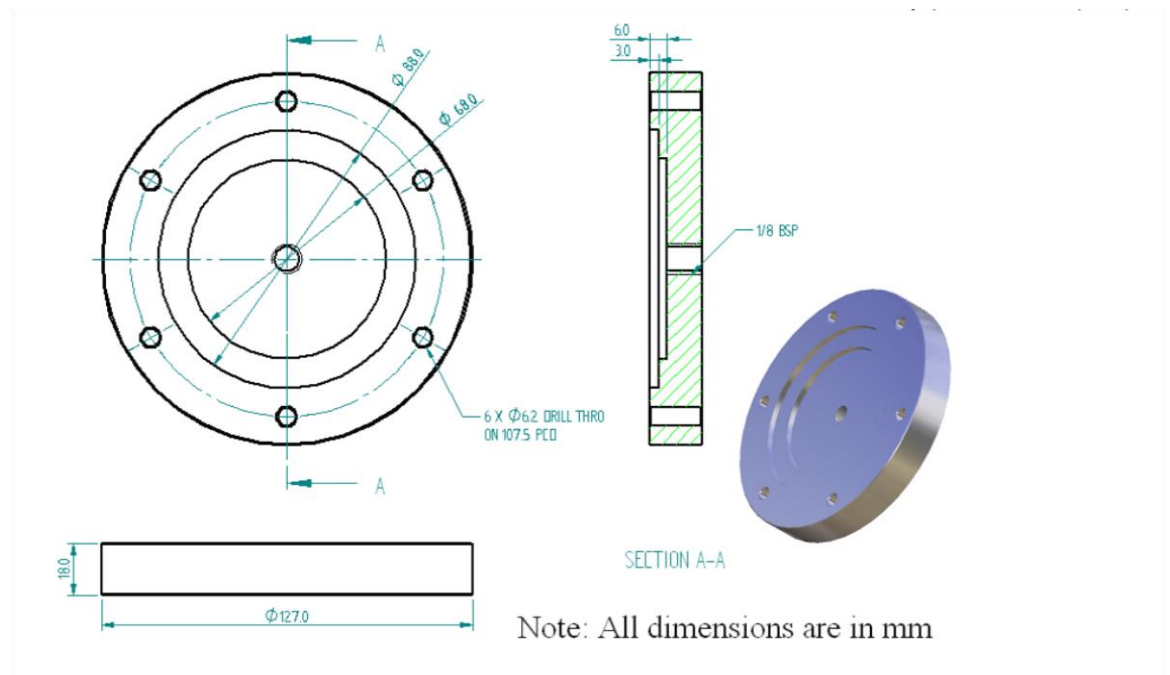


Figure 4.7. Mechanical drawings of the pneumatic compartment cap of the modified cell.

To ensure the acting of air pressure on the total area of the dual spacers and to ensure also that there is no any resistance to the transmission of air pressure through the rubber diaphragm, the dual spacers were designed to be finished above the edge of the cell ring by one millimetre so that the rubber diaphragm is placed to be concaved upward by one millimetre. A schematic section of assembled cell is shown in Figure 4.8.

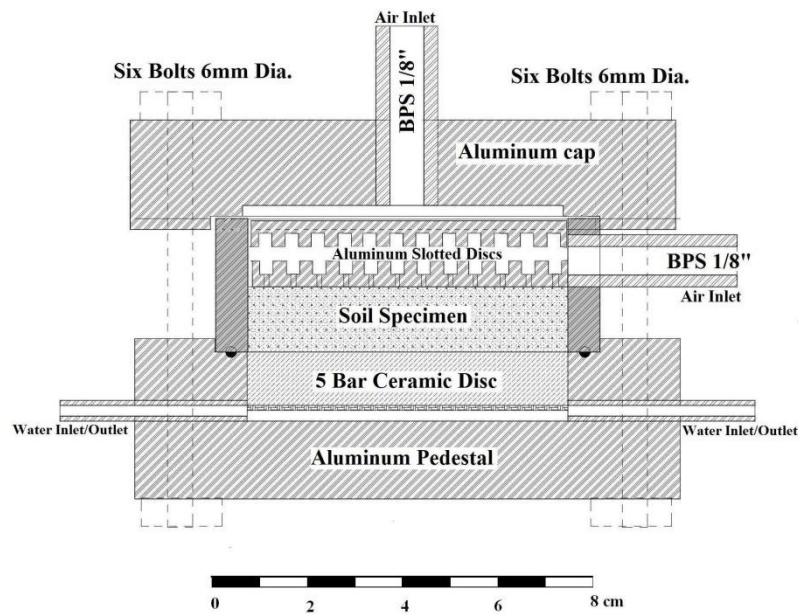


Figure 4.8. Schematic section of modified stress controllable pressure plate cell.

4.2.3.5. The cell assemblage

Six bolts, 6 mm in diameter each, are used to assemble the cell parts. The cell has two air inlets, a side inlet to supply the desired pore air pressure to the soil specimen, and another one located on the centre of the top cap to supply the desired total normal stress on the soil specimen. The difference between the top inlet pressure and the side inlet pressure is the net normal stress applied on the soil specimen. On the other hand, each cell has two outlet/inlet water fittings attached to its water compartment. During testing, one of these fittings is used for diffused air flushing, while the other one is connected to a small water reservoir which has a constant water level adjusted to the same level of the soil-ceramic disc interface.

4.2.3.6. The pressurized air panel

The pressurized air panel contains two main lines; one feeds the pore air pressure inlets of the cells, and the other feeds the total normal pressure inlets of the cells (Figure 4.1). Each pressure line comprises dual pressure regulators and dual pressure gauges for precise control and measurement of air pressure in both low and high values. The opinion from the use of dual pressure regulation was to eliminate the variations in the supplied air pressure values, where high accuracy is desired.

This was achieved simply by using two regulators in series. The first regulator is set at a fairly higher pressure than the second one in order to provide reasonably constant pressure to the second regulator. Pressure from the second regulator in turn could be very constant with source pressure variations greatly diminished. The pressurized air is supplied to the device through a laboratory supply line which delivers pressure up to 700 kPa. If higher air pressure is needed, a bottled nitrogen gas may be used to apply pressures up to 1500 kPa.

For measuring air pressure values less than 10 kPa, a simple water manometer was modified and connected in parallel with the pressure gauges for fine readings. The manometer consists from a cell and a stand pipe fixed on gradual board for water head measurements. The cell includes a base plate, water compartment, flexible diaphragm, air compartment, and top cap. Figure 4.9 shows a photograph of disassembled and assembled cell.



Figure 4.9. A photograph of disassembled and assembled manometer cell.

Stainless steel cylinders, 51 mm internal diameter and 46 mm height, were used as water and air compartments. A funnel shape flexible diaphragm was used to separate these compartments. The water compartment is sealed to the base plate by means of "O" ring sits in a groove in the base plate. The base plate has an outlet water fitting connected to the stand pipe. The air compartment is also sealed to the

top plate by an "O" ring. The top plate is connected to the air pressure manifold through a plastic tube as shown in Figure 4.1.

4.2.4. Specimen preparation and testing procedures

4.2.4.1. Specimen compaction and saturation

The test procedure starts as with the other pressure plate methods, by preparing the specimen inside the cell ring. The specimen is statically compacted to the specified volume, predefined dry density, and predefined compaction water content by using a compaction mould designed specially to be compatible with the newly modified stress controllable pressure plate device.

The mechanical drawings of the compaction mould are presented in Figure 4.10. The components of the compaction mould and their assembly are shown in Figure 4.11. A loading frame machine is used to apply the required static load with a constant displacement rate of 0.2 mm/min.

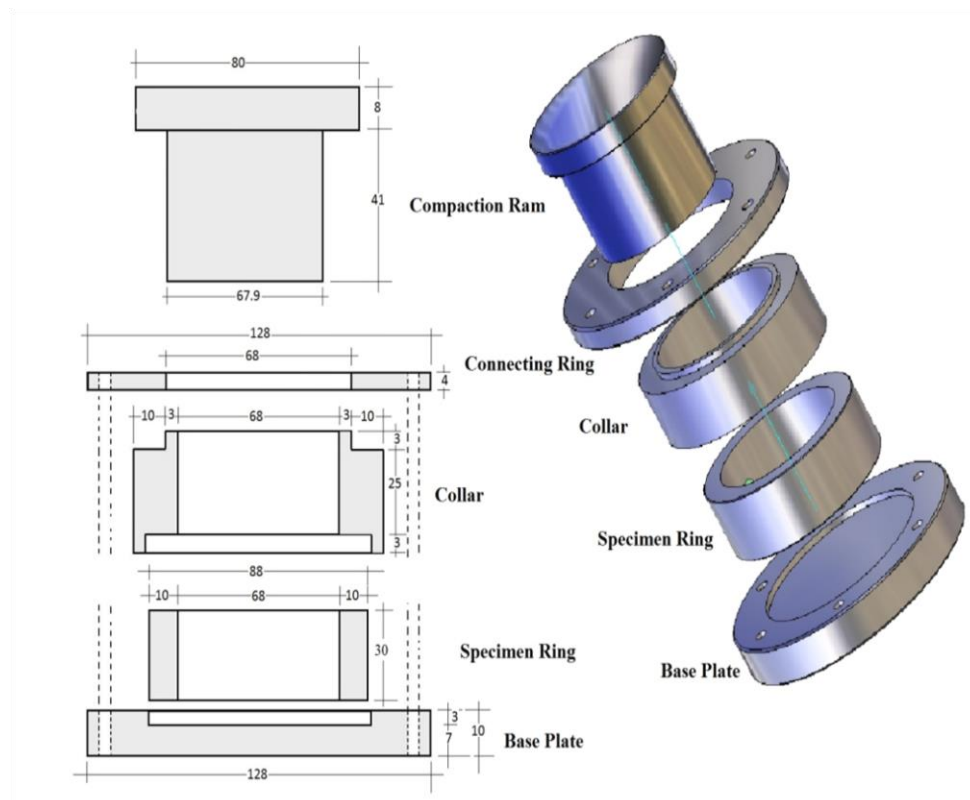


Figure 4.10. The mechanical drawings of compaction mould compatible with specimen ring of the modified device.

The cell ring containing the prepared specimen is placed subsequently on the top of the saturated ceramic disc for saturation. The cell is assembled whereas one of the water inlet tubes is attached to the water reservoir for water intake. The level of water in the reservoir is adjusted to be at the same level of the soil-ceramic disc interface. During the saturation process, the entire cell is weighed periodically until reaches a constant weight at the completion of saturation. Before any weighing process, all the inlet/outlet tubes of the cell are disconnected and the water level in the stand pipes is adjusted to a certain level mark. This is usually done by adding some drops of water to one of the stand pipes using a syringe.

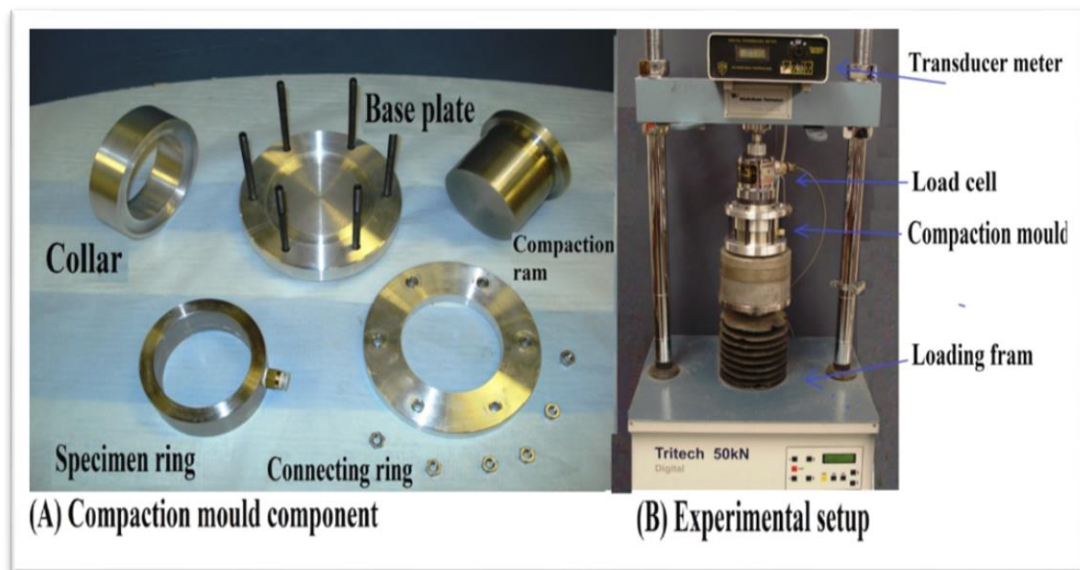


Figure 4.11. A photograph showing; (a) the compaction mould components, (b) the compaction setup.

4.2.4.2. Testing procedure for SD-SWCCs determination

After saturating the soil specimen, the desired normal stress (σ) is applied pneumatically so that the pore water starts to drain under consolidation process and the entire cell weight reduces until reaches a constant value at the end of consolidation. Subsequently, the air pressure inside the cell (u_a) is raised to apply the desired increment of matric suction. Simultaneously, the normal stress should be increased to keep the difference ($\sigma - u_a$) constant, which is equal to the applied net normal stress. When the equilibrium water content of the soil specimen is reached, air bubbles below the ceramic plate is removed first and then the entire cell is weighed to find the amount of water mass lost due to pore water drainage. The equilibrium water content can be calculated by considering the saturated cell weight,

the prepared dry weight of soil specimen, and the entire weight of the cell at equilibrium point. The weight process may then be repeated at successive water content equilibrium points corresponding to successive increments of matric suction. The differences in weight from one soil suction value to another are measured, and then the corresponding water contents are calculated.

Upon completion of the drying process, the test can be continued with the wetting process by successive decrements in matric suction, and this causes water to flow back from the water reservoir to the soil specimen. At the end of the run after the last equilibrium value has been established, the water content of the whole specimen is determined gravimetrically. Depending on the final water content, water contents corresponding to different equilibrium points can be back-calculated by considering the changes in the entire weight readings between successive values of matric suction reversibly.

The drying and the wetting SD-SWCCs can be constructed depending on the equilibrium water content values calculated from the initial water content or final water content. Slight differences between these two sets of water contents may be found when there are some water drops condense on the spacers placed above the soil specimen. This condensation usually makes values calculated from initial water content seem greater than those calculated from final water content. To eliminate the condensation on the inside cell parts, the test is conducted in a temperature-controlled laboratory room.

4.2.4.3. Testing procedure for SD-HCF determination

The measuring of unsaturated hydraulic conductivity function can be carried out simultaneously with the determination of the soil-water characteristic curve in both the drying and the wetting processes under different applied net normal stress levels. During the application of each increment in matric suction, the time-dependent decrease in weight of the specimen is monitored, and then the accumulative outflow volume of water from the specimen with time can be found. Similarly, during the wetting process, the time-dependent increase in weight of the specimen during each decrement in matric suction is monitored and, therefore, the accumulative inflow volume of water with time is determined.

As introduced in Section 3.4.7, two of the transient outflow methods are suitable to be applied in measuring the unsaturated SD-HCF by using the newly modified stress controllable pressure plate device. These methods are the multistep method (Gardner, 1956) and the one step method (Doering, 1965). The multistep method needs periodic monitoring of the specimen weight throughout the whole matric suction step. Time steps of 2, 4, 8, 24, 48, 96 hours, and the final reading at equalization time were found to be appropriate for the tested specimens.

Doering's one step method was modified in this study to be applied in successive increments, or decrements, in matric suction and considering each of these increments as a one small step. In other words, a series of steps in matric suction were applied instead of applying one large step throughout the whole test as specified in the original method. Following this modified approach, only once the weight of the specimen has to be taken during each matric suction increment, or decrement, beside the final specimen weight at equalization. This reading was suggested to be taken after 4 hours from the applying of suction increment or decrement. This time was chosen to be at the second stage of the flow stages, i.e., when the soil permeability is controlling the flow, not the saturated permeability of the ceramic plate, see Section 2.5.5.

Unlike the original Doering's one step approach, the use of one step method with the above modification yields the soil-water characteristic curve simultaneously, while in the original method the SWCC has to be determined independently. Moreover, one of the disadvantages of the original one step method is the large initial hydraulic gradient associated with applying one large step in matric suction. This large gradient varies considerably throughout the test and may causes significant changes in the state of stress of soil specimen during the test. This disadvantage is avoided in the modified approach when series of small suction steps are applied successively instead of one large step.

4.2.4.4. Diffused air removal

Unlike the standard and modified volumetric pressure plate devices, the remove of air bubbles here is carried out in a very simple, swift, and efficient manner. A syringe of de-aired water is injected from one of the outlet/inlet tubes, and this lets

water to circulate through the spiral groove beneath the ceramic disc, carries the air bubbles in its advance, and seeps out from the other outlet tube toward the attached water reservoir. The difference in weight of the entire cell before and after flushing of air bubbles represents the weight of water that replaces the volume which is occupied by air bubbles. Thus, the volume of diffused air through the ceramic disc could be evaluated readily.

The simplicity and reliability of this flushing technique results from the fact that the measurements of water content differences, at successive equilibrium points, are related directly to the differences in the weight of water inside the soil specimen not to the volume or weight of water in an outside measuring system. In other words, in this device, the weight or volume of water in the water compartment and the stand pipes is kept constant throughout the entire test. The water level in the stand pipes has to be adjusted simply to a certain level mark at each weight reading. Thus, there are no any constraints arise from the necessity to retain accurately and measure the weight or volume of water expelled from the soil specimen during each increment in matric suction or the returned water during each decrement in matric suction. Moreover, there is no concern about the amount of evaporation from the outside water system whatever the testing duration is, since that does not affect the water content measurements. On the contrary, in all volumetric pressure plate devices, the evaporation of water from the open ends of the burettes and the ballast tube especially in long run tests affects significantly the determination of water content at different equalization points if it is not estimated and taken into consideration.

4.3. Testing programme

The testing programme was undertaken primarily to study the effect of gypsum content on the two key hydraulic characteristic functions, the soil-water characteristic curve and the unsaturated hydraulic conductivity function of the sandy soil. These two functions were studied during both drying and wetting processes under the influence of different net normal stress levels by using the newly modified stress controllable pressure plate device. The second objective was to use the SD-SWCCs data in conjunction with the results of constant water content-direct shear tests which were carried out on air-dried specimens. Thus, the matric suction values of the

unsaturated sheared specimens can be defined, and then the significant shear parameters can be evaluated.

The third objective of the testing programme was to demonstrate the repeatability and reliability of the newly modified device in measuring the SD-SWCCs and the SD-HCFs during both drying and wetting processes. Thus, the testing programme contains implicitly two parts, SD-SWCCs tests and SD-HCFs tests. These two parts were carried out simultaneously on the same soil specimens, under the same loading conditions.

4.3.1. SD-SWCCs tests

In total, fifty SWCCs were established for five sand-gypsum mixtures having 0, 20, 40, 65, and 80% gypsum content by weight. The drying and the wetting SWCCs for each mixture were determined under five different net normal stress levels, which were 0, 100, 200, 300, and 400 kPa. These values of net normal stress were taken to be the same of those used in the direct shear tests. The increments of applied matric suction were decided after the evaluation of different SWCCs parameters by using the results of the conventional pressure plate. These parameters are the water content and matric suction at the air-entry point and the residual point of the SWCCs. Matric suction increments of 4, 10, 20, 50, 100, 200, and 400 kPa were found to be suitable for all sand-gypsum mixtures tested. These matric suction steps were used with different levels of net normal stress, except with 400 kPa net normal stress, the maximum matric suction applied was 300 kPa since the maximum value of the air pressure source was 700 kPa. A period of approximately one week for each suction increment to reach equalization was found appropriate for all mixtures tested.

Five identical specimens from each sand-gypsum mixture were prepared by statically compacting the soil at its optimum water content to reach 90% of its maximum dry density determined from the standard compaction test. These specimens were tested under five different net normal stress levels. The initial conditions of the prepared specimens for different sand-gypsum mixtures are shown in Table 4.1.

Table 4.1. Initial conditions for specimens statically compacted from different sand-gypsum mixtures.

Term	Values				
Gypsum content %	0	20	40	65	80
Compaction water content %	9.8	9.4	9.4	11.6	14.6
Target dry density (Mg/m ³)	1.809	1.812	1.775	1.660	1.506
Initial void ratio	0.47	0.43	0.42	0.47	0.59

4.3.2. SD-HCFs tests

The SD-HCFs tests were carried out simultaneously with the SD-SWCCs tests on the same specimens under the same loading conditions. The unsaturated hydraulic conductivity function was determined for each sand-gypsum mixture under four different net normal stress levels (0, 100, 200, and 400 kPa), during both the drying and the wetting processes. In total, forty SD-HCF tests were conducted on five sand-gypsum mixtures.

4.4. Calculations

4.4.1. Calculations of SD-SWCCs

The gravimetric water content (w) at different equalization points was calculated based on the total weight of the assembled cell (W_t) at equalization, the weight of assembled saturated cell without soil specimen (W_o), and the dry weight of soil specimen (W_s). The relationship is as follows:

$$w = 100 \times \frac{(W_t - W_o - W_s)}{W_s} \quad 4.1$$

Furthermore, upon completion of test, the final water content of the specimen was determined gravimetrically. Water content values at different equalization points were back-calculated by considering the final water content in conjunction with the incremental differences in the total weight of the cell. From these two sets of water content data, the condensation of water vapour on the inside faces of the grooved spacers was evaluated.

The volumetric water content (θ) at different equalization points was calculated by considering the gravimetric water content (w), specific gravity (G_s), and the void ratio of the specimen at successive equalization points (e) as follows:

$$\theta = \frac{G_s}{e + 1} w \quad 4.2$$

In general, the void ratio of soil specimen at different equalization points could be evaluated by considering: (i) the initial void ratio of the specimen after saturation and consolidation under the applied net normal stress, (ii) the decrease in void ratio resulting from the drying process, and this can be evaluated from CLOD test results.

During the SD-SWCC tests of different sand-gypsum mixtures, it was noticed that both the radial and vertical volume changes of the soil specimens due to the application of matric suction steps were of negligible values. This behaviour can be attributed to the reason that the initial void ratio of these specimens after consolidation under the applied net normal stress levels was small enough that the application of the matric suction steps could not decrease the void ratio noticeably. Accordingly, the initial void ratio after consolidation was considered to be constant under different applied matric suctions, for all sand-gypsum mixtures tested.

The initial void ratio of a statically compacted specimen may be calculated using the mass-volume relationships. During specimen saturation some dilation to the specimen is usually occurred, and the corresponding void ratio can be defined based on the saturated water content of the specimen. After applying the desired net normal stress, the void ratio decreases due to normal consolidation. This decrease can be evaluated from the decreasing in the saturated water content which is continuously monitored by taking the overall weight of the cell.

The results of SD-SWCCs in terms of gravimetric water content were mathematically described by using Fredlund and Xing (1994)'s model, Equation 3.3. Furthermore the matric suction was described as a function to the water content by using the reversed form of Fredlund and Xing (1994)'s model as follows:

$$\psi = a[e^{(\frac{w_s}{w})^{\frac{1}{m}}} - e]^{1/n} \quad 4.3$$

where ψ is the matric suction, w is the gravimetric water content at any soil suction, w_s is the saturated water content, e is the base of the natural logarithm, whereas a , n , and m are fitting parameters related to the SD-SWCC under consideration. The reversed form of the SD-SWCC was very useful when it has been used in conjunction with the direct shear tests to describe many shear strength functions.

4.4.2. Calculations of SD-HCFs

The transient outflow/inflow data of the SD-HCF tests were analysed by following two different methods. These methods are the original multistep method (Gardner, 1956) and the one step method (Doering, 1965). To establish the SD-HCF, seven incremental matric steps were applied during the drying process and seven decrements during the wetting process. The hydraulic conductivity (k) was calculated for each suction increment or decrement to define one point on the SD-HCF under consideration. The calculated hydraulic conductivity was considered to be corresponding to the mean value of matric suction or water content over the applied suction increment or decrement. The relationship between matric suction and water content was assumed linear throughout small suction steps in both the multistep and the one step methods (Gardner, 1956; Doering, 1965).

During each suction step, the time-dependent weight of the specimen was monitored, and the corresponding gravimetric water contents were simply calculated by using Equation 4.1. Then, the volumetric water contents were calculated by applying Equation 4.2. Consequently, the specific moisture capacity (C), which is defined as the change in volumetric water content relative to the change in matric suction as a head (Lu and Likos, 2004), over the incremental suction step, was calculated as follows:

$$C = \Delta\theta/\Delta h \quad 4.4$$

The accumulative outflow/inflow volume of water from the specimen with time was found from the incremental differences in total weight of the cell. Therefore, Gardner's expression for cumulative outflow was applied as follows:

$$\ln\left(\frac{V_f - V_t}{V_f}\right) = \ln\left(\frac{8}{\pi^2}\right) - \left(\frac{D \cdot \pi^2}{4 L^2}\right) \cdot t \quad 4.5$$

where V_f is the total volume of water accumulated for the applied suction increment and V_t is the outflow volume during a time t , D is the hydraulic diffusivity, and L is the specimen thickness.

To calculate the hydraulic conductivity by following Gardner (1956)'s approach, a linear relationship between $\ln((V_f - V_t)/V_f)$ and the elapsed time (t) was drawn. According to Equation 4.5, the slope of this linear relationship is equal to $(D \cdot \pi^2 / 4 L^2)$. Therefore, the hydraulic diffusivity was determined and the hydraulic conductivity was calculated by using the following expression:

$$K = C \times D \quad 4.6$$

where C is the specific moisture capacity over the incremental matric step and D is the hydraulic diffusivity. The calculated K value was considered to be corresponding to the average water content during the specified matric suction increment, or corresponding to the mean matric suction of that increment, which was taken as $\psi_o + \Delta\psi/2$ where ψ_o is the matric suction before the applying of suction increment $\Delta\psi$.

Furthermore, the hydraulic conductivity was calculated by following Doering (1965)'s approach. Only one reading of the weight of the specimen cell during the suction step was used here. This value was taken usually after 3 to 5 hours from the beginning of applying the incremental suction step. From this reading, the gravimetric water content and then the volumetric water content were calculated by using Equations 4.1 and 4.2. Therefore, the hydraulic diffusivity (D) was calculated by using Doering's solution as follows:

$$D = - \frac{4L^2}{\pi^2(\theta_t - \theta_f)} \cdot \frac{\Delta\theta}{\Delta t} \quad 4.7$$

where L is the thickness of the specimen, θ_t is the volumetric water content at time t , θ_f is the volumetric water content at equilibrium, and $(\Delta\theta/\Delta t)$ is the change in volumetric water content during the elapsed time t . After calculating the hydraulic diffusivity, the hydraulic conductivity was calculated by using Equation 4.6. This value was considered to be corresponding to the average water content during the elapsed time.

To clarify and compare the calculation procedures for the above two approaches a numerical example for an incremental suction step is presented below:

Numerical Example:

A series of SD-HCF tests were carried out on silty clayey sand has 40% gypsum content. When the specimen was under 400 kPa net normal stress at K_o condition, the applied matric suction was increased from 20 to 50 kPa and the time-dependent weights of the specimen cell were taken. These readings and the basic data of the tested specimen are listed below:

Elapsed time (days)	0.00	0.17	3.06	5.05	6.01
Overall weight of the cell (g)	2764.33	2763.86	2762.21	2761.88	2761.73

Basic data of the tested specimen	Value
Specimen thickness at compaction, L (cm)	1.393
Specimen's ring diameter (cm)	6.810
Specimen's dry weight, W_s (g)	90.02
Assembled cell weight, W_o (g)	2660.71
Gypsum content (%)	40
Compacted dry density, γ_{dry} (Mg/m^3)	1.775
Void ratio of the compacted specimen, e_o	0.42
Net normal stress (kPa)	400
Overall weight of the cell at saturation under applied net normal stress, W_t (g)	2764.39

It is required to calculate the hydraulic conductivity for this incremental suction step by following the multistep and the one step methods.

Calculations:

Considering the overall weight of the cell at saturation under 400 kPa net normal stress, the assembled cell weight, the dry weight of the specimen, and the specimen

specific gravity, the saturated water content of the specimen and the corresponding void ratio are calculated to be 15.17% and 0.38, respectively. Therefore, by using the volume mass relationships and considering the time-dependent weight, the following parameters are calculated as shown:

Soil matric suction (kPa)	20				50
Elapsed time (days)	0.00	0.17	3.06	5.05	6.01
Gravimetric water content, w %	15.10	14.58	12.75	12.38	12.21
Volumetric water content, θ %	27.54	26.59	23.24	22.58	22.27
Outflow volume (cm ³)	0.00	0.47	2.12	2.45	2.60
$\ln ((V_f - V_t)/V_f)$		-0.20	-1.69	-2.85	

The specific moisture capacity (C) can be calculated by considering the volumetric water contents and the corresponding matric suction heads at the beginning and the end of the incremental step as follows:

$$C = \frac{\Delta\theta}{\Delta h} = \frac{\frac{27.54-22.27}{100}}{\frac{100(50-20)}{9.81}} = 1.7 \times 10^{-4} \text{ (cm}^{-1}\text{)}$$

To find the hydraulic diffusivity by following Gardner (1956)'s approach, the elapsed time versus $\ln ((V_f - V_t)/V_f)$ is plotted on Figure 4.12 and the line slope is defined to be (-0.54). Therefore, the hydraulic diffusivity (D) could be calculated as follows:

$$0.54 = D \cdot \pi^2 / 4 L^2$$

$$D = 0.54 \times 4 \times 1.393^2 / \pi^2 = 0.43 \text{ cm}^2/\text{day}$$

Accordingly, the hydraulic conductivity could be calculated as:

$$k = C \cdot D = 1.7 \times 10^{-4} \times 0.43 = 7.25 \times 10^{-5} \text{ cm/day} = 8.39 \times 10^{-12} \text{ m/sec.}$$

This value of hydraulic conductivity is corresponding to the average values of water content of $((15.10+12.21)/2 = 13.66 \text{ %})$ and average value of matric suction of $((20+50)/2 = 35 \text{ kPa})$ over the suction step.

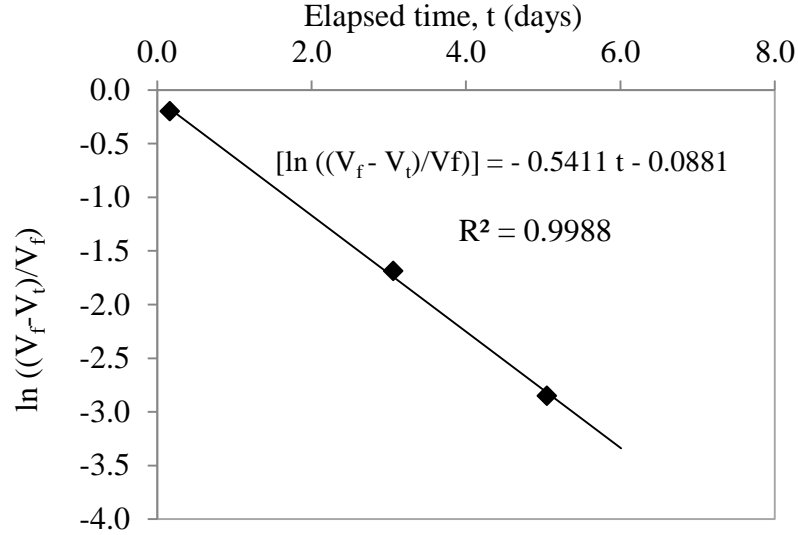


Figure 4.12. Elapsed time versus $\ln((V_f - V_t)/V_f)$ for calculating the hydraulic diffusivity according to Gardner (1956)'s approach.

Following Doering (1965)'s approach, the hydraulic diffusivity could be calculated as follows:

$$D = - \frac{4L^2}{\pi^2(\theta_t - \theta_f)} \times \frac{\Delta\theta}{\Delta t} = \frac{4 \times 1.393^2}{\pi^2(0.2659 - 0.2227)} \times \frac{(0.2754 - 0.2659)}{(0.17 - 0.0)} = 0.96 \text{ cm}^2/\text{day}$$

and then the hydraulic conductivity is:

$$k = C \cdot D = 1.7 \times 10^{-4} \times 0.96 = 1.64 \times 10^{-4} \text{ cm/day} = 1.9 \times 10^{-11} \text{ m/sec.}$$

This value of hydraulic conductivity is corresponding to the average values of water content and matric suction over the period between elapsed time 0 and 0.17 day. The matric suction at the elapsed time 0.17 can be calculated by interpolation as follows:

$$\psi_{0.17} = 20 + (50 - 20) \times \frac{(15.10 - 14.58)}{(15.10 - 12.21)} = 25.4 \text{ kPa}$$

The average values of water content and matric suction corresponding to ($k = 1.9 \times 10^{-11} \text{ m/sec}$) are $(15.10 + 14.58)/2 = 14.84 \%$ and $(20 + 25.4)/2 = 22.7 \text{ kPa}$, respectively.

4.5. Summary

The design and construction details of a modified stress controllable pressure plate device are presented in this chapter. The device is used to determine

conveniently and efficiently two important stress dependent-hydraulic characteristic functions during both drying and wetting processes. These functions are the stress-dependent soil-water characteristic curve (SD-SWCC) and the stress dependent-unsaturated hydraulic conductivity function (SD-HCF). The device has the flexibility to be used also to measure the matric suction for a given soil specimen by applying the null type technique. Several improvements have been done in the design of this device. Among these are:

- (1) The desired normal stress is applied pneumatically inside the cell without the need to a loading frame machine, and this reduces greatly both the cost and the laboratory space required.
- (2) The changes in the water content of the soil specimen corresponding to successive increments/decrements in the applied matric suction are monitored continuously by weighing precisely the whole cell without dismantling it during testing. Therefore, there is no need to an external measuring system to monitor the inflow or outflow into or from the specimen, and consequently there is no evaporation problem during long term tests.
- (3) The volume of diffused air could be measured and removed simply, quickly, and efficiently. This feature results from the use of spiral groove below the ceramic disc which forces the water to move in one direction, and this minimises the possibility of air bubbles entrapment. Furthermore, there is no any necessity to retain accurately and measure the volume of expelled or intake water in the outside water system, and this greatly simplify the flushing process.

An extensive experimental programme was designed and implemented by using the newly modified device. The SD-SWCCs and the SD-HCFs for five sand-gypsum mixtures were established at five different net normal stress levels in both the drying and the wetting processes. The testing procedures and tests calculations are presented in this chapter. The detailed results and discussion of these tests are presented in Chapters 6 and 7.

CHAPTER FIVE

RESULTS AND DISCUSSION OF BASIC TESTS

5.1. Introduction

In this chapter, the test results for standard compaction tests, one-dimensional consolidation tests, shrinkage characteristics (CLOD) tests, and three series of standard soil-water characteristic curve tests are presented. Laboratory tests were carried out on several sand-gypsum mixtures using statically compacted specimens prepared at the optimum water content to 90% of the maximum dry density obtained from the standard compaction tests. The first objective of these tests was to study the effect of gypsum content on some basic characteristics of the sandy soil by following standard approaches. The second objective was to prepare a database that includes the water retention characteristics and the volume change characteristics of several sand-gypsum mixtures. The prepared database was intended to be used in evaluating and comparing the hydraulic test results obtained from the modified stress controllable pressure plate device.

5.2. Effect of gypsum content on compaction characteristics

Eight sand-gypsum mixtures were tested using standard Proctor effort to evaluate the effect of gypsum content on the compaction characteristics of the soil used in this investigation. These mixtures had 0, 10, 20, 30, 40, 50, 65, and 80% gypsum content by weight. The compaction test results for the tested mixtures are shown in Figure 5.1. The values of optimum water content and the corresponding maximum dry density, minimum void ratio, minimum porosity, and the degree of saturation are presented in Table 5.1 for these eight mixtures.

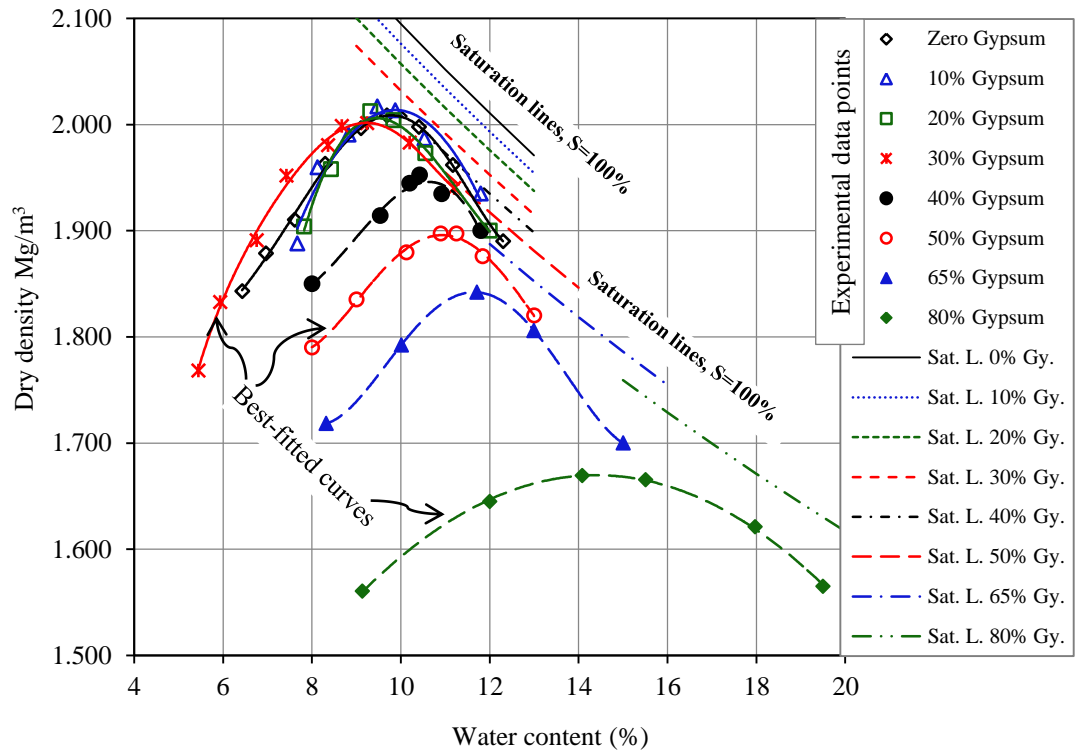


Figure 5.1. Standard compaction curves for different sand-gypsum mixtures.

Table 5.1. Compaction characteristics of the sandy soil with different gypsum additives (standard Proctor tests).

Gypsum content (%)	0	10	20	30	40	50	65	80
Max. dry density (Mg/m^3)	2.01	2.01	2.01	2.00	1.95	1.89	1.83	1.68
Optimum water content (%)	9.8	9.6	9.4	9.3	10.5	11.1	11.9	14.6
Specific gravity, G_s	2.65	2.62	2.59	2.55	2.52	2.49	2.44	2.39
Minimum void ratio, e	0.32	0.30	0.28	0.28	0.29	0.31	0.33	0.42
Minimum porosity, n (%)	24	23	22	22	23	24	25	30
Degree of saturation, S (%)	82	85	85	86	91	89	87	83

The test results presented in Figure 5.1 and Table 5.1 show that at low gypsum contents (i.e., gypsum content ranging from zero to about 30% by weight) the changes in the compaction parameters are insignificant. The effects of gypsum content on the maximum dry density and on the optimum water content are presented in Figure 5.2. It can be noticed from Figure 5.2 that there is a slight increase in the maximum dry density associated with a slight decrease in the optimum water content when gypsum content increases up to 15%. On the contrary, when gypsum content increases more than 30%, the maximum dry density starts to decrease noticeably associated with a clear increase in the optimum water content.

Similar trends have been reported by Kattab (1986) on silty gypsiferous soils and Al-Dilaimy (1989) on clayey gypsiferous soils, but the defined percentage of gypsum that results with an improvement in compaction characteristics was 5% in Al-Dilaimy's results and 15% in Kattab's results. This difference between Al-Dilaimy's and Kattab's results can be attributed to the difference in the pore size distribution of the silty soil from that of the clayey soil.

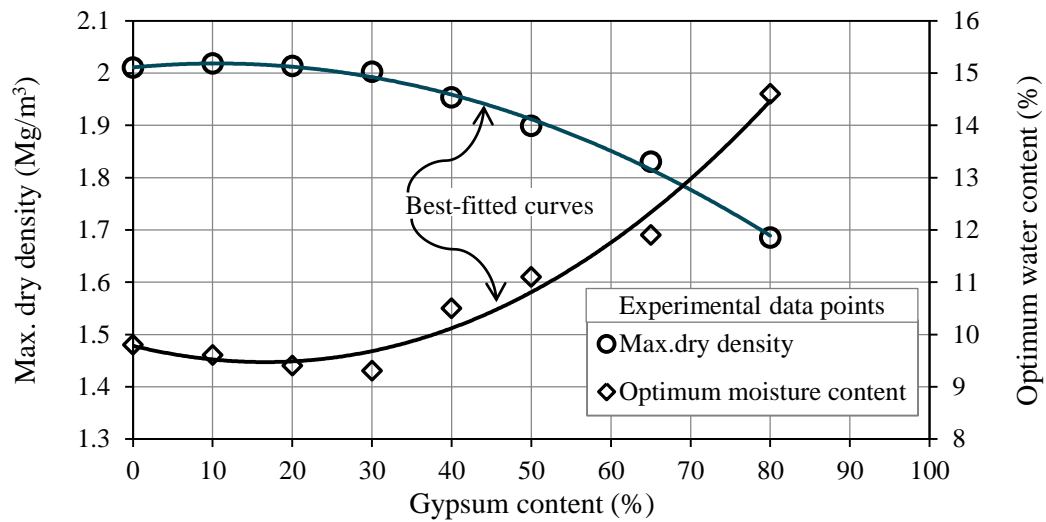


Figure 5.2. Maximum dry density and optimum water content for the soil with different percentages of gypsum.

The effect of gypsum content on compaction characteristics can be explained by visualizing the roles of gypsum in the soil matrix. Two influencing factors associated with the presence of gypsum have to be considered here. The first factor is the role of gypsum particles as a filling material to the intergranular voids of the soil matrix. This is due to the fineness of gypsum particles as described through its particle size distribution curve presented in Figure 3.1. An addition of gypsum to the sandy soil leads to improve the gradation curve of the mixture in such a manner that allows the particles to pack more closely, resulting in an increase in the maximum dry density. Furthermore, gypsum is considered susceptible to crushing during compaction, since gypsum particles are soft crystals (Section 2.2.1), and accordingly there is a possibility for gypsum to fill different void shapes. The second factor is the decrease in the overall specific gravity of the soil mixture associated with the increase in gypsum content, since the specific gravity of the sandy soil used is 2.65 while it is 2.33 for gypsum.

At low gypsum percentages (0 - 30%), the predomination was for the first factor (gypsum served as a filling material) which caused the dry density to increase with increasing gypsum content. However, further increase in gypsum content, exceeding about 30%, the second factor (effect of specific gravity) became dominant which in turn caused a clear decrease in the maximum dry density. Correspondingly, the optimum water content showed remarkable increase with increasing gypsum content. This increase can be attributed in part to the need to release the excess in capillary tension arises from the increasing of gypsum content. For particular water content, the capillary forces are expected to increase with increasing gypsum content, and this can be verified from comparing the soil-water characteristic curves of different sand-gypsum mixtures.

The main purpose of soil compaction is to pack more closely the soil particles and then reduces the air voids in order to improve the engineering properties of the soil under consideration. Thus, to circumvent over the variation in the specific gravity of the sand-gypsum mixtures with varying gypsum content, the standard compaction curves can be expressed here in terms of void ratio instead of dry density, as presented in Figure 5.3. In this representation the minimum void ratio is the analogue to the maximum dry density.

It can be noticed from Figure 5.3 that there is a clear decrease in minimum void ratio and a slight decrease in optimum water content associated with increasing gypsum content up to 30% by weight. This trend is attributed to the role of gypsum in filling the voids between sand particles. However, further increase in gypsum content, exceeding about 30%, causes gypsum particles to begin separate adjacent sand particles, resulting in an increase in the minimum void ratio. This behaviour can be attributed to the fact that at a certain packing array, uniform fine particles like gypsum have void ratio greater than a coarser graded particles like the sandy soil used.

The minimum void ratio, minimum porosity, and the degree of saturation corresponding to the maximum compaction for different sand-gypsum mixtures are presented in Figure 5.4. This figure shows that the greatest compaction (min void ratio or min porosity) results at 30% gypsum content, not 15% as it is corresponding

to max dry density, since the effect of the reduction in the specific gravity is eliminated by this representation.

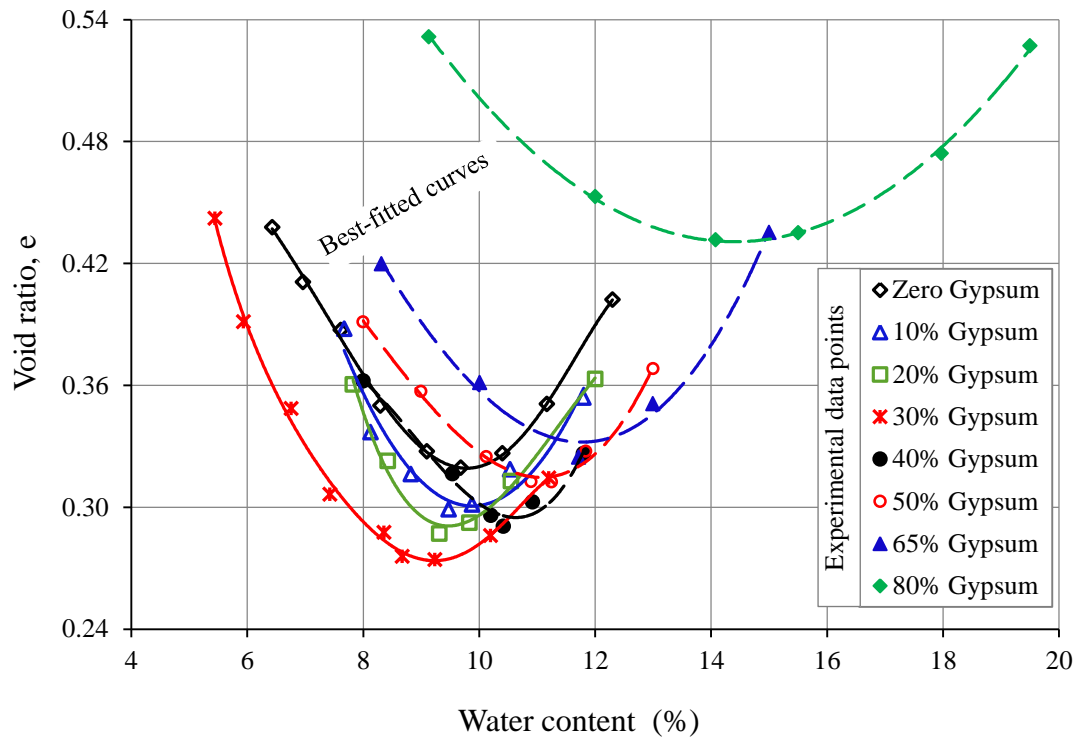


Figure 5.3. Void ratio-water content curves for different sand-gypsum mixtures.

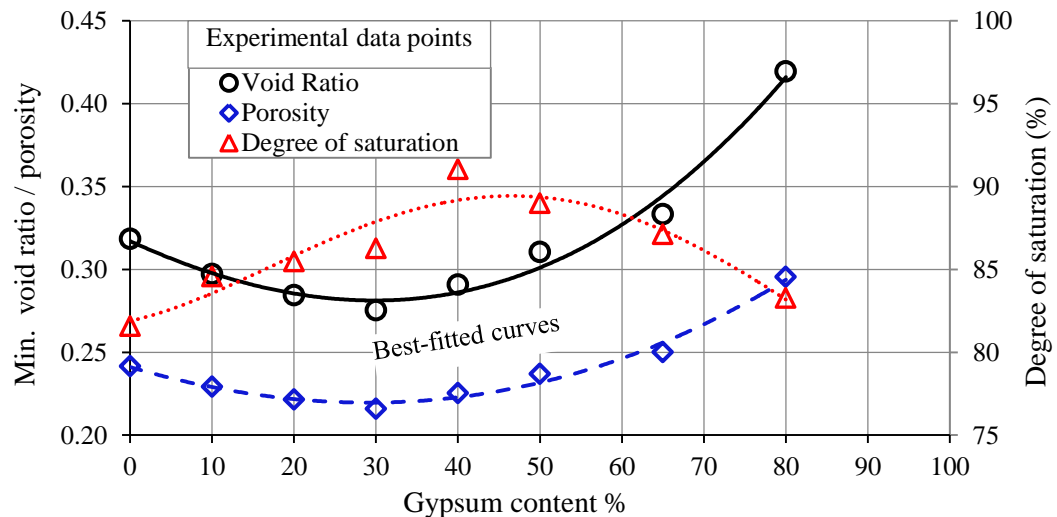


Figure 5.4. Minimum void ratio, minimum porosity, and the corresponding degree of saturation for different sand-gypsum mixtures.

Figure 5.4 also shows that the degree of saturation corresponding to min void ratio clearly increased with increasing gypsum content, reaching a peak of 91% at a gypsum content around 40% by weight, and then starts to decrease for further

increase in gypsum content. Thus, a minimum percentage of air voids of 9% is achieved at 40% gypsum, where the void ratio is 0.29, and the water content is 11.1% as shown in Table 5.1. This trend can be explained by taking into consideration that during compaction process there is an expulsion of air without significant change in the amount of water in the soil mass. Thus, the degree of saturation seems to be increased with increasing compaction.

Furthermore, a close inspection of the compaction curves in Figure 5.1 or in Figure 5.3 reveals that the degree of curvature decreases remarkably with increasing gypsum content. Soils having low gypsum contents react sharply to slight changes in water content, producing sizable changes in dry density, whereas high gypsum content soil specimens seem having smooth changes in dry density with water content variations.

5.3. Effect of gypsum content on compressibility characteristics

A series of oedometer tests were carried out to investigate the effect of gypsum content on one-dimensional compressibility parameters such as the compression index (C_c) and the rebound index (C_r) of the sandy soil. Five sand-gypsum mixtures were tested having gypsum contents of 0, 20, 40, 65, and 80% by weight. The initial conditions of the prepared specimens were the same as those prepared for the other tests. The soil specimens were prepared by static compaction to achieve 90% of the maximum dry density obtained from standard compaction tests.

For each sand-gypsum mixture, the compression curve, which defines the void ratio (e) as a function to the logarithm of applied effective stress ($\log \sigma'$), was obtained from oedometer tests during the loading course. Accordingly the compression index (C_c) corresponding to each increment of the applied effective stress was calculated as described in Section 3.4.2. Similarly, the rebound curve (e - $\log \sigma'$ relationship) was obtained during the unloading course for each sand-gypsum mixture, and then the rebound index (C_r) was calculated for each decrement in the applied effective stress.

The compression and rebound curves for the sandy soil with different gypsum additives are presented in Figure 5.5. It can be noticed from Figure 5.5 that with

increasing gypsum content, the compression and rebound curves move upward with higher initial void ratio (e_0). The initial void ratios after saturation stage are 0.39, 0.46, 0.50, 0.52, and 0.62 corresponding to 0, 20, 40, 65, and 80% gypsum content, respectively.

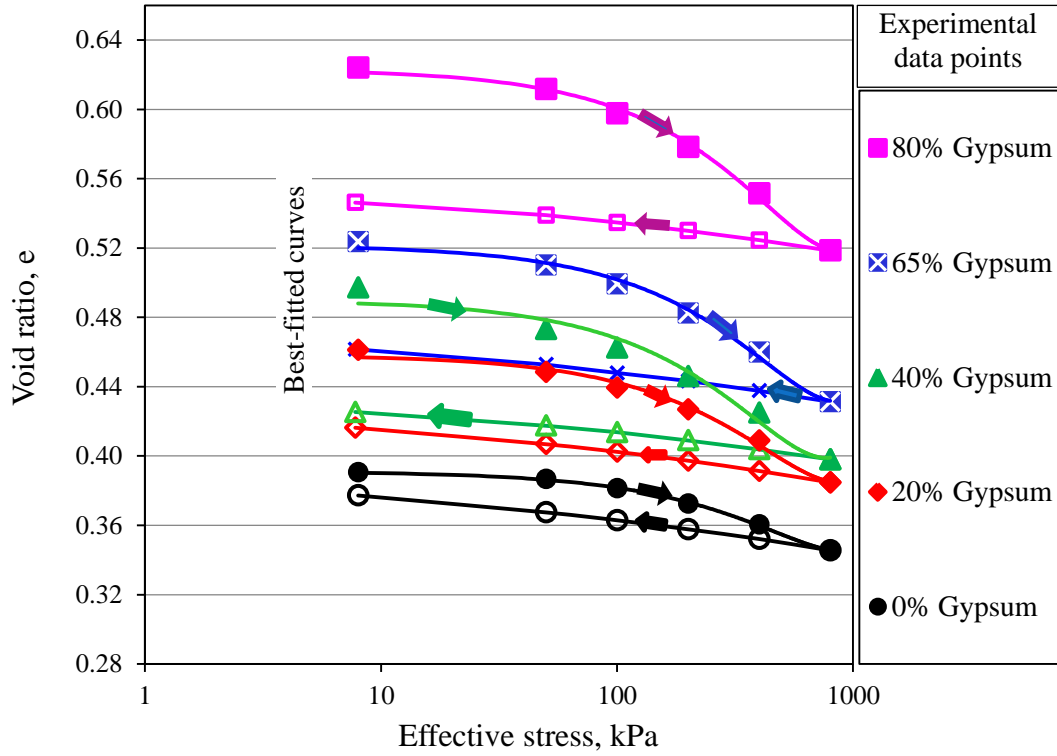


Figure 5.5. Loading and unloading void ratio-log effective stress curves for different sand-gypsum mixtures.

The difference between the compression and the rebound curves exhibits a clear increase with increasing gypsum content. This behaviour can be explained via a purely mechanical approach, where the rebound represents the elastic part of compression and the difference between the compression and rebound curves is the inelastic part resulting from grain slippage and breakage. Gypsum particles are soft crystal with a hardness, on Mohs scale, rating of 2 (Blyth, 1971). Accordingly, with increasing gypsum content, the slippage of particles is anticipated to be easier and the breakage is more. Thus, the increasing in distance between the compression and the rebound curves (the plastic deformation) associated with increasing gypsum content can be explained by considering the properties of gypsum.

The compressibility parameters, C_c and C_r , for different sand-gypsum mixtures are presented against the mean effective stress of each applied increment or

decrement in Figures 5.6 and 5.7, respectively. Figure 5.6 shows that the one-dimensional compression index (C_c) is clearly affected by the amount of gypsum content, while Figure 5.7 shows that the rebound index (C_r) has slight, inconsistent variations with increasing gypsum content.

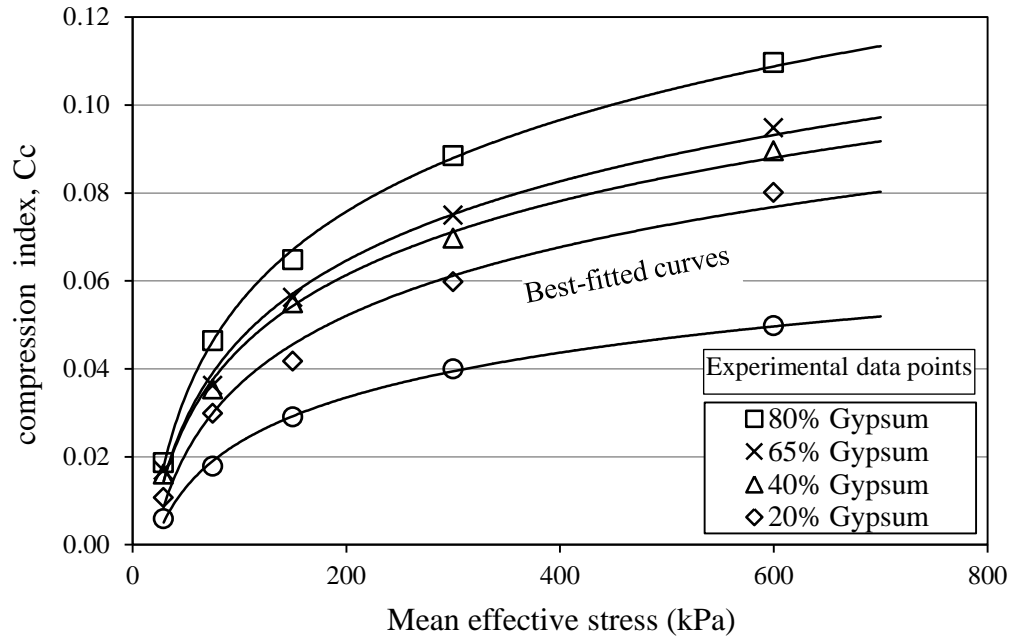


Figure 5.6. Compression index (C_c) versus mean effective stress curves for different sand-gypsum mixtures.

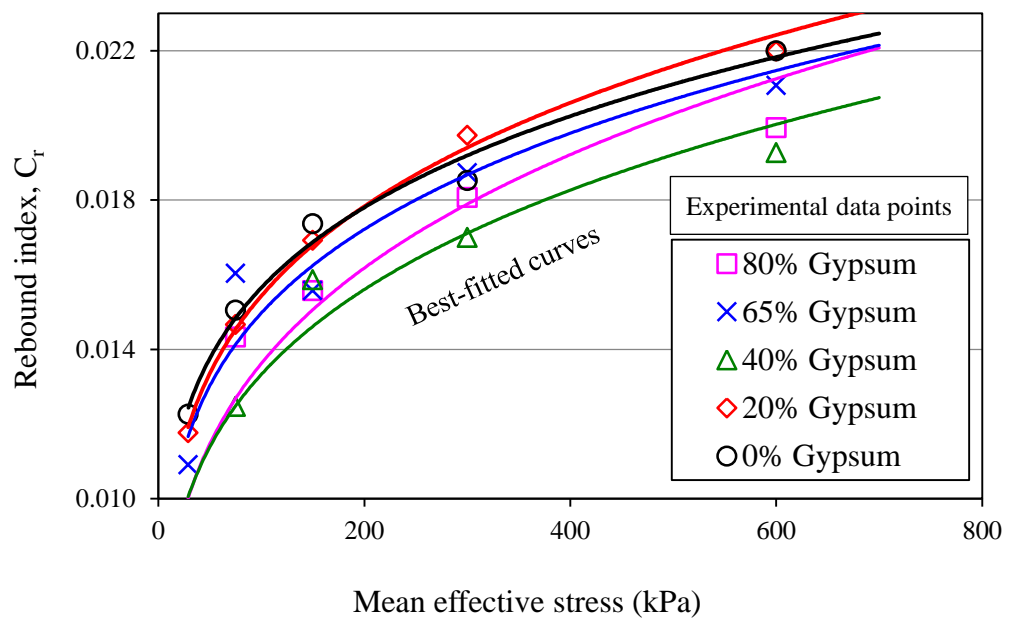


Figure 5.7. Rebound index (C_r) versus mean effective stress for different sand-gypsum mixtures.

Figure 5.6 shows also that there is a remarkable increase in compression index with increasing the level of applied effective stress, and this trend is consistent for different sand-gypsum mixtures. This behaviour can be attributed to the effect of the static load used during compaction of the specimens which is analogous to the influence of preconsolidation pressure in undisturbed specimens. In other words, at low levels of the applied effective stress, the compression index is affected by the previous compaction pressure, whereas at higher effective stress levels, the process is likely to be virgin compression and the compression curve will principally be straight line.

The compression index is defined practically as the slope of the linear portion of the $e - \log \sigma'$ curve. Referring to Figure 5.5, the linear portion of the plotted compression curves is mostly started at effective stress greater than 200 kPa. For comparison, the C_c values corresponding to effective stress increment between 400 to 800 kPa were considered in this investigation.

It is obvious from Figure 5.6 that the compression index increases noticeably with increasing gypsum content. For a mean effective stress of 600 kPa, C_c varies from 0.050 to 0.110 corresponding to 0 and 80% gypsum contents, respectively. This behaviour may be referred in part to the increase in the void ratio with increasing gypsum content, and that is reflected directly on increasing the compression index. Within the framework of this study, a linear relationship between C_c and e_o is noticed. Figure 5.8 shows a plot between e_o and C_c based on the test results of different sand-gypsum mixtures. Two sets of C_c values are represented; the first set is corresponding to effective stress increment from 400 to 800 kPa, while the second set is corresponding to effective stress increment from 200 to 400 kPa. It is possible to say that a linear relationship exists between e_o and C_c , despite some slight scattering. The obtained relationships are: $\{C_c = 0.25e_o - 0.04\}$ and $\{C_c = 0.21e_o - 0.04\}$ for the first and the second set, respectively. These relationships are agreed to some degree to those found by (i) Azzouz et al. (1976) which was $\{C_c = 0.4e_o - 0.01\}$ for all natural soils, (ii) Hough (1957) which was $\{C_c = 0.3e_o - 0.08\}$ for silty clays, and (iii) Sowers (1970) which was $\{C_c = 0.75e_o - 0.37\}$ for very low plasticity soils.

Furthermore, an attempt was done to correlate the values of C_c with other soil parameters such as the initial dry density or the consistency limits, but the obtained statistical indices were less than that obtained from $C_c - e_o$ relationships.

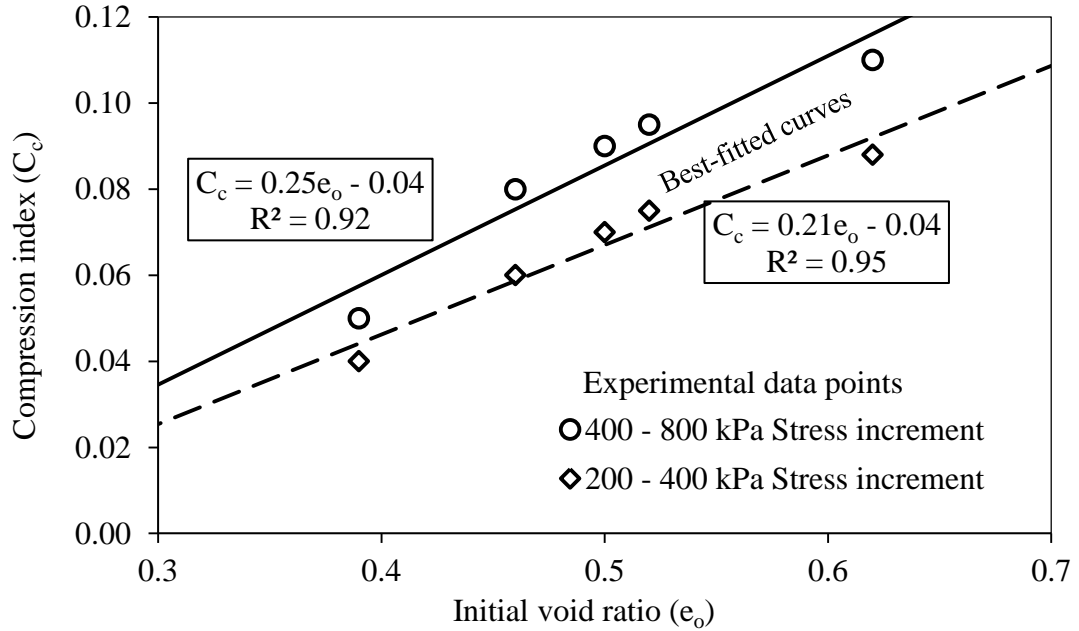


Figure 5.8. Compression index vs. initial void ratio for different sand-gypsum mixtures.

5.4. Soil-water characteristics

Two series of tests were carried out to establish the soil-water characteristic curve for six sand-gypsum mixtures by using the commercial pressure plate equipment (see Section 3.4.3). Two possible approaches according to the ASTM D 6836-02 were followed. In the first series, the same soil specimens were used under different applied suction increments, whereas, in the second series, separate specimens were used for each suction increment. The second approach allowed measuring the volume changes of the specimens under different applied suction increments by using the wax method (ASTM D 4943-08). The main objective of these tests was to study the effect of gypsum content on soil-water retention characteristics of the sandy soil. The second objective was to form a base through which the reliability and accuracy of the modified stress controllable pressure plate device could be compared and evaluated.

5.4.1. Same specimen approach-SWCC tests

The SWCCs for various sand-gypsum mixtures established by following the same specimen approach are presented in Figure 5.9. These curves were best-fitted by using the mathematical model suggested by Fredlund and Xing (1994), Equation 3.3. The fitting parameters and the corresponding statistical indices are listed in Appendix A, Table A.1.

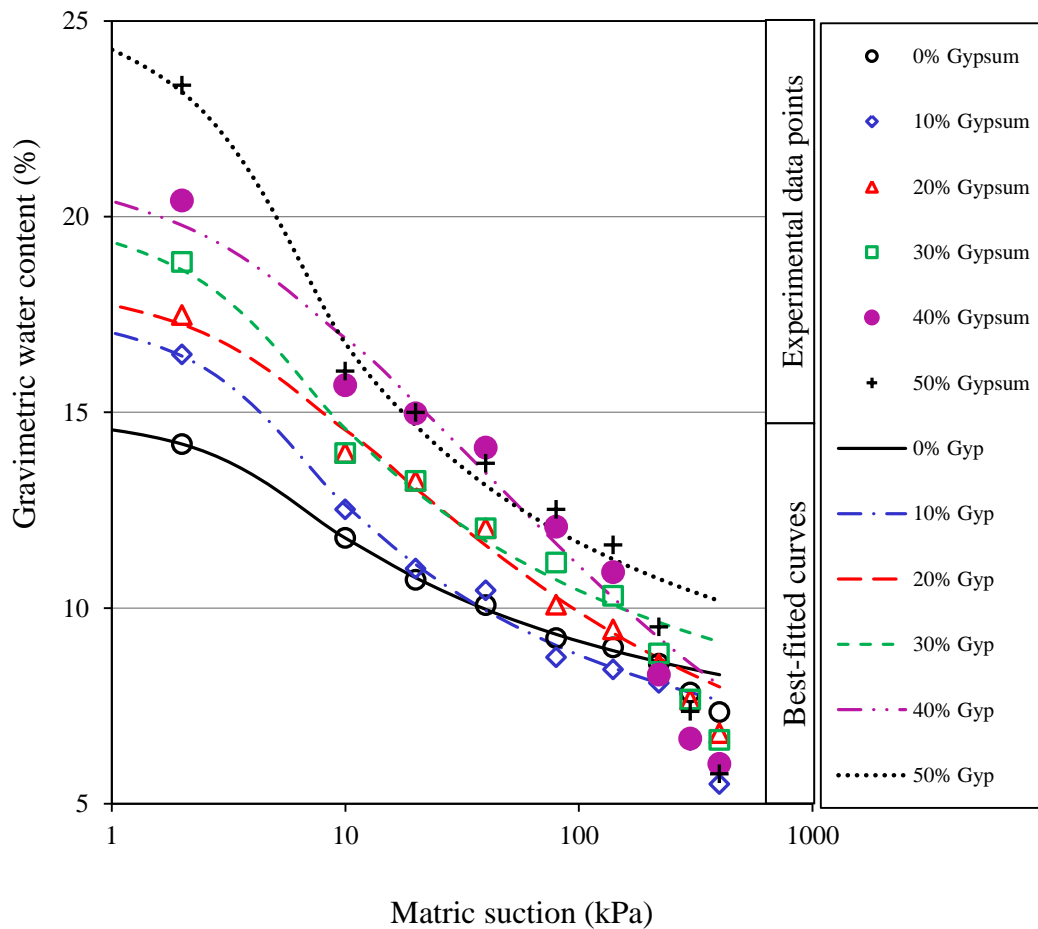


Figure 5.9. SWCCs of different sand-gypsum mixtures carried out by using commercial pressure plate according to ASTM D 6836-02 (same specimen approach).

A noticeable scattering of the experimental test data around the best-fitted curves can be shown in Figure 5.9. Furthermore, comparing with a typical S-shape SWCC, the three desaturation zones which are the boundary effect zone, the transition zone, and the residual zone cannot be identified clearly from these tests. Thus, the essential points describing the SWCC, the air-entry point and the residual

point, are not distinguished with enough precision. In spite of that, it can be noticed from Figure 5.9 that there is a clear increase in the saturated water content with increasing gypsum content. The saturated water content increases from 15.2 % for the sandy soil without gypsum to 26.5% for the sandy soil with 50% gypsum content. This trend can be attributed to the increase of the initial void ratio with increasing gypsum content. Furthermore, a general tendency of the SWCCs shown in Figure 5.9 to become higher with increasing gypsum content may be noticed, specifically for matric suction values greater than the residual values.

In these tests, each soil specimen was used throughout the entire test and subjected to different suction increments to find the SWCC. Thus, the uncertainty in these test results arises from the concerns of the possibility of re-establishing hydraulic contact between the soil specimen and the ceramic disc after the applying of matric suction and the corresponding dryness of the specimen (ASTM D 6836-02). For that reason, it is recommended to use separate specimen for each suction increment.

5.4.2. Separate specimens approach-SWCC tests

In these tests, duplicated specimens were used for each suction increment as described in Section 3.4.3.3. The soil-water characteristic curves of this test series are presented in Figure 5.10. The test data were best-fitted using Fredlund and Xing (1994)'s model as for the SWCCs presented in the previous subsection. The fitting parameters and the statistical indices of SWCC of different sand-gypsum mixtures are listed in Table 5.2.

The test results presented in Figure 5.10 demonstrate the possibility of getting the same results with very slight differences when testing identical specimens. As a comparison with the test results of the first series, Figure 5.10 shows that the results of this series are more consistent, less scattered, closer to the typical S-shape trend, the three desaturation parts on each of the SWCCs are more distinguishable, and then the locating of the air-entry point and the residual point can be done in more reliability.

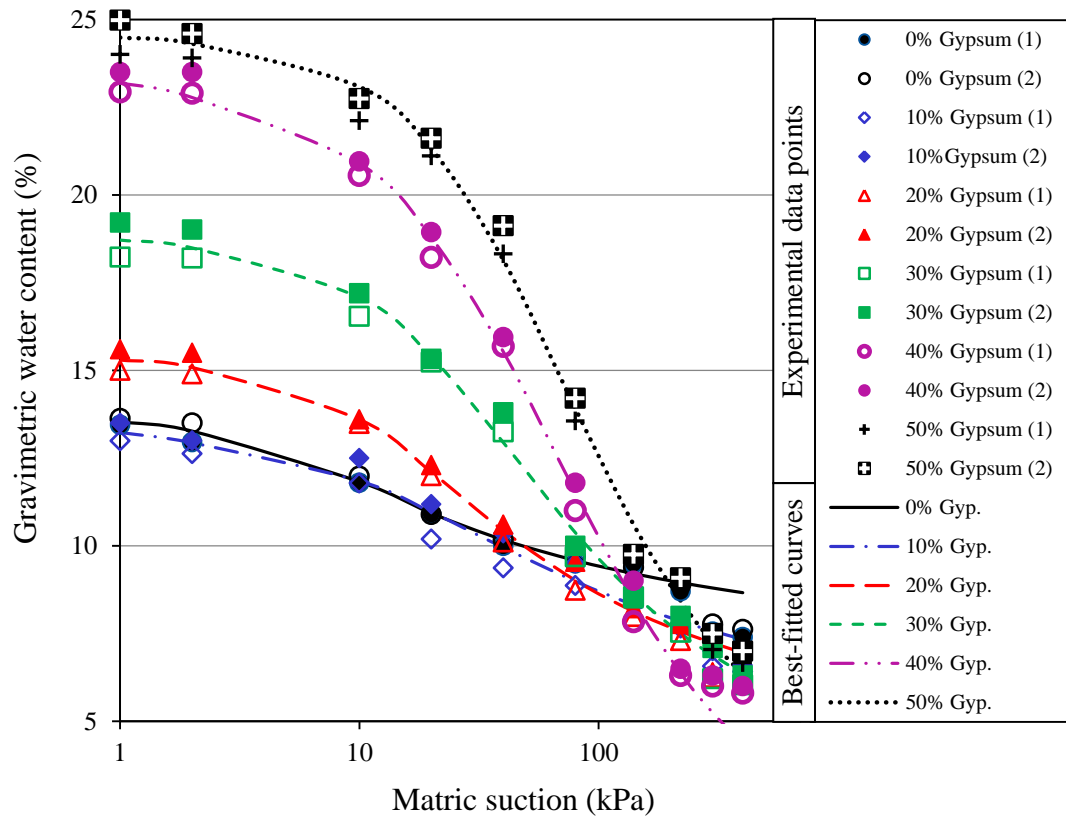


Figure 5.10. The drying SWCCs of different sand-gypsum mixtures carried out by using commercial pressure plate according to ASTM D 6836-02 (separate specimen approach).

Table 5.2. Fittings parameters and statistical indices of SWCCs of different sand-gypsum mixtures, carried out via commercial pressure plate by using separate approach.

Gypsum content	Fitting parameters			Saturated water	R^2
	a	n	m		
0	4.6428	1.5926	0.2275	13.5	0.9956
10	10.2063	1.1169	0.4155	13.6	0.9913
20	10.8349	1.4665	0.4719	15.3	0.9994
30	22.0820	1.3164	0.7959	18.7	0.9945
40	50.9847	1.0960	1.8134	23.2	0.9989
50	43.4977	1.3318	1.1989	24.5	0.9929

5.4.3. Effect of gypsum content on SWCC parameters

Figure 5.10 reveals clearly that with increasing gypsum content, the saturated water content becomes greater, the air-entry and residual suctions show an increase, while the residual water content exhibits moderate decrease. This behaviour can be

attributed to the effect of gypsum content on the grain-size distribution and then on the pore size distribution of these specimens. To evaluate quantitatively the effect of gypsum content on the water retention characteristics, the SWCC parameters were defined by using Vanapalli et al. (1994)'s graphical approach as described in Section 2.4.7. The air-entry suction (ψ_a), air-entry gravimetric water content (w_a), residual suction (ψ_r), and the residual gravimetric water content (w_r) of SWCC for different sand-gypsum mixtures are presented in Table 5.3.

Basically, the difference between residual water content and air-entry water content for a specific soil defines the water holding capacity (WHC) for that soil. The slope of the SWCC in the transition zone can be defined as $[WHC/(\log \psi_r - \log \psi_a)]$. The values of WHC and the corresponding SWCC slope values for different sand-gypsum mixtures are calculated and presented also in Table 5.3.

Table 5.3. SWCC parameters for different sand-gypsum mixtures.

Gypsum content (%)	ψ_a (kPa)	w_a (%)	ψ_r (kPa)	w_r (%)	WHC (%)	SWCC slope
0	10.0	11.8	72	9.5	2.3	0.03
10	10.0	12.0	120	8.3	3.7	0.03
20	11.0	13.6	150	7.6	6.0	0.05
30	12.0	17.0	180	7.0	10.0	0.09
40	14	20.7	210	6.5	14.2	0.12
50	18	22.8	300	7	15.8	0.13

The values of air-entry suction presented in Table 5.3 show slight increases with increasing gypsum content. These values can be closely related to the values of parameter "a" in Fredlund and Xing (1994)'s model as reported by Yang et al. (2004). As such, the values of the measured air-entry suction are supposed to be slightly smaller than the corresponding values of "a" parameter. Comparing the air-entry values with the corresponding "a" values in Table 5.2 reveals some inconsistency to a certain degree. Moreover, results of the SWCC tests implemented by using the modified stress controllable pressure plate device, which are presented

in Chapter 6, demonstrate that the air-entry values, ψ_a , presented in Table 5.3 are under estimated.

The water holding capacity seems to be greatly affected by the amount of gypsum content as revealed in Table 5.3. It varies from 2.3% for the sandy soil without gypsum to 15.8% for sandy soil having 50% gypsum content. This behaviour makes gypsum as an improvement material to the hydraulic characteristics of sandy soil for agricultural purposes. On the other hand, it was noticed from the implemented tests that the time required to reach suction equalization, at any suction level, was remarkably increased with increasing gypsum content. This behaviour could results from the increasing in water holding capacity and consequently the relatively large amount of water which has to leave the specimen before reaching hydraulic equilibrium.

Table 5.3 also reveals that the slope of SWCC clearly increases with increasing gypsum content in the soil mixture. These slope values seem to be consistent with the corresponding uniformity coefficient values of these sand-gypsum mixtures which are shown early in Table 3.1. Uniform soils that have relatively low uniformity coefficient have relatively uniform pore-size and then relatively steep SWCC slope. Thus, the values of SWCC slope are 0.03, 0.03, 0.05, 0.09, 0.12, 0.13 which are corresponding to 114, 87, 70, 30, 18, 7 uniformity coefficient values (Table 3.1), respectively.

5.4.4. Matric suction-volumetric water content relationships

As mentioned in Section 3.4.3, in the second series of SWCC tests, separate specimens were used for each suction increment. Thus, when the equalization for each suction increment was reached, the specimens were removed from the pressure plate, weighed for determining the gravimetric water contents, and then waxed as soon as possible for volume determination. By using the volume-mass relationships, the volumetric water contents corresponding to different suction increments were calculated. The SWCCs in terms of volumetric water content for different sand-gypsum mixtures are presented in Figure 5.11.

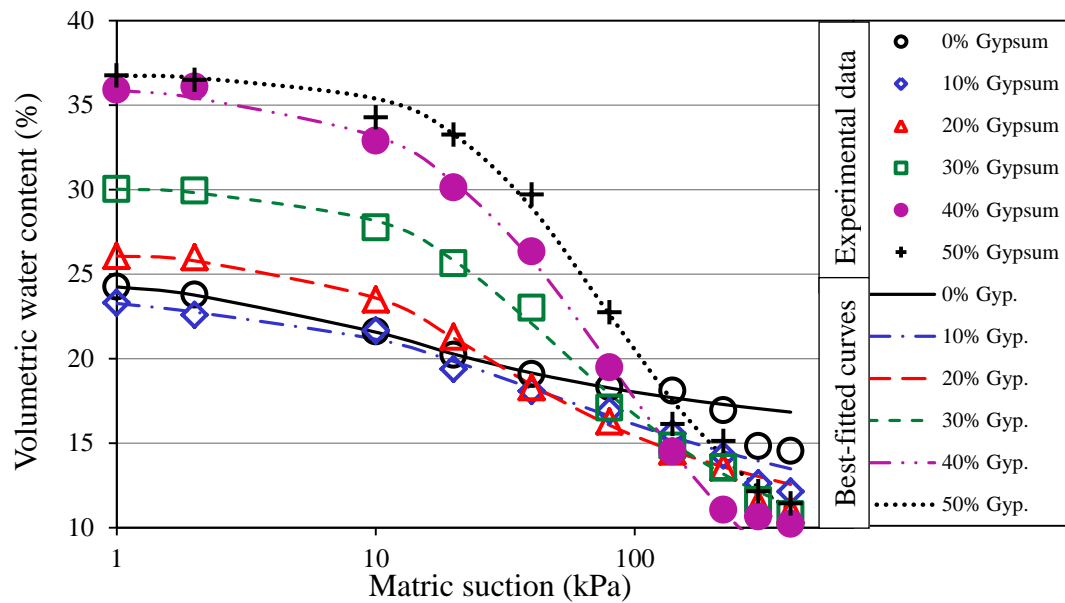


Figure 5.11. Matric suction-volumetric water content curves of different sand-gypsum mixtures found from the pressure plate tests on separate specimens by using the wax method.

5.4.5. Applied suction and volume change

The volume of each soil specimen corresponding to different applied suctions was determined using the wax method (ASTM D 4943-08). Then, the void ratio-matric suction relationships for different sand-gypsum mixtures were found and presented in Figure 5.12.

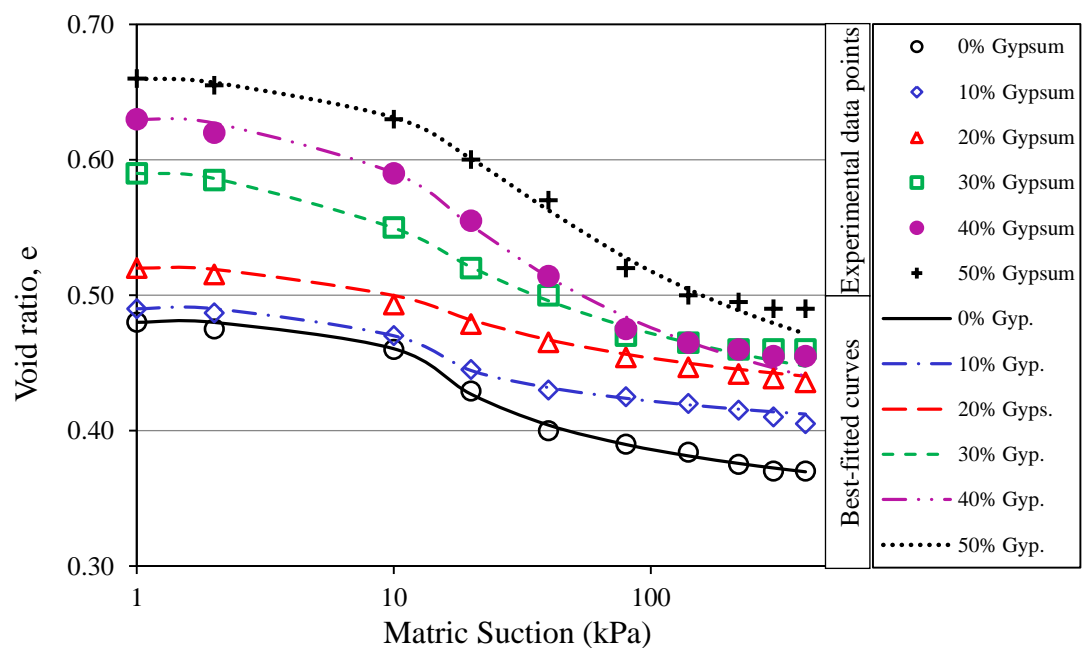


Figure 5.12. Void ratio-matric suction curves of different sand-gypsum mixtures based on pressure plate tests on separate specimens with volume measurements by using the wax method.

Figure 5.12 reveals that the changes in void ratio become greater with increasing gypsum content. This trend is consistent with that of the compression index versus gypsum content which was found from the conventional oedometer test results (Figure 5.6). In conventional consolidation tests, the volume changes result from mechanical external loading that causes skeletal forces propagated through soil grains contacts, while during the drying process, there is a hydraulic loading that causes local forces acts at or near the grains contacts. Both mechanical and hydraulic loading result volume changes but in different magnitudes.

The shrinkage characteristic curve (SCC), which shows the void ratio as a function to the gravimetric water content (McGarry and Malafant, 1987), was found for different sand-gypsum mixtures using the data of the second series of SWCC tests. Figure 5.13 shows the shrinkage characteristic curves for five sand-gypsum mixtures for a range of water contents limited between the saturated water content and nearly the residual water content. These curves are best-fitted using Fredlund et al. (2002)'s mathematical model. The fitting parameters are presented in Table 5.4.

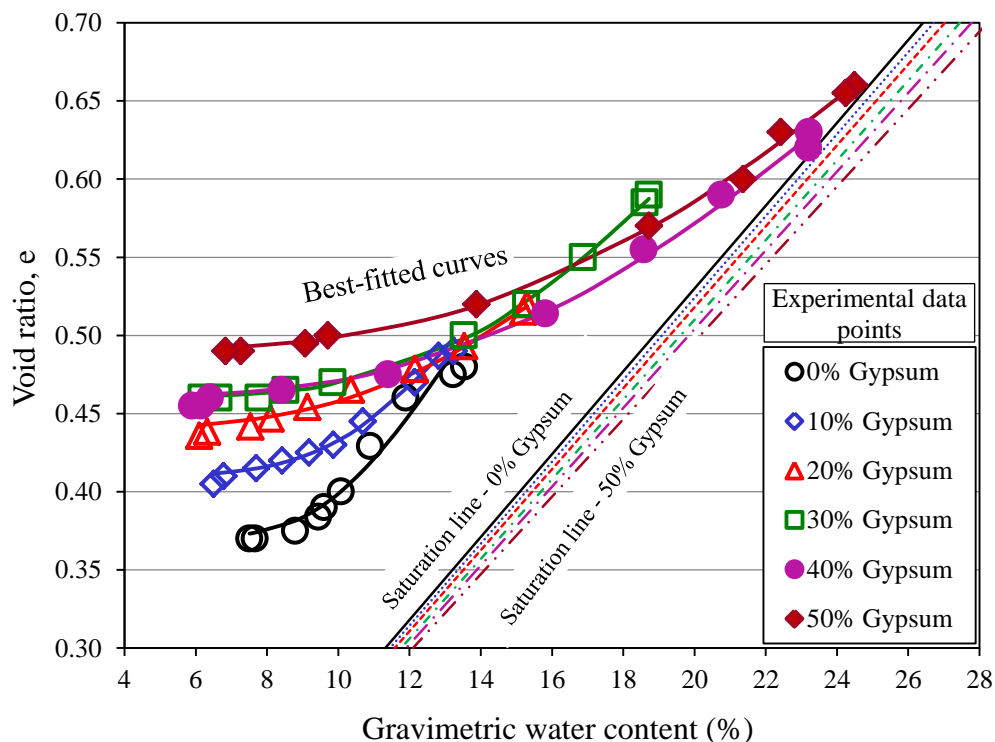


Figure 5.13. Void ratio-gravimetric water content curves of different sand-gypsum mixtures found from the pressure plate tests on separate specimens in conjunction with volume determination using the wax method.

The slope of the linear portion of a SCC (the normal stage of shrinkage) expresses the volume compressibility with respect to water content. This slope is referred to as CLOD index (Fredlund and Rahardjo, 1993), and is expressed as:

$$C_w = \frac{\Delta e}{\Delta w} \quad 5.1$$

where C_w is the CLOD index, Δe is the incremental change in void ratio corresponding to the incremental change in water content Δw .

To evaluate quantitatively the effect of gypsum content on the shrinkage characteristic curve, the fitting parameters a and b , as expressed by Fredlund et al. (2002)'s mathematical model, were used to calculate the slope of the linear portion of the SCCs as follows:

$$C_w = 100 (a / b) \quad 5.2$$

The slope of the SCC for different sand-gypsum mixtures was calculated firstly according to Equation 5.1 and secondly according to Equation 5.2. Both these values are presented in Table 5.4 for comparison. It can be noticed from Table 5.4 that the slope of the SCCs calculated according to Fredlund et al. (2002)'s mathematical model (Equation 5.2) are higher than those calculated according to the basic definition of the CLOD index (Equation 5.1).

Table 5.4. Fitting parameters of the SCCs of different sand-gypsum mixtures found from separate specimens-SWCC tests, implemented by using the commercial pressure plate.

Gypsum content (%)	Fitting parameters			SCC slope, $\Delta e / \Delta w$	SCC slope, 100 (a/b)
	a	b	c		
0	0.37	10.13	8.54	2.27	3.65
10	0.41	11.50	6.35	1.40	3.56
20	0.44	15.67	3.94	1.33	2.81
30	0.46	15.79	4.87	1.68	2.91
40	0.46	18.90	3.69	1.08	2.43
50	0.49	20.15	3.79	1.05	2.43

Figure 5.13 and Table 5.4 reveal that the slope of the linear portion of the SCC decreases with increasing gypsum content. Likewise, the curvature of the SCC becomes flatter with increasing gypsum content, and this could be evaluated quantitatively from the values of "c" parameter. For the soil without gypsum, the parameter "c" is equal to 8.54 and then decreases to 3.79 when the gypsum content reaches 50%. The value of the minimum void ratio, the "a" parameter, shows a clear

increase with increasing gypsum content. Another set of SCCs for different sand-gypsum mixtures were obtained from CLOD test series, and these curves will be presented later in Section 5.6.

5.5. Water content-total suction relationships

As described in Section 3.4.4, a series of tests were carried out to establish the water content-total suction relationship, or as it may be called also the total suction SWCC, for five specimens having gypsum contents of 0, 20, 40, 65, and 80% by weight. These tests were carried out by using the chilled mirror hygrometer, commercial brand "WP4C Dewpoint PotentialMeter". The main objective of these tests is to study the effect of gypsum content on the common parameters of the total suction- SWCC of gypsiferous sandy soil. As a second objective, the osmotic suction component could be evaluated for different sand-gypsum mixtures. The test results are presented in Figure 5.14 for these five sand-gypsum mixtures. The experimental data points were best-fitted by using Fredlund and Xing (1994)'s model.

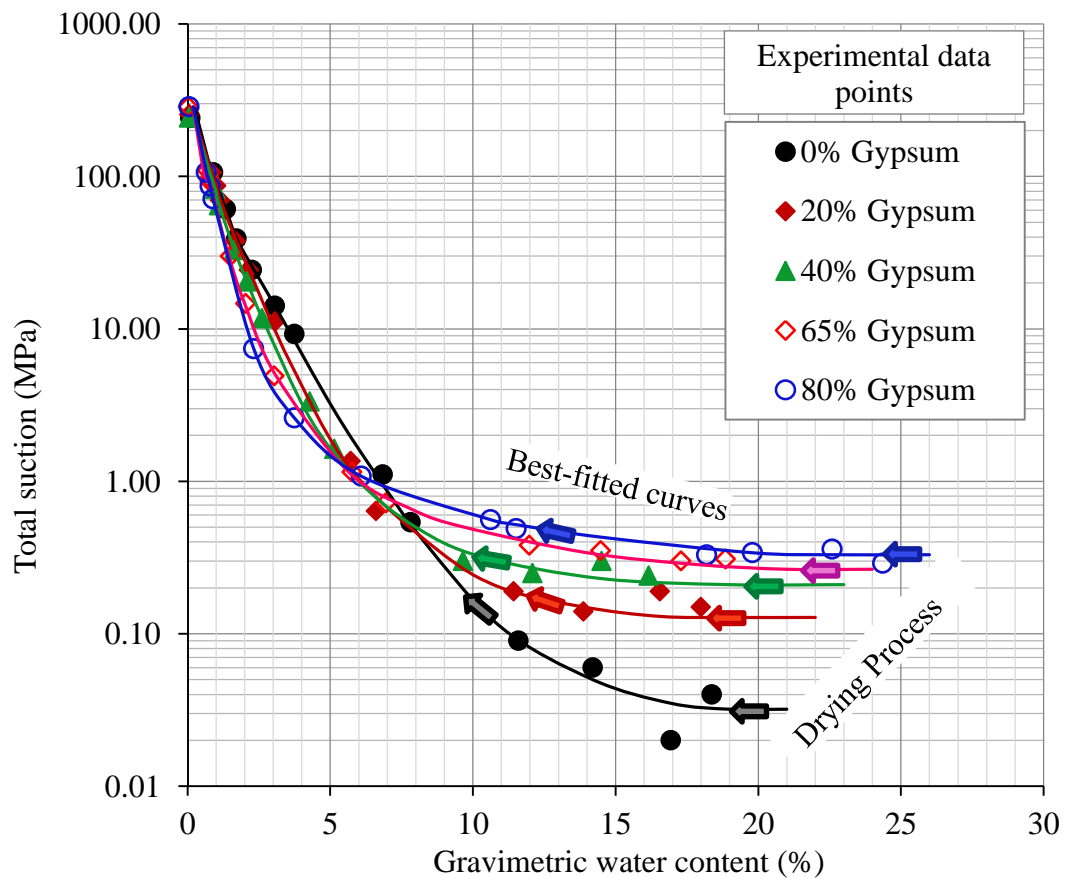


Figure 5.14. Gravimetric water content-total suction relationships of different sand-gypsum mixtures determined by using chilled mirror hygrometer.

Figure 5.14 shows that the experimental results exhibit some scattering near saturated water contents especially for specimens have low gypsum content, whereas this scattering seems to be reduced for specimens have high gypsum contents. This behaviour may be resulted from the small measured suction values for the specimens that have 0 and 20% gypsum content. The suction values of those specimens are smaller or close to the lower limit of the recommended measuring range of the device used (0.10 to 300 MPa). However, with the progress of the specimens drying, when the suction exceeding 0.10 MPa, the experimental results of different sand-gypsum mixtures show consistent trends with minimum scattering.

Figure 5.14 reveals clearly that there is a remarkable increase in total suction function with increasing gypsum content as long as the water content is greater than the residual value. However, all these total suction characteristic curves are intersecting at a suction value of about 1 MPa and their ordering are reversed. Specimens that have higher trend near saturation get the lower position after the intersection point, and eventually all curves approach to each other and then unify to a single constant slope line at low water contents. This behaviour results from the effect of gypsum content on the component of osmotic suction which is generated at high values of water content and diminish gradually with decreasing water content, since osmotic suction is attributed to the dissolved salt solutions in the soil pores. This finding confirms with the conclusion of Fredlund and Xing (1994) who pointed out that when the value of soil suction is greater than 1.5MPa, the total and matric suctions refer nearly to the same meaning, i.e., the osmotic suction is eliminated.

Furthermore, Figure 5.14 reveals that there is a clear correlation between gypsum content and the degree of curvature near residual point. Specimens with high gypsum content have comparatively sharp corner near residual point and relatively steeper curve at residual stage.

The measurements of total suction were started from saturated water contents or slightly above that and continued through a multi-stages drying process to near zero water contents. In such a case, the initial suction readings contain only one component of suction which is the osmotic component, since the matric suction can be considered zero at saturation. The initial suction readings which represent the

osmotic suction values are drawn in Figure 5.15 against gypsum content of the soil specimens tested. Figure 5.15 reveals that the osmotic suction increases with increasing gypsum content, and that is related to the increase of dissolved salts in the soil pore water.

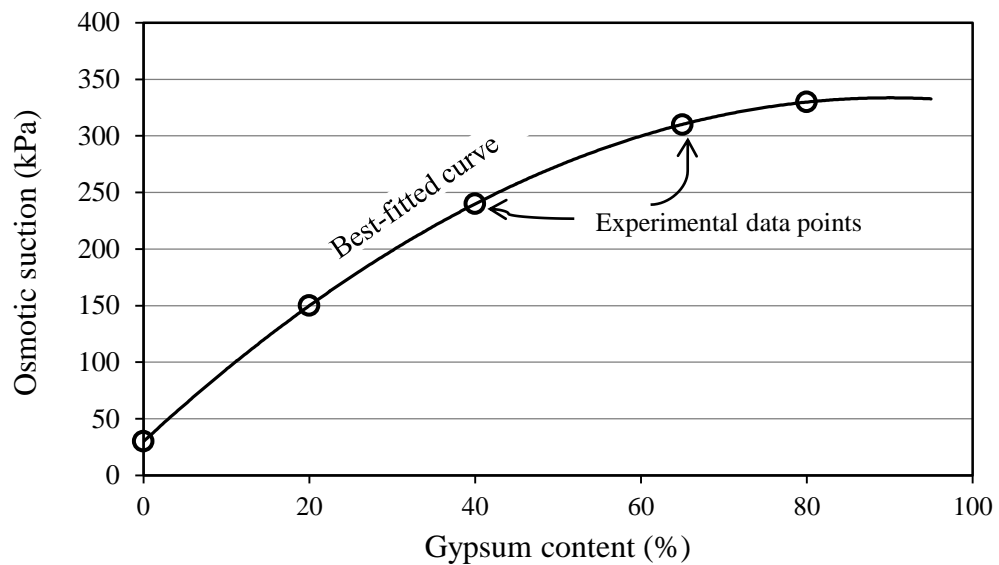


Figure 5.15. Effect of gypsum content on osmotic suction of the sandy soil used.

To determine the residual suction and the corresponding water content for different sand-gypsum mixtures, Vanapalli et al. (1994)'s graphical approach have been applied regardless of the reversed axis presentation of the measured SWCCs. These residual values are presented in Figure 5.16 as functions to gypsum content.

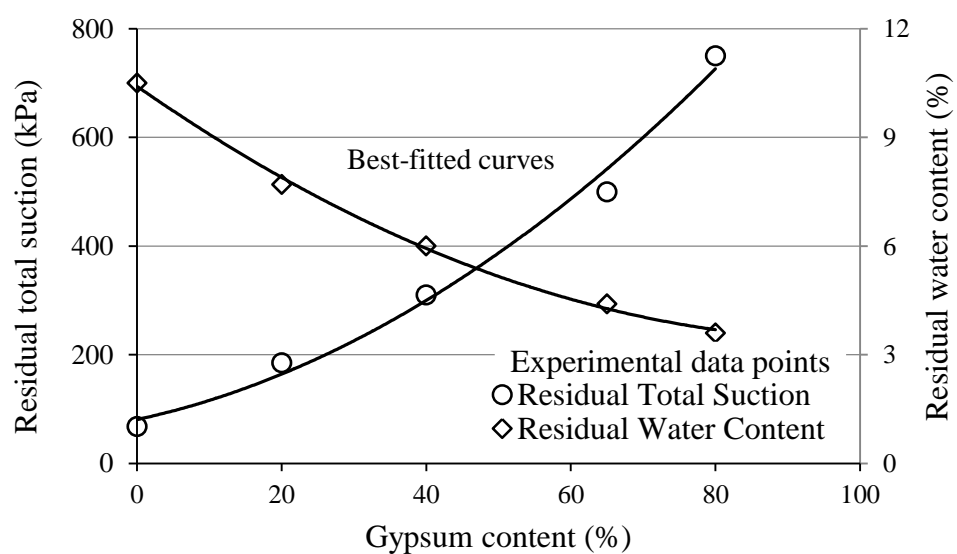


Figure 5.16. Parameters of total suction SWCCs for different sand-gypsum mixtures (based on Figure 5.14).

Figure 5.16 shows that there is a clear increase in residual suction with increasing gypsum content. The residual suction increases from 68 kPa for specimen has 0 % gypsum content to 750 kPa for 80% gypsum content. On the other hand, the corresponding residual water content shows a clear decrease with increasing gypsum content. It decreases from 10.5% for specimen without gypsum to 3.6% for specimen has 80% gypsum content.

5.6. Shrinkage characteristics

A series of CLOD tests were carried out to establish the shrinkage characteristic curve (SCC) for seven sand-gypsum mixtures having gypsum percentages of 0, 10, 20, 30, 40, 65, and 80% by weight. The objectives from these tests were (i) to evaluate the effect of gypsum content on the behaviour of the soil shrinkage characteristic curve of the sandy soil, and (ii) to compare the SCCs found from CLOD tests with the corresponding ones found from the SWCC tests on separate specimens with volume determination using the wax method. Moreover, it is possible to combine the SCCs with the corresponding SWCCs to establish the relationships of void ratio versus soil suction for different sand-gypsum mixtures.

The SCCs for different sand-gypsum mixtures are presented in Figure 5.17 in terms of void ratio versus water content. These curves were best-fitted by using Fredlund et al. (2002)'s model. The fitting parameters are presented in Table 5.5. Figure 5.17 shows the entire shrinkage curves from initial high water content conditions to completely dry conditions. The initial water content values were corresponding to applied matric suction ranging from 10 kPa to 30 kPa. Specimens with high gypsum content demonstrated good consistency to deal with at relatively high water contents without dislodging or disturbing. Accordingly, the shrinkage curves for those mixtures are extended from higher water content values.

As a comparison between the shrinkage curves presented in Figure 5.17 and the analogous curves obtained from SWCC tests (Figure 5.13) a good agreement may be noticed, even though, the former curves do not cover the entire range of water contents. Nevertheless, the comparison between the fitting parameters of the shrinkage curves under consideration (Table 5.5) and those presented in Table 5.4 for

the former curves can be quantitatively characterizes these curves. Referring to Table 5.4, the values of parameter "a", which represents the minimum void ratio, for mixtures having 0, 10, 20, 30, and 40% gypsum content are 0.37, 0.41, 0.44, 0.46, and 0.46, respectively. The corresponding ones from CLOD tests are 0.38, 0.40, 0.44, 0.47, and 0.47, respectively. Similarly, the values of the slope of the SCCs for the above mentioned mixtures are 3.65, 3.65, 2.81, 2.91, and 2.43 from the SWCC tests, while the analogous slopes from CLOD tests are 3.74, 3.11, 2.81, 2.93, and 2.47. These values show a good agreement between the two approaches of finding the SCC.

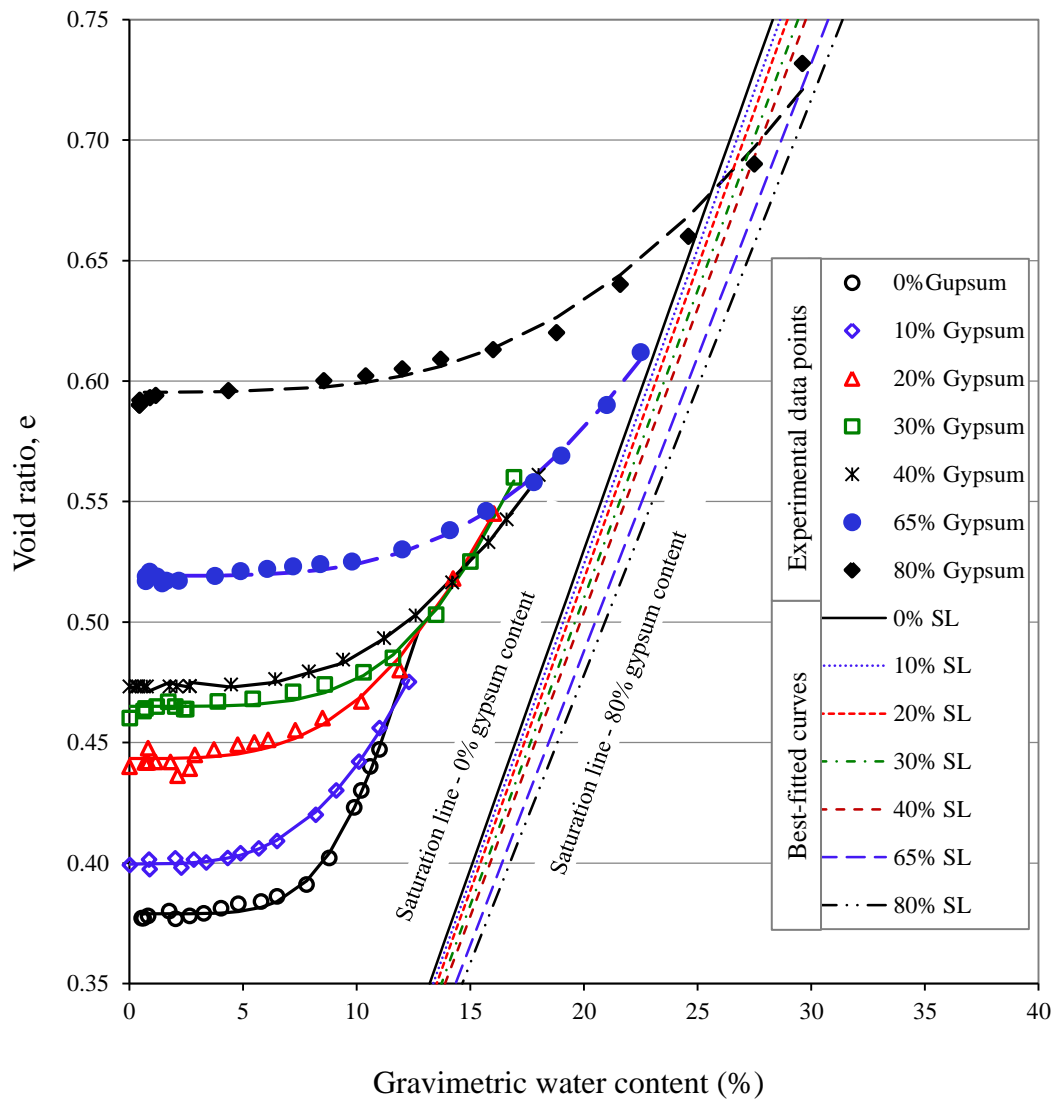


Figure 5.17. Shrinkage characteristic curves for different sand-gypsum mixtures determined from CLOD tests.

Table 5.5. Fitting parameters of the SCCs of different sand-gypsum mixtures determined from CLOD tests.

Gypsum content (%)	Fitting parameters			SCC Slope (a/b)
	a	b	c	
0	0.38	10.12	5.73	3.74
10	0.40	12.87	3.53	3.11
20	0.44	15.80	3.49	2.81
30	0.47	15.88	4.64	2.93
40	0.47	19.16	3.47	2.47
65	0.52	23.36	3.89	2.22
80	0.60	30.02	3.50	1.98

The shrinkage limit of different sand-gypsum mixtures can be identified from the shrinkage curves according to shrinkage limit definition (i.e., the water content at which drying-shrinkage ceases). The values of the shrinkage limit identified from the SCCs in Figure 5.17 are 8, 7, 8.5, 11, 11.3, 13.5, and 17 % for sand-gypsum mixtures having 0, 10, 20, 30, 40, 65, and 80% gypsum content, respectively. On the other hand, the values of shrinkage limits of these mixtures measured by using the standard shrinkage limit determination method (Section 3.3) are 13, 11.5, 10.7, 10.5, 12.5, 17.6, and 22.5%, respectively. It is clear that the values of shrinkage limit found from CLOD tests are smaller than those found from the standard method. This behaviour can be attributed to the difference in the preparation condition of the specimens in these two different methods. In the standard shrinkage limit determination method (ASTM D 4943-08), the specimens were prepared at slurry condition with values of water content greater than the liquid limit values, and then they were placed in small cans without any compaction and oven dried. In contrary, in the CLOD tests, the specimens were statically compacted at the optimum water content to 90% of the maximum dry density obtained from the standard compaction tests. Thus, there are considerable variations in the microstructure and pore spaces of the specimens in this method.

Results of the CLOD tests demonstrate that with increasing gypsum content, the slope of the linear portion of the SCC reduces, the curvature of the SCC becomes smaller (flatter curves), and the final void ratio at the dry condition becomes greater. As well as, the results clearly show that it is important to measure the shrinkage curve especially for high volume change soils when the volume-mass properties versus soil suction have to be evaluated.

5.7. Concluding remarks

Standard laboratory tests of grain size distribution, compaction, one-dimensional consolidation, shrinkage characteristics (CLOD), SWCC in terms of matric suction, and SWCC in terms of total suction revealed that the water retention characteristics and the volume change characteristics of the sandy soil are highly influenced by gypsum content in the soil mixture.

The grain-size distribution parameters (coefficient of uniformity and coefficient of curvature) of the prepared sand-gypsum mixtures were clearly affected by gypsum, with a degree depends on the gypsum percentage added. That is resulting from the very uniform size distribution of the gypsum used which has 60% by weight between 0.010 and 0.020 mm equivalent particle diameter.

The standard compaction tests revealed that there is a slight increase in the maximum dry density associated with a slight decrease in the optimum water content with increasing gypsum content up to 15% by weight. On the contrary, when gypsum content increases more than 30% by weight, the maximum dry density starts to decrease noticeably associated with a clear increase in the optimum water content.

Gypsum influences compaction characteristics through two different roles. At relatively low gypsum contents, gypsum acts as a filling material to the intergranular voids of the soil matrix, and then increases the maximum dry density. At relatively high gypsum contents, gypsum decreases the overall specific gravity of the soil mixture, and then decreases the maximum dry density. That is because the specific gravity of gypsum is smaller than that of the sandy soil used.

Results of the consolidation tests exhibited that the one-dimensional compression index (C_c) of the sandy soil increases clearly with increasing gypsum content in the soil mixture. This behaviour may be referred in part to the increase in the void ratio with increasing gypsum content. As well as, there is a remarkable increase in compression index with increasing the applied normal stress. The difference between the compression and rebound curves exhibits clear increase with increasing gypsum content as well. This difference represents the plastic part of compression resulting from grain slippage and breakage.

Results of the CLOD tests demonstrated that with increasing gypsum content, the slope of the linear portion of the shrinkage characteristic curve (SCC) reduces, the curvature of the SCC becomes flatter, and the final void ratio at the dry condition becomes greater. A good agreement has been noticed between the SCCs obtained from the SWCC tests and the analogous curves obtained from CLOD tests.

The shrinkage limit values of different sand-gypsum mixtures found out from CLOD tests were smaller than those determined from the standard shrinkage limit tests (ASTM D 4943-08). This can be attributed to the difference in the specimens' preparation condition. Where the specimens were prepared at slurry condition in the standard shrinkage method, the specimens were statically compacted at the optimum water content in the CLOD tests.

Clear increases in the SWCC parameters were noticed with increasing gypsum content in the soil mixture. These parameters are; the saturated water content, the air-entry and residual suctions, the water holding capacity, and the slope of SWCC. Furthermore, the volumetric changes associated with desaturation (increasing matric suction) were greater with increasing the gypsum content in the soil mixture. This trend is consistent with increasing the compression index (C_c) when gypsum content increases, as shown from the conventional oedometer tests.

Results of the chilled mirror hygrometer tests revealed clearly that there is a remarkable increase in total suction function with increasing gypsum content in the soil mixture as long as the water content is greater than the residual value. This behaviour can be attributed primarily to the effect of gypsum content on increasing the osmotic suction component. At suction value of about 1 MPa, all total suction characteristic curves are approached an intersecting point and their ordering is reversed. Soil mixtures that have higher trend near saturation get the lower position after that intersection point. This can be attributed to the eliminating of osmotic suction component at this level of suction. This interpretation agrees to some degree with the conclusion of Fredlund and Xing (1994) who pointed out that the osmotic suction is eliminated when the value of soil suction is greater than 1.5 MPa. Furthermore, with increasing gypsum content, the residual total suction showed remarkable increase, while the residual water content showed clear decrease.

CHAPTER SIX

STRESS-DEPENDENT SOIL-WATER CHARACTERISTICS

6.1. Introduction

The experimental programme, described in Chapter 4, was suggested to study the influence of gypsum content and stress state on two unsaturated hydraulic key functions of gypsiferous sandy soils. These hydraulic functions are the soil-water characteristic curve and the unsaturated hydraulic conductivity function. This chapter presents the test results of the experimental programme related to the stress-dependent soil-water characteristic curves (SD-SWCCs) during both the drying and the wetting processes. The modified stress controllable pressure plate device was used to establish the SD-SWCCs for five sand-gypsum mixtures. The room temperature was controlled at 20-22°C and the relative humidity at 40-50%. The influence of five different levels of net normal stress was considered. These levels were 0, 100, 200, 300, and 400 kPa. For clarity purpose, the drying and the wetting curves determined at 300 kPa are excluded from the following presentation since they have consistent, in between trends of those found at 200 and 400 kPa. The results of SWCCs tested at 300 kPa were used to confirm the experimental accuracy of the adjacent curves that tested at 200 and 400 kPa.

The results of SD-SWCCs are presented in the following section, and then they will be discussed in detail in the subsequent sections for the effect of gypsum content firstly, and for the effect of net normal stress secondly.

6.2. Test results preview

The test results of the SD-SWCCs are previewed in Figures 6.1 to 6.6. These results will be discussed in the subsequent sections for the effect of gypsum content and the effect of net normal stress on each SWCC parameter. Figure 6.1 shows the drying and the wetting SWCCs for five sand-gypsum mixtures tested at 0 kPa net normal stress. The other SWCCs established at 100, 200, and 400 kPa net normal stress levels are presented through Figures 6.2 to 6.6, in sets each have the same gypsum content and various net normal stress levels. This presentation shows primarily the influence of various net normal stress levels on the behaviour of the SWCCs.

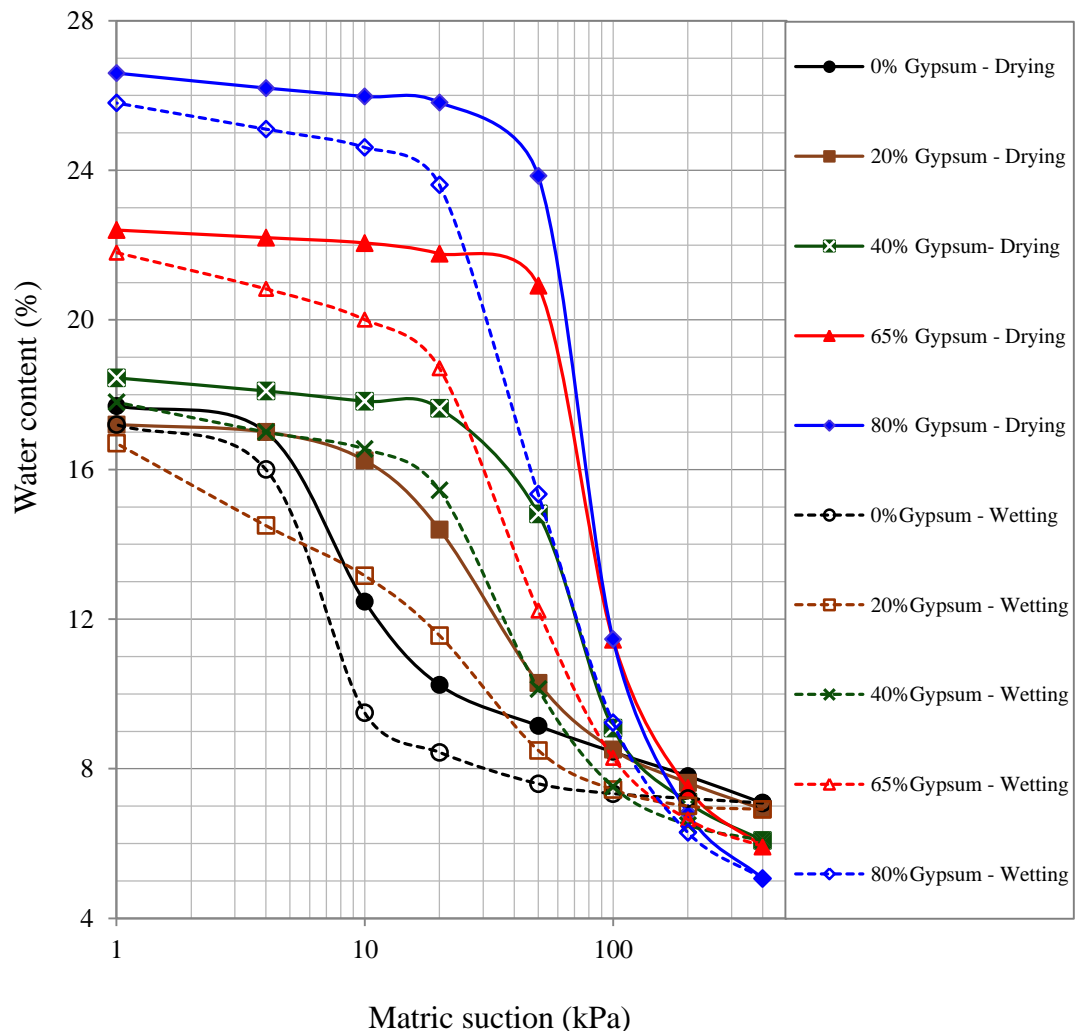


Figure 6.1. Effect of gypsum content on the drying and the wetting SWCCs of specimens tested under 0 kPa by using the modified stress controllable pressure plate device.

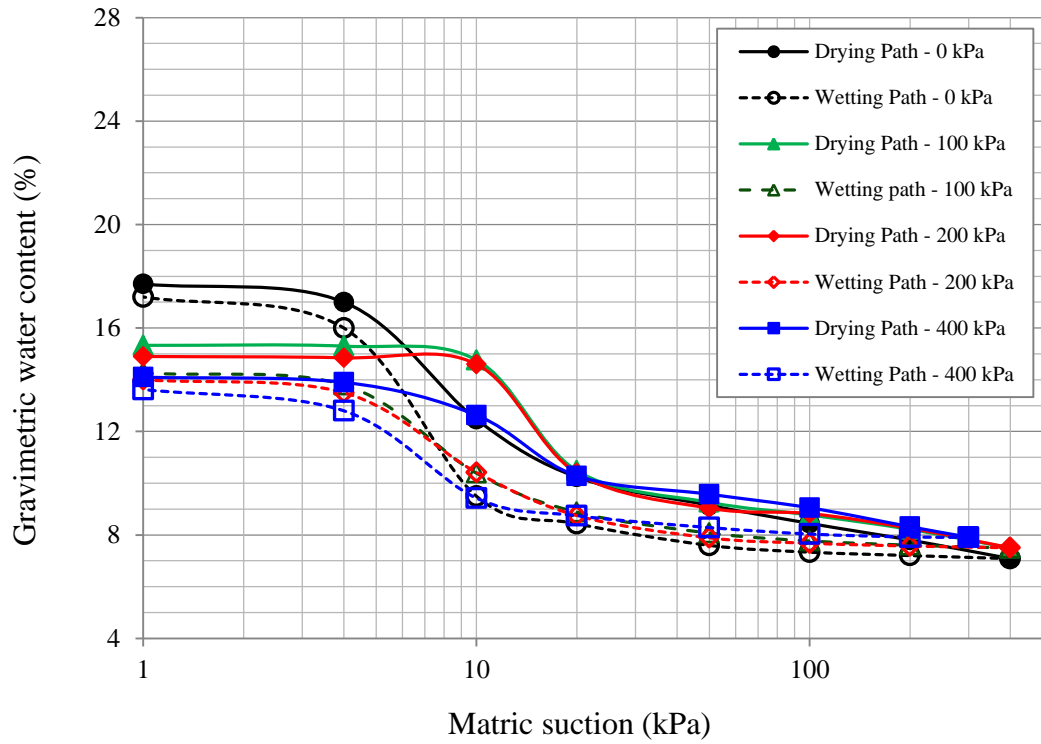


Figure 6.2. The drying and the wetting SD-SWCCs of the sandy soil having 0% gypsum content.

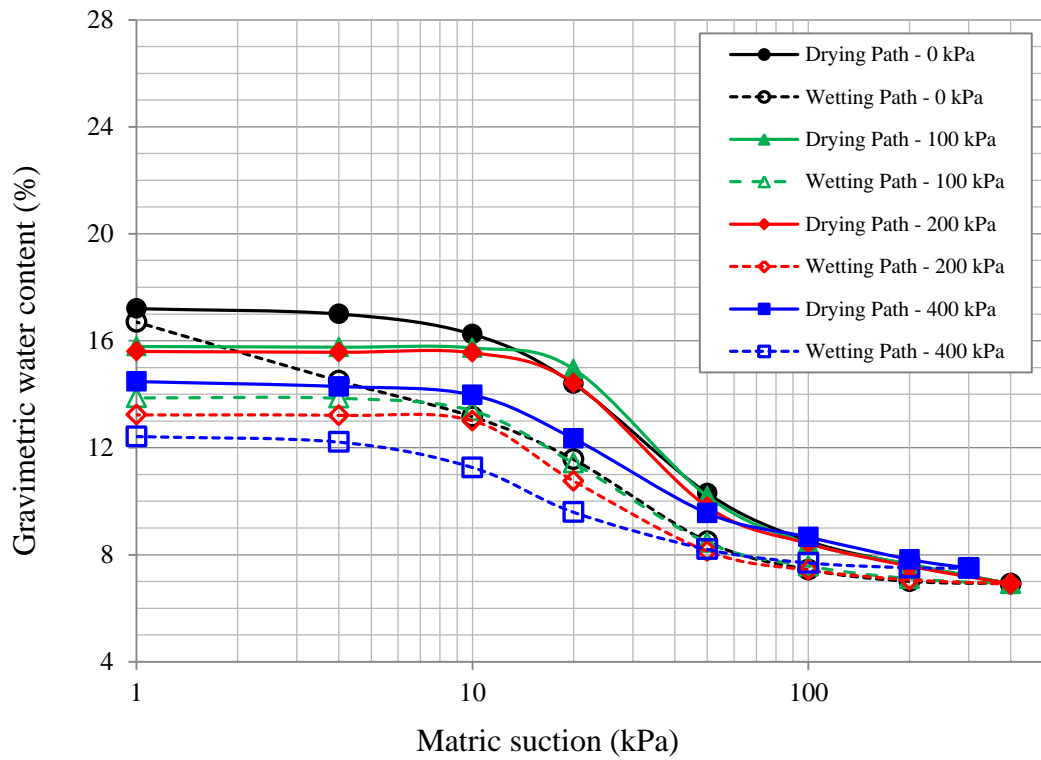


Figure 6.3. The drying and the wetting SD-SWCCs of the sandy soil having 20% gypsum content.

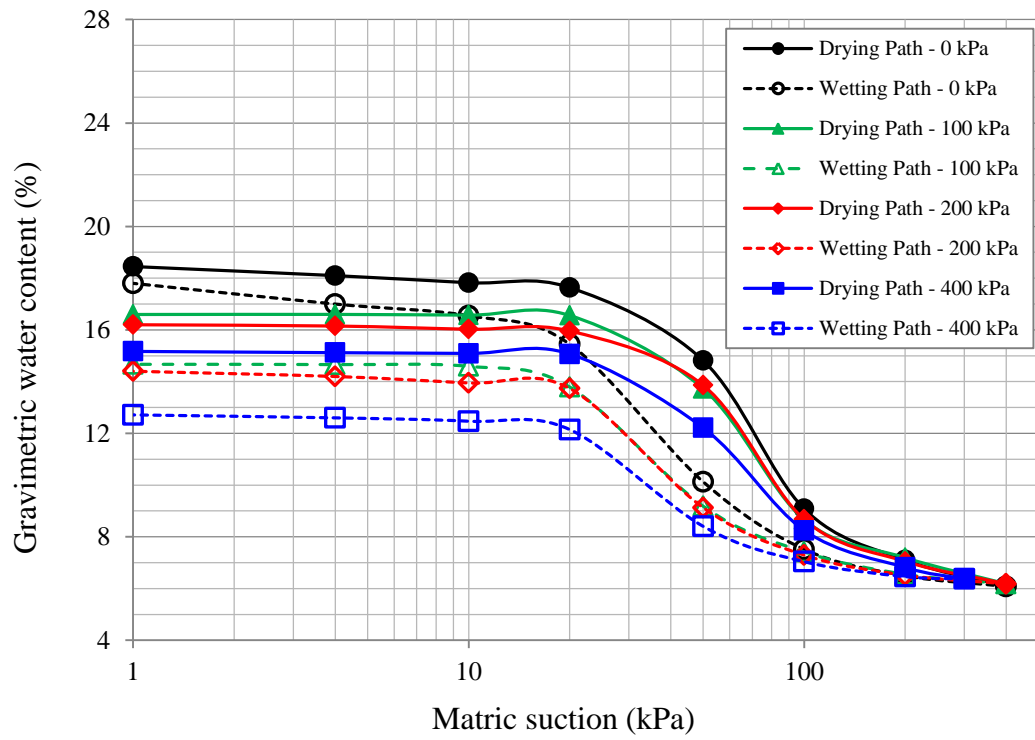


Figure 6.4. The drying and the wetting SD-SWCCs of the sandy soil having 40% gypsum content.

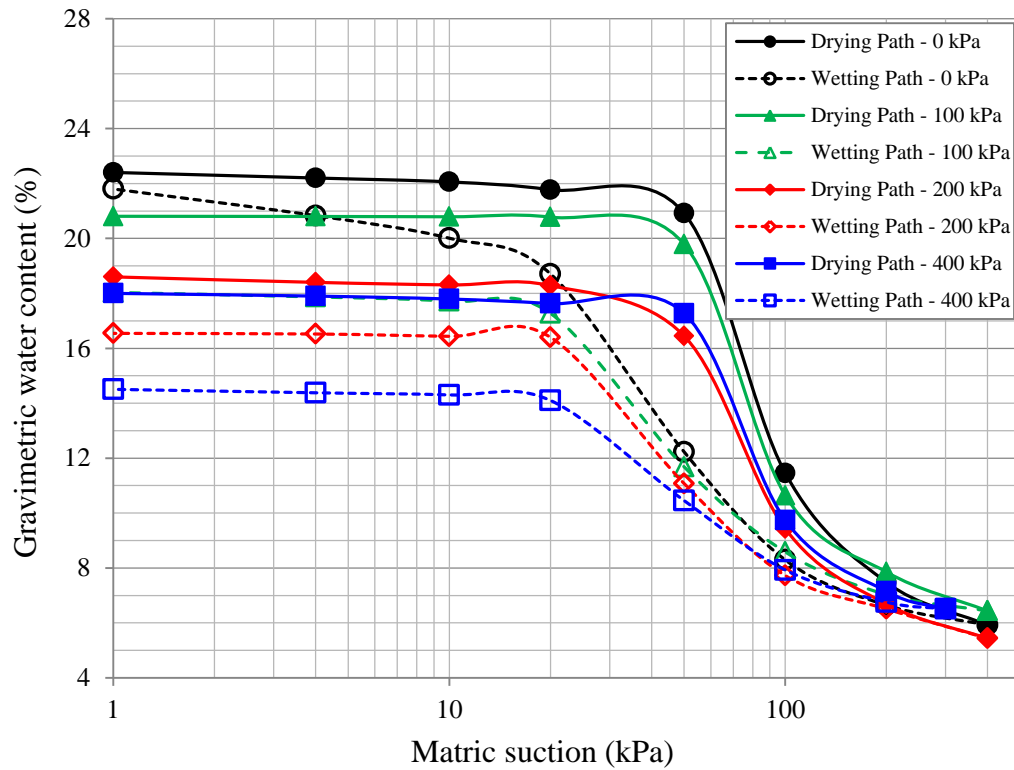


Figure 6.5. The drying and the wetting SD-SWCCs of the sandy soil having 65% gypsum content.

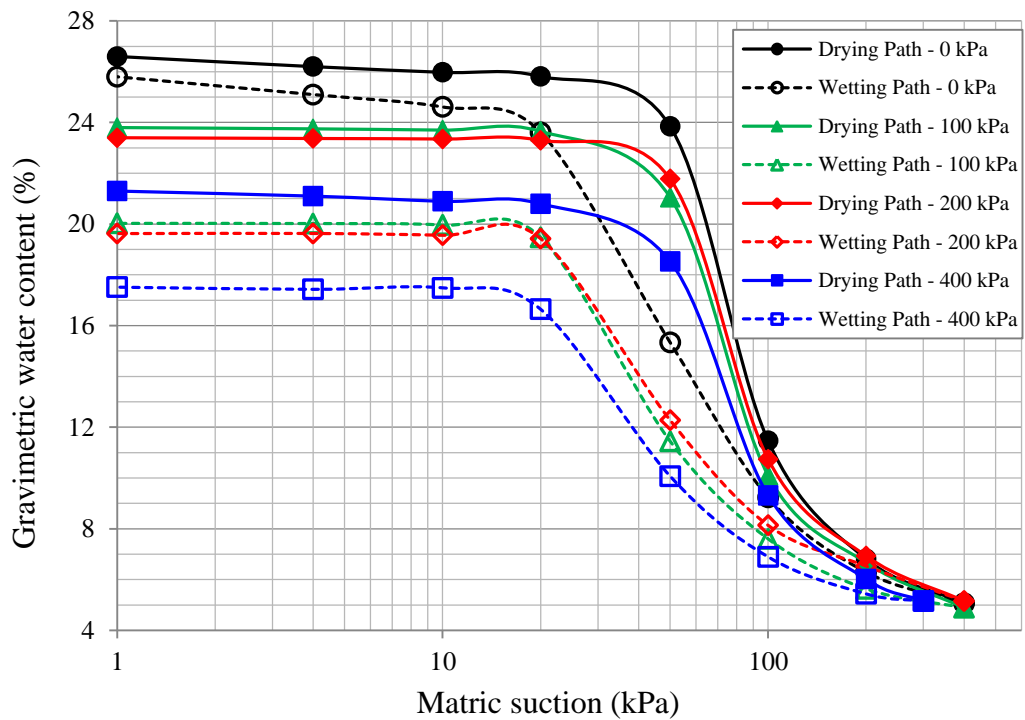


Figure 6.6. The drying and the wetting SD-SWCCs of the sandy soil having 80% gypsum content.

In general, the SD-SWCCs shown in Figures 6.1 to 6.6 show harmonious trends to each other when they are compared regarding to their gypsum content variations or to the net normal stress variations. The water content-matric suction points of each curve are directly linked by a curved line to form together a consistent "S" shape, without the need to reconditioning them by a best fit curve. Unlike the SWCCs test results of the commercial pressure plate which are presented in the preceding chapter, the SD-SWCCs of the modified stress controllable pressure plate device are presented here without curve fittings to show their reliability, consistency, and their accuracy. However, these curves are characterized mathematically later on in this chapter with an attempt to correlate the obtained fitting parameters with the characteristic points of these curves.

It can be noticed from Figure 6.1 that the gypsum content greatly influences the soil-water characteristics. However, both the drying and the wetting SWCCs still adopt typical S-shapes for different sand-gypsum mixtures when the soil suction is plotted on logarithmic scale. Based on the S-shape of a SWCC, Vanapalli et al. (1994) identified three zones of desaturation which are the boundary effect zone, the

transition zone, and the residual zone. These zones are separated by the "air-entry point" and the "residual point" respectively. Similar to that identification of the drying SWCC, the wetting SWCC could be also designated by three parts separated by two points. These points may be referred to as "air-expulsion point" and "water-entry point". The air-expulsion point is analogous to the air-entry point on drying path but here it represents the point on the wetting SWCC where imbibition of water and the corresponding expulsion of air nearly come to an end. The water-entry point, which is analogous to the residual point, could be defined as the point on the wetting SWCC where water starts to release air and enter specimen voids significantly. Matric suction and water content corresponding to air-expulsion point are referred to as "air-expulsion suction" and "air-expulsion water content", respectively. Similarly, matric suction and water content related to water-entry point are referred to as "water-entry suction" and "water-entry water content", respectively. Some of these terms have been used also by other researchers such as Uchaipichat (2010), Yang et al. (2004), and Stormont (1997).

To evaluate quantitatively the effects of both gypsum content and net normal stress level on the SD-SWCCs, the air-entry suction (ψ_a), the air-entry water content (w_a), the residual suction (ψ_r), and the residual water content (w_r) were determined for all the established drying SD-SWCCs (Figures 6.1 to 6.6) by using Vanapalli et al. (1994)'s graphical method. Analogically, the air-expulsion suction(ψ_{ex}), the air-expulsion water content(w_{ex}), the water-entry suction(ψ_{we}), and water-entry water content (w_{we}) for the wetting SD-SWCCs were found as well.

The SD-SWCC-suction parameters (ψ_a , ψ_r , ψ_{ex} , and ψ_{we}) for different applied levels of net normal stress are presented in Figure 6.7 as functions to gypsum content. Similarly, the SD-SWCC-water content parameters (w_a , w_r , w_{ex} , and w_{we}) for different applied levels of net normal stress are presented in Figure 6.8 as functions to gypsum content. Furthermore, the SD-SWCC-suction parameters, the SD-SWCC-water content parameters, the corresponding water holding capacity values, and the slope values of the transition segments of the SD-SWCCs are presented in Table 6.1.

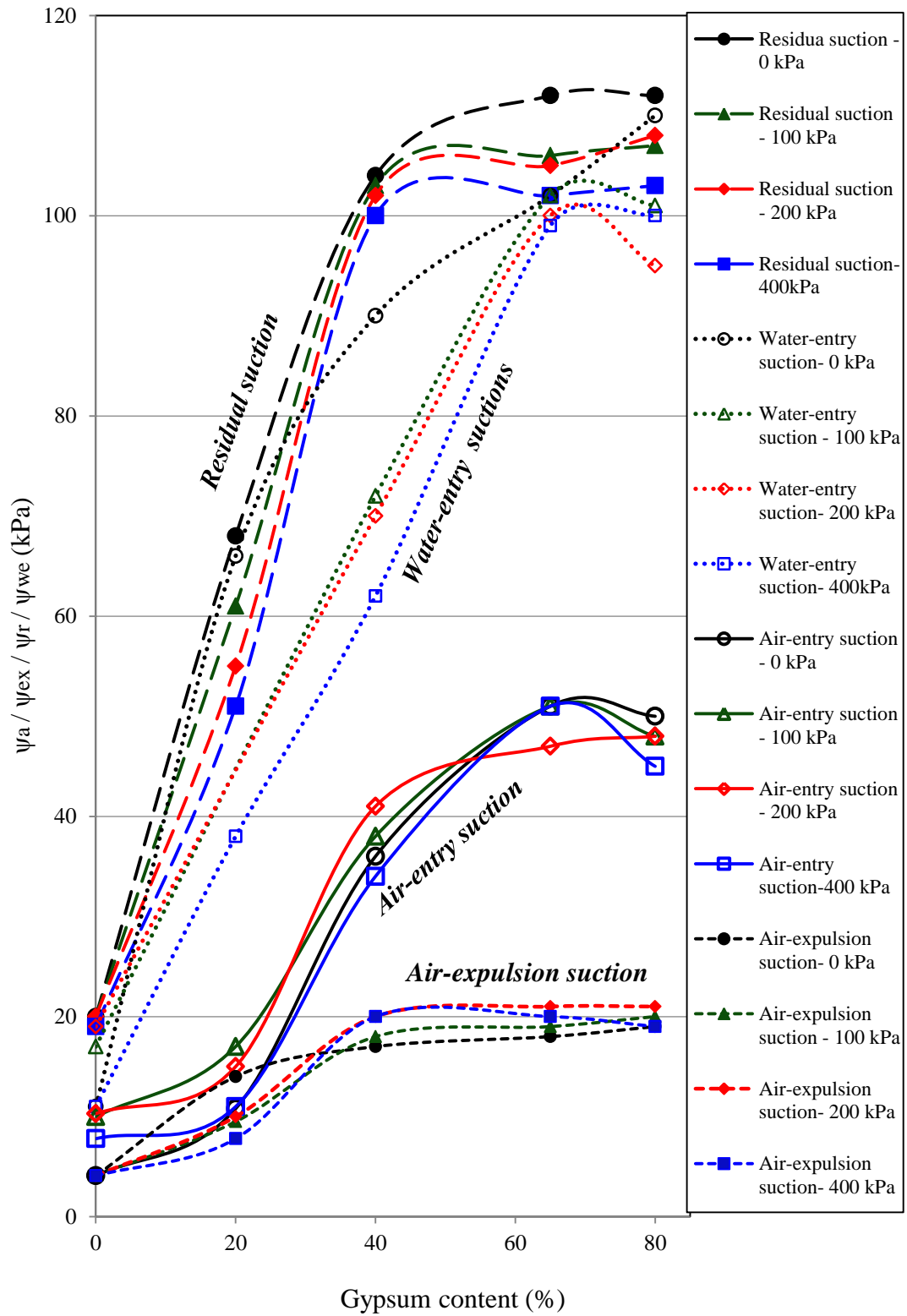


Figure 6.7. Air-entry, air-expulsion, water-entry, and residual suction values of different sand-gypsum mixtures, tested under different net normal stress levels.

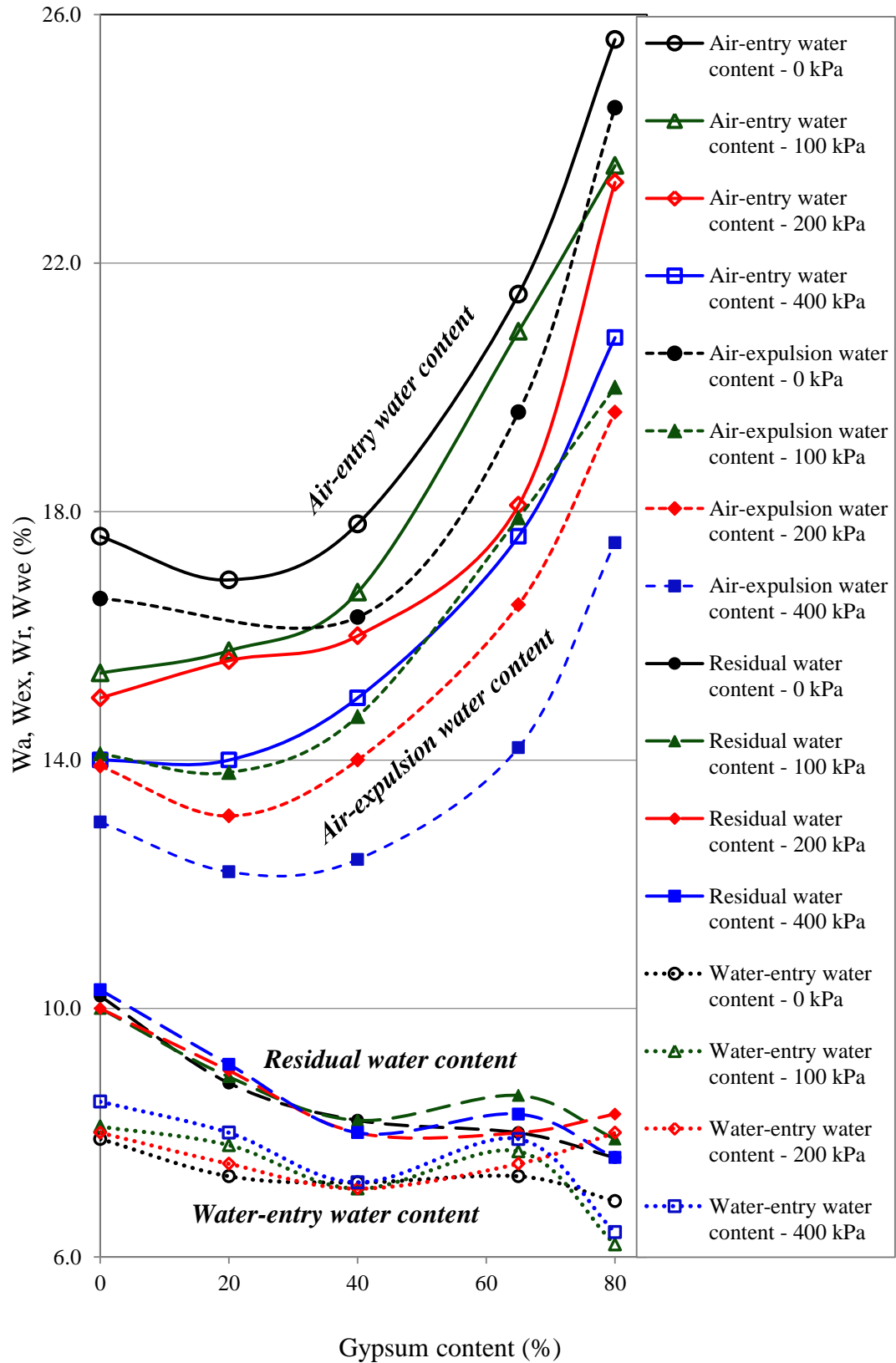


Figure 6.8. Air-entry, air-expulsion, water-entry, and residual water contents of different sand-gypsum mixtures tested under different net normal stress levels.

Table 6.1. SWCCs parameters for specimens having different gypsum contents tested under different loading conditions.

Gypsum content (%)	Ψ_a (kPa)	W_a (%)	Ψ_r (kPa)	W_r (%)	WHC (%)	Slope of SWCC	Ψ_{ex} (kPa)	W_{ex} (%)	Ψ_{we} (kPa)	W_{we} (%)	WHC (%)	Slope of SD- SWCC
	Drying path						Wetting path					
SWCCs parameters for specimens tested under 0 kPa net normal stress												
0	4.1	17.6	20	10.2	7.4	0.11	4.1	16.6	11	7.9	8.7	0.20
20	10.8	16.9	68	8.8	8.1	0.10	14.0	12.4	66	7.3	5.1	0.08
40	36.0	17.8	104	8.2	9.6	0.21	17.0	16.3	90	7.2	9.1	0.13
65	51.0	21.5	112	8.0	13.5	0.40	18.0	19.6	102	7.3	12.3	0.16
80	50.0	25.6	112	7.6	18.0	0.51	19.0	24.5	110	6.9	17.6	0.23
SWCCs parameters for specimens tested under 100 kPa net normal stress												
0	10.0	15.4	20	10.0	5.4	0.18	4.1	14.1	17	8.1	6.0	0.10
20	17.0	15.8	61	8.9	6.9	0.12	9.5	13.8	60	7.8	6.0	0.07
40	38.0	16.7	103	8.2	8.5	0.20	18.0	14.7	72	7.1	7.6	0.13
65	51.0	20.9	106	8.6	12.3	0.39	19.0	17.9	102	7.7	10.2	0.14
80	48.0	23.6	107	7.9	15.7	0.45	20.0	20.0	101	6.2	13.8	0.20
SWCCs parameters for specimens tested under 200 kPa net normal stress												
0	10	15.0	20	10.0	5.0	0.17	4	13.9	19	8.0	5.9	0.09
20	15	15.6	55	9.0	6.6	0.12	10	13.1	60	7.5	5.6	0.07
40	41	16.0	102	8.0	8.0	0.20	20	14.0	70	7.1	6.9	0.13
65	47	18.1	105	8.0	10.1	0.29	21	16.5	100	7.5	9.0	0.13
80	48	23.3	108	8.3	15.0	0.43	21	19.6	95	8.0	11.6	0.18
SWCCs parameters for specimens tested under 400 kPa net normal stress												
0	8	14.0	19	10.3	3.7	0.10	4.1	13.0	11	8.5	4.5	0.10
20	11	14.0	51	9.1	4.9	0.07	7.8	12.2	38	8.0	4.2	0.06
40	34.0	15.0	100	8.0	7.0	0.15	20	12.4	62	7.2	5.2	0.11
65	51	17.6	102	8.3	9.3	0.31	20	14.2	99	7.9	6.3	0.09
80	45	20.8	103	7.6	13.2	0.37	19.0	17.5	100	6.4	11.1	0.15

6.3. Effects of gypsum content on the SD-SWCCs parameters

6.3.1. Effects of gypsum content on SD-SWCCs-water content parameters

The term SD-SWCCs-water content parameters is used to refer to the water content at different characteristic points of the drying and the wetting SD-SWCCs. These parameters include the saturated water content, air-entry water content, residual water content, water-entry water content, and the air-expulsion water content of the SD-SWCC under consideration.

The drying and the wetting SWCCs for specimens of different sand-gypsum mixtures are presented in Figure 6.1. These specimens were tested under 0 kPa net normal stress. One of the remarkable points, which could be noticed from Figure 6.1, is the increase of saturated water content with increasing gypsum content. It increases from 17.7 % for the sandy soil without gypsum to 26.6% for 80% gypsum content, and this may be attributed in part to the increase of initial void ratio in the specimens having high gypsum contents as described in Chapter 4 (Table 4.1). It is obvious from Figure 6.1 that the SWCC becomes higher with increasing gypsum content as long as matric suction is greater than the residual value. In contrary, at residual zone, the higher gypsum content specimen the lower SWCC is. This trend may be quantitatively evaluated by presenting the air-entry water contents and the residual water contents as functions to gypsum content as shown in Figure 6.8. The difference between these two values for a certain soil represents the water holding capacity (WHC) for that soil. At any net normal stress level, the increase of gypsum content causes a noticeable increase in the air-entry water content and a slight decrease in the residual water content, i.e., there is a clear increase in the water holding capacity with increasing gypsum content under different net normal stress levels as shown in Figure 6.9. As well as, Figure 6.8 reveals that there is a clear increase in the air-expulsion water content and a slight decrease in the water-entry water content with increasing gypsum content.

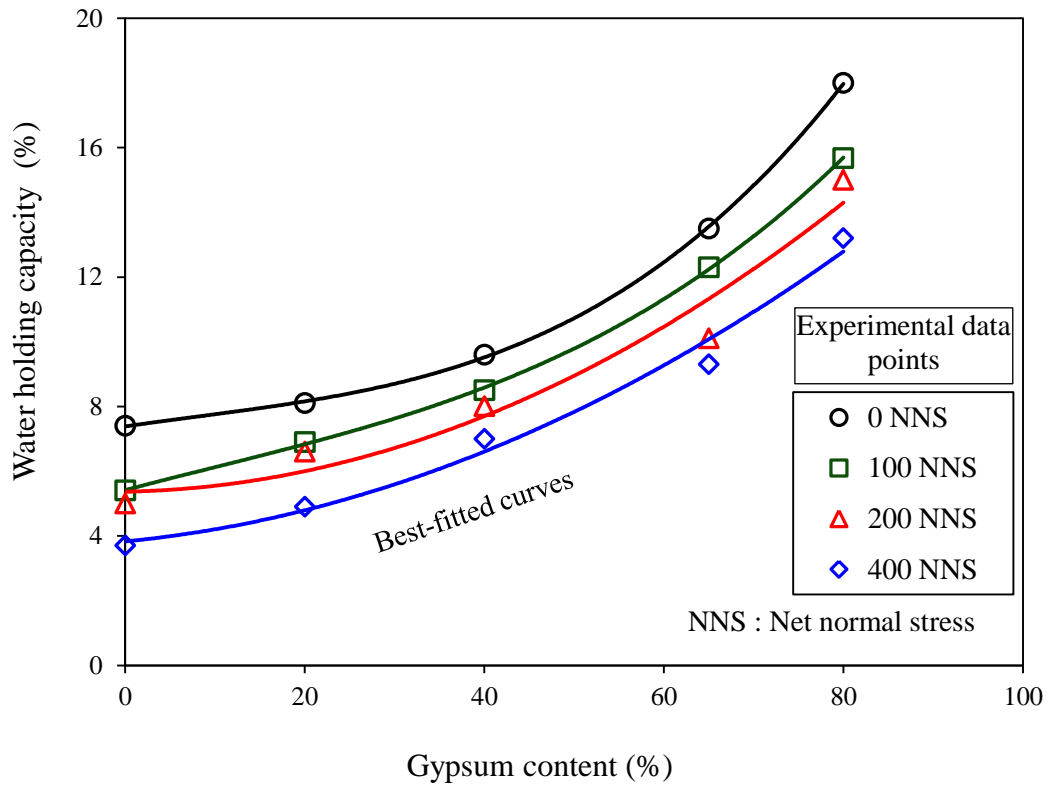


Figure 6.9. Effect of gypsum content on the water holding capacity of the sandy soil under different net normal stress levels.

6.3.2. Effects of gypsum content on the SD-SWCCs-suction parameters

The SD-SWCC-suction parameters are referred to matric suction values corresponding to the four characteristic points of the drying and the wetting SD-SWCCs. These parameters include the air-entry suction, residual suction, water-entry suction, and the air-expulsion suction. Referring to Figures 6.1 and 6.7, it can be noticed that there is a clear increase in both the air-entry suction and the residual suction with increasing gypsum content, under different levels of net normal stress. Figure 6.7 and Table 6.1 reveal that the influence of increasing gypsum content on the air-entry suction and the residual suction is more pronounced when gypsum content increases from 0% to about 40%. Then, further increasing in gypsum content seems to be slightly affected these parameters. This behaviour could be directly related to the effect of gypsum content on the grain-size distribution and then on the pore-size distribution of these sand-gypsum specimens as described in Chapter 3 (Figure 3.1). Moreover, there is a significant effect of gypsum particles on the geometry of pore spaces. This effect results from the brittle nature of gypsum

particles which can be shaped during compaction to take the shapes of the existent pore spaces that formed between sand particles. At low gypsum contents, the increase in gypsum percentage highly influences the pore spaces, but this influence becomes insignificant when gypsum content increases over a certain percentage.

6.3.3. Effects of gypsum content on the slope of the SD-SWCC

The slope of the SD-SWCC at the transition zone reveals a clear increase with increasing gypsum content as can be noticed from Figure 6.1 and Table 6.1. This trend is consistent with the trend of the grain-size distribution curve with increasing gypsum content as shown Figure 3.1. Soils of relatively narrow pore size distribution have relatively wide water content domain corresponding to narrow range of suction, i.e. steep SD-SWCC slope.

It is worth to mention here that the slope of SD-SWCC is normally used to determine the specific moisture capacity, which is defined as the decrease in volumetric water content corresponding to the increase in suction, where the suction is expressed as a hydraulic head (Lu and Likos, 2004). This term, specific moisture capacity, is usually used in conjunction with hydraulic diffusivity to describe the unsteady flow of water in unsaturated porous media, where the hydraulic conductivity is the product of hydraulic diffusivity by the specific moisture capacity (Gardner, 1956; Binson and Gribb, 1997; Doering, 1965, Gupta et al., 1974; Lu and Likos, 2004). Therefore, the increase of gypsum content causes a clear increase in the unsaturated hydraulic conductivity through the increase in the slope of the SD-SWCC. The slope of the SD-SWCC through the transition zone can be measured as $[(w_a - w_r)/(\log \psi_r - \log \psi_a)]$. The slopes of different SD-SWCCs are presented in Table 6.1. The effect of gypsum content on the slope of the drying and the wetting SWCC under different levels of net normal stress is shown in Figure 6.10. It can be noticed from Figure 6.10 that the drying SD-SWCCs are more pronounced to be affected with the increasing of gypsum content than the wetting SD-SWCCs which exhibit marginal effects.

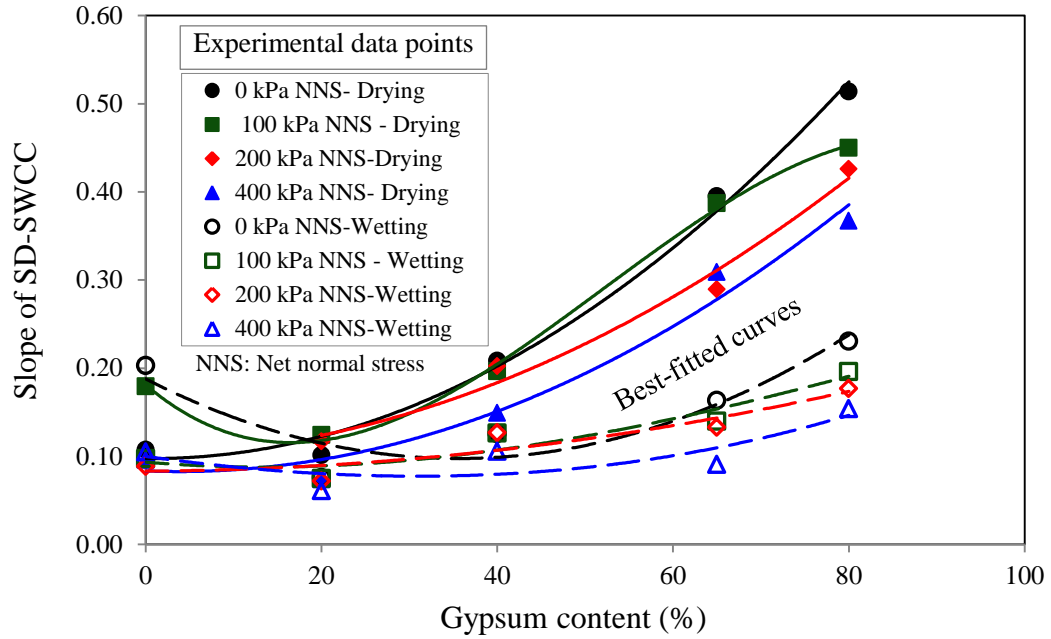


Figure 6.10. Effect of gypsum content on the slope of SD-SWCC of the sandy soil under different loading condition.

6.3.4. Effects of gypsum content on hysteresis phenomenon

There is a marked hysteresis between the drying and the wetting soil-water characteristic curves for all soil specimens (see Figure 6.1). Specimens undergoing drying processes usually tend to retain a greater amount of water than those under wetting processes. This may be mainly attributed to the non-homogenous pore size distribution (Haines, 1930; Miller and Miller, 1988), the contact angle hysteresis (Bear, 1972), and the entrapped air effects. By estimating the area between the drying and the wetting paths of SWCCs, the hysteresis can be evaluated (Yang et al., 2004). Following this concept, Figure 6.1 shows that the hysteresis loop size seems to increase with increasing gypsum content.

However, comparing the values of residual suction by the corresponding values of water-entry suction and the values of air-entry suction by the corresponding values of air-expulsion suction gives a better quantitative evaluation to the hysteresis phenomenon. This concept has been proposed and adopted in this study. Figure 6.7 and Table 6.1 show that the difference in the residual suction and the corresponding water-entry suction markedly increases with increasing gypsum content, reaches a maximum difference at 40% gypsum content and then starts to decrease at higher gypsum contents. This observable trend is more pronounced with increasing the

applied net normal stress. Figure 6.7 and Table 6.1 also show that the difference between the air-entry suction and the corresponding air-expulsion suction noticeably increases with increasing gypsum content under all levels of applied net normal stress. The comparison of these suction parameters provides the horizontal shifts between the drying and the wetting SD-SWCCs, while the vertical shifts could be evaluated by comparing the water content parameters of the SD-SWCCs.

Furthermore, it can be noticed from Figure 6.1 that the breadth of the hysteresis loop is most pronounced in the transition zone when the water retention is governed by capillary mechanism, while it is less pronounced at the residual zone when the pore water retention falls under adsorption mechanism. Figure 6.8 also shows that under any level of net normal stress there are clear differences between the air-entry water contents and the corresponding air-expulsion water contents, which are mostly due to air entrapment in some closed voids. These differences seem to be slightly changed with increasing gypsum content.

6.3.5. Effect of gypsum content on suction-water content equalization time

Figure 6.11 shows the elapsed time required for matric suction-water content equalization. These values were determined during the establishing of the drying and the wetting SD-SWCCs for different sand-gypsum mixtures, tested under 0 kPa net normal stress. It can be noticed from Figure 6.11 that the elapsed time required for equalization for a soil specimen depends on the amount of the applied suction increment and the zone of SD-SWCC at which the specimen is. At boundary effect zone, the time required to reach equalization was found to be short comparing with that at transition zone. After passing the air-entry value, ψ_a , the time required for equalization was found to be significantly increased for the drying path because large pores start to drain and large amount of water is leaving the specimen. During the wetting path the elapsed time needed to reach equalization was increased when passing the water-entry suction value, ψ_{we} , where large pores start to soak up water (see Figure 6.11).

Figure 6.11 reveals that at any level of matric suction, the elapsed time required to reach equalization noticeably increases with increasing gypsum content. This may

be attributed to the increase in the water holding capacity with the increasing of gypsum content and consequently there is a relatively large amount of water leaving the specimen. Furthermore, the elapsed time required to reach equalization during the wetting process is much greater than that during the drying process. On the other hand, it was noticed from the inflow/outflow time dependent readings of specimens tested under 100, 200, 300, and 400 kPa net normal stress that the equalization time is affected also with the level of the applied net normal stress. As the applied net normal stress increases, the time required to reach equalization decreases markedly.

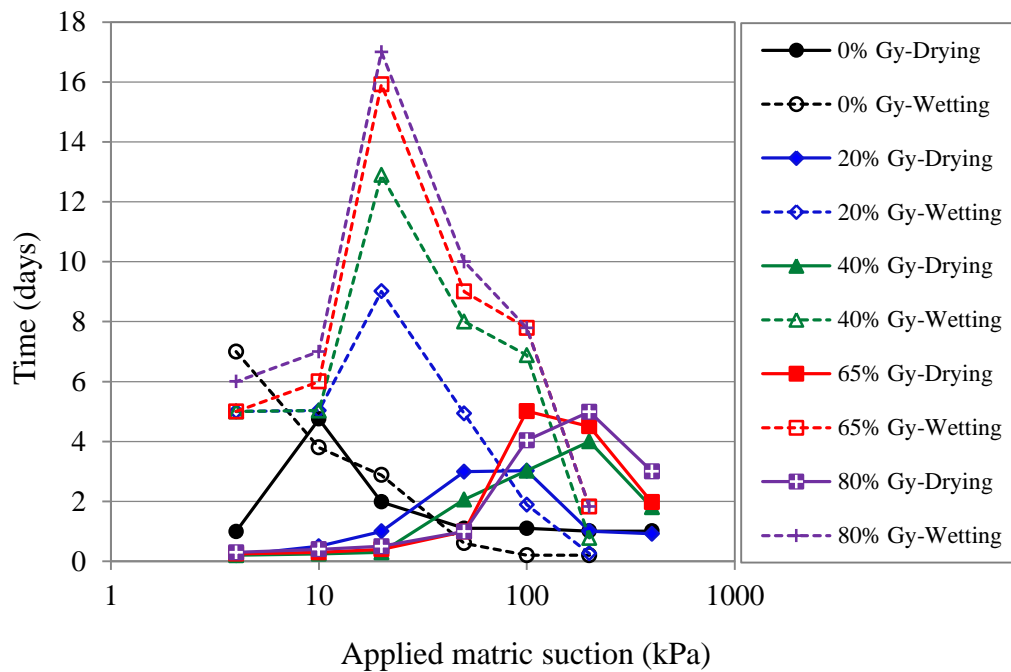


Figure 6.11. Time required for matric suction-water content equalization versus applied matric suction during the drying and the wetting processes for different sand-gypsum mixtures tested under 0 kPa net normal stress level.

6.4. Effects of net normal stress on SD-SWCCs parameters

6.4.1. Effect of net normal stress on initial water content of SD-SWCC

The stress-dependent soil-water characteristic curves for five sand-gypsum mixtures tested under different levels of net normal stress are presented in Figures 6.2 to 6.6. These figures reveal that for all gypsum contents, at the beginning of the test when the applied matric suction is zero, soil specimens subjected to a higher net normal stress exhibit lower initial gravimetric water contents. This result is agreed

with that found by Ng and Pang (2000b). The decrease in the initial water content can be attributed to the decrease in the void ratio associated with the increasing of net normal stress. This decrease depends on the compressibility characteristics of soil specimens. Specimens contain high gypsum contents exhibit higher decrease in void ratio under normal stress comparing with specimens having low gypsum content. That is because the compressibility indices of these specimens are higher than those having low gypsum contents, as discussed in Chapter 5 (Figures 5.5 and 5.6). The initial gravimetric water contents of the SD-SWCCs of different sand-gypsum mixtures are shown in Table 6.2. It can be noticed from Table 6.2, when the applied net normal stress increases from 0 to 400 kPa, the initial gravimetric water content varies from 17.2 to 14.5% for specimens having 20% gypsum content, and from 26.6 to 21.3% for 80% gypsum content.

Table 6.2. Initial gravimetric water contents of the SD-SWCCs of different sand-gypsum mixtures.

Applied net normal stress (kPa)	Gypsum content (%)				
	0	20	40	65	80
	Initial gravimetric water content (%)				
0	17.7	17.2	18.5	22.4	26.6
100	15.3	15.8	16.6	20.8	23.8
200	14.9	15.6	16.2	18.6	23.4
300	14.4	15.2	15.5	18.2	21.5
400	14.1	14.5	15.2	18.0	21.3

6.4.2. Effect of net normal stress on characteristic zones of SD-SWCC

The test results of the SD-SWCCs presented in Figures 6.2 to 6.6 reveal that the effect of the applied net normal stress on the SWCCs is more pronounced within the boundary effect zone, and it is extended to some degree through the transition zone. The effect of the applied net normal stress decreases with increasing matric suction till reaches a slight effect at the beginning of the residual zone. This behaviour can be attributed to the reason that at low matric suction values water is retained in pore spaces under capillary mechanism, while at high matric suctions the predomination is to the hydration mechanism (see Section 2.4.7). Capillary mechanism depends mainly on particle and pore structure and pore-size distribution which are directly

influenced with the increasing of net normal stress. In contrary, the hydration mechanism which is related mainly to the surface properties of soil particles does not influenced by the value of the applied net normal stress.

6.4.3. Effects of net normal stress on SD-SWCCs characteristic points

The characteristic points of the SD-SWCCs include the air-entry and residual points on the drying curve, and the water-entry and air expulsion points on the wetting curve. It can be noticed from Figures 6.2 to 6.6 that for all gypsum contents, the increasing of net normal stress causes remarkable decrease in the air-entry water contents and slight increase in the air-entry suctions. Thus, the air-entry points shift mostly vertically downwards with increasing net normal stress. Similar stress dependency of the air-expulsion points can be noticed on the wetting paths. At residual side, it may be shown that for all gypsum contents the increase of net normal stress causes slight decrease in the residual suctions and slight increase in the residual water contents. Thus, the net normal stress seems to be has limited effects on the residual points. On the wetting paths, for any sand-gypsum mixture, the water-entry suction reveals clear decrease with increasing the net normal stress, while the variation in water-entry water content seems to be insignificant, i.e., the water-entry points on the wetting paths move horizontally with increasing the net normal stress.

6.4.4. Effect of net normal stress on the slope of SD-SWCCs

The test results shown in Figures 6.2 to 6.6 indicate that with increasing the applied net normal stress, the SD-SWCCs show reduction in desorption rate as well a greater reduction in absorption rate, i.e., the SD-SWCCs become flatter. Thus, the water holding capacity clearly decreases with increasing the net normal stress, and this could be noticed also from Figure 6.9, Figure 6.10, and Table 6.1. Same behaviour of SD-SWCCs was also noticed by other researchers like Tse (2007), see Section 2.4.9.

6.4.5. Effect of net normal stress on hysteresis phenomenon

Comparisons between the residual suctions and the corresponding water-entry suctions (Figure 6.7), and between the air-entry water contents and the corresponding

air-expulsion water contents (Figure 6.8), under different levels of net normal stress show that there is a general tendency to the hysteresis loops to be moderately greater with the increasing of net normal stress. This finding does not comply with the results of Zhou (2008), Tse (2007), and Sharma (1998), see Section 2.4.9.

6.5. Mathematical modelling of SD-SWCCs

There are several mathematical models that have been proposed to describe SWCCs. Fredlund and Xing (1994)'s model is one of the most commonly used SWCC models in geotechnical engineering discipline (Equation 3.3). As recommended by Fredlund and Xing (1994), for the range of suctions applied in this study, the correction function $F(\psi)$ may be taken equal to one and Equation 3.3 is reduced to the following form for representing the gravimetric water content as a function to the soil suction:

$$w(\psi) = \frac{w_s}{\{\ln[e + (\psi/a)^n]\}^m} \quad 6.1$$

where $w(\psi)$ is the gravimetric water content at any soil suction, w_s is the saturated water content, e is the base of the natural logarithm, and a , n , m are fitting parameters related to the SWCC under consideration.

To characterize the measured SD-SWCCs, Equation 6.1 was used to describe mathematically each of the drying and the wetting SD-SWCC. The fitting parameters and the corresponding statistical indices (coefficients of determination, R^2), were found. These parameters are listed in Table 6.3 for different sand-gypsum mixtures, which were tested under different net normal stress levels.

Trials have been done to fit the experimental data using two other different models, such as those proposed by van Genuchten (1980) and Pereira & Fredlund (2000). Good representations were also found but with statistical indices marginally less than those obtained by applying Fredlund and Xing (1994)'s model. The applicability of different mathematical models to represent the experimental test results reveals the laboratory reliability of SD-SWCCs measurements by using the newly modified stress controllable pressure plate device. As well as, this could also be shown from the consistency of the experimental results and the possibility of

getting the same results with very slight differences when testing identical specimens.

Table 6.3. The fitting parameters and the coefficient of determination (R^2) for specimens having five different gypsum contents tested under four different net normal stress levels.

Net normal stress (kPa)	Gypsum content (%)	Drying curve					Wetting curve				
		Fitting parameters			Ws (%)	R^2	Fitting parameters			Ws (%)	R^2
		a	n	m			a	n	m		
0	0	4.8	4.3	0.30	17.7	0.98	3.9	24.9	0.19	17.2	0.99
	20	15.3	2.6	0.43	17.2	0.98	5.5	1.3	0.55	16.7	0.97
	40	42.2	5.2	0.46	18.5	0.98	18.7	2.6	0.55	17.8	0.97
	65	57.8	6.2	0.53	22.4	0.98	21.7	2.1	0.77	21.8	0.96
	80	56.1	5.7	0.69	26.6	0.97	31.3	2.5	0.91	25.8	0.96
100	0	10.2	11.9	0.18	15.3	0.99	4.5	6.6	0.20	14.3	0.99
	20	22.1	5.2	0.30	15.8	0.98	13.5	4.5	0.27	13.9	0.98
	40	43.6	8.2	0.34	16.6	0.98	22.0	5.1	0.33	14.7	0.98
	65	55.7	8.8	0.41	20.8	0.98	27.0	4.0	0.44	18.0	0.98
	80	53.2	6.3	0.61	23.8	0.97	29.7	4.8	0.56	20.0	0.97
200	0	10.6	13.9	0.16	14.9	0.99	4.5	6.0	0.20	14.0	0.99
	20	20.0	5.3	0.29	15.6	0.98	16.8	20.7	0.16	13.2	0.99
	40	45.4	8.2	0.33	16.2	0.98	22.8	5.4	0.32	14.4	0.98
	65	51.1	5.7	0.50	18.6	0.97	32.3	5.5	0.41	16.5	0.97
	80	57.5	6.8	0.58	23.4	0.98	32.3	5.2	0.50	19.6	0.97
400	0	7.7	4.9	0.19	14.1	0.99	3.8	23.9	0.12	13.6	0.99
	20	14.0	3.1	0.29	14.5	0.98	8.0	4.3	0.19	12.4	0.98
	40	40.9	7.1	0.33	15.2	0.98	21.8	6.2	0.25	12.7	0.98
	65	56.7	8.8	0.38	18.0	0.98	29.0	4.1	0.36	14.5	0.97
	80	52.1	5.8	0.61	21.3	0.97	26.9	4.3	0.53	17.5	0.97

As mentioned in Section 2.4.7, there are two distinctive changes in slope along SWCC. These changes in slope define two essential points for describing the SWCC, the air-entry point and the residual point. The parameter "a" in Fredlund and Xing (1994)'s model is closely related to the air-entry suction as reported by Yang et al. (2004). The parameter "n" governs the change in slope of the soil-water characteristic curve near the air-entry point, and the parameter "m" governs the

change in slope near the residual point. Comparing the air-entry suction/air-expulsion suction values which are presented in Table 6.1 with the corresponding "a" values in Table 6.3 shows that the values of the parameter "a" are slightly higher than the air-entry suction/air-expulsion suction values. A highly correlated linear relationship, $a = 1.11 \psi_a + 1.93$, was found by plotting the values of parameter "a" against those of air-entry/air-expulsion values as shown in Figure 6.12. The coefficient of determination, R^2 , for this relationship was found to be 0.96. This relationship complies to some degree with that found by Yang et al. (2004) which was $a = 1.40 \psi_a - 0.08$. Yang et al. (2004)'s relationship was found for five different sandy soils with a coefficient of determination, R^2 , equal to 0.987.

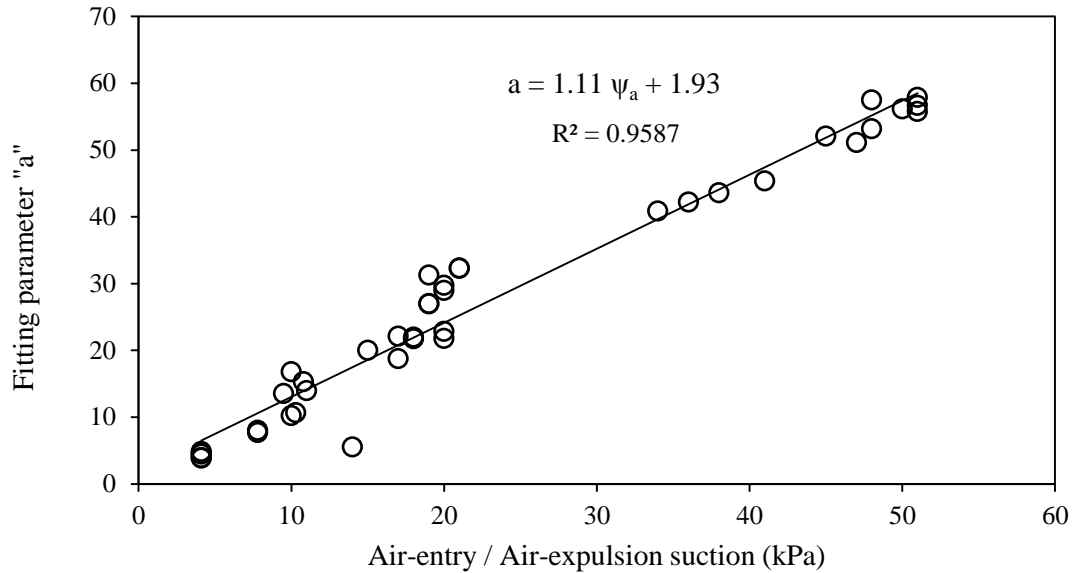


Figure 6.12. The relationship between the fitting parameter "a", Fredlund and Xing (1994)'s model, and the air-entry/air-expulsion suction values for various sand-gypsum mixtures that tested under different net normal stress levels.

As well as, the SD-SWCCs parameters in Table 6.1 and the fitting parameters presented in Table 6.3 reveal that there is a clear correlation between the fitting parameter "m" and the corresponding residual suction/water-entry suction values. The larger the ψ_r value, the greater the "m" value as shown in Figure 6.13. Furthermore, the parameter "m" may be expressed the degree of curvature near the residual point. Large values of "m" reflect a sharp corner near the residual point and a steeper curve at residual zone.

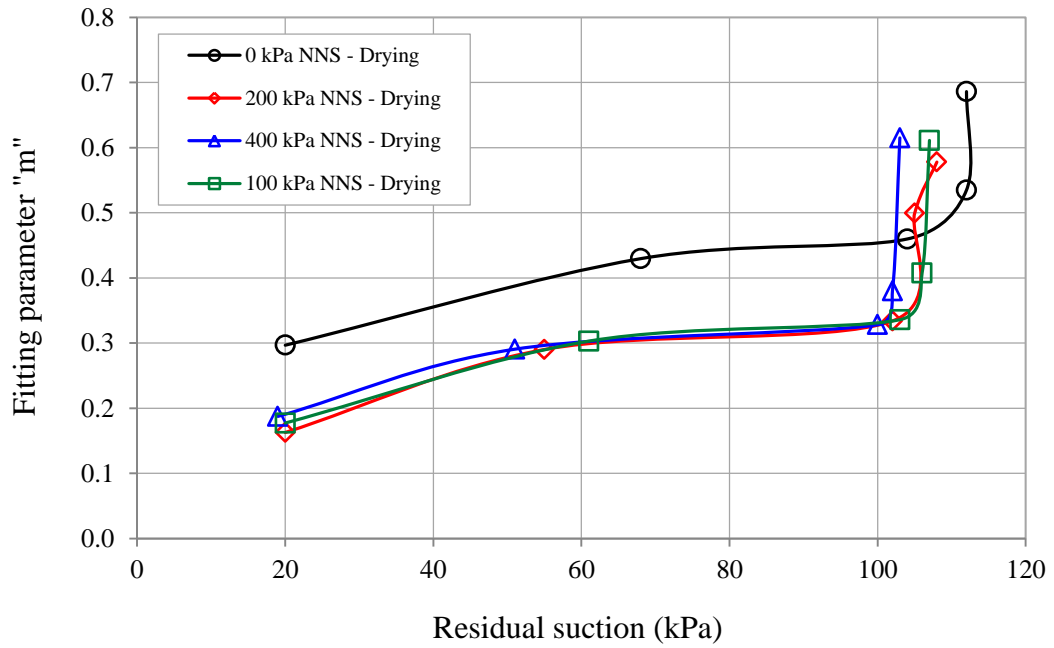


Figure 6.13. The relationship between the fitting parameter "m", Fredlund and Xing (1994)'s model, and the residual suction value for various sand-gypsum mixtures that tested under different net normal stress levels.

Referring to Figures 6.1 to 6.6, the slope of the SD-SWCCs at the transition zone and the degree of curvature near the air-entry point can be evaluated by considering the values of "n" parameter that shown in Table 6.3. Large value of n reflects a steeper slope for SWCC and a sharp corner near air-entry point. For all gypsum contents, there is a general tendency for the "n" value to increase with increasing the net normal stress till reach a peak value corresponding to a net normal stress around 200 kPa, then it shows some decrease with higher levels of net normal stress. In other words, the increasing of net normal stress causes the desorption rate, near the air-entry points, to increase reaching a peak under 200 kPa and then tends to decrease under higher net normal stress levels.

6.6. Comparison of SWCCs obtained from different equipment

The consistency and reliability of the SWCCs established by using the modified stress controllable pressure plate device and those established by using the commercial pressure plate are compared in this section. For comparison, the SWCCs of specimens having 0, 20, and 40% gypsum contents are considered and presented in Figure 6.14.

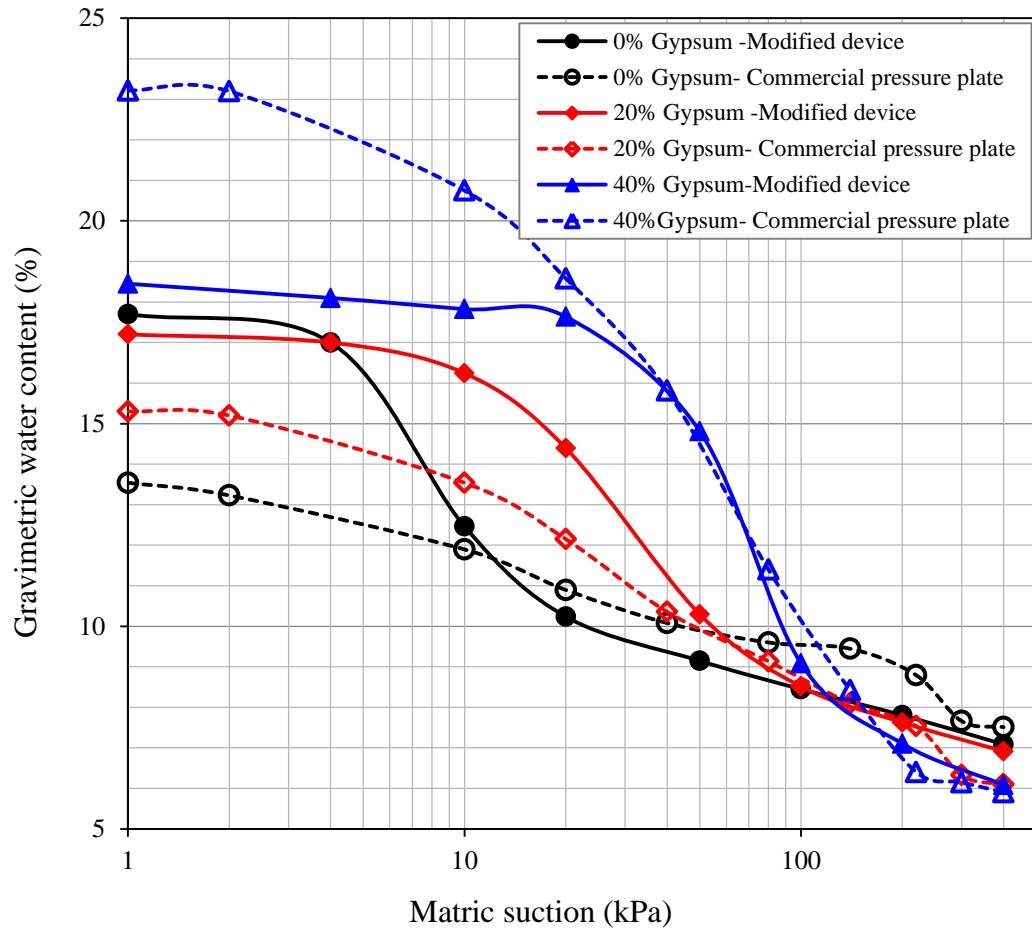


Figure 6.14. Comparison of the SWCCs established from the modified stress controllable pressure plate device with that established by using the commercial pressure plate.

It can be noticed from Figure 6.14 that there are clear differences between these two curve sets in the general shapes, saturated water contents, air-entry points, residual points, water holding capacities, and the desaturation rates or the slope of the SWCCs. For comparison, these parameters are listed in Table 6.4 for the two sets of the SWCCs. The SWCCs obtained from the modified device have well defined "S" shapes, well distinguishable desaturation zones, and accordingly well defined air-entry and residual points. On contrary, the SWCCs established by using the commercial pressure plate do not have well expressive "S" shapes and their characteristic points (the air-entry and residual points) cannot be defined with enough precision.

Table 6.4. Comparison of SWCCs parameters obtained by using the modified stress controllable pressure plate device and those obtained from the commercial pressure plate.

Parameters	Modified device			Commercial device		
	Gypsum content			Gypsum content		
	0%	20%	40%	0%	20%	40%
$w_{sat.}(\%)$	17.7	17.2	18.5	13.5	15.3	23.2
ψ_a (kPa)	4.1	10.8	36.0	10.0	11.0	14.0
ψ_r (kPa)	20	68	104	72	150	210
w_a (%)	17.6	16.9	17.8	11.8	13.6	20.7
w_r (%)	10.2	8.8	8.2	9.5	7.6	6.5
WHC (%)	7.4	8.1	9.6	2.3	6.0	14.2
SWCC slope	0.11	0.10	0.21	0.03	0.05	0.12

The differences between the results of the commercial pressure plate and that of the modified device may be resulted in part from the variation in the size of specimens used. At the commercial pressure plate tests, the specimen size was 45 mm diameter and 7.6 mm thickness, while it was 68 mm diameter and 14 mm thickness in the modified stress controllable pressure plate device tests.

The saturation process of soil specimens used with the modified device is different from that used with the commercial pressure plate. This difference may be the main reason causing the variations at the initial saturated water content of the two sets of the SWCCs. At the commercial pressure plate, an excess of water is left on the top of the ceramic disc to saturate the soil specimens while they are in contact with the ceramic disc (see Section 3.4.3.3). At the modified device, there is no excess of water standing on the top of the ceramic disc, and the water level in the outside standing tubes is adjusted to be at the level of the soil-ceramic disc interface (see Section 4.2.4.1).

At the modified device, the specimen covers the entire surface area of the ceramic disc. Thus, there is no exposed area of ceramic disc in contact directly with the pressurized air of the cell, which may have some effect on continuity of the water phase as pointed out lately by some researches such as Leong et al. (2011), Power et al. (2011). In contrary, the exposed area to air pressure in the commercial pressure plate is mostly greater than the covered area by the soil specimens.

The soil specimen at the modified device occupies the entire volume of the cell, and that is preventing the soil from drying by evaporation. On the other hand, the volume of the commercial vessel is too large in compare with the volume of the soil specimens tested, which may results in remarkable evaporation especially when the attached vapour saturator that saturates the inflow air is disregarded.

Furthermore, as a comparison with published investigations on nearly similar soils, the SD-SWCCs established in this study on the silty clayey sand without gypsum additives are compared to matric suction measurements carried out by Tripathy et al. (2012). The soil used in these measurements was a low-plastic , poorly graded silty sand, taken from North-West Libya that contains 3.5% coarse sand, 12.8% medium sand, 71% fine sand, and 12.7% silt and clay fractions. Three groups of Tripathy et al. (2012)'s data points related to statically compacted specimens under three levels of load (high, intermediate, and light) are presented in Figure 6.15. In these groups the matric suction values of as compacted water content specimens were measured by using null-type axis-translation technique.

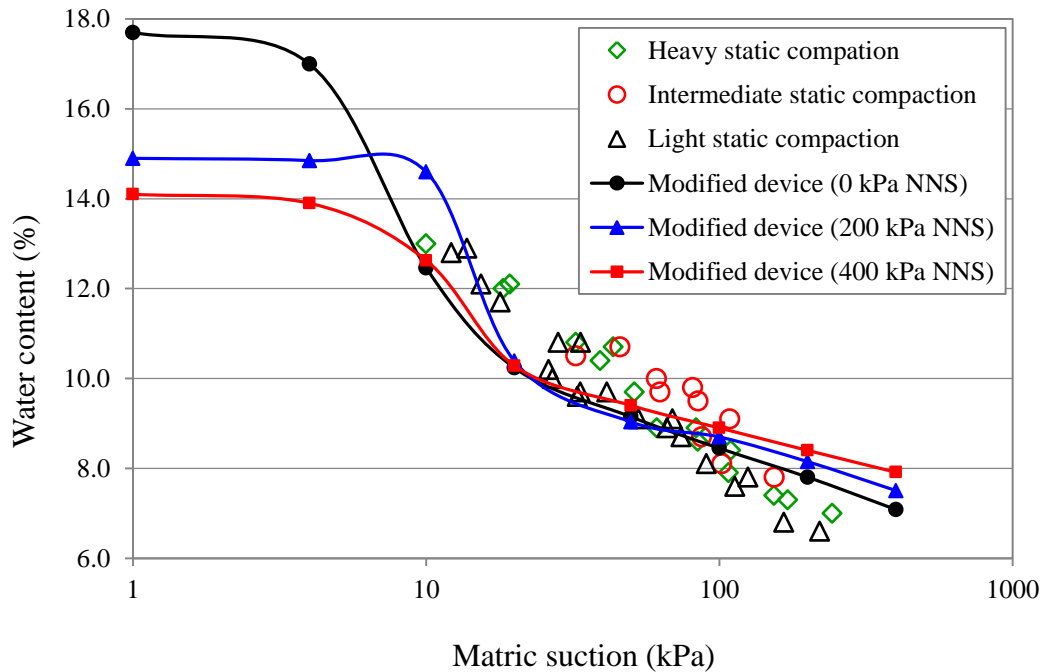


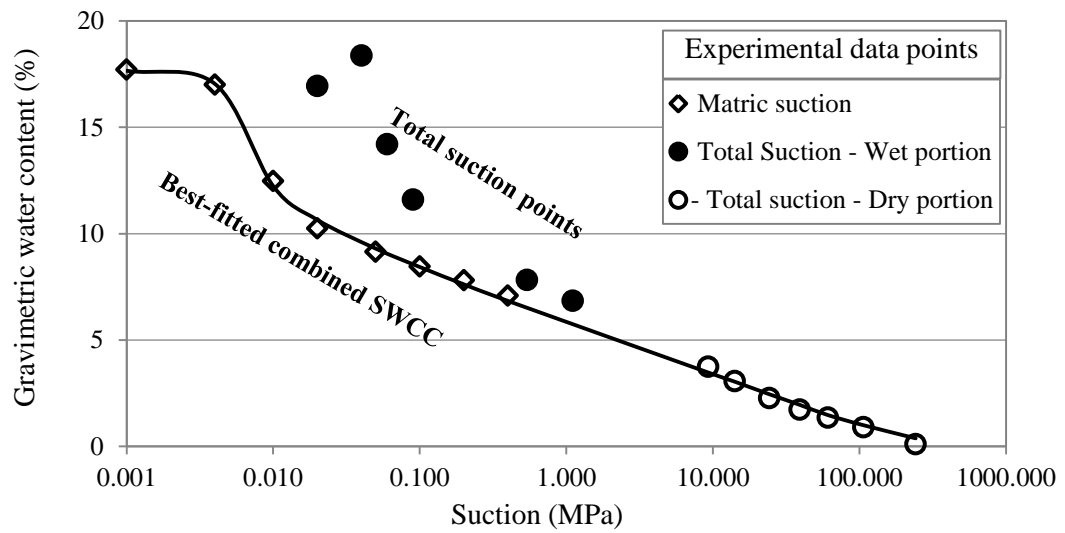
Figure 6.15. Comparison of the drying SD-SWCCs established from the modified stress controllable pressure plate device for the silty clayey sand with published matric suction measurements on poorly graded silty sand using null-type technique (Tripathy et al., 2012).

It can be noticed from Figure 6.15 that the variations between the established SD-SWCCs and Tripathy et al. (2012)' measurements are acceptable to some extent. These variations result mainly from the differences in the grain-size distribution of the soils used, and the differences in the compaction dry densities and water contents of the prepared specimens.

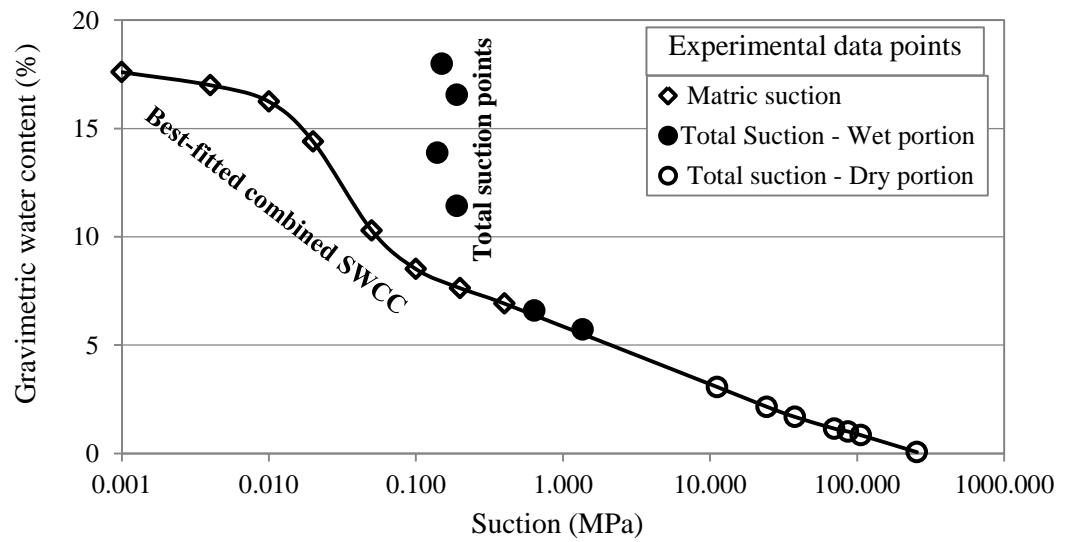
6.7. Combined SWCCs of different sand-gypsum mixtures

Results of the SWCCs found from the modified stress controllable pressure plate device were combined with those obtained from the dew point potentiometer to establish nearly the entire SWCCs for different sand-gypsum mixtures (ASTM D 6836-02). The resulting curves are referred to as the combined SWCCs. The drying SWCCs tested at 0 kPa net normal stress which are presented earlier in Figure 6.1 are employed to establish the segments of the combined SWCCs corresponding to high water contents (wet segments). Results of the dew point potentiometer at low water contents, typically corresponding to total suction values greater than 1 to 1.5 MPa, are used to define the dry segments (dry ends) of the SWCCs. Under this condition, the osmotic component of the total suction is generally small, and the matric and total suctions are comparable (Fredlund and Xing, 1994; ASTM D 6836-02).

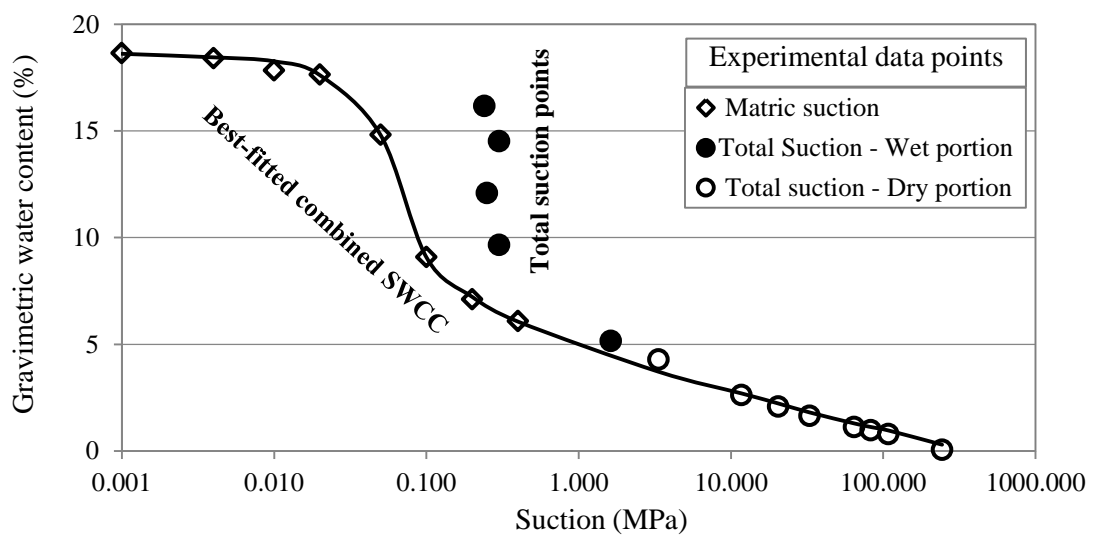
The combined SWCCs for different sand-gypsum mixtures are presented in Figure 6.16. The experimental data points of the dew point potentiometer at relatively high water contents are presented as well. The combined curves show the gravimetric water content as a function to the matric suction, whereas the single data points show the gravimetric water content as a function to the total suction (matric + osmotic) and they are referred to as the " total suction-data points ". The combined SWCCs points are designated by using open symbols, square for the wet portions and circular ones for the dry ends. The total suction-data points are symbolized by circular solid signs at wet portions and circular open ones at dry portions.



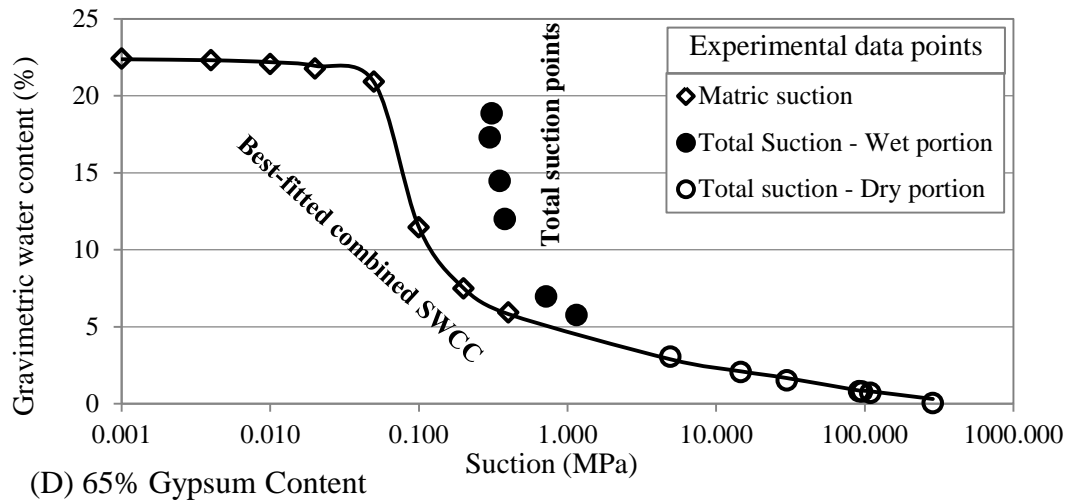
(A) 0% Gypsum Content



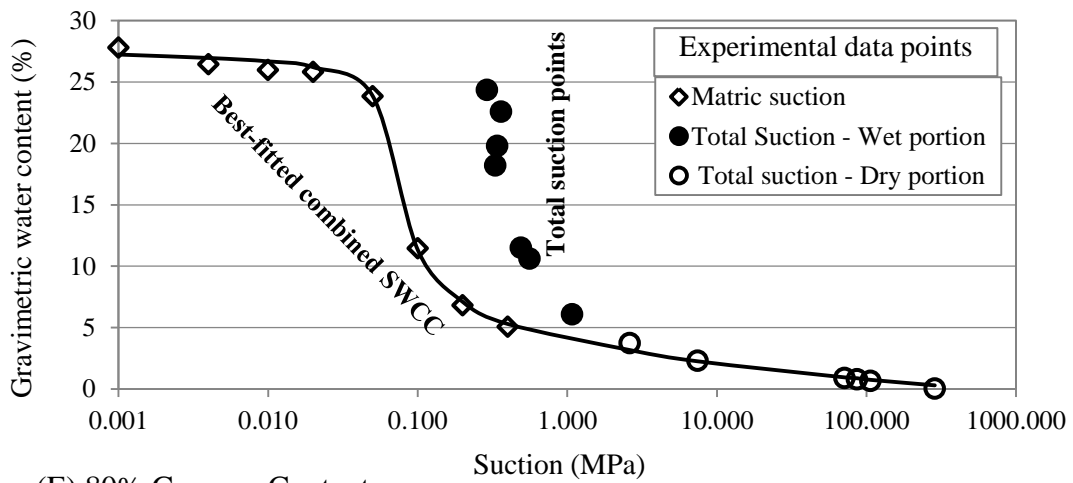
(B) 20% Gypsum Content



(C) 40% Gypsum Content



(D) 65% Gypsum Content



(E) 80% Gypsum Content

Figure 6.16. Combined SWCCs for different sand-gypsum mixtures, (A) 0%, (B) 20%, (C) 40%, (D) 65%, and (E) 80% gypsum content.

The combined data points of wet and dry portions of the SWCCs were best fitted by using Fredlund and Xing (1994)'s mathematical model. The fitting parameters and the statistical indices for these curves are shown in Appendix A, Table A. 2A.2. The coefficient of determination (R^2) was greater than 0.997 for all these fitted curves. Very good matching between the two portions of the combined SWCC can be noticed for different sand-gypsum mixtures.

The wet portions of the combined curves exhibit remarkable consistency with the corresponding total suction-data points with lateral shifting seems to be harmonic for different gypsum contents as long as the suction values are represented on logarithmic scale. Nevertheless, both the combined and total suction-data points shift to the right, to a higher logarithm cycle, with increasing gypsum content, thus, the

numerical difference between these two curves which represent the osmotic suction increases significantly with increasing gypsum content. On the other hand, the combined and the total suction-data points converge from each other with increasing suction till match at suction values around 2 MPa for different sand-gypsum mixtures.

Examining Figure 6.16 closely, two distinguished constant slope segments could be noticed at each of the combined SWCCs of different sand-gypsum mixtures. The first segment dominates over the capillary mechanism zone (transition zone), while the second segment extends over the hydration mechanism zone (residual zone). A curvature part joints these two segments. The slope of the capillary segment exhibits clear increase with increasing gypsum content, while the slope of the hydration segments on the contrary shows obvious decrease with the increase of gypsum content. The degree of curvature of the joining part between these two segments seems to increase remarkably with increasing gypsum content, i.e., relatively sharp corner may be noticed at the SWCC of high gypsum content specimens.

The effect of gypsum content on the slope of the capillary segment is attributed directly to the effect of gypsum on the pore-size distribution, since gypsum has highly uniform grain-size distribution. Soils of relatively narrow pore size distribution have relatively steep SWCC slope at capillary zone. On the other hand, the slope of the residual segment is related to the specific surface of soil particles and surface charge properties.

The residual points of the SWCCs for different sand-gypsum mixtures can be defined by using the combined SWCCs (Figure 6.16). These points have more accuracy and reliability comparing with those defined by considering only the wet parts of the SWCCs (Figure 6.1). This reliability results from the possibility of defining the tangent line to the residual part of the SWCC precisely. The residual suction and the corresponding water content for different sand-gypsum mixtures, which were determined from the combined SWCCs, are presented in Table 6.5. For comparison, the corresponding values defined from the single SWCCs shown in Figure 6.1 are presented in the same table as well.

Table 6.5. Residual suction and residual water content for different sand-gypsum mixtures defined from the combined SWCCs in comparison to those found from the single SWCCs.

Gypsum content (%)	Combined SWCCs		Single SWCCs	
	ψ_r (kPa)	w_r (%)	ψ_r (kPa)	w_r (%)
0	12	10.8	20	10.2
20	72	8.9	68	8.8
40	115	6.3	104	8.2
65	140	5.0	112	8.0
80	120	5.0	112	7.6

Table 6.5 reveals that the residual suction values defined from the combined and the single SWCCs are comparable to each other, while the residual water contents exhibit noticeable variations, especially for specimens have 40, 65, and 80% gypsum content.

6.8. Summary and concluding remarks

An extensive laboratory programme has been designed to study the influences of gypsum content, net normal stress, and drying-wetting cycle on the soil-water characteristic curve (SWCC) of the sandy soil by using the modified stress controllable pressure plate device. Results of the experimental programme revealed that there is a remarkable dependency of the SWCC on the applied net normal stress. This dependency becomes more pronounced with increasing gypsum content, and this may be attributed in part to the changes of the compressibility characteristics associated with increasing gypsum content in the soil specimen. There is a clear decrease in each of saturated water content, desorption rate, absorption rate, and water holding capacity with increasing net normal stress level for various sand-gypsum mixtures. On contrary, all these parameters are increasing clearly with increasing gypsum content in the soil specimen at different levels of net normal stress. Furthermore, both the air-entry suction and the residual suction show significant increase with increasing gypsum content in the soil mixture. The consistency of the experimental results and the possibility of getting relatively identical results for identical specimens demonstrate the reliability and accuracy of the measurements of the SD-SWCC by using the newly modified device.

CHAPTER SEVEN

STRESS DEPENDENT-UNSATURATED HYRAULIC CONDUCTIVITY FUNCTIONS

7.1. Introduction

Forty tests of stress dependent-hydraulic conductivity function (SD-HCF) were carried out on five sand-gypsum mixtures by using the modified stress controllable pressure plate device. The mixtures had gypsum contents of 0%, 20%, 40%, 65%, and 80%. The specimens were tested during the drying and the wetting path conditions under four different net normal stress levels of 0, 100, 200, and 400 kPa. The room temperature was controlled at 20-22°C and the humidity at 40-50%. The tests were carried out by considering two different approaches at the same time. These approaches are the one step outflow method by Doering (1965) and the multistep outflow method by Gardner (1956) as described in Chapter 4. Accordingly, two groups of SD-HCFs were obtained, one calculated by following Doering's approach and the other by following Gardner's approach. In each group, the hydraulic conductivity was represented first as a function to the matric suction, and second as a function to the gravimetric water content. The results of SD-HCFs according to Doering's approach are presented in Section 7.2 in sets each under the same level of net normal stress, while the results according to Gardner's approach are presented in Section 7.4 in sets each has the same gypsum content.

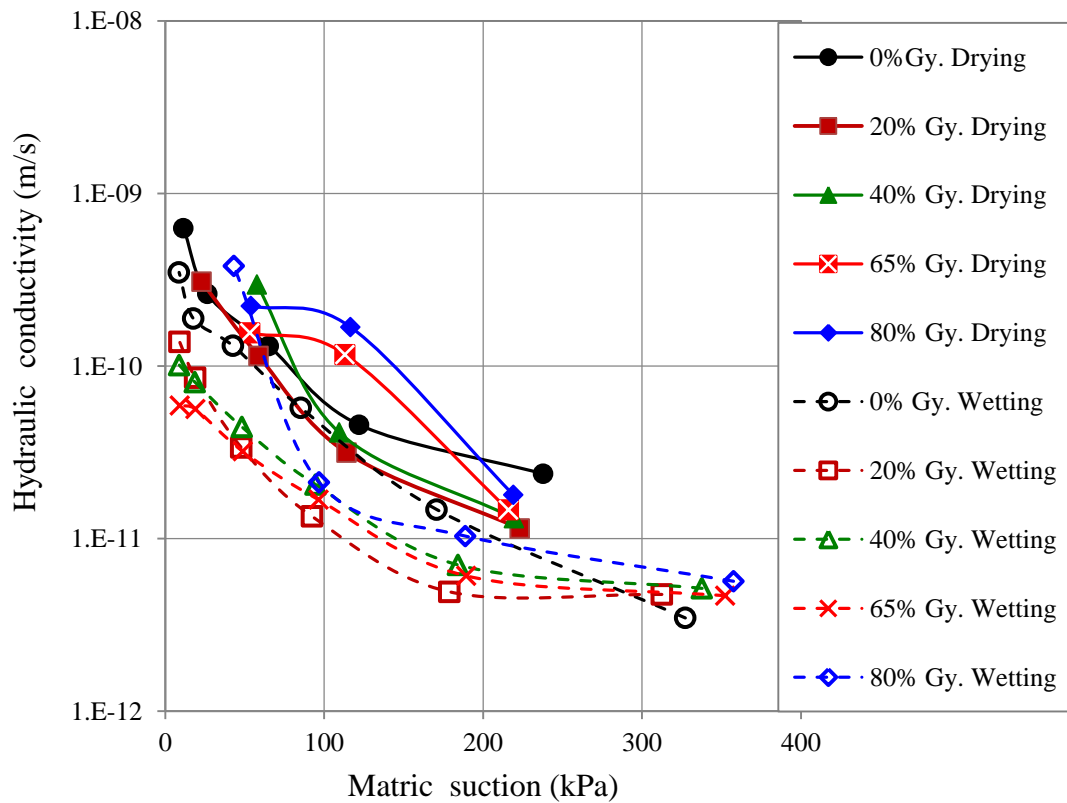
7.2. Effect of gypsum content on SD-HCFs

In this section, the influences of gypsum content, soil suction, and drying-wetting cycle on the hydraulic conductivity function under different levels of net

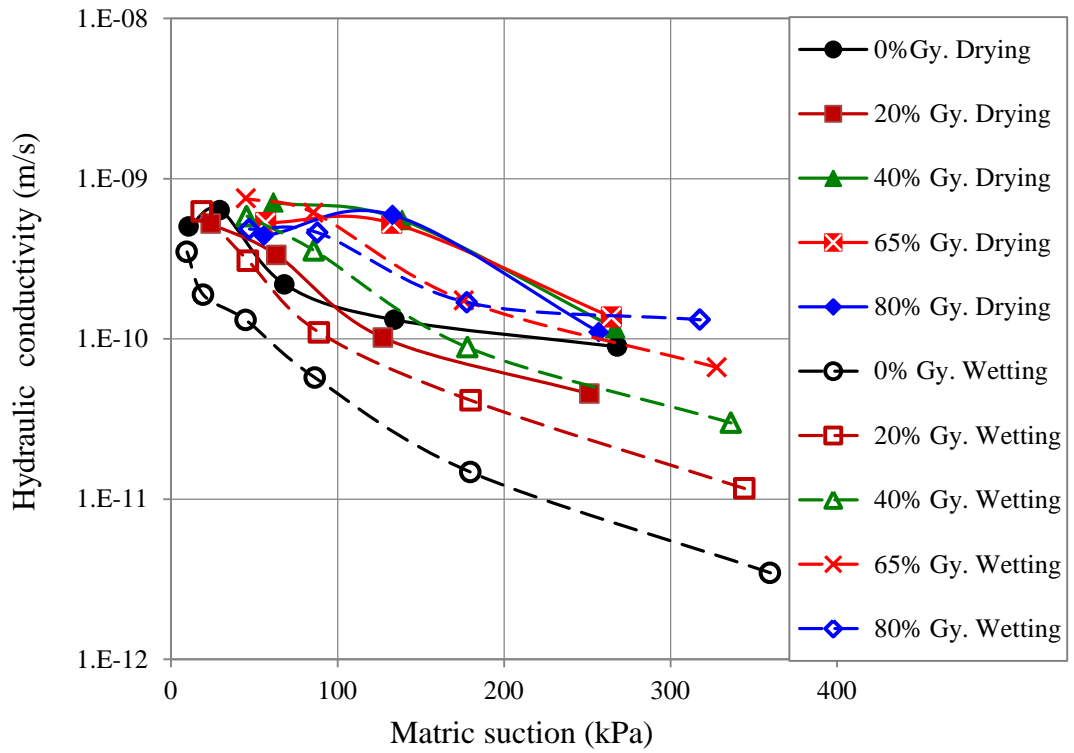
normal stress are presented and discussed. The stress dependent-hydraulic conductivity functions (SD-HCFs) presented in this section were calculated according to Doering's approach after some modification. This approach was applied in each of the successive increments, or decrements, in matric suction instead of applying it through only one large step as specified in the original method. Accordingly, each suction increment or decrement was treated here as a one independent step.

7.2.1. Hydraulic conductivity-matric suction relationships

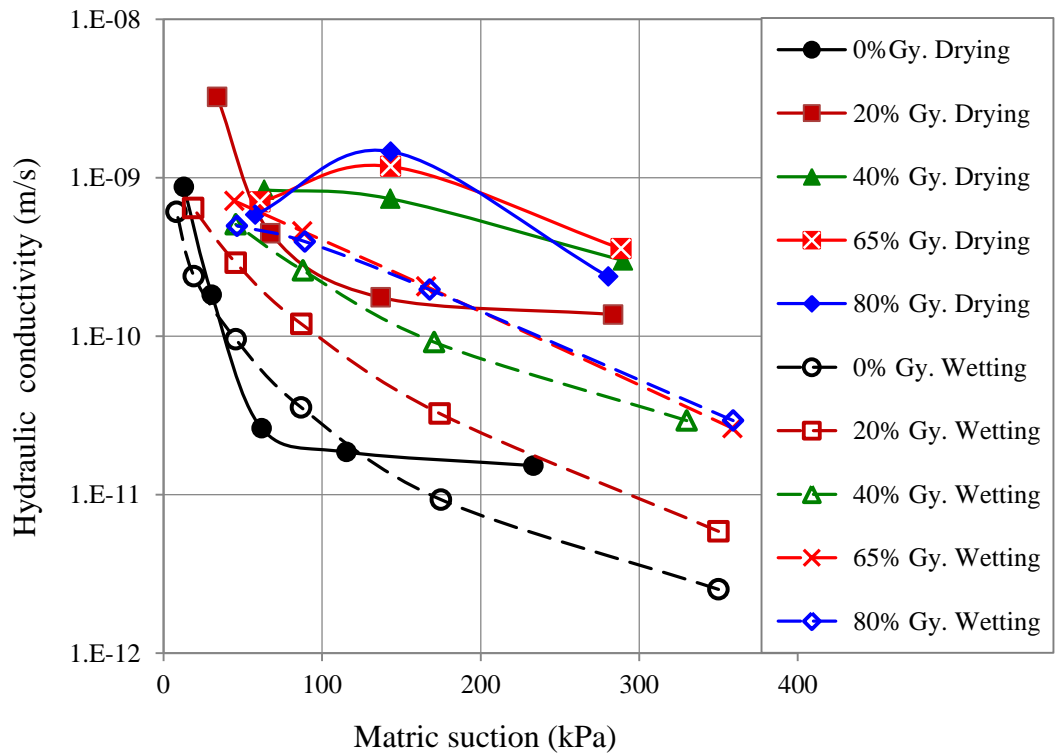
Figures 7.1 A, B, C, and D show the drying and the wetting hydraulic conductivity functions (HCFs) in terms of matric suction, $k(\psi)$, for different sand-gypsum mixtures under net normal stress levels of 0, 100, 200, and 400 kPa, respectively. The measured $k(\psi)$ for the five sand-gypsum mixtures are denoted by using five different symbols and colours, while the drying and the wetting $k(\psi)$ are designated by using solid and open symbols, respectively.



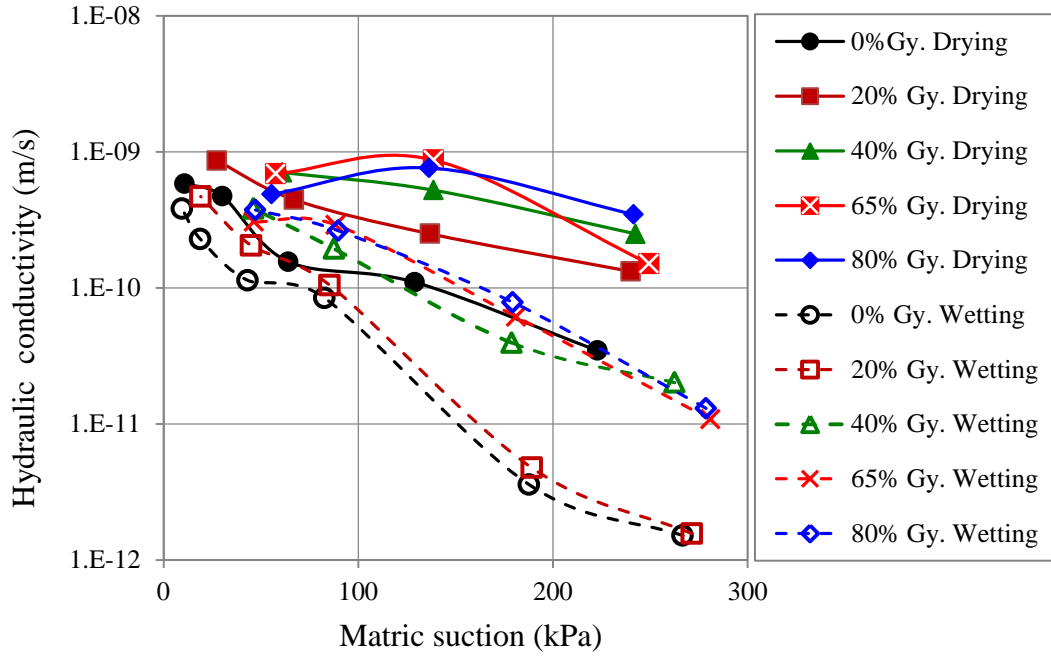
(A) HCFs under 0 kPa net normal stress



(B) HCFs under 100 kPa net normal stress



(C) HCFs under 200 kPa net normal stress.



(D) HCFs under 400 kPa net normal stress.

Figure 7.1. The drying and the wetting hydraulic conductivity functions in terms of matric suction, according to Doering's approach, for different sand-gypsum mixtures, tested under net normal stress levels of (A) 0, (B) 100, (C) 200, and (D) 400 kPa.

In general, Figures 7.1 A, B, C, and D show that the unsaturated hydraulic conductivity values of different sand-gypsum mixtures (corresponding to different levels of net normal stress and matric suction) seem realistic comparing with a saturated hydraulic conductivity of 4×10^{-9} m/s for the host sandy soil without gypsum additives.

It can be noticed from Figures 7.1 A, B, C, and D that the general trend of these functions shows a clear increase in hydraulic conductivity with increasing gypsum content under different levels of net normal stress, for both the drying and the wetting paths, at any value of matric suction. However, for the drying functions, this increase is more pronounced throughout the transition zone, i.e., at matric suction values located between the air-entry and the residual suction values of the sand-gypsum mixtures tested. As matric suction increases more, the hydraulic conductivity functions start to converge to each other reaching minimum differences at the residual suction zones of the mixtures tested. This trend is harmonic with the trend of SWCCs of these mixtures which are presented earlier in Section 6.2. Figures

6.2 to 6.6 reveal that the SWCC becomes higher with increasing gypsum content as long as matric suction is greater than the residual value. At residual zone, the ordering is reversed, thus the higher gypsum content specimen becomes the lower SWCC is. In other meaning, the water content of a specimen increases with increasing gypsum content at any suction value below the residual value. Thus, the flow paths and then the hydraulic conductivity increase with increasing gypsum content. On the other hand, there is a clear increase in the initial void ratio of the prepared specimens with increasing gypsum content as described in Chapter 4, Table 4.1, and consequently this causes the hydraulic conductivity to increase proportionally as well.

Experimentally, it was noticed in this study that the outflow transient methods are inapplicable at matric suction values below the air-entry value (boundary zone) because there is no flow of water. On the other hand, at residual zone, the flow of water is very little making the outflow methods inapplicable as well. Thus, the applicability of the outflow transient methods may be limited to the transition zone only. For this reason, values of hydraulic conductivity measured at suction values below the air-entry points are omitted in this presentation.

Moreover, it can be noticed from Figures 7.1 A, B, C, and D that the general shape of the drying hydraulic conductivity functions is convex upward for mixtures having gypsum content more than 40%, while it has a concave shape for those having 0% and 20% gypsum content. This behaviour may be attributed to the reason that the values of air-entry suctions of the 65% and 80% gypsum content mixtures are relatively high and the initial parts of their functions, $k(\psi)$, are corresponding to matric suction values very close to their air-entry points where the outflow is restricted.

It is clear from Figures 7.1 A, B, C, and D that the drying hydraulic conductivity decreases with increasing matric suction under different net normal stress values, but at a decreasing rate has some dependency on gypsum content. As gypsum content increases, the decreasing rate or the slope of the hydraulic conductivity function shows a clear increase. This trend is consistent with the increasing in slope of the SWCC, or the increasing in desorption rate with increasing gypsum content as

discussed in Section 6.3. Ultimately, this behaviour may be attributed directly to the effect of gypsum content on the grain-size distribution and then on the pore-size distribution.

Like the drying hydraulic conductivities, Figures 7.1 A, B, C, and D reveal that the wetting conductivities show clear increases with decreasing matric suction but at increasing rates depends on gypsum content as well. In contrary to the drying functions, the wetting functions of specimens have higher gypsum content showing lower increasing rate in hydraulic conductivity with decreasing matric suction. In other words, at any specific suction, the slope of the wetting $k(\psi)$ decreases with increasing gypsum content.

The general trend of the wetting and the drying $k(\psi)$, presented in Figures 7.1 A, B, C, and D, shows that the slope of these functions seems to be steeper with high curvature at low suction values and then becomes flatter and goes nearly asymptotic to the suction-axis at high suction values. This trend is consistent with the slopes of the wetting and the drying SWCCs presented in Figures 6.1 to 6.6, where these slopes seem steeper at the transition zones and then become flatter at residual zones. In other words, the rate at which the unsaturated hydraulic conductivity decreases /increases is directly dependent on the water desorption/absorption rate of the soil specimen.

In general, the wetting HCFs seem to be more consistent than the drying HCFs, and could be found for suction values less than the air-entry point with the application of the transient outflow methods. It is worthy to mention here that the practical applicability of the transient outflow methods for a wetting path is extended between the water-entry suction and the air-expulsion suction. These points are analogous to the residual suction and the air-entry suction on the drying path, respectively.

For all specimens that have different gypsum contents, tested under different net normal stress levels, the wetting hydraulic conductivity function was always lower than the corresponding drying function, as may be seen from Figures 7.1 A, B, C, and D. The hysteresis of $k(\psi)$ between the wetting and the drying is consistent with

the results published by Ng and Leung (2012), shown in Figure 7.2, on compacted decomposed silty clay (36% sand, 42% silt, and 22% clay). They adopted the instantaneous profile method using a stress-controllable soil column. The soil specific gravity was 2.68 and placed at dry density of 1.552 Mg/m³.

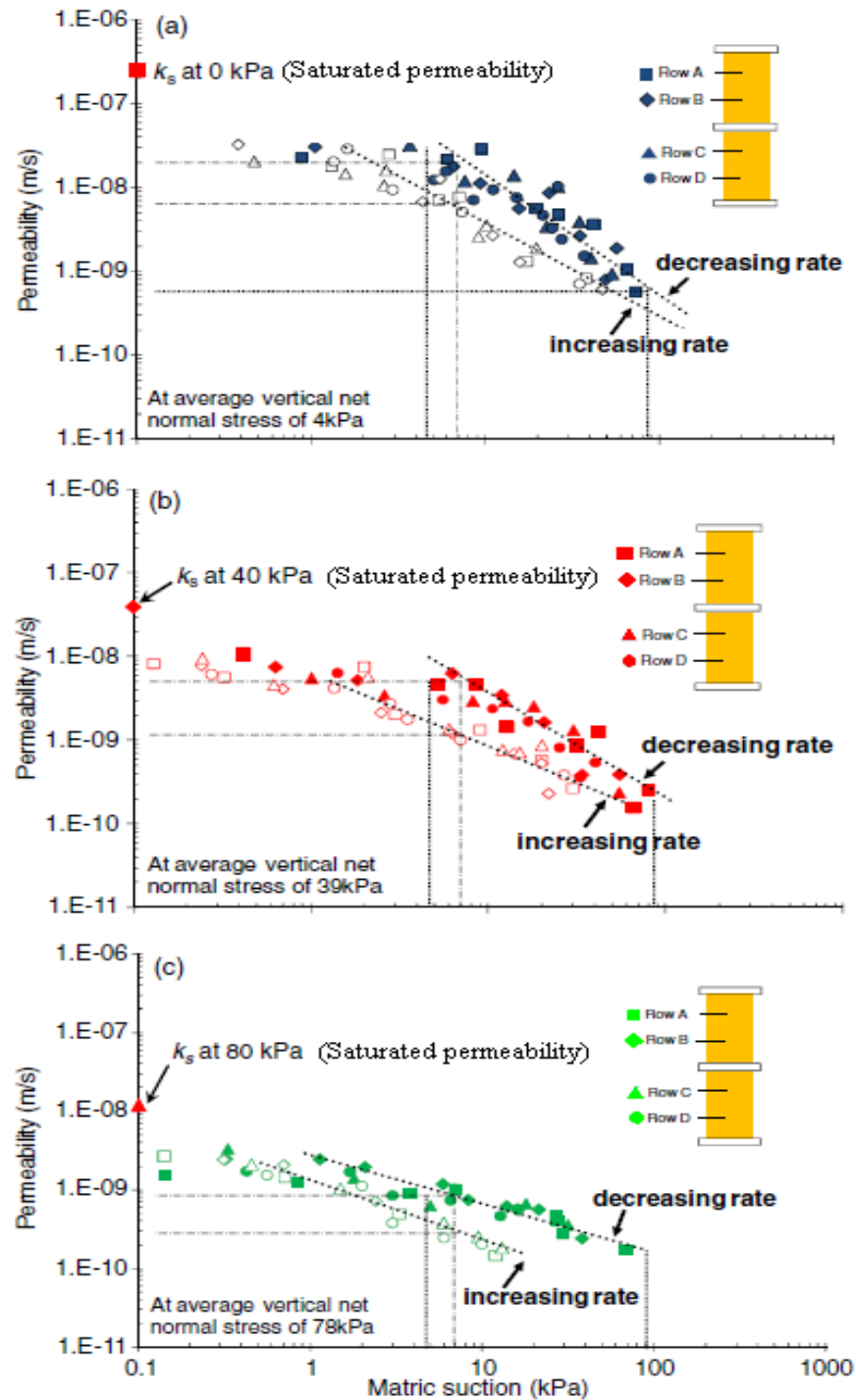


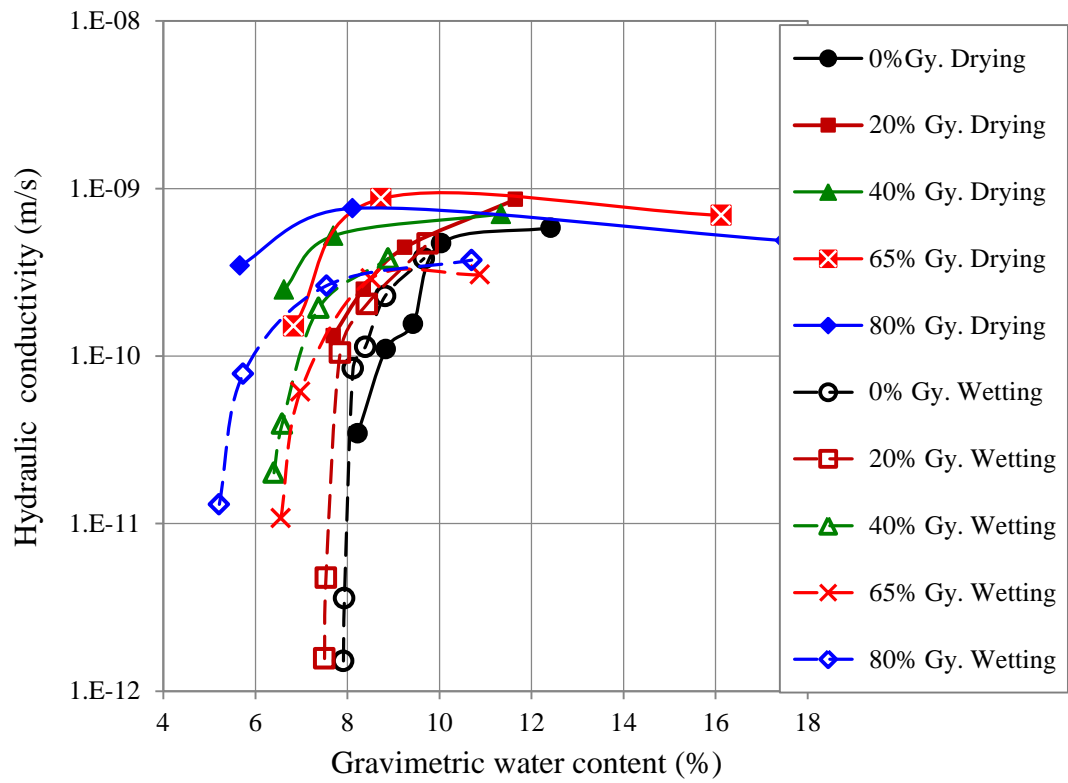
Figure 7.2. Measured drying and wetting stress dependent $k(\psi)$ s at (a) 4 kPa, (b) 39 kPa, (c) 78 kPa net normal stress levels for a compacted decomposed silty clay using the instantaneous profile method (Ng and Leung, 2012).

The hysteresis of $k(\psi)$ is likely because the soil-water characteristic curve exhibits hysteresis, and because the hydraulic conductivity is directly related to the soil-water content. In other words, the water content along the wetting path is always less than that along the drying path at any given suction and this leads to lesser hydraulic flow paths and hence lower wetting hydraulic conductivity. Thus, only minor hysteresis is noticed when the hydraulic conductivity is plotted against the gravimetric water content as discussed in the following section.

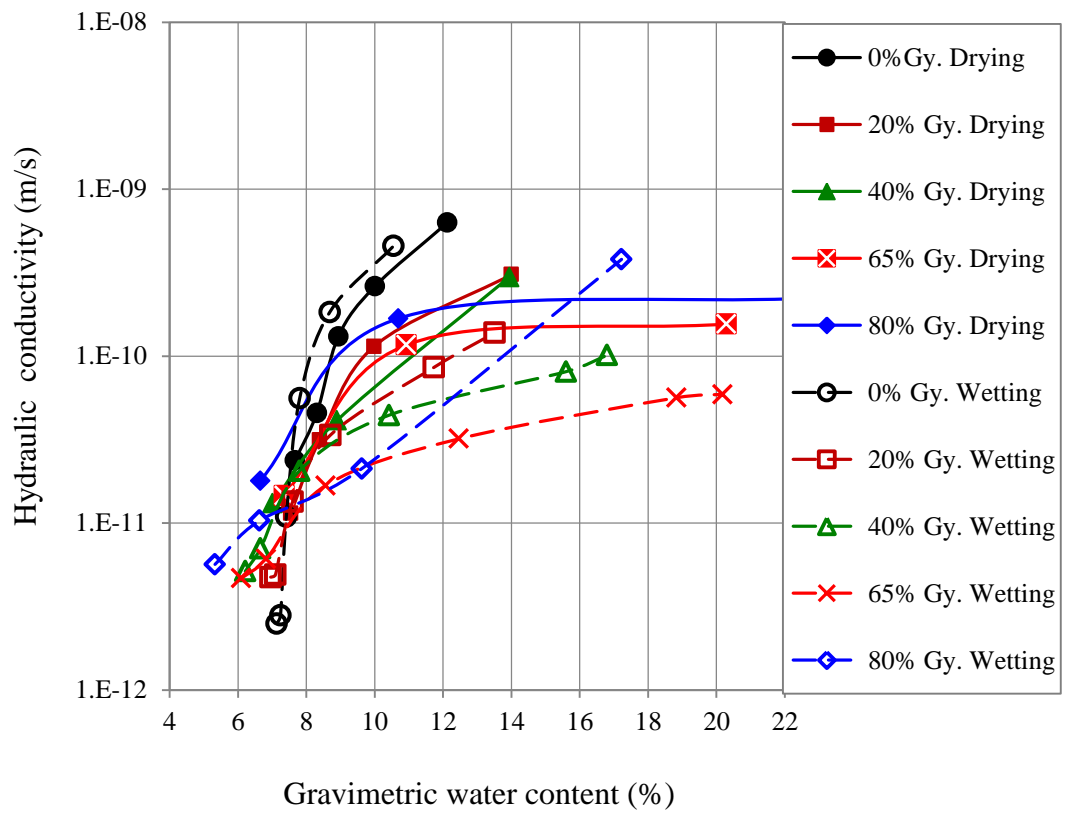
7.2.2. Hydraulic conductivity-gravimetric water content relationships

As discussed in the previous section, the increase in $k(\psi)$ with increasing gypsum content is related in part to the increase in water content of the specimen associated with the increase of gypsum content at any specific matric suction. As well as, the hysteresis of $k(\psi)$ between the drying and the wetting paths is also related to the variation in the water content between these two paths. For that reason, the hydraulic conductivity function is represented in this section in terms of gravimetric water content, and it is designated as $k(w)$. Figures 7.3 A, B, C, and D show the drying and the wetting $k(w)$ for different sand-gypsum mixtures tested under net normal stress of 0, 100, 200, and 400 kPa. These functions were calculated according to Doering's approach after some modification as mention earlier. The $k(w)$ for different sand-gypsum mixtures are denoted by using different symbols with different colours. Solid symbols with solid lines are used for the drying functions, and open symbols with dashed lines are used for the wetting functions.

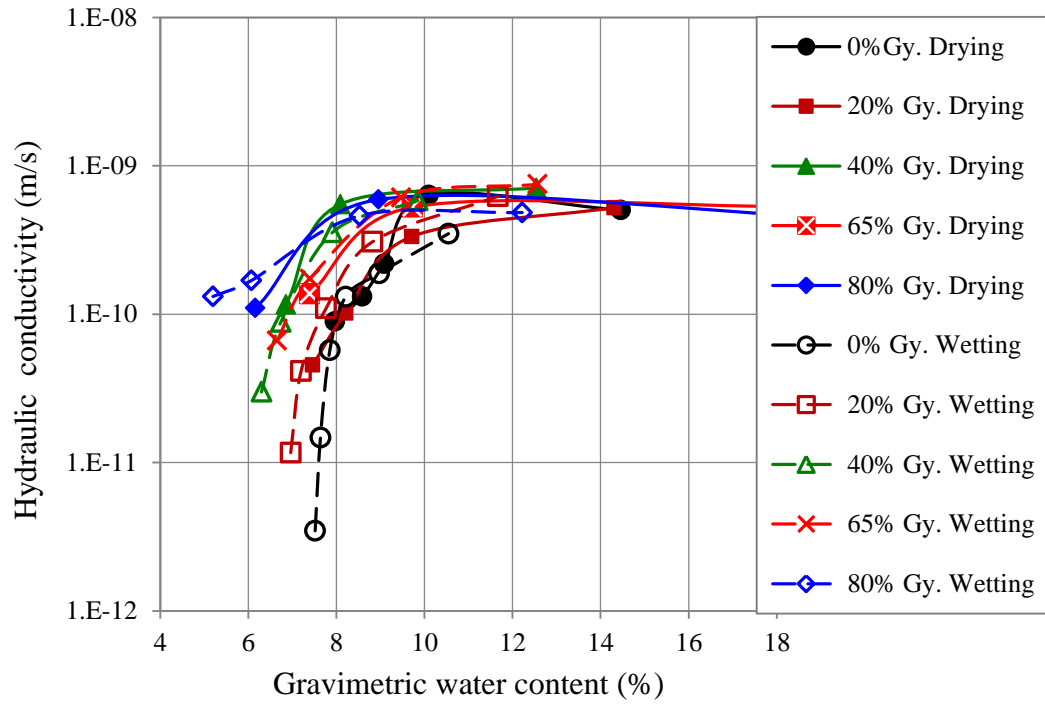
It can be noticed from Figures 7.3 A, B, C, and D that there is a minor effect to the gypsum content on both the drying and the wetting $k(w)$ at high water content values (low suctions), while this effect becomes more pronounced at low water content values (high suctions). This behaviour is noticed under different levels of net normal stress. In general, $k(w)$ exhibits a tendency to increase with increasing gypsum content under various applied net normal stress levels. This trend is mainly attributed to the increase in specific surface, initial void ratio, and the changes in the pore-size distribution associated with increasing gypsum content.



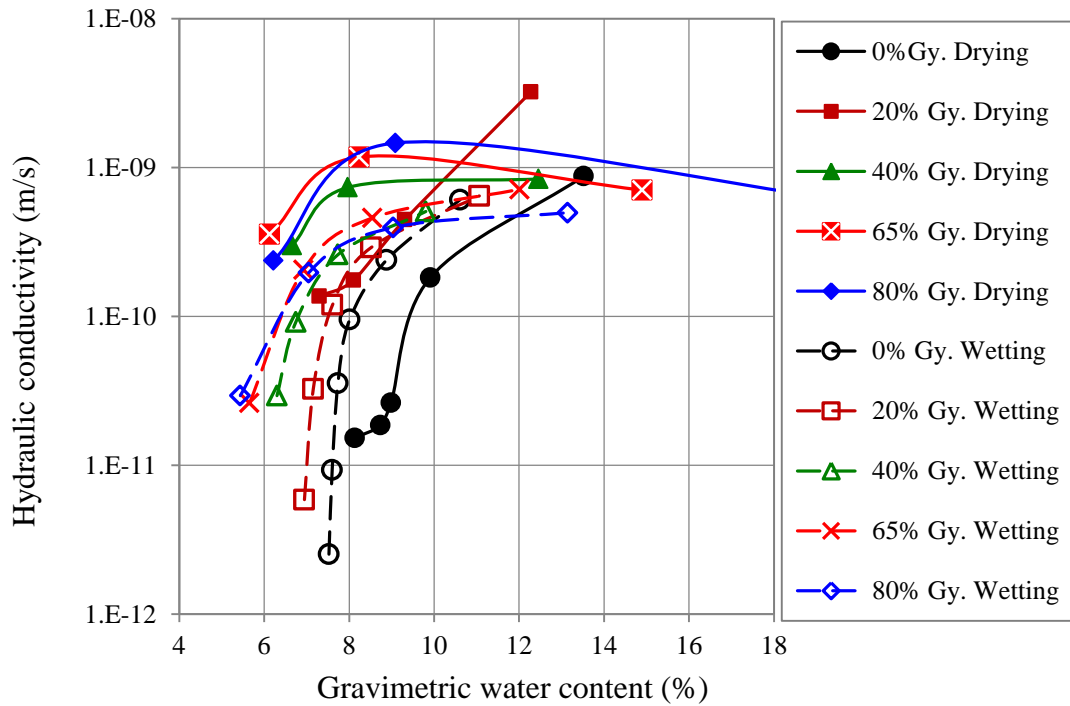
(A) HCFs under 0 kPa net normal stress



(B) HCFs under 100 kPa net normal strss.



(C) HCFs under 200 kPa net normal stress.



(D) HCFs under 400 kPa net normal stress.

Figure 7.3. The drying and the wetting hydraulic conductivity functions in terms of gravimetric water content, according to Doering's approach, for different sand-gypsum mixtures, tested under net normal stress of (A) 0, (B) 100, (C) 200, and (D) 400 kPa.

It is clear from Figure 7.3A, B, C, and D that the hysteresis effects on $k(w)$ is less than that on $k(\psi)$ presented in Figures 7.1 A, B, C, and D. That is likely because the water content hysteresis is eliminated when the hydraulic conductivity function is represented in terms of water content. Ng and Leung (2012) have investigated the effects of the drying-wetting cycle on $k(\theta)$. They pointed out that these effects appear to be less significant when compared with those observed on $k(\psi)$, as shown in Figure 7.4. Where $k(\theta)$ is the unsaturated hydraulic conductivity function in terms of volumetric water content.

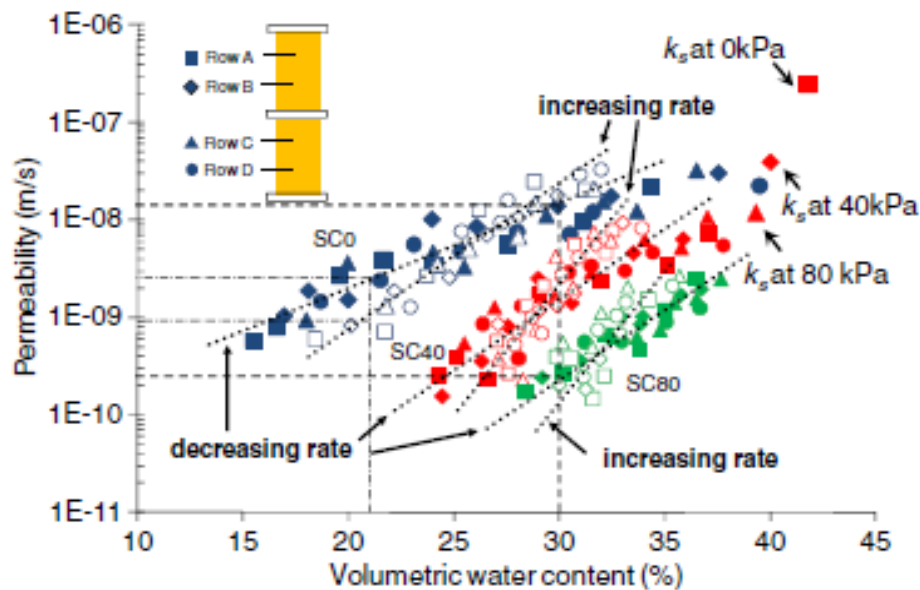


Figure 7.4. The hydraulic conductivity functions in terms of volumetric water content, at average net normal stresses of 4 kPa, 39 kPa, and 78 kPa for a compacted decomposed silty clay using the instantaneous profile method (Ng and Leung, 2012).

The general trend of $k(w)$ for various sand-gypsum mixtures which were tested under different levels of net normal stress shows that the slope of these functions (i.e., the change in hydraulic conductivity corresponding to the change in water content) is relatively flat at high water content (low suction) and gradually increases to be steep at low water content (high suction). This trend conflicts with the trend of $k(\psi)$ where the slope seems steep at low suction values and then becomes flatter with the increase in matric suction (Figures 7.1 A, B, C, and D).

Under different levels of net normal stress, the slope of the drying or the wetting $k(w)$ shows a clear decrease with increasing gypsum content at any specific suction.

In other words, specimens with high gypsum content have flatter curves than those of low gypsum.

It is worthy to mention here that the water content has a direct effect on the hydraulic conductivity, while matric suction affects the hydraulic conductivity indirectly, i. e., through his effect on the water content. In other words, the slope of $k(\psi)$ of a particular specimen depends implicitly on the slope of the SWCC of that specimen, while the slope of $k(w)$ is not so.

When the soil specimen is nearly saturated, the decrease in hydraulic conductivity associated with de-saturation is linearly proportional to the reduction in cross sectional area of the water flow paths, and then to the reduction in the water content as long as the water phase is continuous. In this stage, the slope or the decreasing rate of $k(w)$ seems relatively constant, especially when the change in void ratio corresponding to the change in water content is slight near saturation.

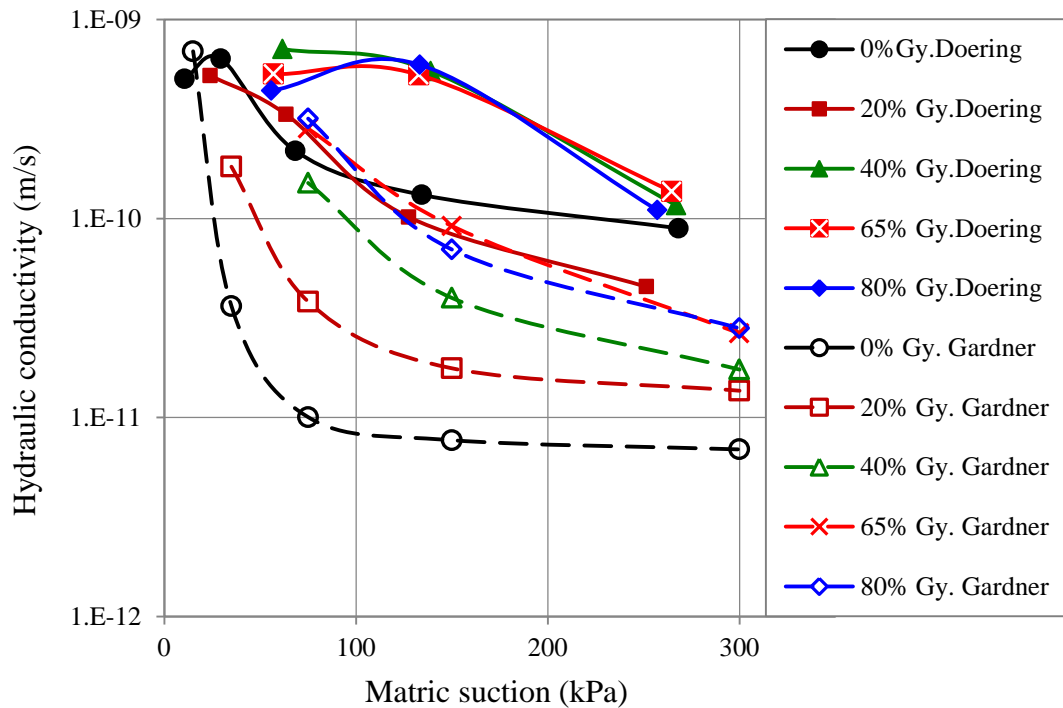
As the desorption progresses beyond the residual point and the water phase starts to be discontinuous, the slope of the $k(w)$ or the decreasing rate in hydraulic conductivity starts to increase dramatically and becomes steeper since the diffusion mechanism starts to control the system in this stage. Furthermore, the soil shrinkage and the corresponding reduction in void ratio is more pronounced in this stage of de-saturation, as may be noticed from the SCCs presented in Figure 5.17.

In more details, the flow of water near the air-entry point is at liquid phase where the water phase is continuous with the possibility of some isolated air pocket existence. Thus, the slope of $k(w)$ is mild and seems relatively constant. With increasing matric suction, water is drained causing soil to dry and produce a reduction in the continuity of the water phase. Ultimately, at the end of the transition zone and the beginning of the residual zone, the water phase starts to be discontinuous due to low soil water content while the air phase begins to be well continuous. Thus, the flow of water transforms gradually to a vapour flow and the diffusion will be the dominant mechanism at this zone. Due to this transformation, dramatic decreases in $k(w)$ can be noticed in this stage (Figures 7.3 A, B, C, and D).

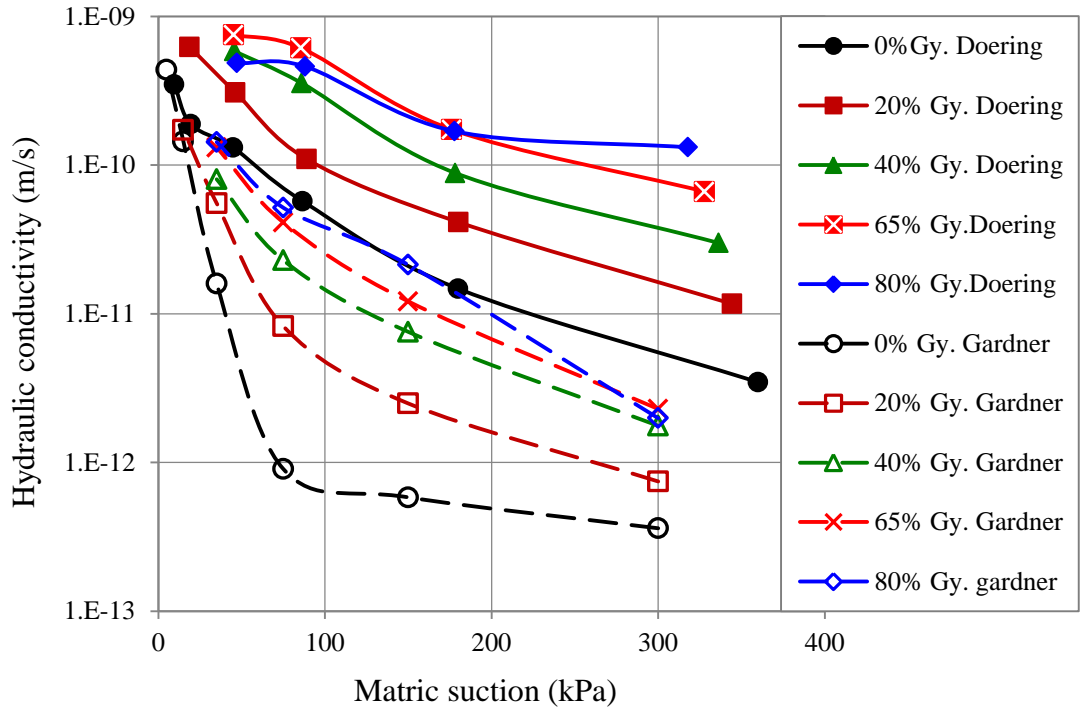
7.3. Comparison of Doering's approach with Gardner's approach

The experimental programme of the stress dependent-hydraulic conductivity tests was designed by considering two of the outflow methods, and consequently the results were analysed twice by following these approaches for all the implemented tests. These approaches are the multistep outflow method by Gardner (1956) and the one step outflow method by Doering (1965). The experimental procedures adopted by both these approaches were approximately the same but the methods used to analyse the outflow data were different depending on the assumptions, and the initial and boundary conditions which had been considered to solve Richard (1931)'s equation. This equation is the governing equation for the one-dimensional transient flow in homogenous soils.

For comparison, results of the drying and the wetting hydraulic conductivity functions, for different sand-gypsum mixtures tested under 100 kPa net normal stress, are selected among the complete results obtained. These results are presented in Figures 7.5 A, and B.



(A) Drying process.



(B) Wetting process

Figure 7.5. A comparison between hydraulic conductivity functions found according to Doering's approach and that found according to Gardner's approach for different sand-gypsum mixtures tested under 100 kPa net normal stress, (A) during drying process, (B) during wetting process.

One of the remarkable points arises from Figures 7.5 A, and B is that the hydraulic conductivity functions calculated according to Gardner's analytical solution are always lower than the corresponding functions calculated according to Doering's solution by one to one and half an order, for both the drying and the wetting paths, for all specimens that have different gypsum contents. This result is due to the assumptions which had been adopted in these two approaches. In Gardner's approach, the hydraulic conductivity of the specimen is assumed constant over the whole applied suction increment, while in Doering's approach, each suction increment is divided to small time steps and the hydraulic conductivity could be calculated for each of these steps. In other words, the hydraulic conductivity according to Doering's approach is considered variable with time during the period of each suction increment.

As mentioned in Section 4.2.4.3, a time step of 4 hours, from the applying of each suction increment, was taken to measure the hydraulic conductivity according

to Doering's method, whereas periodic monitoring of the outflow/inflow throughout the whole period (around one week) of suction increment/decrement was taken to determine the hydraulic conductivity by using Gardner's approach. The calculated hydraulic conductivity value was considered to be corresponding to the mean of matric suction or water content over the applied suction increment or decrement. This value is usually smaller than that taken during the first 4 hours of the suction increment period, because the outflow rate and then the hydraulic conductivity is relatively high once the suction increment is applied and then decreases with time till reach the suction equalization after approximately 7 days, for the specimens tested.

According to Green et al. (1998), the outflow of water from the specimen could be categorized into three stages. The first stage starts with the beginning of the test, at which the cumulative outflow volume is linearly proportional to the elapsed time, since the saturated permeability of the ceramic plate controls the flow through the system. This stage takes a short time, thereafter, the second stage is started, at which the accumulated outflow volume is linearly proportional to the second root of elapsed time (\sqrt{t}). At this stage, the core soil specimen behaves as a semi-infinite column, and the soil permeability controls the flow. This stage takes the most of suction increment period and it is ceased by the beginning of the third stage when the top layer of the soil specimen starts to influence the flow.

According to the above categorization, it is worthy to mention that both approaches adopted, Gardner's and Doering's approaches include the first and the second stages of flow. However, the hydraulic conductivity calculated according to Doering's approach is more affected by the first stage flow regime than that found according to Gardner's approach. This is because the time of the first stage could be significant within a time step of 4 hours, but it is negligible within the whole period of the suction increment, which is around 7 days.

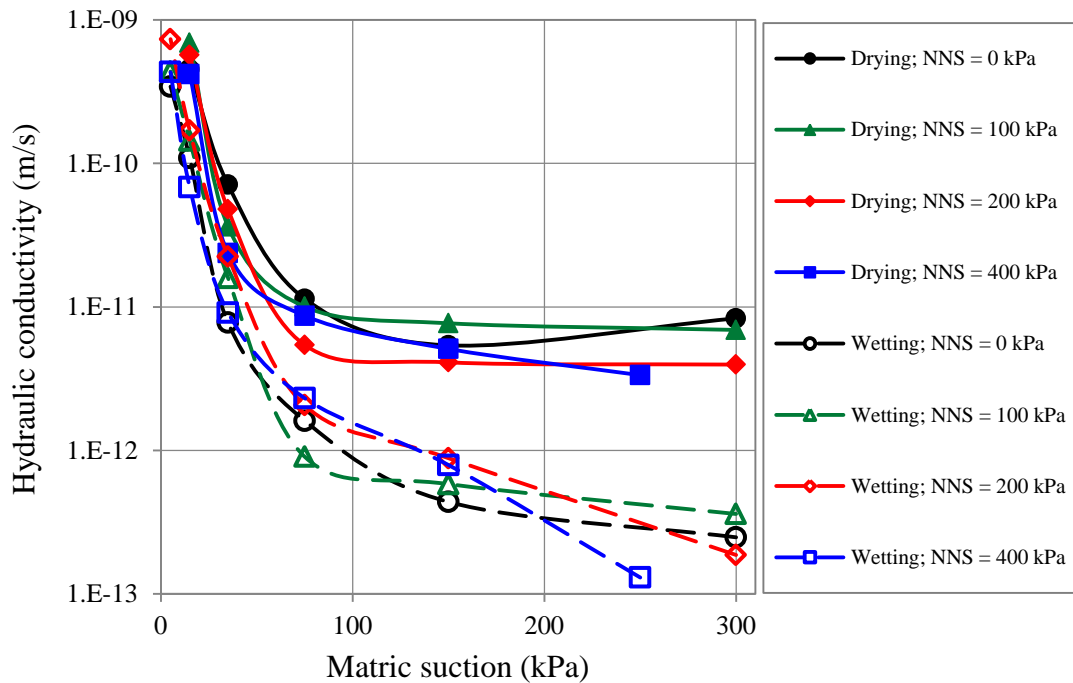
The other interesting point which can be noticed from Figures 7.5 A, and B is the hydraulic conductivity functions calculated by Gardner's method are more comparable and more consistent with the corresponding soil-water characteristic curves when the matric suction of the SWCCs are represented on an ordinary scale.

7.4. Effect of net normal stress on SD-HCFs

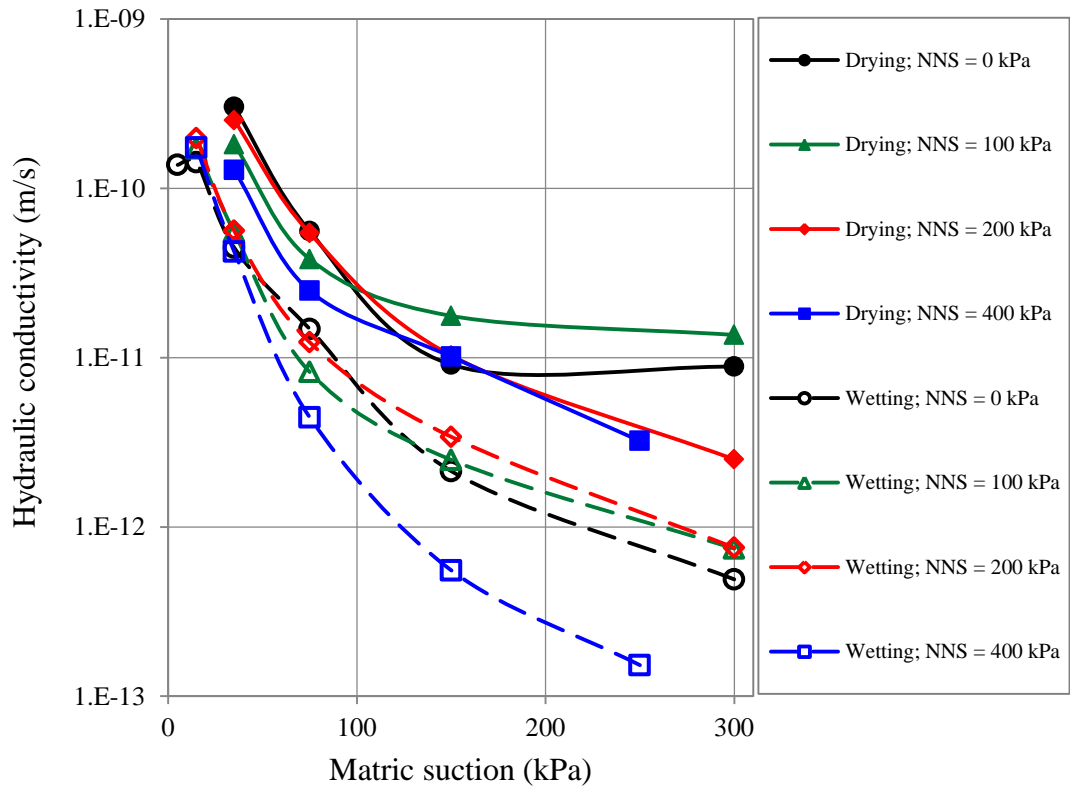
In this section, the effect of net normal stress on the drying and the wetting hydraulic conductivity functions are presented and discussed for sand-gypsum mixtures having 0, 20, 40, 65, and 80% gypsum content. The specimens were examined under four levels of net normal stress which were 0, 100, 200, and 400 kPa. The stress dependent-hydraulic conductivity functions (SD-HCFs) were calculated here according to Gardner's approach. These functions are presented and discussed first in terms of matric suction and then in terms of gravimetric water content.

7.4.1. Hydraulic conductivity-matric suction relationships

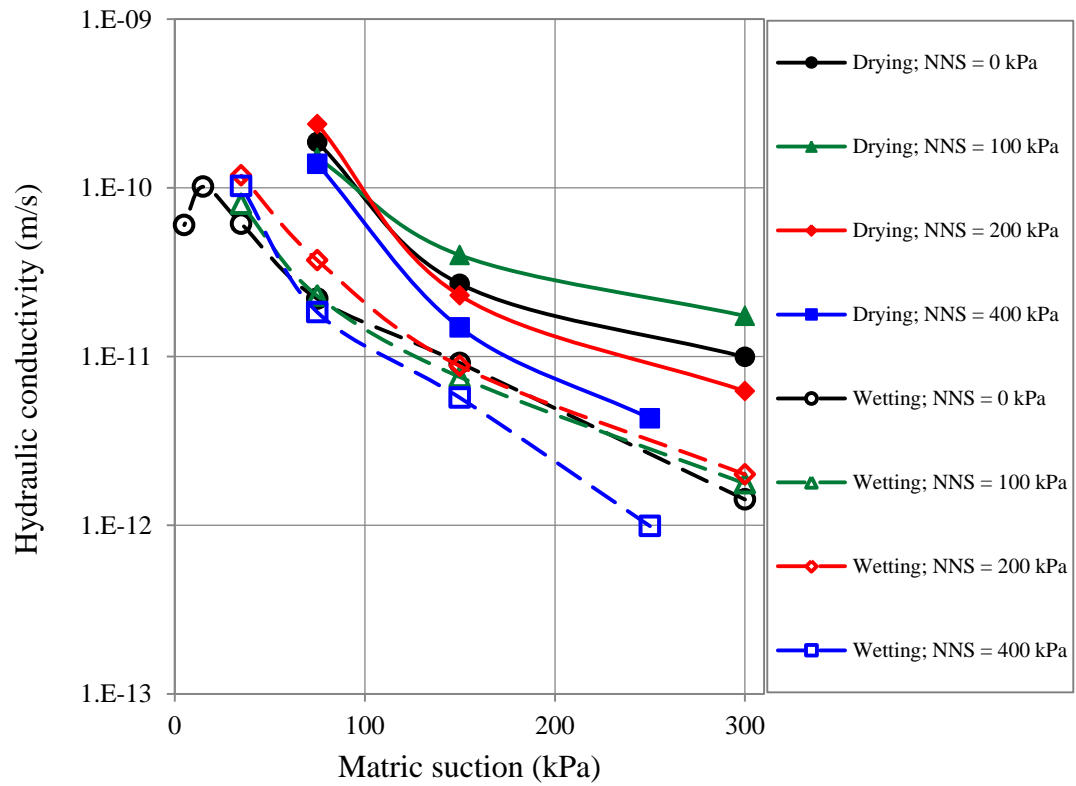
The drying and the wetting hydraulic conductivity functions (HCFs) in terms of matric suction, $k(\psi)$, under different net normal stress levels are presented in Figures 7.6 A, B, C, D, and E for different sand-gypsum mixtures. The measured $k(\psi)$ corresponding to different levels of net normal stress are denoted by using four different symbols and colours, while the drying and the wetting $k(\psi)$ are designated by using solid and open symbols, respectively.



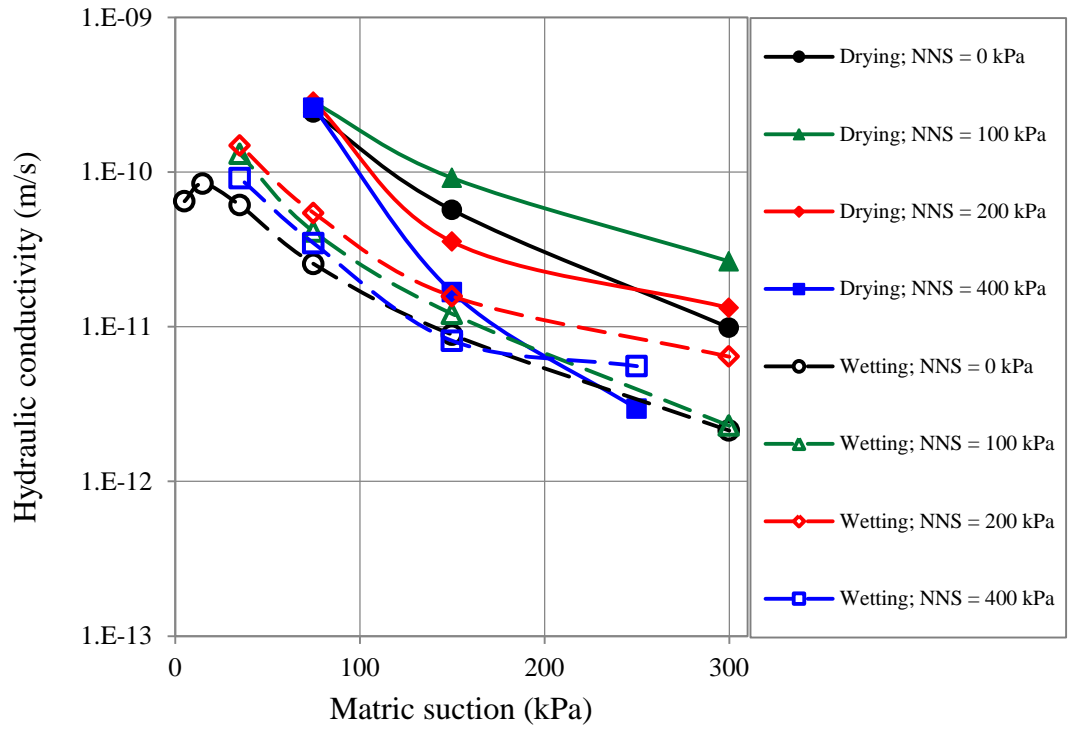
(A) 0% Gypsum content.



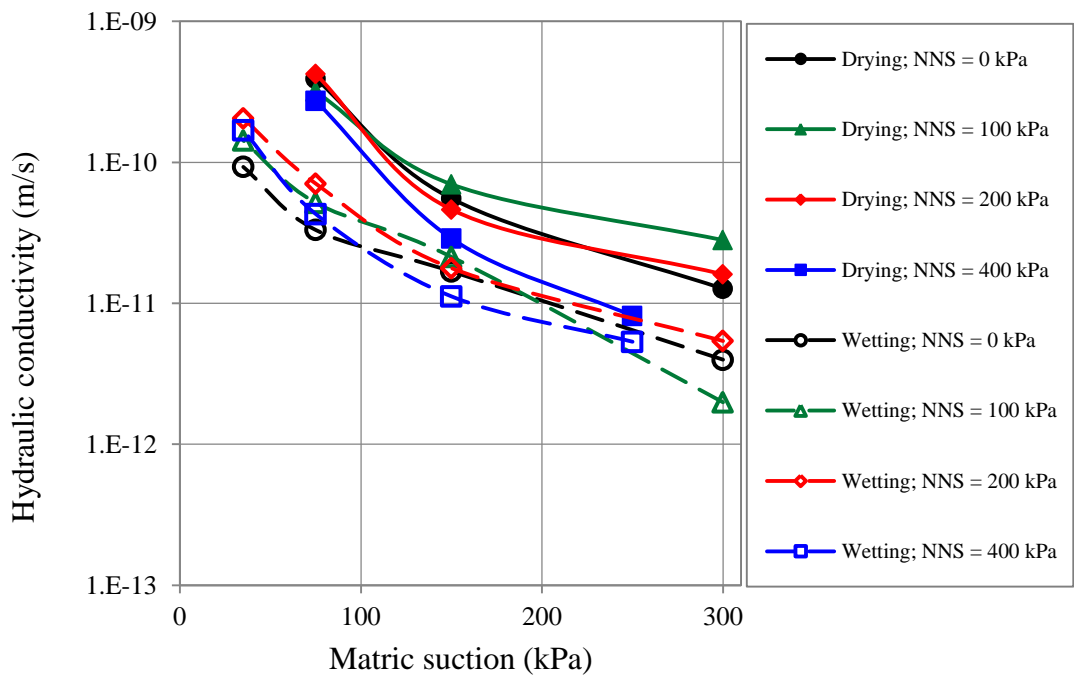
(B) 20% Gypsum content.



(C) 40% Gypsum content.



(D) 65% Gypsum content.



(E) 80% Gypsum content.

Figure 7.6. The drying and the wetting hydraulic conductivity functions in terms of matric suction, according to Gardner's approach, tested under different levels of net normal stress for sand-gypsum mixtures having (A) 0% , (B) 20%, (C) 40%, (D) 65%, and (E) 80% gypsum content by weight.

Figures 7.6 A, B, C, D, and E appear that the trends of both the drying and the wetting $k(\psi)$ under the four levels of net normal stress, for different sand-gypsum mixtures, are consistent to each other. In general, at any given suction the variation in the measured hydraulic conductivities for the drying conductivities or the wetting ones is within half an order of magnitude. Thus, the influence of net normal stress do not appears to affect the hydraulic conductivity of the specimens tested significantly. This behaviour may be attributed to the matter that the tested specimens were compacted to 90% of their maximum dry densities, which are considered relatively high densities. The static loads required to reach these densities were much greater than the applied net normal stress levels during hydraulic conductivity testing. Thus, the specimens could be considered as pre-consolidated under pressure much more than the applied one during hydraulic conductivity determination. For that reason, the effect of the applied net normal stresses on the void ratio of the specimens and then on the pore-size distribution is limited. Particularly, the effect of the applied net normal stress on the void ratio can be evaluated to some degree from the saturated consolidation test results which are presented in Chapter 5 (Figures 5.5 and 5.6). Nevertheless, soil compressibility is strongly influenced by the level of the applied suction. As soil suction increases, the compression index reduces distinctly, Cui et al. (2010). As such, the effect of applied net normal stress on soil-pore structure and then on hydraulic conductivity appeared to be limited.

In general, it can be noticed from Figures 7.6 A, B, C, D and E that the trends of $k(\psi)$ seem more distinguished at residual zone, where it can be noticed that the increase of net normal stress to a level between 100 and 200 kPa causes some increase in the hydraulic conductivity. Thereafter, the hydraulic conductivity show clear decrease with further increasing in the applied net normal stress, reaching lowest values at 400 kPa. This behaviour can be interpreted by considering two conflicting factors. The first factor can be the anticipated increase in the water phase continuity with increasing net normal stress (squeezing action). Thus, the hydraulic conductivity increases with increasing net normal stress to some extent. The second factor can be the substantial decrease in pore spaces and then in the water flow paths of the soil specimen associated with the increase in net normal stress level. The second factor can be demonstrated by referring to the stress-dependent soil-water characteristic curves presented through Figures 6.2 to 6.6 which reveal clear decrease

in gravimetric water content of soil specimen with increasing the applied net normal stress at any specific suction level. Furthermore, highly gypsiferous specimens seem to be more influenced with increasing net normal stress level. This can be attributed to the increase in the compressibility indices of those specimens associated with the increasing of gypsum content, see Figure 5.6. In brief, both the net normal stress and the gypsum content have clear effect on specimen water content which in turn reflects on the hydraulic conductivity of that specimen.

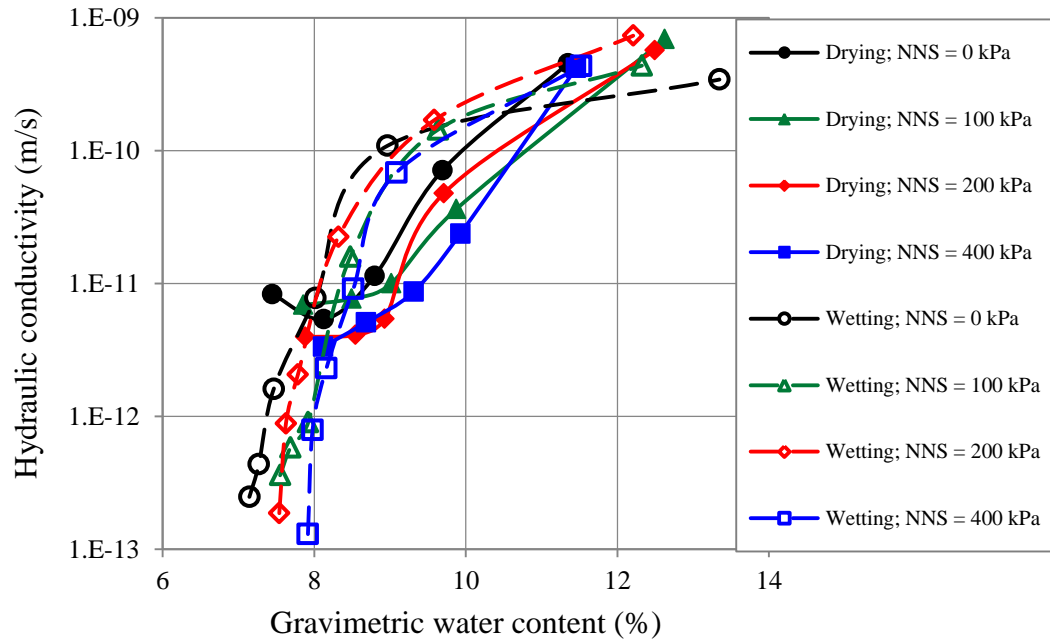
Like the effect of gypsum content on the slope of $k(\psi)$, Figures 7.6 A, B, C, D and E reveal that there is a general tendency of an increase in the slope of both the drying and the wetting $k(\psi)$ with increasing net normal stress level for different sand-gypsum mixtures. This behaviour is likely related to the decrease in water holding capacity with increasing the net normal stress level, as could be noticed from Figure 6.9. This trend disagrees with that found by Ng and Leung (2012) as shown in Figure 7.2, where the slope of $k(\psi)$ decreases with increasing the applied net normal stress in the range from 0 to 78 kPa. However, results of Ng and Leung (2012) shown in Figure 7.4 reveal that the slope of $k(\theta)$ increases with increasing the average net normal stress from 0 kPa to 39 kPa or to 78 kPa, and that it agrees with the results found in this study.

7.4.2. Hydraulic conductivity-gravimetric water content relationships

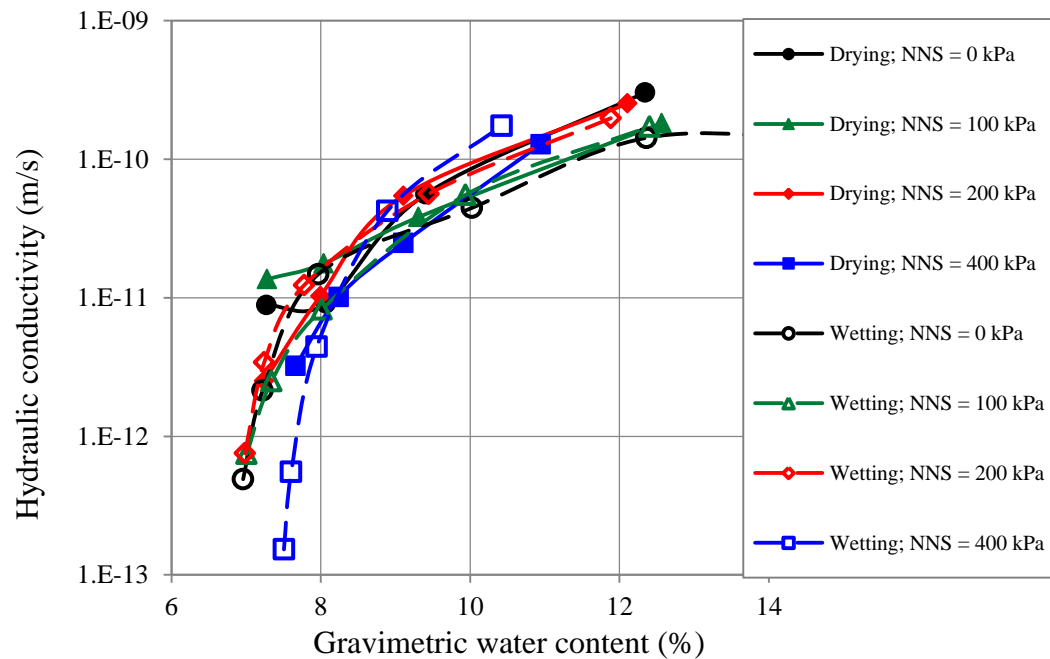
As indicated in the previous sections, the main factors that affect the unsaturated hydraulic conductivity are the water content of the soil mass, pores structure and pore-size distribution. To eliminate the changes in water content related to the changes in the applied net normal stress, the hydraulic conductivity function is represented in this section as a function to water content, $k(w)$. Figures 7.7 A, B, C, D, and E show the drying and the wetting $k(w)$ under different net normal stress for different sand-gypsum mixtures.

Figures 7.7 A, B, C, D, and E reveal that at any specific water content the effect of net normal stress on the drying or the wetting $k(w)$ is so limited for different sand-gypsum mixtures under investigation. This diminution in the effect of net normal stress could be attributed first to the elimination of the implicit effect of water

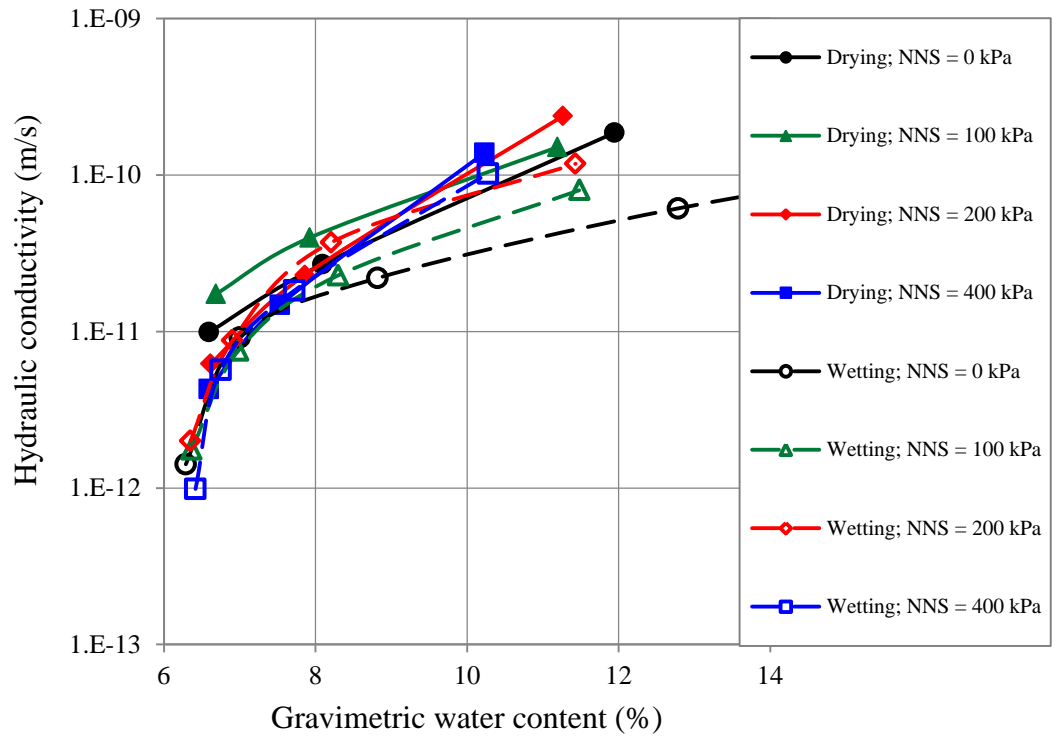
content changes, since the water content in this representation is taken as the independent variable. As a second reason, the effect of net normal stress on pore size distribution is mostly diminished as long as the specimens were statically compacted under loads much greater than the applied net normal stress levels.



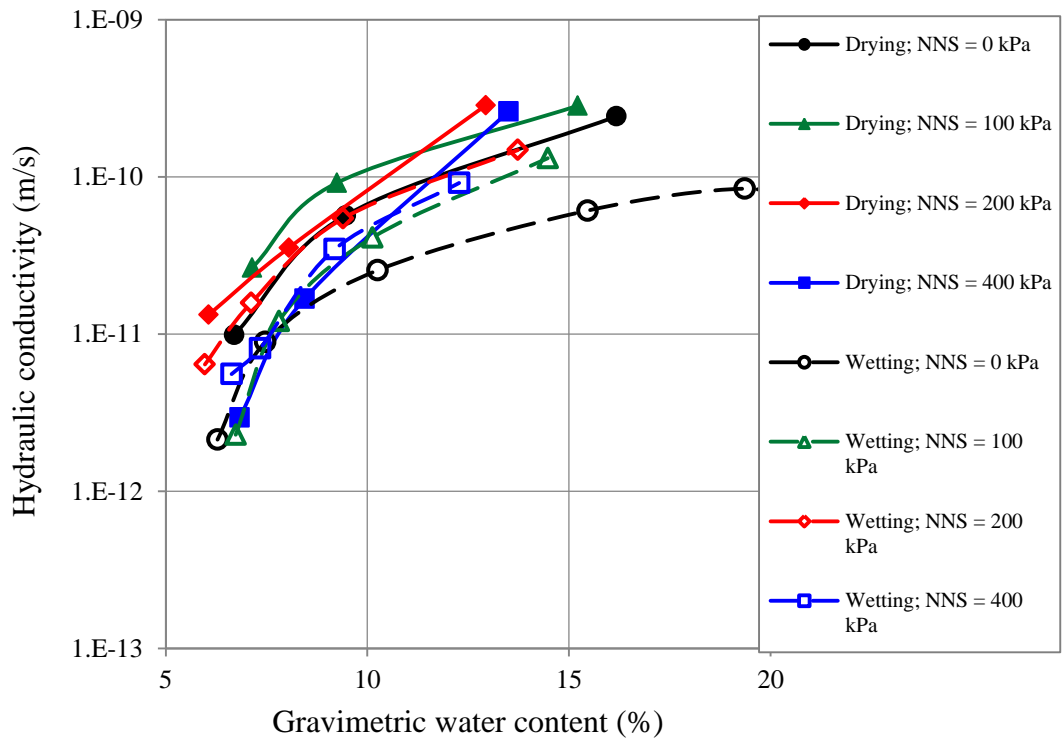
(A) 0% Gypsum content.



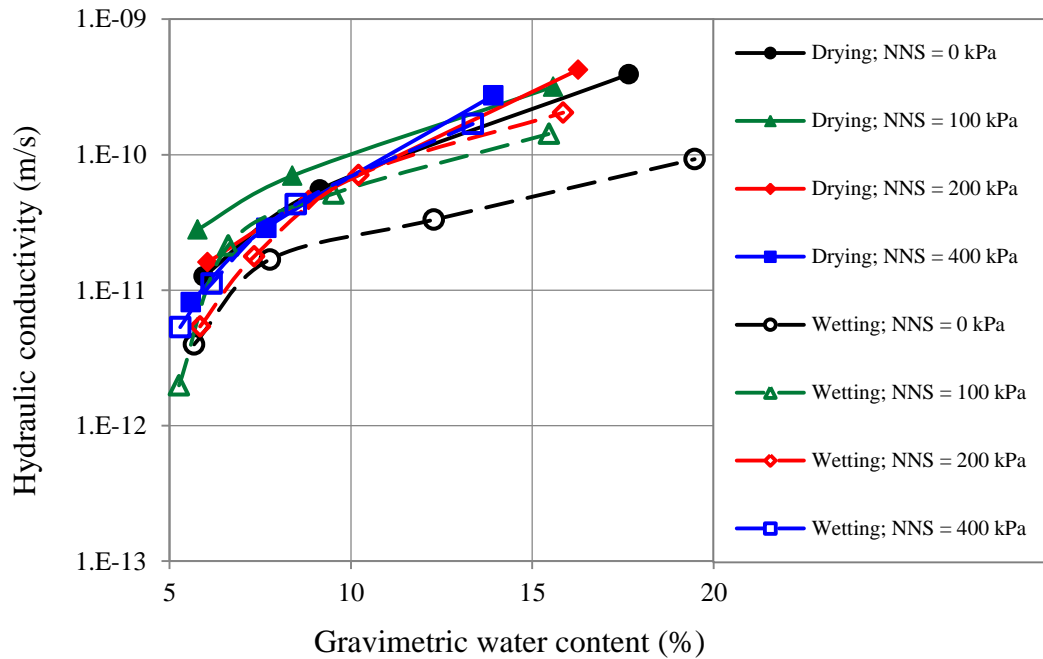
(B) 20% Gypsum content.



(C) 40% Gypsum content.



(D) 65% Gypsum content.



(E) 80% Gypsum content.

Figure 7.7. The drying and the wetting stress dependent-hydraulic conductivity functions in terms of gravimetric water content, according to Gardner's approach for sand-gypsum mixtures having (A) 0% , (B) 20%, (C) 40%, (D) 65%, and (E) 80% gypsum content by weight.

The other point which can be noticed from Figures 7.7 A, B, C, D, and E is that the slope of the wetting $k(w)$ is greater than that for the drying functions, and that is more pronounced in the low water content values. The change in hydraulic conductivity between the highest and lowest water content values is about three orders of magnitude for the wetting functions, while it is around one and a half order for the drying functions. This trend is consistent under different levels of net normal stress, for all sand-gypsum mixtures under investigation.

7.5. Summary and concluding remarks

The SD-HCFs testing programme was designed to study the influence of gypsum content, net normal stress, and drying-wetting cycle on the unsaturated hydraulic conductivity function by using the modified stress controllable pressure plate device. The results were analysed by following two of the transient outflow methods, the one step outflow method by Doering (1965) and the multistep outflow method by Gardner (1956).

Doering's one step outflow method was modified in this study to be applied in successive increments, or decrements, in matric suction instead of applying one large step. Each of these increments/decrements was considered as a one small step. This modification yields the SD-SWCCs simultaneously with the SD-HCFs.

The SD-HCFs calculated by Gardner's method are always lower than the corresponding functions calculated according to Doering's method by more than one order of magnitude. In spite of that, the test results show that there is a clear increase in hydraulic conductivity function with increasing gypsum content under different levels of net normal stress, for both the drying and the wetting paths. This can be attributed to the increase of water content, void ratio, and then the water flow paths with increasing gypsum content.

The influence of net normal stress on the hydraulic conductivity of compacted specimens seems depend mainly on the initial conditions of the prepared specimens. Specimens compacted to high densities appear slight effect with the level of applied net normal stress. However, highly gypsiferous specimens seem to be more influenced with the increasing of net normal stress level due to their compressibility characteristics.

For all specimens that have different gypsum contents, tested under different net normal stress levels, there is clear hysteresis effects on the $k(\psi)$ with wetting function always lower than the corresponding drying one. Nevertheless, only minor hysteresis is noticed on $k(w)$, and that is likely because the water content hysteresis is eliminated. The $k(w)$ is more representative to the physical state of the soil mass, whereas $k(\psi)$ is more mimic and consistent with the SWCC. On the other hand, experimentally, it was noticed from this study that the applicability of the outflow transient methods may be limited corresponding to matric suction values between the air-entry point and the residual point (the transition zone) only.

CHAPTER EIGHT

SHEAR STRENGTH AND DEFORMATION CHARACTERISTICS

8.1. Introduction

This chapter presents the shear strength and shear deformation characteristics of various sand-gypsum mixtures tested under different loading conditions. The first part of this chapter presents the direct shear test results carried out on saturated specimens. The effect of gypsum content on saturated shear strength parameters (c' & ϕ'), and on shear deformation characteristics are presented. In the second part, the results of direct shear tests carried out on air-dried specimens under water content controlled conditions are presented. Three different common criteria for describing the shear strength of unsaturated soils are considered. The effects of gypsum content, desaturation, and net normal stress level on the unsaturated shear strength parameters of different sand-gypsum mixtures are discussed in detail. The peak/maximum shear stress was adopted as the failure criteria.

8.2. Results of direct shear tests on saturated specimens

As mentioned in Section 3.4.8, the experimental programme includes a series of direct shear box tests on saturated specimens. These tests were conducted for two reasons: (i) to evaluate the effect of gypsum content on the stress-deformation characteristics, contraction-dilation behaviour, and the saturated shear strength parameters of the sandy soil tested, and (ii) to use the values of the saturated shear strength as a reference to find the excess in shear strength resulting from desaturation. Thus, the contribution of matric suction to shear strength for different soil mixtures can be evaluated.

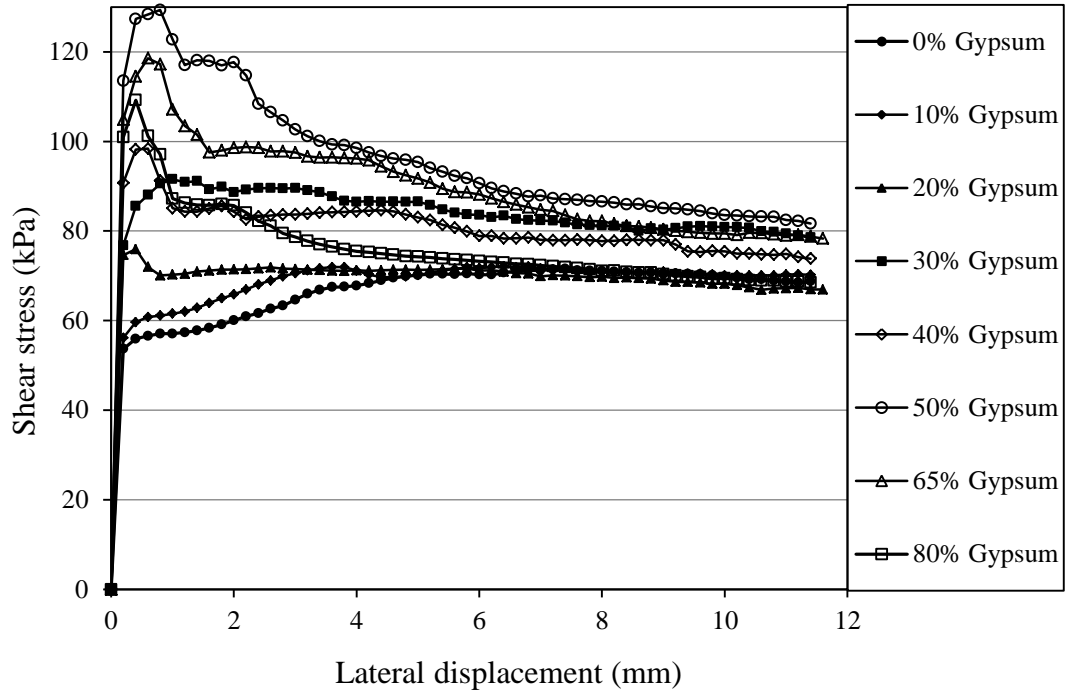
Single stage direct shear tests were carried out on initially saturated specimens having gypsum percentages of 0, 10, 20, 30, 40, 50, 65, and 80% by weight. The specimens were statically compacted, saturated, consolidated, and then sheared under drained conditions at constant strain rate of 0.02 mm/min. Each soil mixture was tested under three different normal stress levels (100, 200, 400 kPa). The results are presented and discussed in the following sections.

8.2.1. Stress-strain characteristics

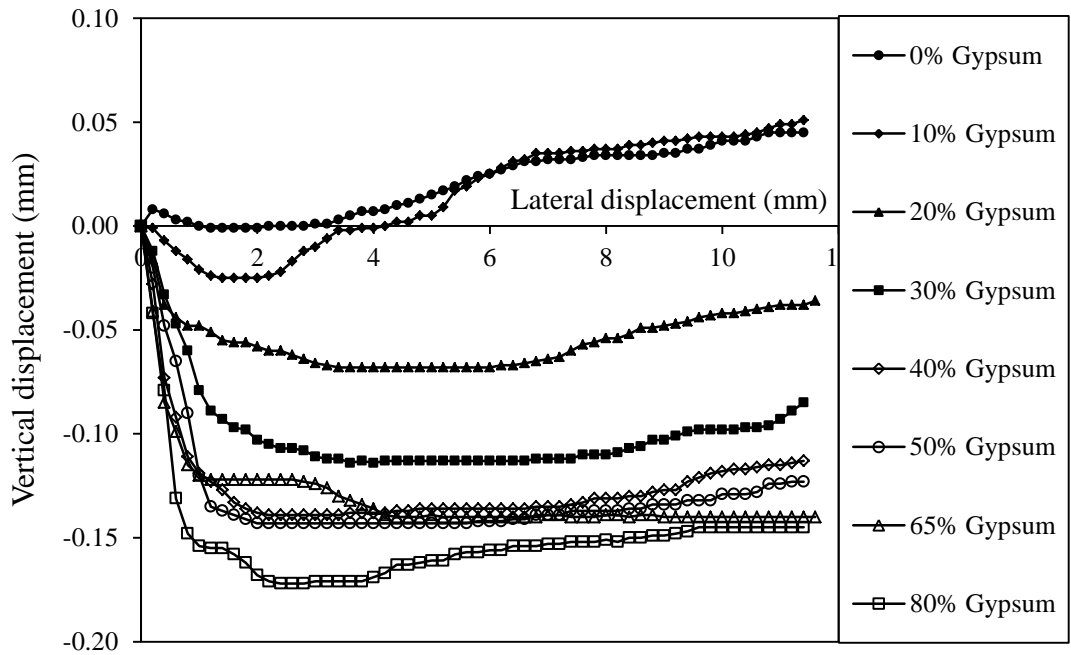
Typical direct shear box test results are best illustrated through the graphs of shear stress versus horizontal displacement and the related graphs of vertical deformation versus horizontal displacement. Figures 8.1 and 8.2 show these relationships for eight sand-gypsum mixtures tested under 100 and 400 kPa normal stress levels, respectively. The stress-strain relationships for specimens tested under 200 kPa normal stress, which exhibit an intermediate behaviour comparing to that tested under the lowest (100 kPa) and highest (400 kPa) normal stress levels, are shown in Appendix B, Figure B.1.

Different symbols are used to designate specimens having different gypsum contents. On the lateral displacement-vertical deformation graphs, negative vertical displacement values indicate the occurrence of dilation (an increase in volume of the sheared specimen), whereas the positive values indicate contraction (a decrease in volume of the sheared specimen).

Test results presented in Figures 8.1 and 8.2 exhibit that the shear strength and the volume change characteristics are clearly influenced by the amount of gypsum in the soil mixture. In addition, it can be noticed that the dilation or contraction properties of the soil mixtures are highly dependent on the applied normal stress levels. This behaviour agrees with the review of Bolton (1986) who mentioned that both effective stress and soil density affect the rate of dilatancy of soils and thereby their strength parameters.

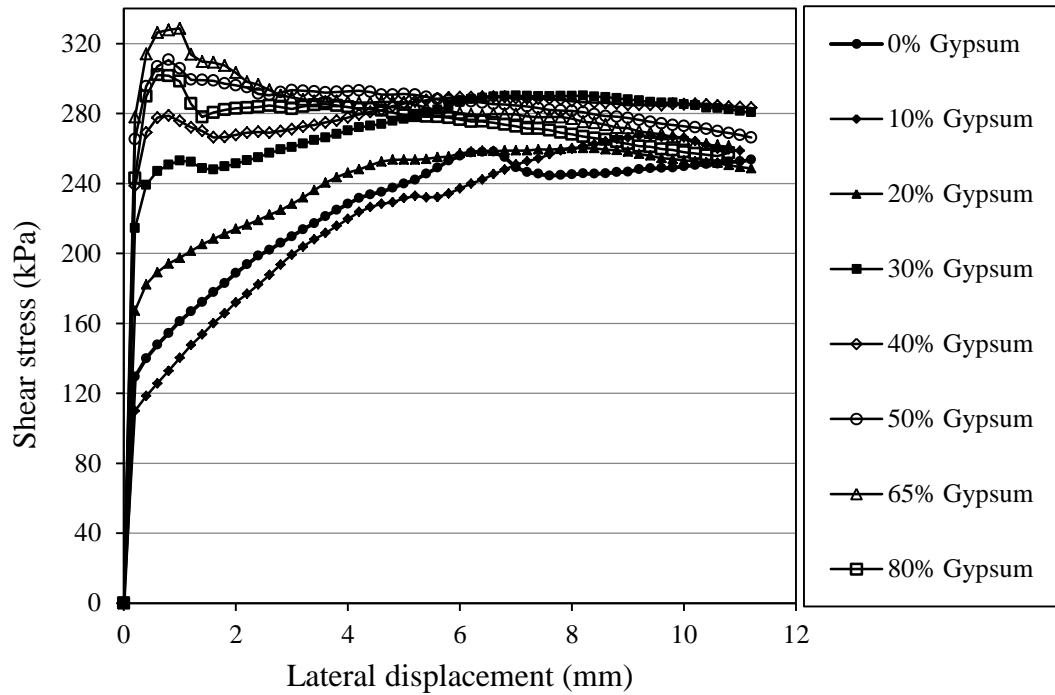


(A) Lateral displacement-shear stress curves.

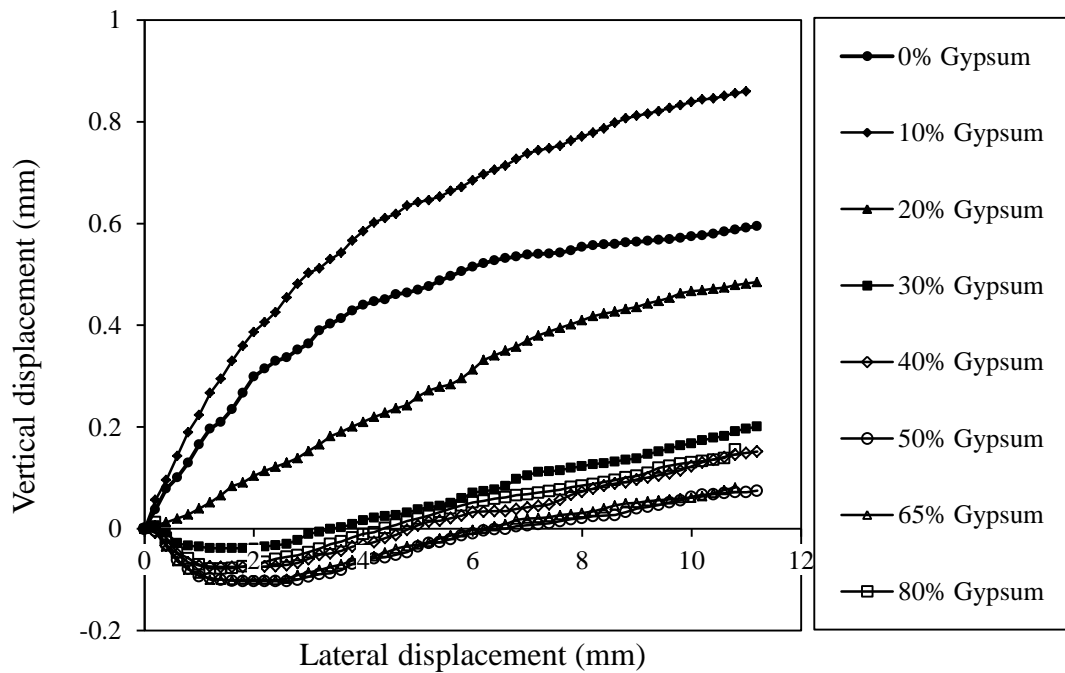


(B) Lateral displacement-vertical deformation curves .

Figure 8.1. Stress-deformation characteristic curves for different sand-gypsum mixtures tested under normal stress of 100 kPa, (A) Shear stress versus lateral displacement, and (B) Vertical deformation versus lateral displacement.



(A) Lateral displacement-shear stress curves.



(B) Lateral displacement-vertical deformation curves.

Figure 8.2. Stress-deformation characteristic curves for different sand-gypsum mixtures tested under normal stress of 400 kPa, (A) Shear stress versus lateral displacement, and (B) Vertical deformation versus lateral displacement.

Shear stress-shear displacement plots (Figures 8.1A and 8.2A) show two distinguished patterns, peak patterns which indicate stiff behaviour, also referred to

as strain softening behaviour (Mofiz et al., 2004), and non-peak patterns which indicate ductile behaviour, also referred to as strain hardening behaviour (Mofiz et al., 2004). Specimens with high gypsum content exhibit peak patterns, while those of low gypsum content exhibit non-peak patterns.

More specifically, Figure 8.1A indicates that the shear displacement corresponding to maximum/ peak shear stress shows a clear decrease with increasing gypsum content. On the other hand, the comparison of lateral displacement-shear stress plots of the specimens tested under 400 kPa normal stress (Figure 8.2A) with those tested under 100 kPa (Figure 8.1A) demonstrates that the shear displacement corresponding to peak shear stress exhibits an increase with increasing the applied normal stress. In other words, the specimen ductility increases as the applied normal stress is increased. The lateral displacement required to reach the maximum/peak shear stress at different normal stress levels for the eight sand-gypsum mixtures tested are presented in Table 8.1.

Table 8.1. Lateral displacement corresponding to maximum shear stress under different normal stress levels for different sand-gypsum mixtures.

Gypsum content (%)	Lateral displacement related to maximum/peak shear stress (mm)		
	Applied normal stress (kPa)		
	100	200	400
0	7.4	9.4	6.6
10	6.4	7.6	9.2
20	0.4	7.8	8.0
30	1.0	7.6	8.2
40	0.6	6.6	6.8
50	0.8	0.6	0.8
65	0.6	0.6	1.0
80	0.4	0.6	0.6

As expected, highly gypsiferous specimens exhibit higher shear strength than specimen with low gypsum content. However, significant changes in the stress deformation characteristics can be noticed when gypsum content increases over 20% by weight (Figures 8.1 and 8.2). Specimens having gypsum content more than 50% exhibit stiff behaviour with peak shear stress achieved at low shear strain, mostly not exceeded 1%. The shear stress of these specimens reveals reduction after the peak value, reaching to a yield stress and then goes to relatively steady stress value at higher shear displacements. Typically, similar strain softening trend could be noticed

as well with shearing of dense sand specimens. On the other hand, specimens without gypsum or low gypsum contents show ductile behaviour or what is called also strain hardening behaviour where the shear stress gradually increases to reach a maximum value at relatively large shear displacements.

It can be concluded from Figures 8.1A and 8.2A that the gypsum content at which the soil shearing behaviour is changed from ductile behaviour to stiff behaviour is about 30 % for the sandy soil tested. This gypsum content is just enough to fill the voids of the original sandy soil and yields the sand-gypsum mixture to be at the minimum porosity or minimum void ratio (see Figure 5.4 and Table 5.1). At 30% gypsum content and more, the structure of the soil mixture is governed by gypsum portion, and then, gypsum characteristics will dominate the overall mixture properties.

At relatively small shear displacement, stress patterns (shear stress-shear displacement patterns) of different sand-gypsum mixtures show clear distinctions as can be noticed from Figures 8.1A and 8.2A. However, at relatively large shear displacements, all specimens tend to come to nearly the same steady or critical shear stress value. The stress pattern of highly gypsiferous specimens show clear decrease with increasing shear displacement, while the pattern of low gypsum content specimens show an increase to approach the first pattern.

At initial shearing stage, relatively linear shear stress-shear displacement relationship with well defined straight line segment can be noticed for all sand-gypsum mixtures tested (Figures 8.1A and 8.2A). The slope of the initial straight-line is referred to as "the initial shear stiffness (K_i)", and it has units of kPa/mm. This terminology has been used by many researchers such as Lun (2005) and Vassallo et al. (2007). In practical geomechanics, the initial shear stiffness is commonly used in characterisation of soil stiffness. However, complete characterisation of an isotropic elastic soil material requires the determination of two possible stiffness parameters, Young's modulus E and Poisson's ratio ν , or shear modulus G and bulk modulus K (Clayton, 2011). A sound evaluation of stiffness parameters at small strain is essential, if realistic predictions of the soil movements that may affect adjacent infrastructure are to be made (Clayton, 2011).

Figures 8.1A and 8.2A reveal that the initial shear stiffness has clear dependency on both gypsum content and the applied normal stress level. The initial shear stiffness for different sand-gypsum mixtures corresponding to different normal stress levels are defined and presented in Figure 8.3. This figure shows clear increase in the initial shear stiffness associated with the increase in gypsum content. Furthermore, remarkable increase in the initial shear stiffness could be noticed with increasing the applied normal stress level. Similar trends have been reported by Clayton et al.(2010) after studying the cementation effect of methane hydrate deposition on the very small strain stiffness moduli (shear modulus G_0 and Young's modulus E_0) of a selection of sand-sized materials having different grain sizes, shapes and gradings. They noticed clear increases in the stiffness moduli at very small strain with increasing the proportion of methane hydrate deposited and/or with increasing the mean effective confining stress.

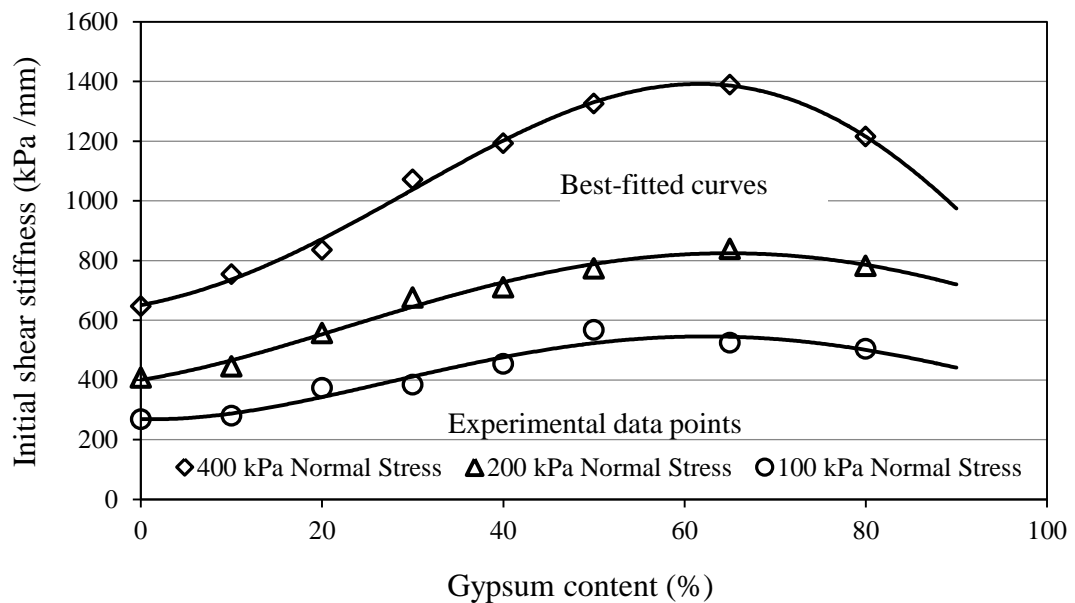


Figure 8.3. Effect of gypsum content on initial shear stiffness of specimens tested under different normal stress levels.

Best explanation and interpretation of the stress-strain behaviour needs to consider closely the dilation/contraction behaviour associated with the shearing process. The vertical displacement versus shear displacement plots (Figures 8.1B and 8.2B) reveal that most sand-gypsum mixtures exhibit dilation, especially at lower normal stress level, with an amount shows a clear increase with increasing gypsum content. This interprets the strain softening behaviour and the increase of the initial

shear stiffness with increasing gypsum content in the soil mixture. As well as, Figures 8.1B and 8.2B indicate that the amount of dilation gradually decreases with the increasing of the applied normal stress level. Thus, at 400 kPa normal stress level, the contraction becomes more pronounced for most sand-gypsum mixtures, even though, the initial volume change for most specimens tested were dilatant behaviour. That is why soil mixtures exhibit relatively more ductility at higher normal stress levels.

The shear stress-lateral displacement curves (Figures 8.1A and 8.2A) are consistent with their corresponding vertical displacement-lateral displacement curves (Figures 8.1B and 8.2B). Thus, the maximum rate of dilatancy is approximately coincided with the peak shear stress point, whereas the dilatancy rate at the study stage (critical state) is equal to zero.

8.2.2. Effect of gypsum content on saturated shear strength

The peak/maximum shear stress for different sand-gypsum mixtures tested under 100, 200, and 400 kPa normal stress levels were defined from shear stress-lateral displacement plots (Figures 8.1A, B.1A, and 8.2A). These values which were adopted as the soil shear strength values are presented against gypsum content in Figure 8.4.

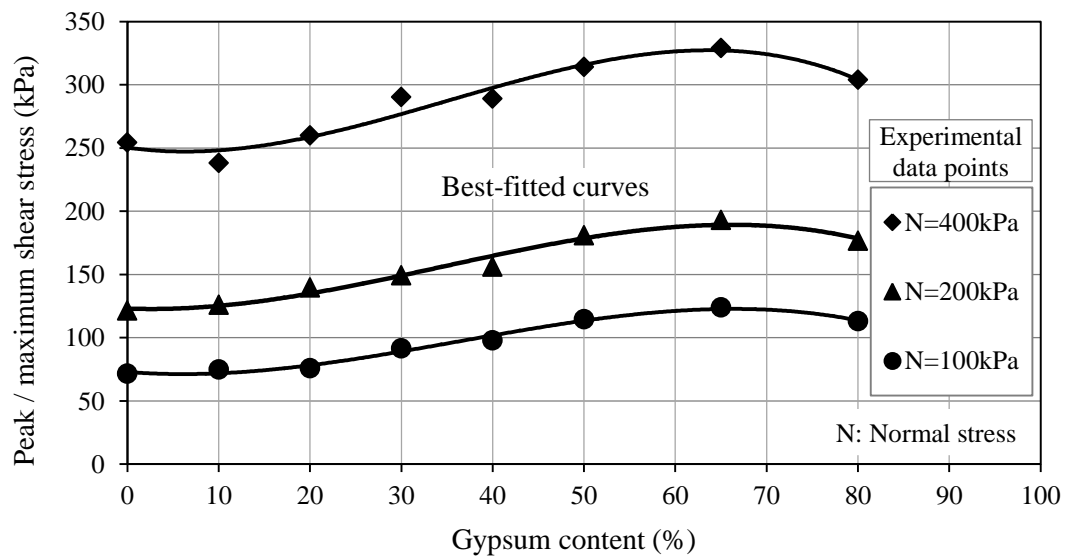


Figure 8.4. Effect of gypsum content on peak/maximum shear stress for specimens tested under different normal stress levels.

Figure 8.4 shows a clear increase in the peak/maximum shear stress with increasing gypsum content. Consistent trends corresponding to different normal stress levels can be noticed. This behaviour agrees with that found by Seleam (1988) and Al-Qaissy (1989) for gypsiferous sandy soil and gypsiferous clayey soil, respectively (see Section 2.2.2).

Results of chilled mirror hygrometer tests which are presented in Section 5.5 show that there is a clear increase in osmotic suction of the sandy soil with increasing gypsum content, and this may lead to an increase in the saturated shear strength. Peterson (1990) has pointed out that the increasing of osmotic suction causes clear increase to the cohesion term (the first term) in the modified Mohr-Coulomb shear strength equation (Equation 2.20) and mild decrease to the contribution of matric suction to the shear strength (the third term).

8.2.3. Mohr-Coulomb failure envelopes and shear strength parameters

The highest level of shear stress measured in the direct shear test under a given normal stress is defined as the "peak strength". With continued shear displacement there is typically a loss of strength. The shear stress at any given displacement past the point of peak strength could be referred to as "post peak strength", and it is usually differentiated by specifying the corresponding shear displacement, Thiel (2001). The strength at which there is no further strength loss, no volume changes, with continued displacement is called the "steady state strength or critical state strength". In practical applications, the decision whether to use peak or steady state shear strengths for a stability analysis depends on the potential relative shear displacement for the specified problem under consideration. To study the effect of gypsum content on the mechanical properties of the sandy soil used in this study, the peak shear strength was adopted. The peak shear strength values for different sand-gypsum mixtures are presented in Appendix B, Table B.1.

To define the peak friction and cohesion parameters, the peak shear stress is plotted against the normal stress in Figure 8.5, for different sand-gypsum mixtures. Linear shear strength envelopes are considered over the range of the applied normal stress levels (100 to 400 kPa), and a best fit lines are drawn. The peak angle of

internal friction is defined from the slope of the envelope line and the cohesion is defined from the y-axis intercept, for different sand-gypsum mixtures.

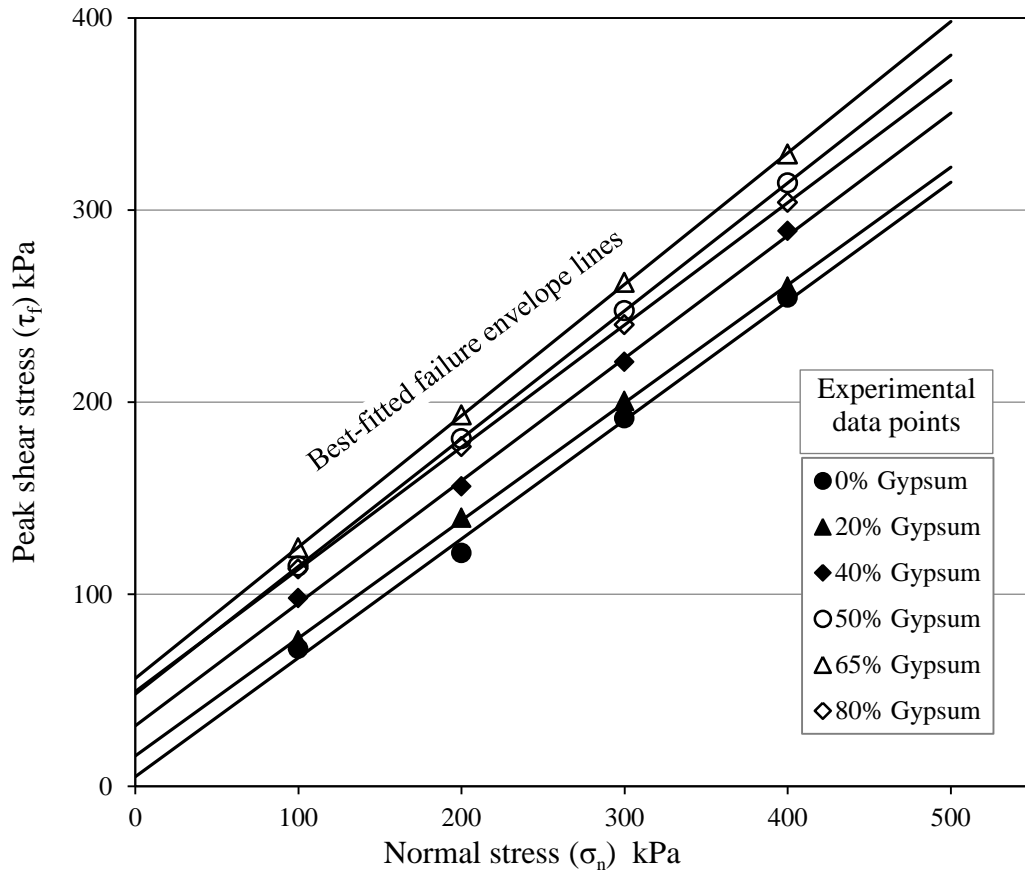


Figure 8. 5. Mohr-Coulomb failure envelopes of different sand-gypsum mixtures.

The peak shear strength parameters for different sand-gypsum mixtures obtained from Figure 8.5 are presented in Figure 8.6, and their numerical values are shown in Appendix B, Table B.2. Figure 8.6 reveals that the increase of gypsum causes a clear increase in the effective cohesion up to 65% gypsum content by weight, and then the cohesion shows a slight decrease at a gypsum content of 80%. Likewise, the general tendency of the friction angle shows moderate increase with increasing gypsum content up to 65%, and then a slight decrease could be noticed at higher gypsum content. This trend highly agrees with results of Seleam (1988) on a gypsiferous sandy soil, and agrees to some extent with results of Al-Qaissy (1989) on a gypsiferous clayey soil (see Section 2.2.2). The trend of shear strength parameters shown in Figure 8.6 may be attributed to the matter that the cohesion between gypsum-gypsum particles is greater than gypsum-sand particles and this in turn is greater than sand-sand particles. On the other hand, the initial increase in the angle of

internal friction with increasing gypsum content may be attributed in part to the decrease in void ratio associated with the increase of gypsum content, as shown in Figure 5.4. In other words, gypsum particles act as filling material to pore spaces of the sandy soil up to 30% gypsum content when the void ratio reaches a minimum value.

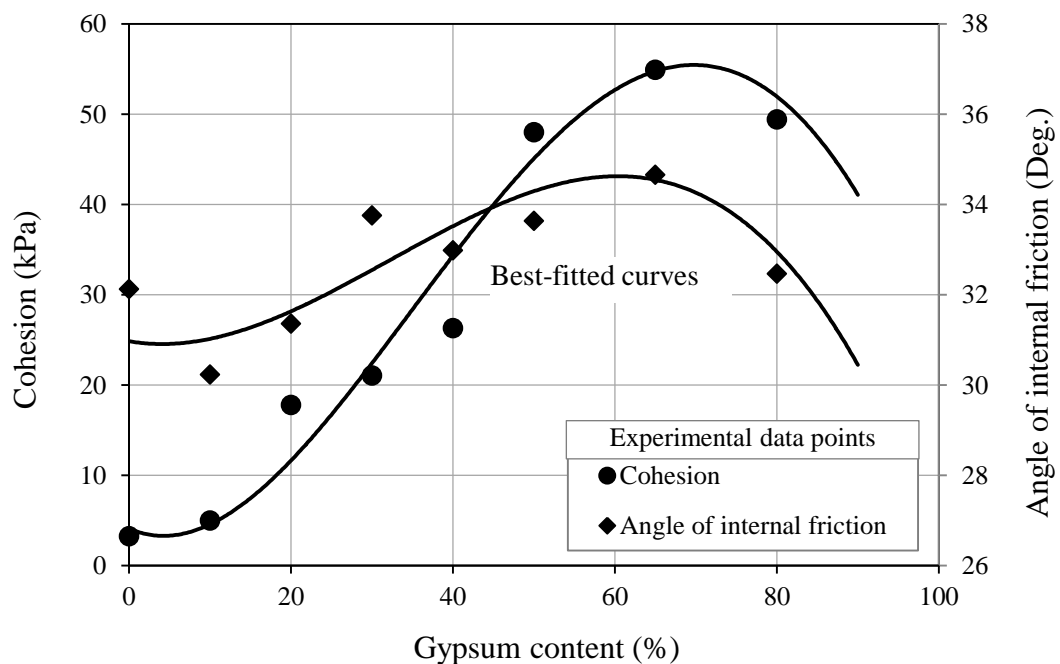


Figure 8.6. Effect of gypsum content on saturated shear strength parameters.

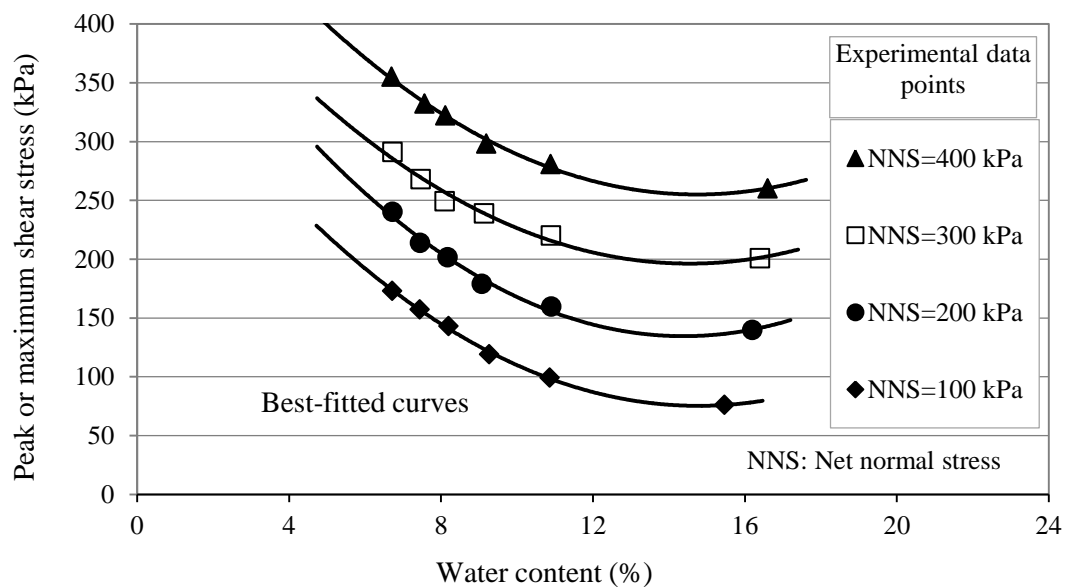
8.3. Results of direct shear tests on unsaturated specimens

The main objective of these tests is to examine the effect of gypsum content and the effect of desaturation on the shear strength of the sandy soil. As described earlier in Section 3.4.9, five extensive series of tests on five sand-gypsum mixtures having gypsum contents of 0, 20, 40, 65, and 80% by weight were carried out. Each soil mixture was tested at various water contents under four net normal stress levels (100, 200, 300, and 400 kPa). These tests were carried out in conventional shear box device under water content controlled conditions instead of suction controlled conditions. The room temperature was controlled at 20-22°C and the humidity at 40-50%. The specimens were sheared at a rate of 0.50 mm/min under undrained conditions for the water phase while the air phase was allowed to be under atmospheric conditions (see Section 3.4.9.5 for detailed procedure). The peak shear stress or the maximum shear stress was adopted as a failure criterion.

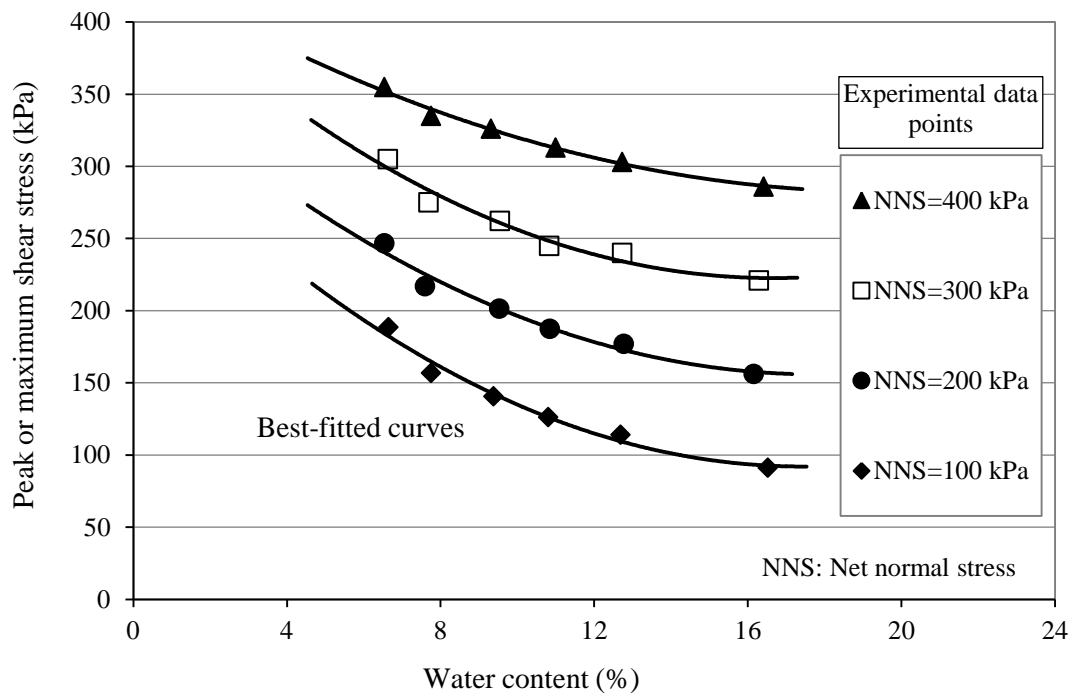
The test results were incorporated with the data obtained from the stress dependent soil-water characteristic curve (SD-SWCC) tests to evaluate the shear strength as a function to the matric suction (see Section 3.4.9.6). Three main approaches were considered in analysing the test results which are the single stress-state variable approach (Bishop, 1959), the two stress-state variables approach (Fredlund and Morgenstern, 1977), and the true effective stress concept introduced by Lu and Likos (2006). The contribution of matric suction to shear strength (τ_s), the internal friction angle related to matric suction (ϕ^b), the effective stress parameter (χ), the suction stress (σ'_s), and the true effective stress (σ'') were evaluated for different sand-gypsum mixtures under different loading conditions. These parameters are presented and discussed in the following sections.

8.3.1. Shear strength-water content relationships

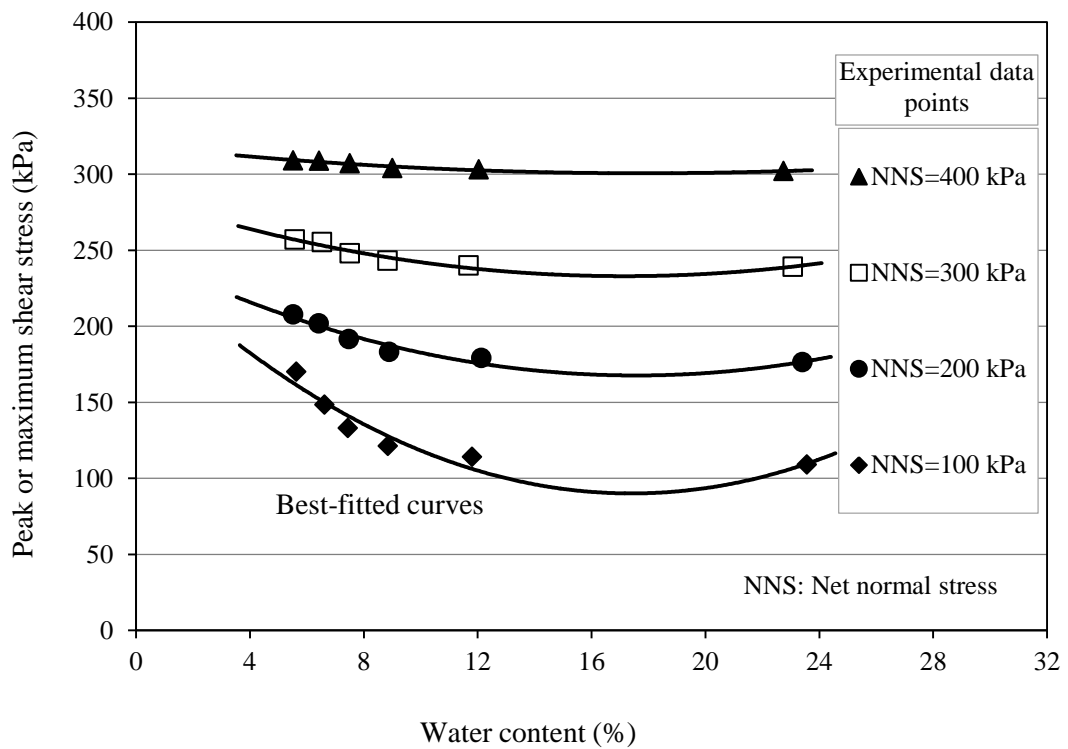
Typical results of the variation of shear strength (peak or maximum shear stress) with gravimetric water content at four levels of net normal stress are presented in Figures 8.7 A, B and C. Three different sand-gypsum mixtures are considered. These mixtures had gypsum contents of 20, 40, and 80% by dry weight. Results of other two sand-gypsum mixtures (0 and 65% gypsum content) are presented in Figures B.2 A and B, Appendix B.



(A) 20% Gypsum content



(B) 40% Gypsum content



(C) 80% Gypsum content

Figure 8.7. Peak or maximum shear stress vs. water content at four levels of net normal stress for sand-gypsum mixtures having (A) 20%, (B) 40%, (C) 80% gypsum content by weight.

The relationship between peak shear stress and water content is curvilinear over the range of water content tested, with a peak shear stress increasing as the water content decreases (Figures 8.7 A, B and C). The degree of curvature seems to be related to the gypsum content and to the level of the applied net normal stress. As gypsum content increases, the peak shear stress-water content curve becomes flatter showing low degree of curvature. Ultimately, at gypsum content of 80%, the peak shear stress -water content relationship approaches linear pattern, especially at net normal stress level of 400 kPa. As well as, for all gypsum contents, the increase of the net normal stress causes the peak shear stress-water content curve to be flatter.

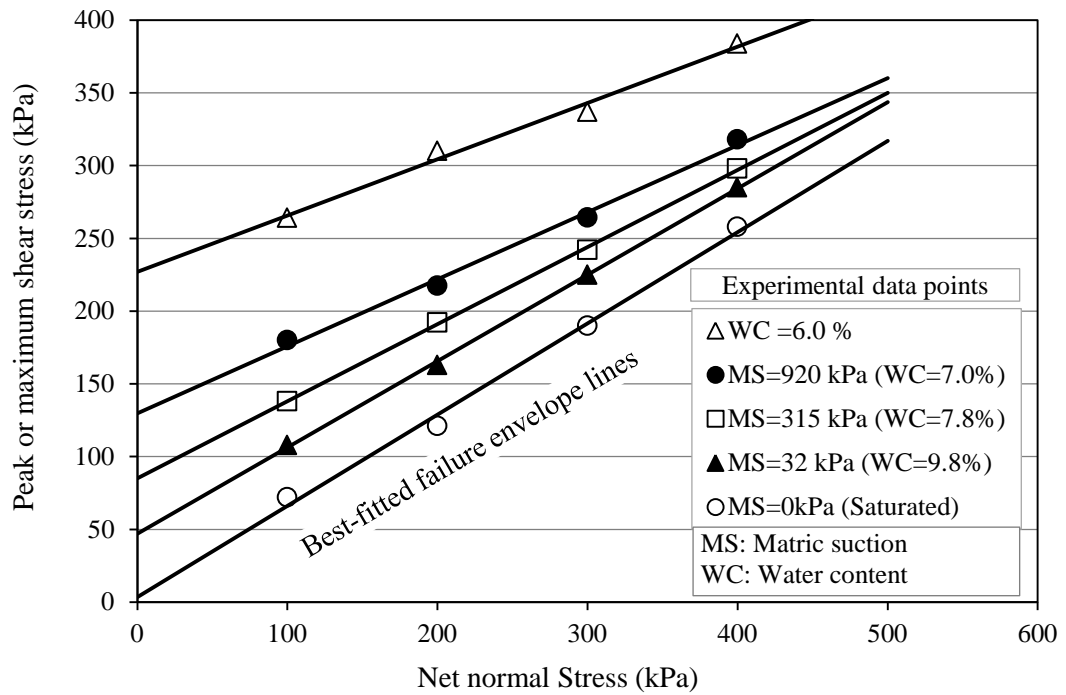
Test results presented in Figures 8.7 A, B and C show also that the slope of the peak shear stress-water content curve, or the rate of increasing peak shear stress with decreasing water content, seems to be affected by each of the gypsum content, net normal stress, and the stage of desaturation. At any specified net normal stress and water content, the slope of peak shear stress-water content curve reveals clear decrease with increasing gypsum content. Thus, the effect of desaturation (increasing of matric suction) in increasing the shear strength decreases with increasing gypsum content in the soil mixture.

For all gypsum contents, the slope of peak shear stress-water content curve at any specified water content shows apparent decrease with increasing the level of the applied net normal stress (Figures 8.7 A, B and C). Thus, the contribution in the shear strength resulting from desaturation exhibits some decrease with increasing the applied net normal stress level. On the other hand, the general slope of peak shear stress-water content curve has relatively small value near saturation and then gradually increases with decreasing water content reaching a maximum constant value near residual water content.

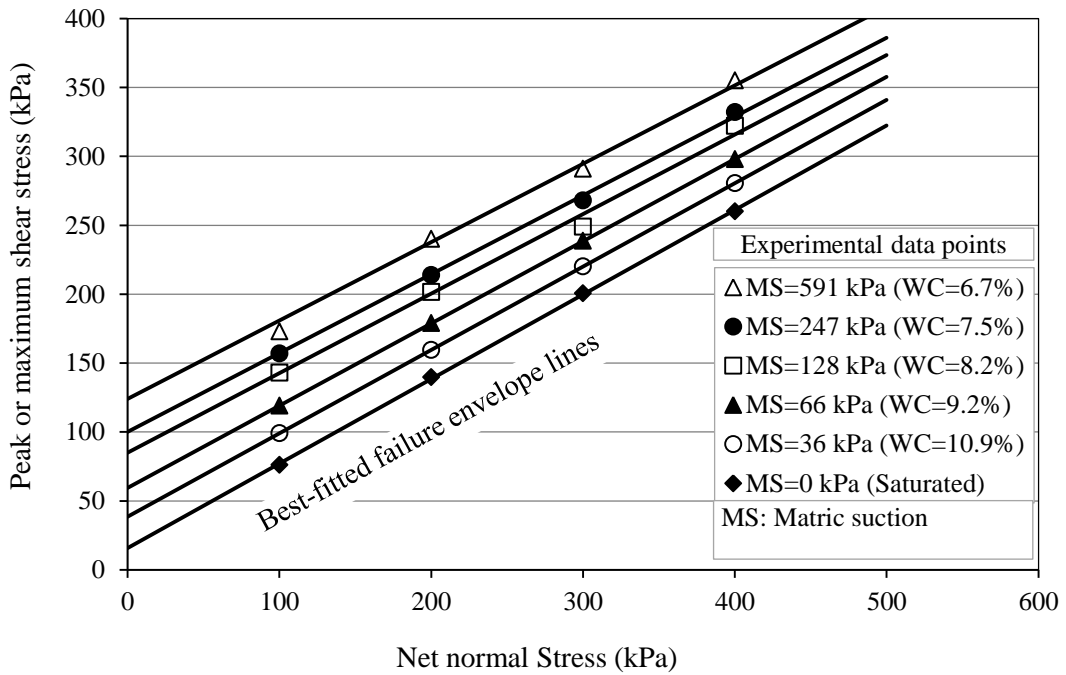
8.3.2. Failure envelopes in plane of net normal stress-shear stress

A series of nearly parallel failure envelopes in the plane of net normal stress-shear stress were constructed corresponding to different water contents (different matric suction) for five sand-gypsum mixtures. These envelopes are presented in Figures 8.8 A, B, C, D and E. The matric suction values corresponding to different

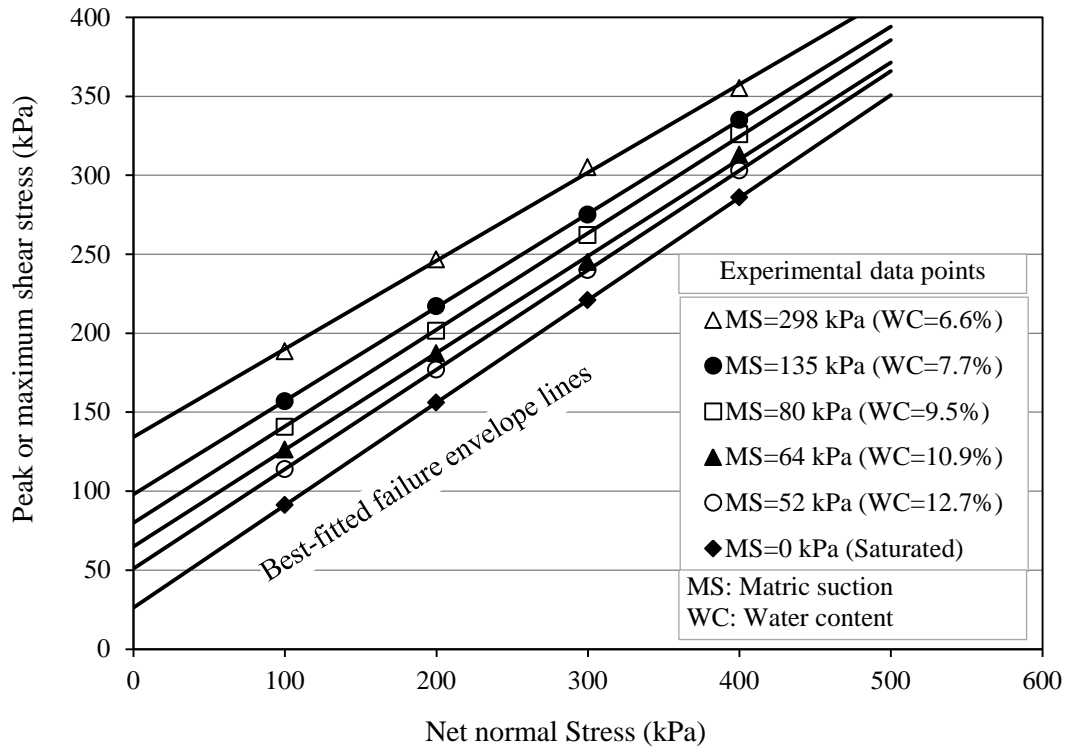
water contents were estimated by using the SD-SWCC tests data as described in Section 3.4.9.6.



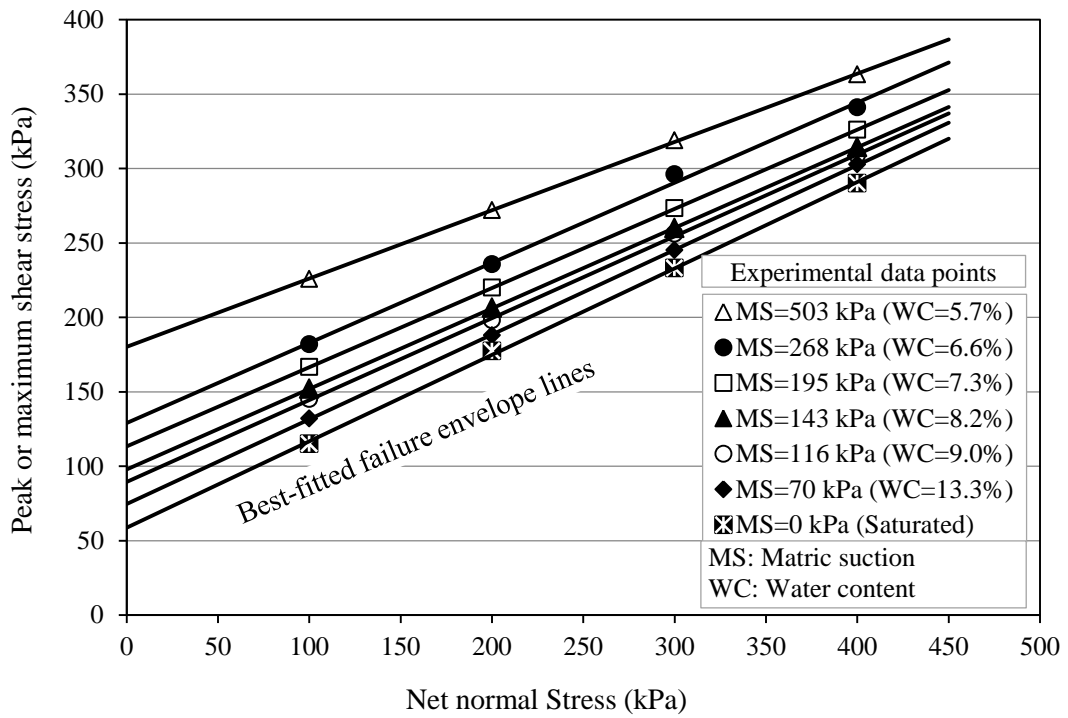
(A) 0% Gypsum content



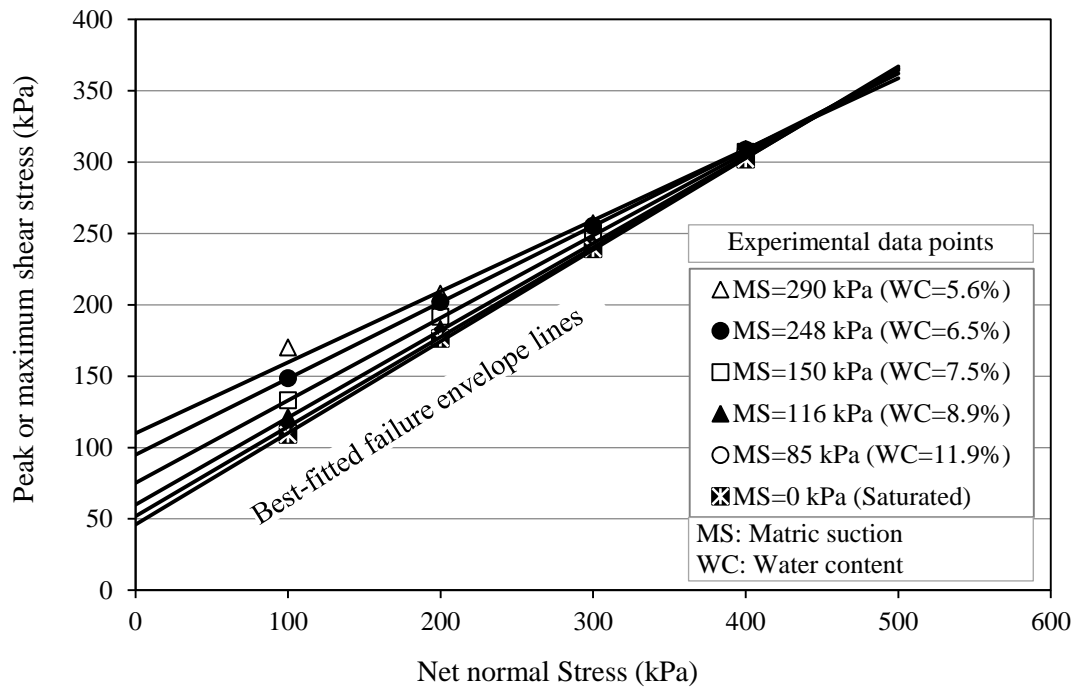
(B) 20% Gypsum content



(C) 40% Gypsum content



(D) 65% Gypsum content



(E) 80% Gypsum content

Figure 8.8. Shear strength failure envelopes at different water contents (different matric suctions) for sand-gypsum mixtures having (A) 0%, (B) 20%, (C) 40%, (D) 65%, and (E) 80% gypsum content by weight.

Like the saturated shear strength envelopes, the shear strength envelopes for unsaturated specimens show good linearity over the normal stress range of 100 to 400 kPa. The linearity between peak shear stress and normal stress is an indication of the existence of an apparent cohesion and friction angle in terms of total stresses. For all tested sand-gypsum mixtures, failure envelopes of unsaturated specimens show good consistency to each other at various water contents. Even though, results of unsaturated specimens show relatively more scattering when compared to the saturated test results that appear fairly unique.

It can be noticed from Figure 8.8E for 80% gypsum content mixture that the shear strength envelopes at different water contents converge towards an intersecting point when the net normal stress level approaches 400 kPa. This behaviour means that at this level of net normal stress, there is no effect to desaturation or matric suction in increasing the shear strength for the soil mixture have 80% gypsum content.

Figures 8.8 A, B, C, D and E reveal also that the decrease of specimen water content causes the apparent cohesion to increase noticeably and the friction angle to decrease moderately. This behaviour makes the effect of desaturation in increasing the shear strength is more pronounced at low levels of net normal stress. The effect of desaturation on the apparent shear parameters is quantified and discussed in detail in the following section.

8.3.3. Apparent cohesion and friction angle versus water content

The shear strength parameters in terms of apparent cohesion intercept and total stress friction angle were determined for five sand-gypsum mixtures, at different water contents, by using the best fitted-straight line failure envelopes presented in Figures 8.8 A, B, C, D and E. These parameters are presented in Figure 8.9 as functions to the gravimetric water content. It can be noticed that the apparent cohesion of different sand-gypsum mixtures exhibits remarkable increase as water content decreases, with an increasing rate dramatically increases at low water contents. On the contrary, the apparent friction angle of those sand-gypsum mixtures shows mild decrease with decreasing water content.

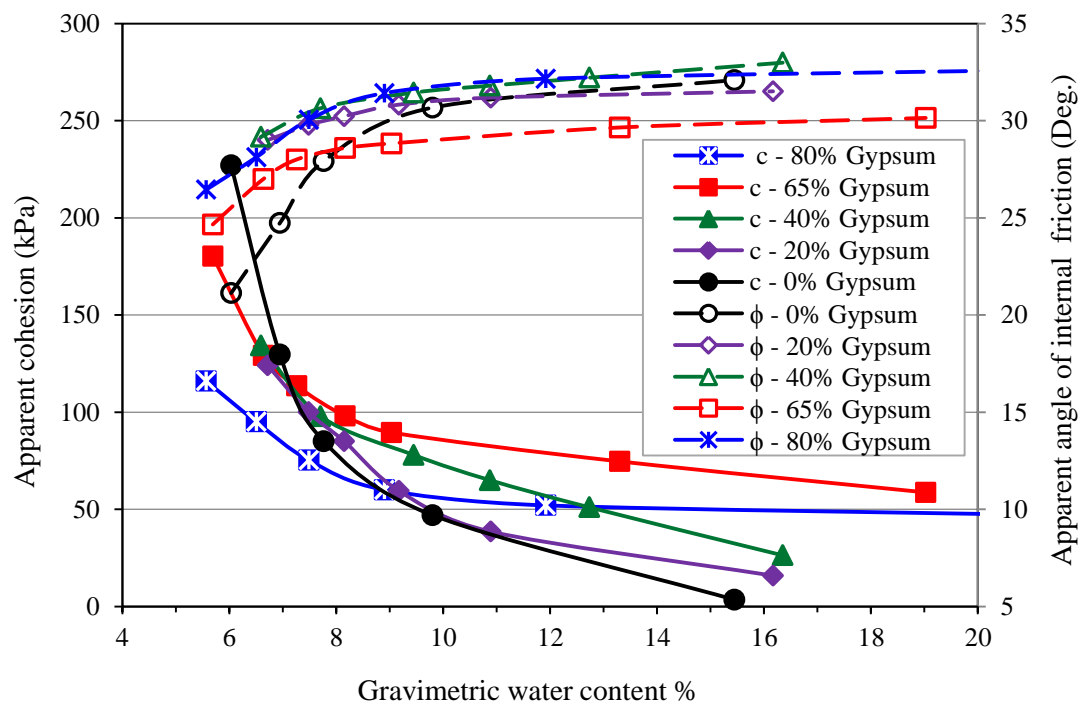


Figure 8.9. Apparent cohesion and apparent friction angle versus gravimetric water content for different sand-gypsum mixtures.

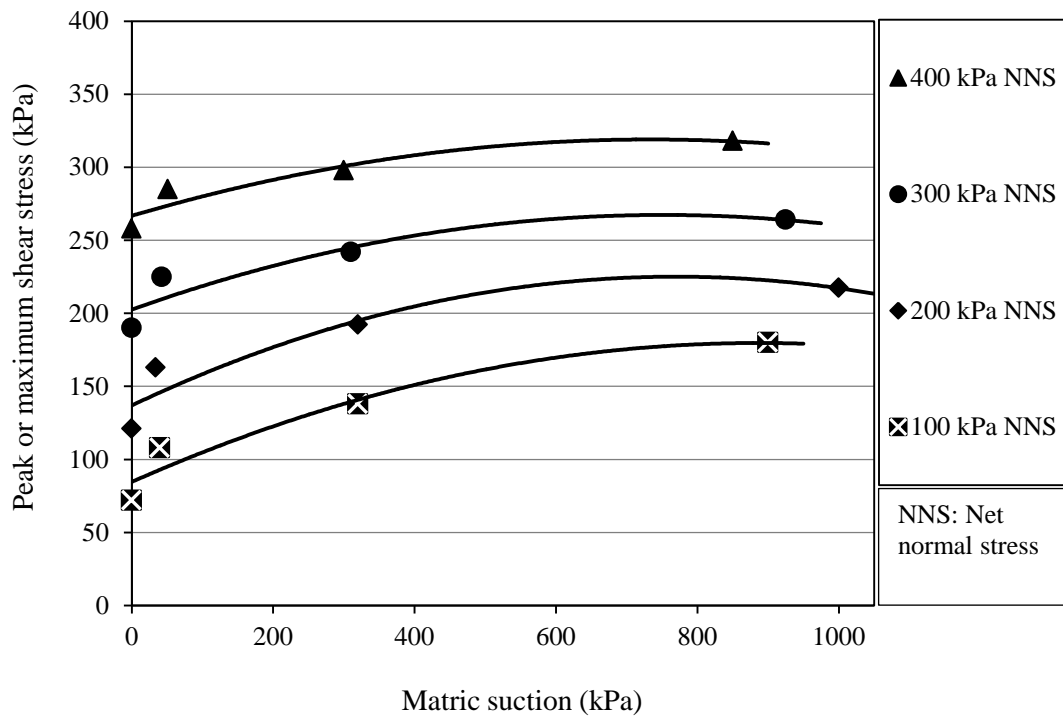
As with the saturated cohesion, there is a general tendency to the apparent cohesion function to increase with increasing gypsum content reaching a highest level at 65% gypsum content. Then, the apparent cohesion function exhibits a decrease with further increase in gypsum content. This behaviour can be attributed to matter that the cementation bonds between gypsum-gypsum particles are greater than the cementation bonds between gypsum-sand particles and these in turn are greater than the bonds between sand-sand particles.

It is recognised from the stress-deformation characteristics of the compacted saturated specimens presented in Section 8.2.1 that the contribution of cementation bonds to the soil cohesion and then to the shear strength may be significant when the shear stress-shear displacement curve has a peak corresponding to small lateral displacement. On the other hand, the cementation cohesion of sand-gypsum mixtures that have non-peak behaviour may be insignificant, especially when the shear displacement required to mobilize the maximum shear stress is much more than the shear displacement required to mobilize the cementation cohesion. When large shear displacement is required to mobilize the maximum shear stress, the majority of cementation bonds would have been destroyed. In other words, for sand-gypsum mixtures of non-peak behaviour, the strength due to cohesion is mobilized at a faster rate than the strength due to frictional component. As a conclusion, when the two components of the shear strength are mobilized at nearly the same lateral displacement, the cementation bonds would be significant, otherwise it would be not.

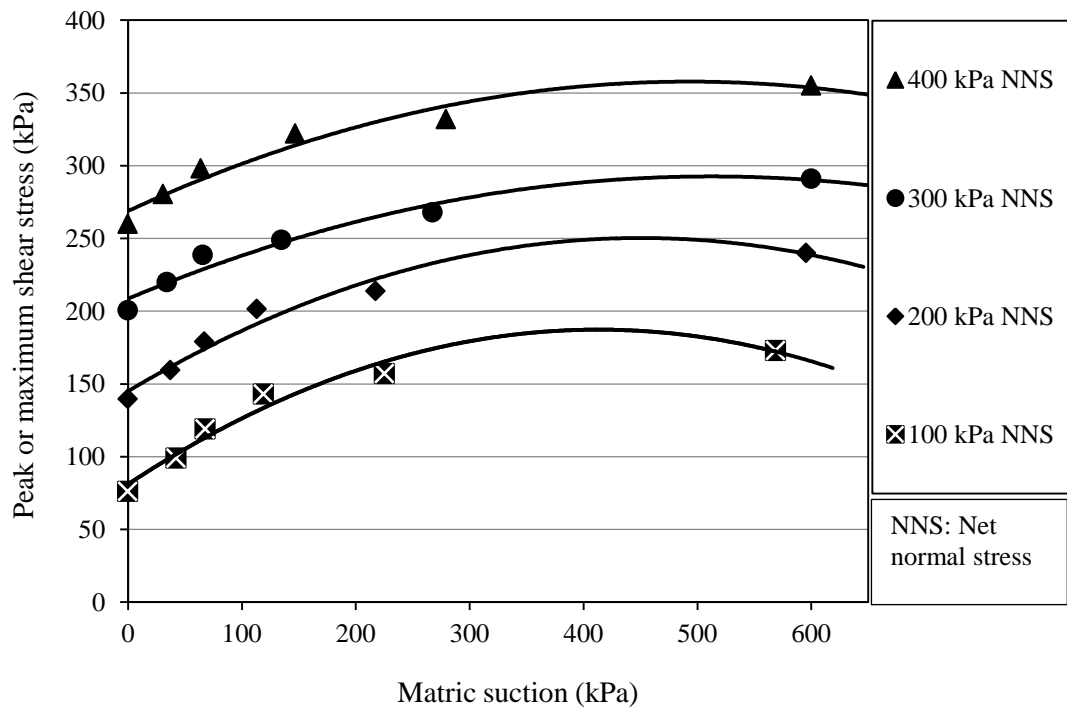
8.3.4. Failure envelopes in plane of matric suction-shear stress

Figures 8.10 A, B, C, D, and E present a summary of the results obtained from about 150 direct shear tests on unsaturated specimens, at different controlled water contents, of five sand-gypsum mixtures. The shear strength data of the unsaturated specimens were incorporated with the results of stress-dependent soil-water characteristic curve tests which were carried out on identical five sand-gypsum mixtures, at identical levels of net normal stress. Thus the matric suction values corresponding to the controlled water content values were estimated by using the mathematical equation of the SD-SWCCs with the fitting parameters which are presented in Table 6.2. Thus, the shear strength results are presented as plots of peak

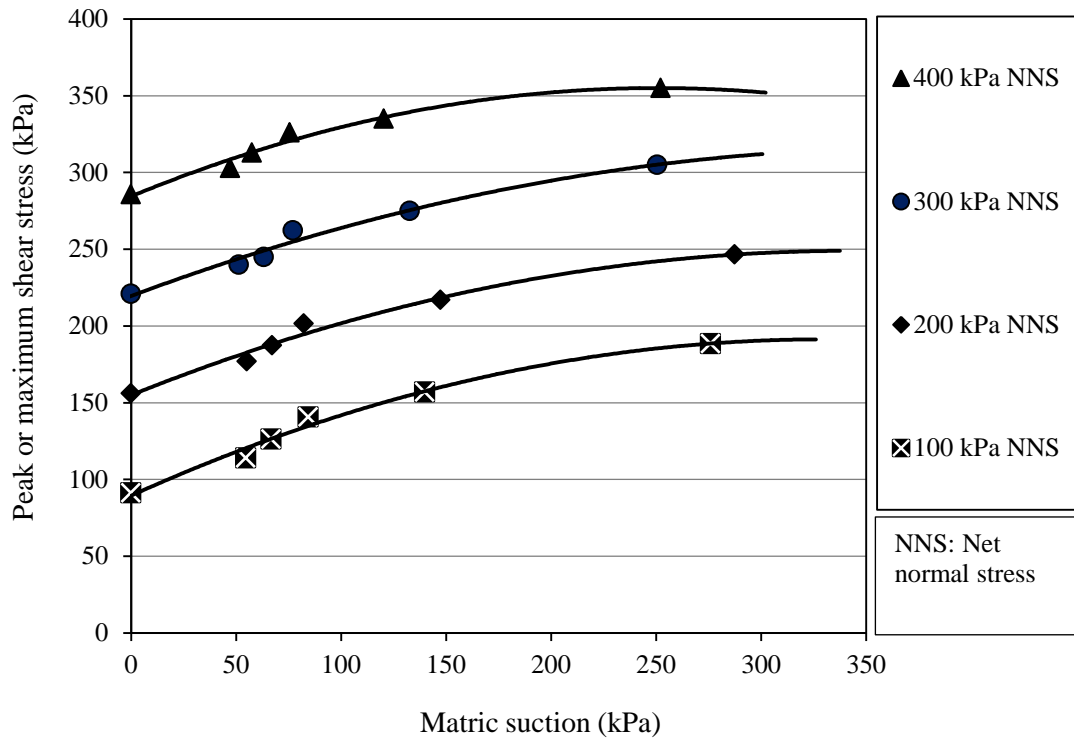
or maximum shear stress versus the estimated matric suction at four constant net normal stress levels, for five sand-gypsum mixtures.



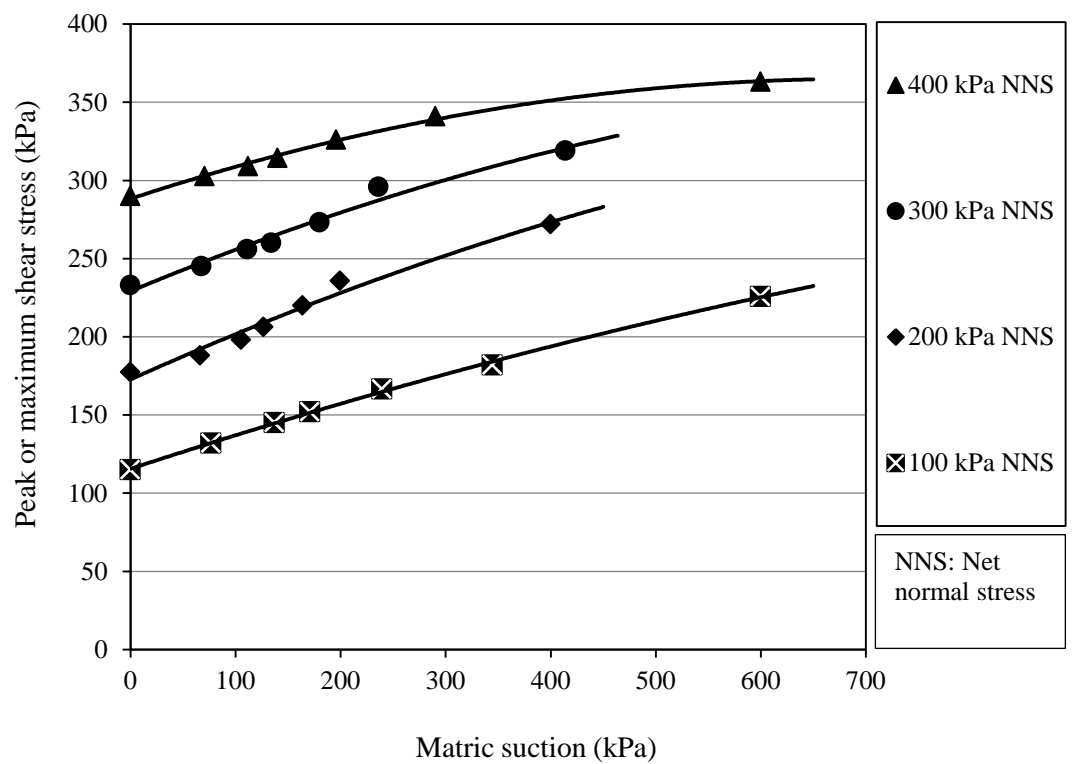
(A) 0% Gypsum content



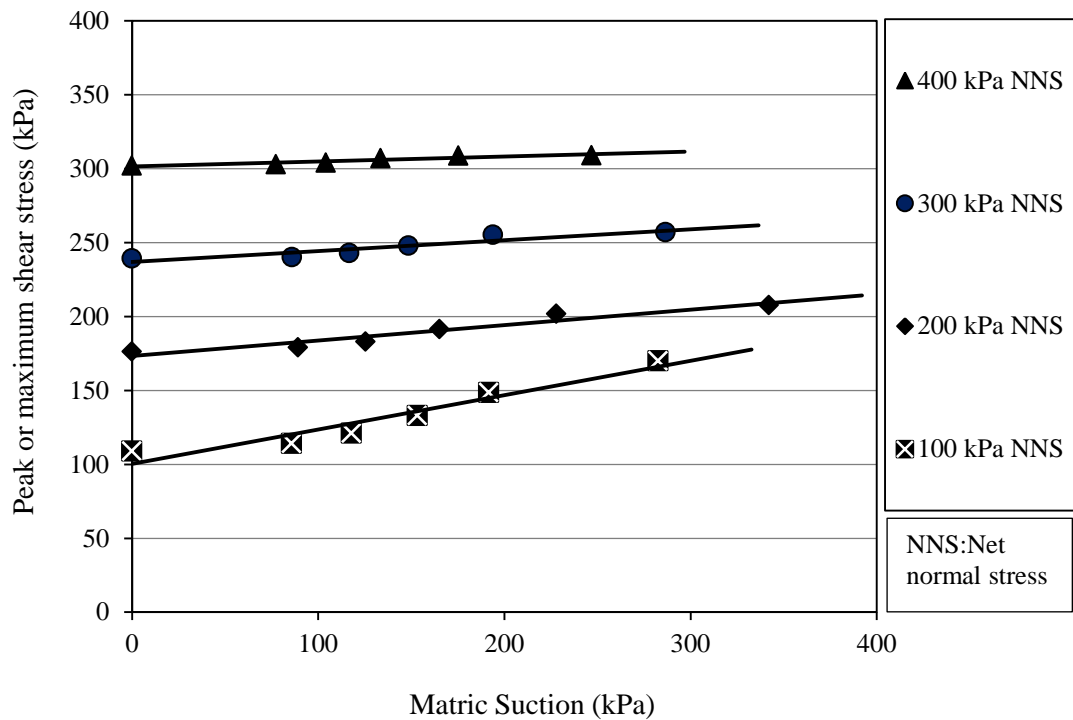
(B) 20% Gypsum content



(C) 40 % Gypsum content



(D) 65% gypsum content



(E) 80% Gypsum content

Figure 8.10. Shear strength failure envelopes with respect to matric suction under four constant net normal stress levels for sand-gypsum mixtures having (A) 0%, (B) 20%, (C) 40%, (D) 65%, and (E) 80% gypsum content by weight.

As discussed earlier in Section 3.4.9.5, it is worthy to mention here that the estimated values of matric suction are essentially very close to the real matric suction values at the end of consolidation stage while some changes may be anticipated during shearing process. However, it is assumed that a relatively fast rate of shearing (which was adopted to be 0.5 mm/min.) results in a small change in matric suction during the shearing stage. Similar assumption for analyses of shear strength test results has been used by Vanapalli et al. (2000) and Vanapalli et al. (2002).

The shear strength envelopes shown in Figures 8.10 A, B, C, D, and E have some nonlinearity with respect to the matric suction axis, especially when a relatively large range of soil suction is considered. The general pattern of these curves comprises of two curvilinear segments, an initial high curvature segment with relatively high average slope followed by a second relatively low curvature segment with smaller average slope. The transition from the high curvature to the low curvature segment of the envelope appears to occur at an estimated matric suction of

about 130 kPa for the five tested sand-gypsum mixtures. This transition point is close to the residual matric suction values of those soil mixtures (see Figures 6.2 to 6.6). The transition may be resulted from the diminishing contribution of matric suction to the shear strength as the water content of the specimen approaches the residual water content. At residual stage, the water phase starts to be discontinuous and the soil-water system transforms from capillary mechanism to hydration mechanism (Lu and Likos, 2004; Ng and Menzies, 2007). As a result, the cross-sectional area through which the water phase acts is decreased, and as such, an increase in the matric suction is not as effective in increasing the shear strength as in the capillary stage (Fredlund and Rahardjo, 1993; Vanapalli et al., 1999). The nonlinearity of the failure envelope with respect to matric suction has been addressed and discussed in detail by Fredlund et al. (1987).

The other remarkable point which can be noticed from the failure envelopes in Figures 8.10 A, B, C, D, and E is that the overall envelope curvature exhibits clear decrease with increasing gypsum content in the sand-gypsum mixture. This behaviour can be noticed at all levels of net normal stress. The matric suction failure envelopes of soil mixtures having gypsum content of 65% and 80% appear good linearity over the entire matric suction range of 0 to 400 kPa, at various levels of net normal stress.

Furthermore, the overall slope of the failure envelopes presented in Figures 8.10 A, B, C, D, and E reveal slight increase with increasing gypsum content up to 40% by weight, then the slope shows clear decrease with further increasing of gypsum content in the soil mixture. This behaviour is quantitatively evaluated in the next section. The effectiveness of the matric suction in contributing an increase in the shear resistance seems highly dependent on the gypsum content. Matric suction contribution in shear strength shows a noticeable decrease at gypsum content of 80% by weight, especially at higher levels of net normal stress (Figure 8.10 E).

It is apparent from Figures 8.10 A, B, C, D, and E that consistent relationships are existed at different net normal stress levels between the peak or maximum shear stress and the matric suction which is estimated from the SD-SWCC tests. This consistency confirms the reliability and the viability of the proposed approach of

testing and analysing the shear strength parameters of unsaturated compacted specimens. The proposed procedures utilize standard laboratory direct shear equipment and take a relatively short time to be completed. Thus, it offers an easy and convenient alternative way for the determination of the unsaturated shear strength parameters.

8.3.5. Effect of gypsum content on ϕ^b and χ

The shear strength of an unsaturated soil consists of an effective cohesion component (c'), frictional component resulting from net normal stress ($\sigma - u_a$), and the independent contribution to shear strength resulting from matric suction ($u_a - u_w$), Fredlund and Rahardjo (1993), Ng and Menzies (2007). The first two components are well defined through the saturated shear strength parameters, c' and ϕ' . The contribution of matric suction to the shear strength can be viewed in terms of being either part of the frictional component or part of the cohesive component of the soil shear strength (Lu and Likos, 2004). As mentioned in Sections 2.6 and 3.4.9.6, the shear strength contribution from matric suction could be characterized by ϕ^b which is a friction angle with respect to matric suction (Fredlund and Morgenstern, 1977) or by the effective stress parameter χ (Bishop, 1959) which represent the matric suction contribution to the effective stress and then to the shear strength through the saturated friction angle.

To evaluate ϕ^b , the shear strength failure envelopes with respect to matric suction, which are presented earlier in Figures 8.10 A, B, C, D, and E, were best fitted by two linear segments. The first segment covers the range of matric suction from 0 to 130 kPa, while the second segment starts from 130 kPa suction value and extends to residual range. Thus, two values of ϕ^b were defined from each matric suction failure envelope, ϕ^b at capillary zone and ϕ^b at residual zone. These values which were defined for different sand-gypsum mixtures, at four levels of net normal stress, are presented in Figures 8.11 A and B. Several procedures for handling the nonlinearity of the shear stress versus matric suction failure envelope have been proposed by Fredlund et al. (1987). One of these procedures is to discretize the failure envelope into several linear segments if the envelope is highly nonlinear, and this may agree to some extent with the proposed procedure in this study.

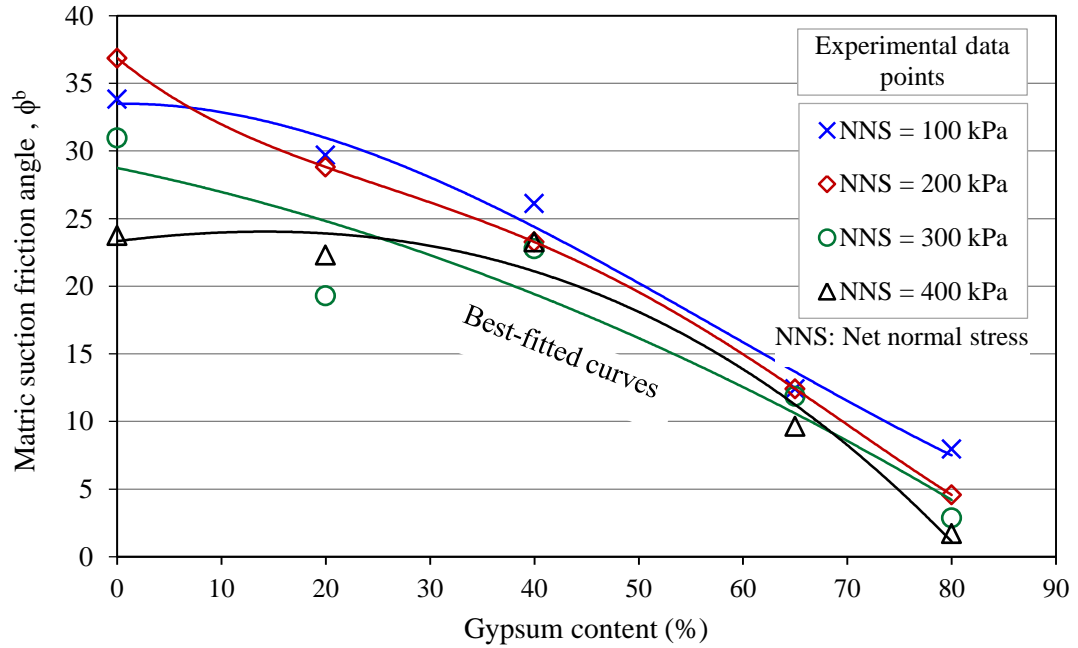
It can be noticed from Figures 8.11 A and B that ϕ^b at capillary zone shows noticeable decrease with increasing gypsum content under various levels of net normal stress. These ϕ^b angles commence at values of 33.8, 36.9, 31.0, and 23.7, corresponding to net normal stress levels of 100, 200, 300, and 400 kPa, for sandy soil without gypsum and decrease with increasing gypsum content reaching values of 8.0, 4.6, 2.9, and 1.7, respectively for soil mixture has 80% gypsum content. Comparing with saturated friction angle value of 32.1 for sandy soil without gypsum, the values of ϕ^b at capillary zone for the same soil are 33.8 and 36.9 under 100 and 200 kPa net normal stress levels, respectively. As such, at this case, an increase in matric suction is more effective in increasing the shear strength as is an increase in the net normal stress.

On contrary to the capillary zone, Figure 8.11 B shows that the values of ϕ^b at residual zone exhibit remarkable increase with increasing gypsum content, under various levels of net normal stress, reaching maximum values at around 50% gypsum content and then clear decrease can be noticed for further increase in gypsum content.

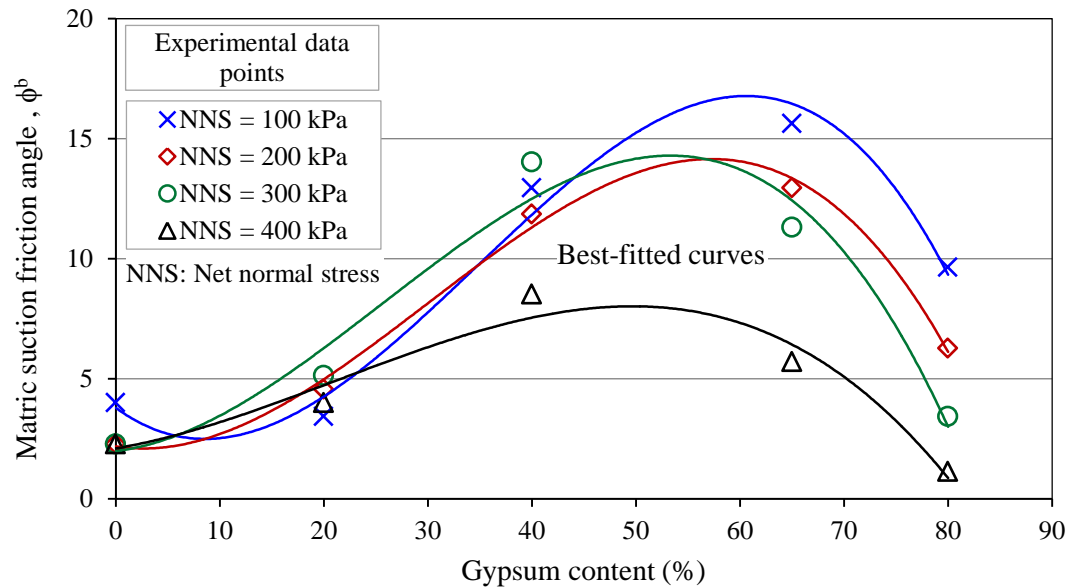
Considering ϕ^b values at capillary zone and using Equation 3.21, the values of effective stress parameter χ at various net normal stress levels are evaluated and presented in Figure 8.12 as functions to gypsum content. It is obvious from Figure 8.12 that χ functions are highly consistent with the corresponding ϕ^b functions under different levels of net normal stress. This behaviour is attributed to the fact that both the single stress approach and the two independent stress-state approach are mathematically the same but physically are different. Similar to ϕ^b , the effective stress parameter χ exhibits remarkable decrease with increasing gypsum content under various net normal stress levels. Thus, regardless the approach adopted in the analysis of shear strength data, it is clear that there is noticeable diminishing in the contribution of matric suction in increasing the shear strength associated with the increase in gypsum content.

However, a precise inspection to Figure 8.12 reveals that the values of χ are greater than one for soil specimens without gypsum, tested at 100 and 200 kPa net normal stress levels, and that is consistent with the corresponding values of ϕ^b which

are greater than the saturated friction angle ϕ' . Similar results of ϕ^b values higher than ϕ' were reported by Vanapalli et al. (1999) on glacial till specimens tested at confining pressure values of 100 and 200 kPa.



(A) Matric suction range of 0 to 130 kPa



(B) Matric suction greater than 130 kPa

Figure 8.11. Effect of gypsum content on matric suction friction angle (ϕ^b) under four levels of net normal stress, (A) For matric suction range of 0 to 130 kPa, (B) Matric suction at residual zone.

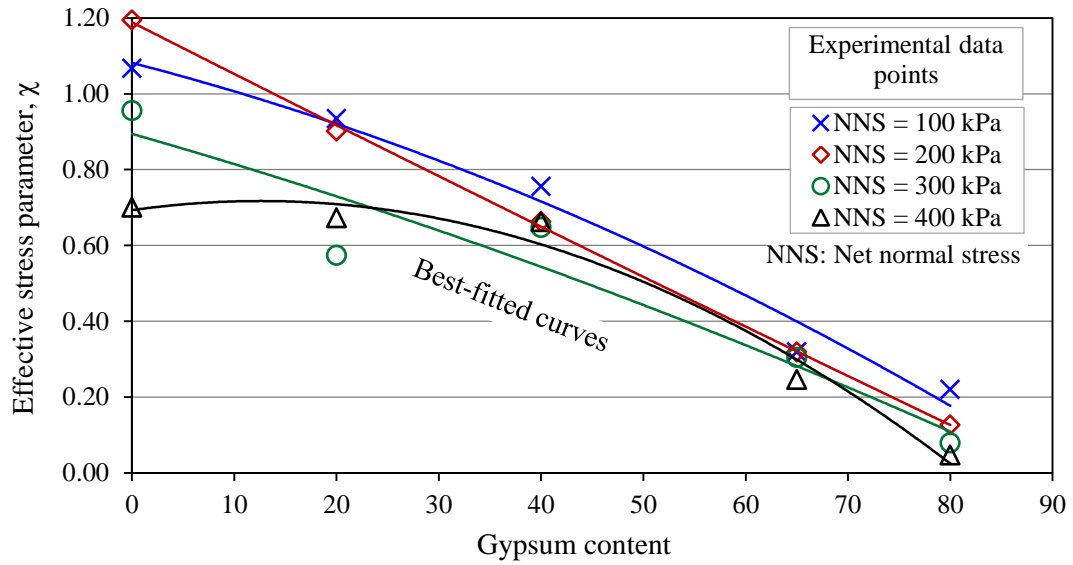


Figure 8.12. Effect of gypsum content on effective stress parameter (χ), under four levels of net normal stress, for matric suction range of 0 to 130 kPa.

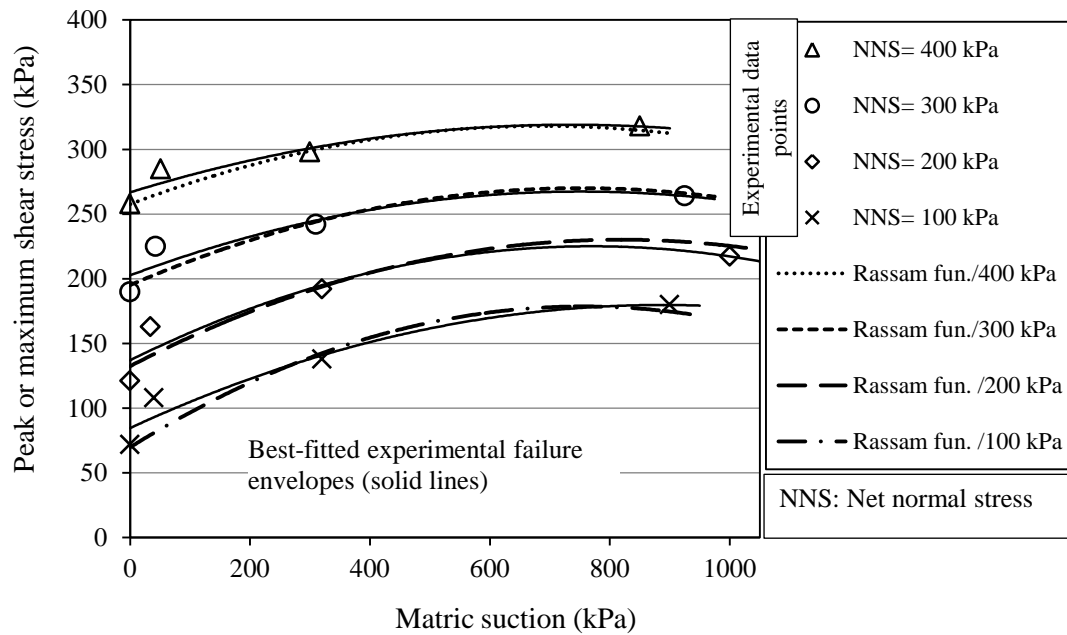
Figures 8.11 A and B and Figure 8.12 also show that for any gypsum content there is a general tendency for ϕ^b and χ to decrease with increasing the level of the applied net normal stress. That is consistent with the mathematical approach for predicting the unsaturated shear strength proposed by Rassam and Williams (1999), as reviewed in Section 2.6.4.

8.3.6. Prediction of unsaturated failure envelopes

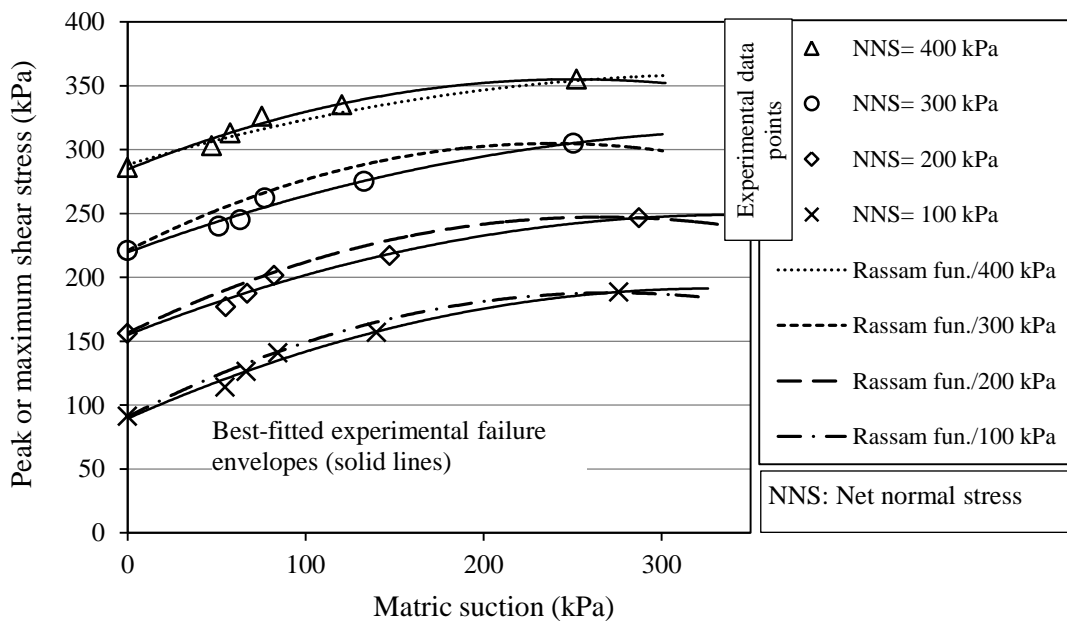
In recent years, several semi-empirical shear strength functions were proposed to predict the shear strength of unsaturated soils. Among these was the semi-empirical predictive model proposed by Rassam and Cook (2002) as reviewed in Section 2.6.4. This model was used in this research to predicate the unsaturated shear strength envelopes for various sand-gypsum mixtures. The saturated shear strength parameters (i.e., c' and ϕ'), the shear strength of air-dried specimen with water content corresponding to the residual suction, along with the stress-dependent soil-water characteristic curve data for various sand-gypsum mixtures were utilized.

Comparisons between the measured shear strength envelopes of unsaturated specimens and the predicted shear strength envelopes, at different levels of net normal stress, are presented in Figures 8.13 A, B and C for sand-gypsum mixtures having 0%, 40%, and 65% gypsum content by weight. The reminder graphs that

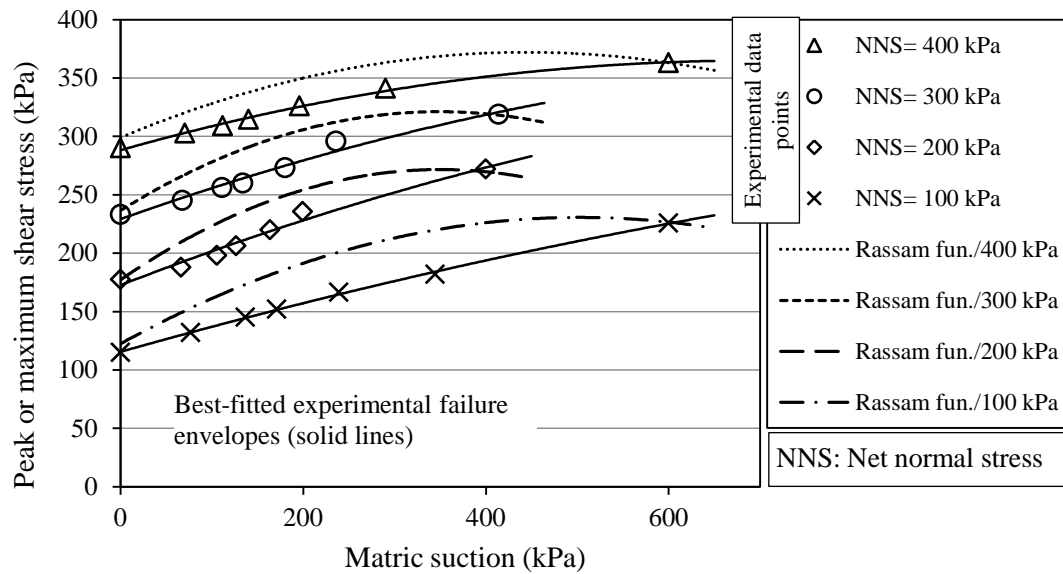
related to 20% and 80% gypsum content mixtures are presented in Appendix B, Figures B.3 A and B. In these figures, the experimental data are designated by different symbols and the resulting envelopes are shown by curve fitted solid lines. Different broken lines are used to show the predicted failure envelopes at different levels of applied net normal stress.



(A) 0% Gypsum content



(B) 40% Gypsum content



(C) 65% Gypsum content

Figure 8.13. Comparison of Rassam and Cook (2002)'s predictive function with the experimental shear strength envelopes, at different levels of net normal stress, for unsaturated sand-gypsum specimens having (A) 0%, (B) 40%, and (C) 65% gypsum content by weight.

Good agreement is observed between the predicted and the measured shear strength results for the sandy soil without gypsum additives as shown in Figure 8.13A. For sand-gypsum mixture of 40% gypsum content, accepted differences could be noticed between the predicted and the measured envelopes as shown in Figure 8.13B. With further increasing of gypsum content, the amount of deviation increases remarkably as shown in Figure 8.13C.

The predictive failure envelopes in matric suction-peak shear stress plane are necessarily matched the experimental envelopes at the beginning points (zero suction points) and at the end points (residual suction points). That is because the predictive function is formulated basically by considering the experimental shear strength values at saturation and residual water content conditions. Thus, the variation between the predictive and the experimental envelopes can be characterized sufficiently by evaluating the matching in the degree of curvature between these two envelopes.

As discussed in the previous section, two factors could influence the degree of curvature of the failure envelopes of the sand-gypsum mixtures, gypsum content

mainly and the level of applied net normal stress secondly. The degree of curvature reveals remarkable decrease with increasing gypsum content and moderate decrease with increasing the level of net normal stress. Rassam and Cook (2002) have considered the effect of net normal stress in developing their predictive model, thereby, the remaining factor that influences the deviation between the predictive and experimental envelopes and then the applicability of the proposed function could be the percentage of gypsum content. Thus, with increasing gypsum content, the experimental matric suction failure envelopes approaching linear pattern and then high deviation from Rassam and Cook's predictive model can be noticed.

The other remarkable point which can be noticed from Figures 8.13 A, B and C is the slope of the failure envelopes (ϕ^b) at residual zone. The experimental results reveal that this slope shows clear increase with increasing gypsum content, as quantitatively evaluated also in Figure 8.11B. Rassam and Cook (2002)'s predictive model based on the assumption that ϕ^b is zero at residual matric suction, i.e., the predictive failure envelopes become horizontal at residual matric suction. This assumption seems reasonable for the sandy soil without gypsum additives (Figure 8.13A), but with increasing gypsum content, there are clear deviations between the experimental and the corresponding predicted envelopes can be noticed under various levels of net normal stress (see Figure 8.13C).

8.3.7. Suction stress characteristic curves

Suction stress refers to the net interparticle force generated within a matrix of unsaturated soil particles due to the combined effects of negative pore water pressure and surface tension (Lu and Likos, 2006). The function of suction stress to the water content or matric suction is termed as the suction stress characteristic curve (SSCC). The SSCC concept was recently proposed to more effectively express and evaluate the influence of matric suction on the effective stress and then on the shear strength of unsaturated soil. This concept is advantageous because it can represent the state of stress for unsaturated soil using a single stress variable by expanding both Terzaghi (1943)'s and Bishop (1959)'s effective stress principles, Oh et al. (2012).

The suction stress characteristic curves (SSCCs) for five sand-gypsum mixtures at various net normal stress levels were found from direct shear strength tests on unsaturated specimens, by following the approach of Lu and Likos (2006). The SSCCs in terms of water content for sand-gypsum mixtures having 0% and 80% gypsum content are presented in Figures 8.14 A and B. The SSCCs for mixtures having 20%, 40%, and 65% are presented in Appendix B, Figure B.4 A, B, and C.

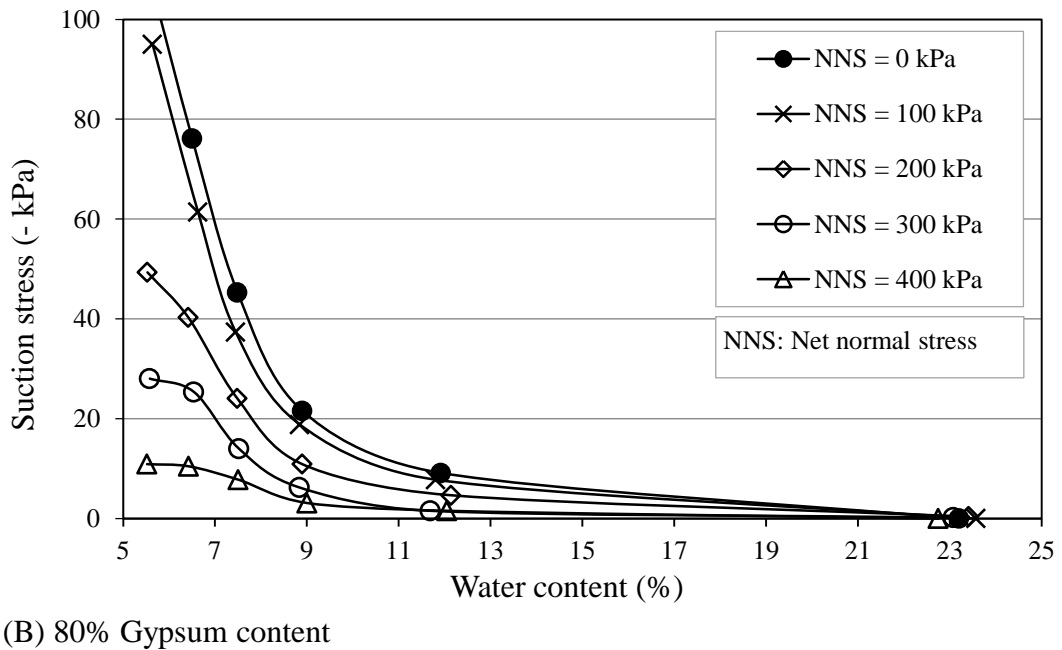
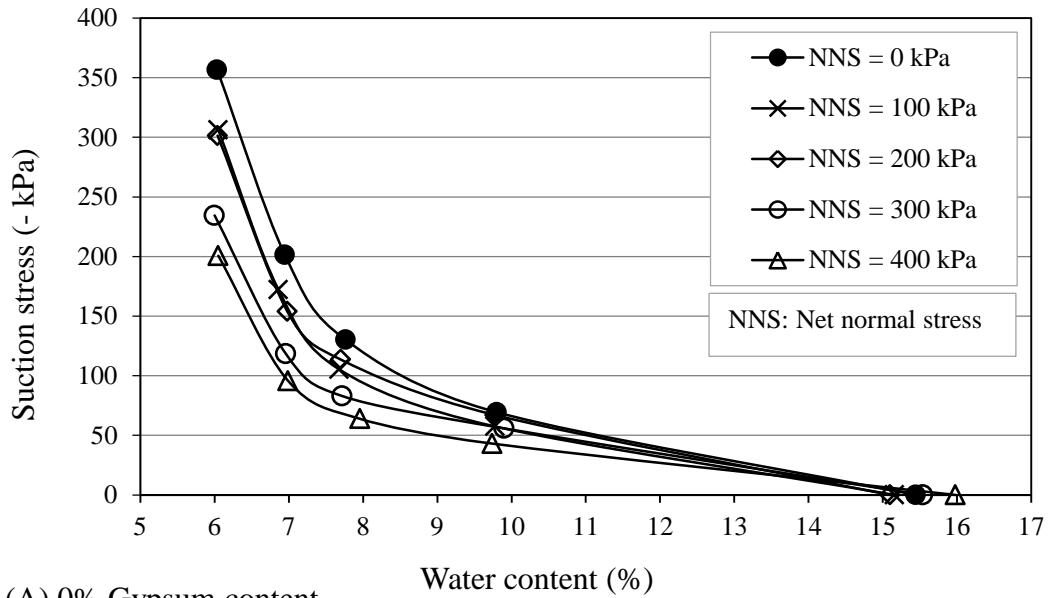


Figure 8.14. SSCCs in terms of water content (According to the approach of Lu and Likos, 2006) for sand-gypsum mixtures having (A) 0%, and (B) 80% gypsum content by weight, at different levels of net normal stress.

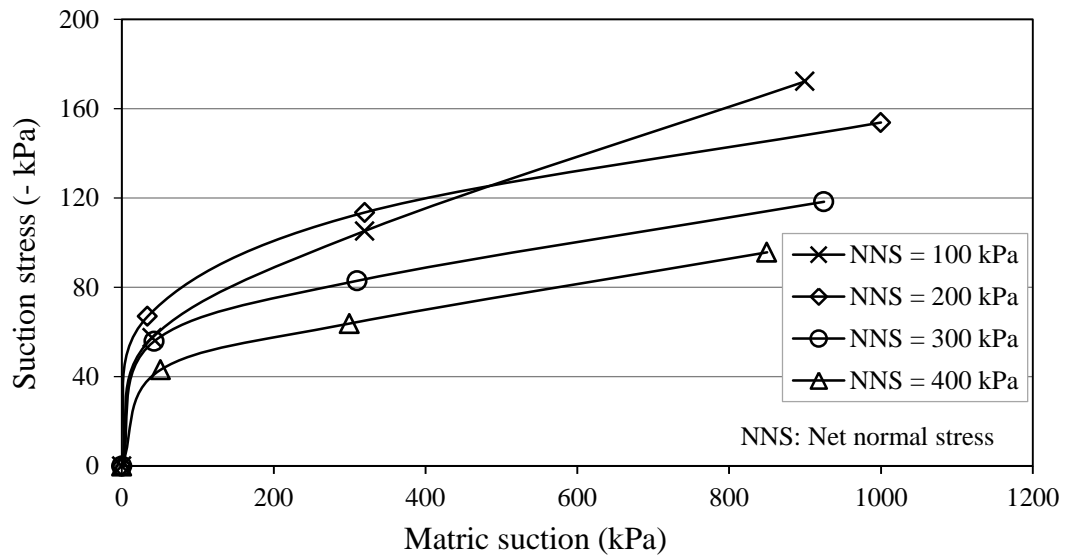
Figures 8.14 A and B reveal that the SSCCs behaviour are significantly depended on gypsum content of the sand-gypsum mixture under consideration. The level of the applied net normal stress is clearly affected the pattern of the SSCC as well. Three segments could be distinguished on each of the determined SSCC; two linear segments with a curvilinear segment in the middle connected them. A precise comparison between the SD-SWCCs presented in Figures 6.2 to 6.6 and the SSCCs in Figures 8.14 A and B reveals that these three segments can be related to the different water retention mechanisms within the matrix of unsaturated soil. These mechanisms are (i) the capillary mechanism which extends from saturation to near residual water content, (ii) the adsorption mechanism that extends behind the residual stage of water retention, and (iii) a transition state between these two different mechanisms (Section 2.4.7). The two linear segments of the SSCC may be related to the capillary mechanism and the adsorption mechanism, respectively. The middle curvilinear segment is related to the transition zone between these two mechanisms.

At relatively high water contents, when the matric suction is smaller than the residual matric suction, the SSCC exhibits linear relationship with relatively small inclination. When the matric suction approaching the residual value, the SSCC in terms of water content shows nonlinear shape with a degree of curvature depends significantly on the material properties, particularly pore size and pore size distribution. As the matric suction exceeds the residual suction of the soil mixture, the SSCC returns again showing a linear pattern but with relatively steep inclination.

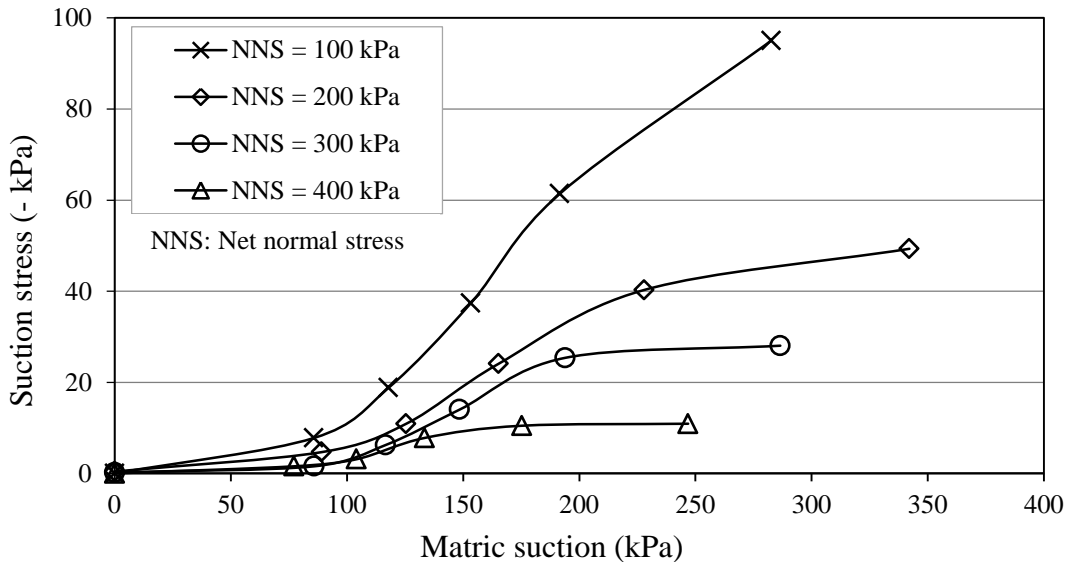
Figures 8.14 A and B reveal that there is a clear decrease in suction stress function with increasing the level of the applied net normal stress, and this decrease becomes more pronounced at high gypsum content soil mixtures. Thus, the slope of the linear segments of the SSCC seem to decrease with increasing net normal stress, associated mostly with clear decrease in the degree of curvature of the transition segment.

As discussed in Section 2.3.2, SSCC could be described as a function to water content or to matric suction. Thus the SSCCs in terms of matric suction for different sand-gypsum mixtures were established after estimating the matric suction values in correspondence to the water content values. The mathematical representations of the

SD-SWCCs data were used. Figures 8.15 A and B present the SSCCs in terms of matric suction, for sand-gypsum mixtures having 0% and 80% gypsum contents. Figures 8.15 A and B show clearly that the general trend of the contribution of matric suction to the suction stress decreases with increasing matric suction, i.e., the slope of SSCC decreases with increasing matric suction. As well as, the suction stress function in terms of matric suction exhibits remarkable decrease with increasing the level of net normal stress.



(A) 0% Gypsum content

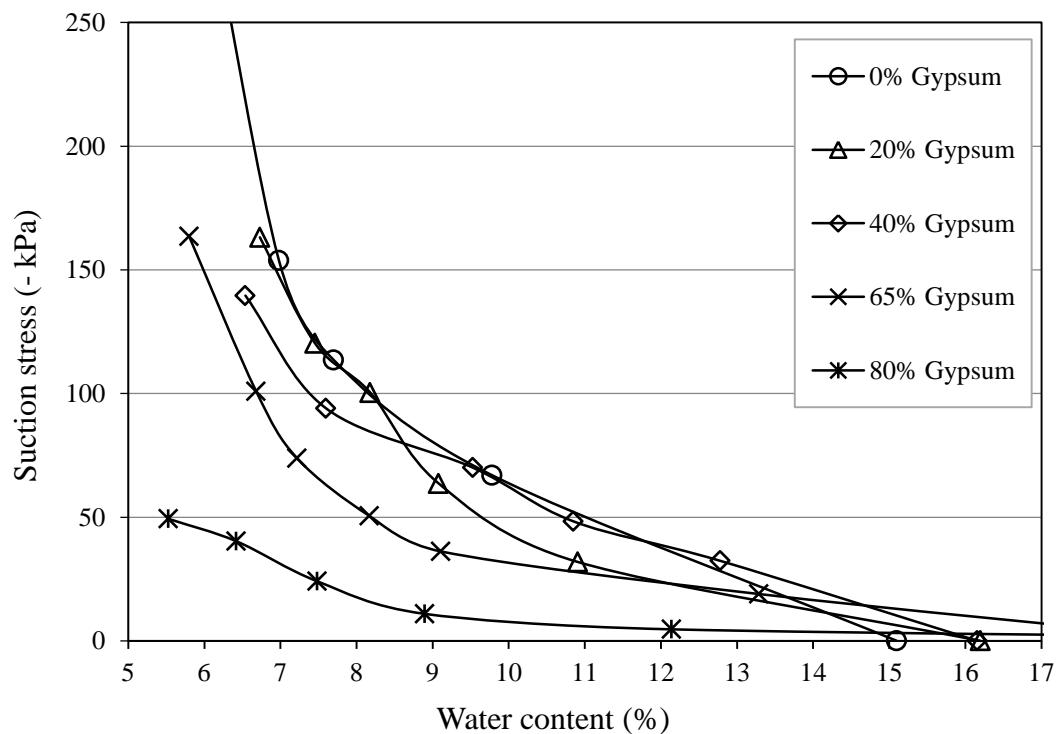


(B) 80% Gypsum content

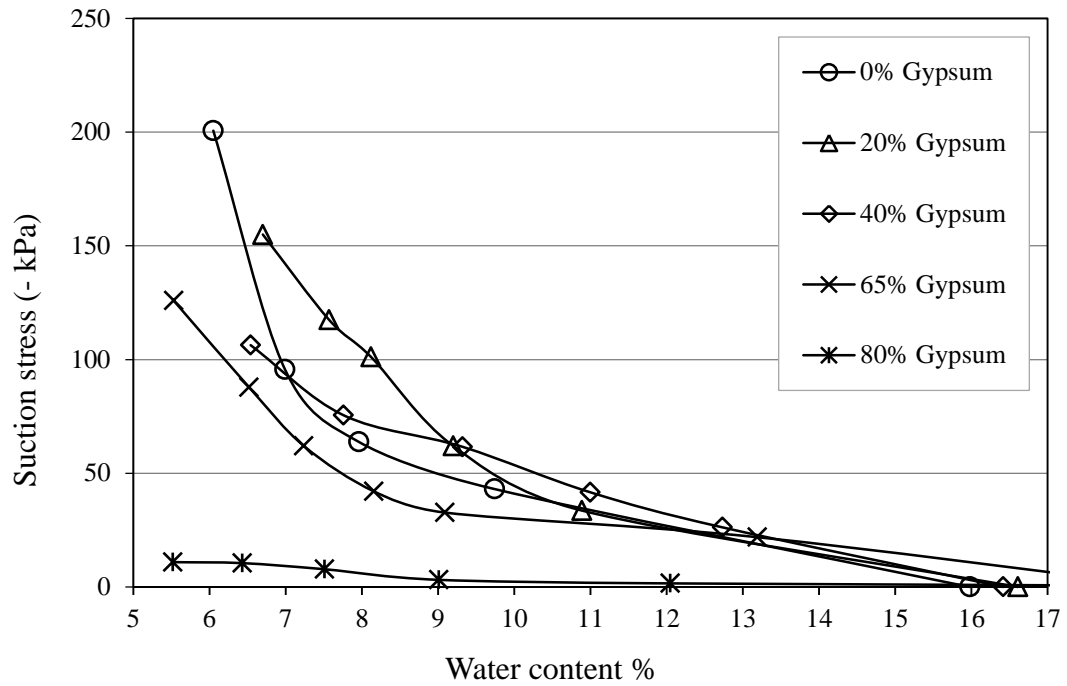
Figure 8. 15. SSCCs in terms of matric suction (According to the approach of Lu and Likos, 2006) for sand-gypsum mixtures having (A) 0%, and (B) 80% gypsum content by weight, at different levels of net normal stress.

The SSCCs in terms of matric suction show high consistency with those in terms of water content. This consistency indicates the validity and reliability of the adopted approach in measuring the unsaturated shear strength by controlling the water content, as well as, the accuracy and reliability in measuring the SD-SWCC by using the modified stress controllable pressure plate device. However, the describing of SSCC as a function to water content is more preferable in practical application, because the measuring of field water content is easier and faster than measuring soil suction.

To evaluate the effect of gypsum content on grain-size and pore-size distribution and then on the behaviour of suction stress function, the SSCCs for five sand-gypsum mixtures are presented in Figures 8.16 A and B under net normal stress level of 200 and 400 kPa. Figures 8.16 A and B reveal that gypsum content has significant effects on the behaviour of SSCC at different levels of net normal stress. The slope of the linear segments, the degree of curvature of the middle segment, and then the whole SSCC exhibit clear decrease with increasing gypsum content in the soil mixture.



(A) At 200 kPa net normal stress



(B) At 400 kPa net normal stress

Figure 8.16. SSCCs in terms of water content (According to the approach of Ning Lu, 2006) for different sand-gypsum mixtures at net normal stress level of (A) 200 kPa, and (B) 400 kPa.

8.3.8. Shear strength failure envelopes in terms of intergranular effective stress

Lu and Likos (2006) introduced the concept of "true effective stress" as discussed in Section 2.3.2. True effective stress is defined as the interparticular stress resulting from three components; bonding stress (apparent tensile stress) that provides cohesion in saturated soil, net normal stress, and suction stress. The combination of net normal stress and suction stress without joining bonding stress is herein referred to as "intergranular effective stress". To present shear strength failure envelopes of different soil mixtures in one graph for comparison, and since these mixtures have different values of bonding stress, the "intergranular effective stress" was used instead of "true effective stress" in this representation.

The excess in shear strength resulting from desaturation (τ_s) was considered together with the applied net normal stress to define the intergranular effective stress in the direct shear tests of different unsaturated specimens. This approach circumvents about the necessity to determine the matric suction in shear strength

tests of unsaturated specimens, since the most relevance variable is not the matric suction but the suction stress which could be defined here as $(-\tau_s / \tan \phi')$.

The shear strength failure envelopes in terms of intergranular effective stress, for saturated and unsaturated specimens, of five different sand-gypsum mixtures are presented in Figure 8.17. It can be noticed from Figure 8.17 that the representation of failure envelope for saturated or unsaturated soil in the intergranular effective stress-shear stress plane results a unique line, having an intercept equal to the saturated cohesion (c'), regardless the degree of saturation. Thus, the failure envelope of each sand-gypsum mixture is best fitted using the data of about 24 direct shear tests which were carried out at four different net normal stress levels on specimens having different water contents.

As shown in Figure 8.17, the coefficients of determination of failure envelope lines of different sand-gypsum mixtures are ranging between 0.9957 and 1.0000 which indicating very limited amount of scattering. That is of course can be referred to the precise method adopted in preparing the test specimens and the well controlling conditions during different tests.

The failure envelopes shown in Figure 8.17 are nearly parallel with an angle of internal friction of about 32° and cohesion intercepts increasing from 4.15 kPa for 0% gypsum mixture to 57.23 kPa for 65% gypsum mixture, and then decreasing to 46.06 kPa for further increasing in gypsum content up to 80%. The values of ϕ' and c' obtained from Figure 8.17 are similar to large degree to those obtained from saturated shear strength tests in Figure 8. 5, since the current representation includes both the saturated and unsaturated shear tests data. Thus, the suction stress characteristic curves together with the saturated shear strength parameters could be considered to be completely defined the shear strength for any particular field problem.

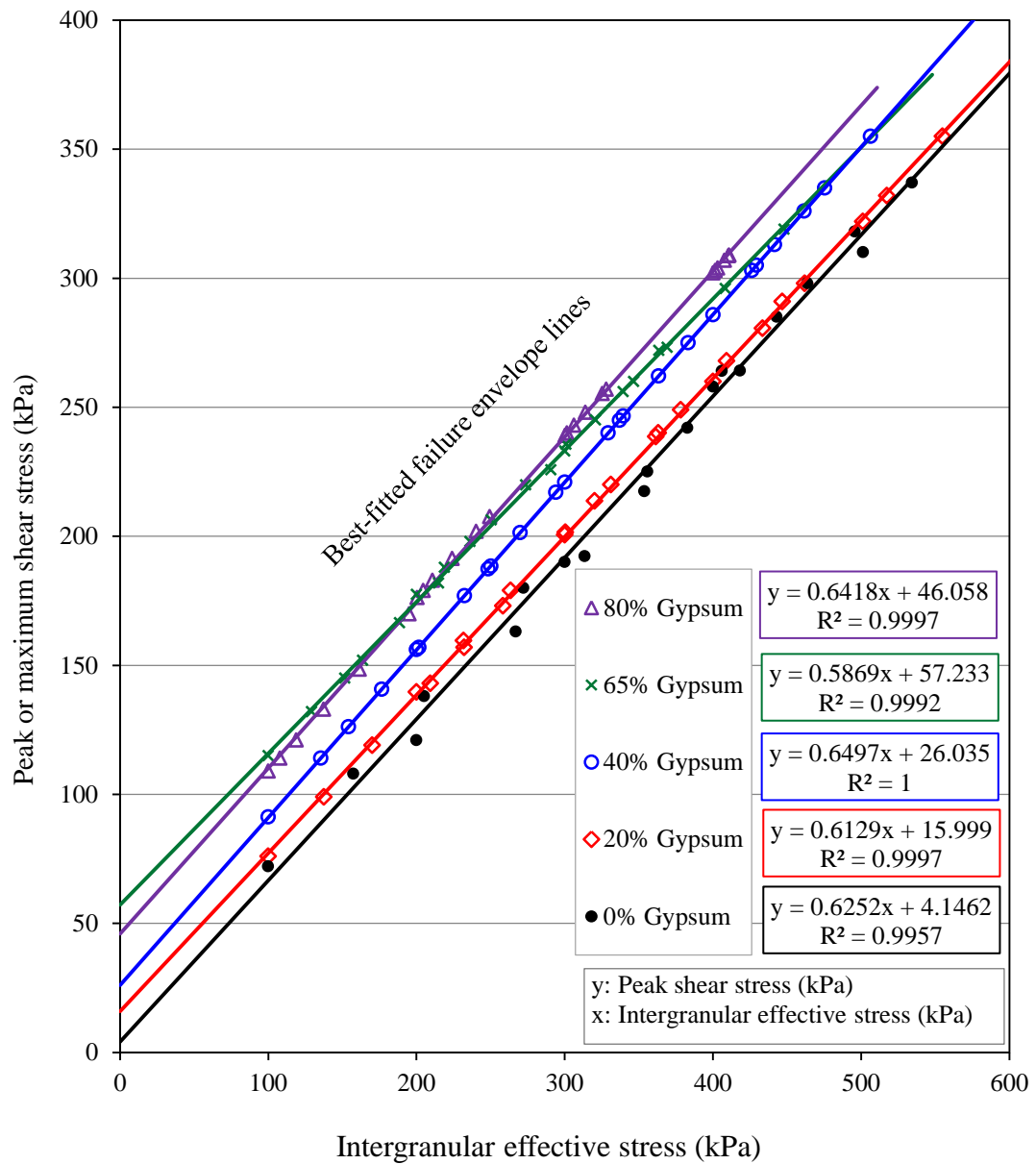


Figure 8.17. Shear strength failure envelopes in terms of intergranular effective stress for different sand-gypsum mixtures.

8.4. Concluding remarks

Results of direct shear tests carried out on saturated and unsaturated specimens of various sand-gypsum mixtures revealed that gypsum content, applied net normal stress, and desaturation have great influence on the shear strength and deformation characteristics of the soil mixtures tested.

There was an increase in the saturated shear strength parameters (c' and ϕ') with increasing gypsum content, reaching maximum values at 65% gypsum content. Slight decreases in c' and ϕ' were noticed for further increase in gypsum content.

There was a general tendency to the shear stress-shear displacement curves of the sand-gypsum mixtures to have peak behaviour with increasing gypsum content. At saturated conditions, under a normal stress of 400 kPa, sand-gypsum mixtures exhibited non-peak behaviour (ductile behaviour) for gypsum contents less than 30% and peak behaviour for gypsum contents greater than that. This limit (30%) decreased to 20% when the applied normal stress was decreased to 100 kPa.

The peak behaviour can be attributed to the increase of effective cohesion with increasing gypsum content. The cohesion component seems to be mobilized at small shear displacement (0.8 to 1.2 mm) while the friction component needs around 12 mm to be mobilized for the specimens tested. Thus, specimens of high gypsum content exhibited peak stress at shear displacement not exceeding 1.2 mm, and then showed clear decrease in shear stress with the progress of shear displacement (softening pattern). In contrast, specimens of low gypsum content (non peak behaviour) showed clear increase in stress pattern with increasing shear displacement, approaching the softening patterns at relatively large shear displacement of about 12 mm. Thus, the increase in shear strength with increasing gypsum content is more pronounced and significant when the peak shear stress is adopted as a failure criterion, while it is less pronounced when the steady shear strength is considered.

The suction stress function and then the contribution of matric suction to the shear strength revealed clear decrease with increasing gypsum content in the soil mixture. Thus, there is clear decrease in each of the friction angle in terms of matric suction (ϕ^b), the effective stress parameter (χ), and the degree of curvature of the shear strength-matric suction failure envelope with increasing gypsum content. As well as, the increasing of applied net normal stress caused decrease in the contribution of matric suction to shear strength by decreasing the suction stress function.

CHAPTER NINE

CONCLUSIONS AND RECOMMENDATIONS

The major objectives of this study were to evaluate experimentally the effect of gypsum content and the effect of stress state on the water flow and retention characteristics, volume change, shear strength and deformation characteristics of unsaturated sandy soils. A sandy soil from the district of Al-Fallujah / Al-Anbar province / Iraq was considered. An extensive laboratory testing programme was undertaken on synthetic sand-gypsum mixtures using compacted soil specimens. The specimens were statically compacted at the optimum water content to 90% of the maximum dry density obtained from the standard Proctor test.

The testing programme comprised of three main parts. The first part included the classification tests and some conventional, standard tests. The effect of gypsum content on the overall particle density, grain-size distribution, consistency limits, compaction behaviour, consolidation characteristics, soil-water characteristic curve, and the shrinkage characteristics of the soil mixtures were investigated in the first part. The second part focused on the detailed investigation of the drying and the wetting stress-dependent soil-water characteristic curves (SD-SWCCs) and the stress dependent-unsaturated hydraulic conductivity functions (SD-HCFs) for different sand-gypsum mixtures. A new stress controllable pressure plate device with test procedures were developed to carry out these two key hydraulic functions. The shear strength and deformation characteristics of saturated and unsaturated soil mixtures were carried out in the third part of the testing programme.

The conclusions corresponding to each of the three testing parts are presented in the following sections. These conclusions are directly related to the results provided

in the previous chapters. Finally, the recommendations for future works are presented in the last section.

9.1. Conclusions from conventional, standard tests

The major conclusions obtained from the classification, compaction, consolidation, soil-water characteristic curve, and the shrinkage characteristics tests are as follows:

- (1) An alternative method was suggested in this study for determining gypsum particles density by using saturated water with gypsum salt instead of using white spirit (BS 1377-2, 1990). When the water is pre-saturated with gypsum salt, it will be unable to dissolve gypsum any more during the particle density test. The results obtained were very close to that obtained from the standard method with differences not exceeding 0.005 Mg/m^3 .
- (2) There was a slight increase in the maximum dry density of the soil mixture associated with a slight decrease in the optimum water content when gypsum content is increased up to 15% by weight. Further increase in gypsum content caused noticeable decrease in the maximum dry density associated with a clear increase in the optimum water content. This conclusion agrees to that reported by Kattab (1986) and Al-Dilaimy (1989).
- (3) A better evaluation of compaction characteristics of gypsiferous soils can be achieved by adopting the minimum void ratio rather than the maximum dry density. This evaluation circumvents over the variations in the overall specific gravity of different sand-gypsum mixtures, since the main purpose from compaction is to pack more closely the soil particles and then reduces air voids. By adopting the minimum void ratio, the defined percentage of gypsum that results maximum improvement in compaction characteristics was 30% instead of 15% for the sandy soil tested.
- (4) A mild decrease in each of the consistency limits (liquid limit, plastic limit, and shrinkage limit) of the sand-gypsum mixtures was observed with increasing gypsum content up to 30% by weight, then the consistency limits exhibited clear increase with increasing gypsum content. This trend is consistent with the effect of gypsum content on the void ratio of the compacted specimens.

(5) The one-dimensional compression index (C_c) of sand-gypsum mixtures increased noticeably with increasing gypsum content. Also there was a remarkable increase in (C_c) with increasing the level of applied effective stress. Greater volumetric changes with desaturation were also noticed from the CLOD tests with increasing gypsum content. This behaviour can be attributed to the soft nature of gypsum particles, and the increase in void ratio of the soil specimen with increasing gypsum content.

(6) A combined procedure was suggested in this study to find simultaneously the gravimetric/ volumetric water content - matric suction - void ratio relationships using the commercial pressure plate extractor. Two of ASTM Standard procedures were incorporated, the SWCC determination using separate specimens (ASTM D 6836-02), and the specimen volume determination using the wax method (ASTM D 4943-08).

(7) The slope of the SWCC in the transition zone showed clear increase with increasing gypsum content in the soil mixture. This trend can be directly related to the uniformity coefficient decrease of the soil mixture with increasing gypsum content. The water holding capacity of the soil mixtures revealed noticeable increase with increasing gypsum content. Thus, gypsum is considered as an improvement material to the hydraulic characteristics of sandy soils for agricultural purposes.

(8) Results of the shrinkage characteristic curves (SCCs) obtained from the CLOD tests revealed high consistency with the analogous curves obtained from the SWCC tests. Both results showed that the slope of the linear portion of the SCC decreases with increasing gypsum content in the soil mixture. Likewise, the curvature of the SCC becomes flatter and the value of the minimum void ratio at the dry condition becomes greater with increasing gypsum content. The shrinkage limit values of various soil mixtures determined from CLOD tests were found smaller than those determined from the standard shrinkage limit tests (ASTM D 4943-08), and that is may be attributed to the differences of the initial conditions and the preparation of specimens tested in these two different approaches.

(9) There was a remarkable increase in water content-total suction function of the soil mixture with increasing gypsum content as long as water content is greater than the residual value, whereas these functions exhibited converging to each other at total suction value of about 1 MPa. This behaviour can be attributed primarily to the effect of gypsum content on increasing the osmotic suction component near saturation and the eliminating of osmotic component at higher level of suction. Sand-gypsum mixtures exhibited clear increase in residual total suction associated with clear decrease in the corresponding residual water content with increasing gypsum content.

9.2. Conclusions from developed-stress dependent-hydraulic tests

The major conclusions obtained from the developed SD-SWCCs and SD-HCFs tests are presented below.

(1) A newly modified stress controllable pressure plate device has been introduced in this study. The modified device was applied to measure conveniently and efficiently both the SD-SWCCs simultaneously with the SD-HCFs during both the drying and the wetting processes under K_0 condition. The device has the flexibility to be used also to measure the matric suction for a given soil specimen by applying the null type technique. Several improvements have been made in the design of this device. Among these are:

(i) The volume of diffused air is evaluated and removed simply, quickly, and efficiently. This feature is attributed to the use of spiral groove below the ceramic disc, and to the manner adopted in monitoring the water content variations in the soil specimen.

(ii) The desired vertical stress is applied pneumatically inside the cell without the need to a loading frame machine, and this reduces greatly both the cost and the laboratory space required.

(iii) Continuous determination of specimen water content during the test is accurately done without dismantling the device by weighing the overall cell and monitoring the differences in consequent weights. Therefore, there is no need to an external measuring system, and there is no evaporation problem during long term tests.

(iv) Single soil specimen is used to obtain the SD-SWCCs simultaneously with the SD-HCFs with any number of data points during both the drying and the wetting processes.

(v) Soil specimen covers the whole surface area of the ceramic disc, i.e., there is no exposed area of ceramic disc in direct contact to the pressurized air of the cell, which may have some effect on water phase continuity.

(vi) Soil specimen occupies the whole inside volume of the cell, thus there is no need to additional attachments such as a vapour saturator to prevent the drying of the specimen by evaporation.

(vii) The high accuracy with which water removal and uptake from or into the specimen can be measured made the device suitable to measure the drying and the wetting SD-HCFs with high reliability and accuracy.

(2) Results of the SD-SWCCs revealed that gypsum content greatly affects the drying and the wetting SWCC parameters. At any level of net normal stress, the increase of gypsum content in the soil mixture causes noticeable increase in the saturated water content, air-entry water content, air-entry suction, residual suction, desorption rate, absorption rate, air-expulsion water content, air-expulsion suction, and the water-entry suction. Conversely, the residual water content and the water-entry water content revealed slight decrease with increasing gypsum content. This behaviour can be directly related to the effect of gypsum content on the grain-size distribution and then on the pore-size distribution of the soil mixture.

(3) Clear hysteresis was noticed between the drying and the wetting SD-SWCCs of the sand-gypsum mixtures with an amount increases with increasing gypsum content. A quantitative evaluation to hysteresis phenomenon between the drying and the wetting SD-SWCCs has been proposed in this study. The values of air-entry suction and residual suction were compared to those of air-expulsion suction and water-entry suction respectively to find the horizontal shift between the drying and the wetting curves. Similarly, the water content parameters of the drying and the wetting curves were compared to find the vertical shift.

(4) At any levels of net normal stress and matric suction, the elapsed time required to reach equalization noticeably increased with increasing gypsum content in the soil mixture. On the other hand, the elapsed time required to reach equalization during the wetting process was much greater than that during the drying process. As the applied net normal stress increased, the time required to reach equalization decreased markedly.

(5) Obvious dependency of SWCC on the applied net normal stress level was noticed. This dependency was more pronounced within the boundary effect zone, extended to some degree through the transition zone, and eliminated at the residual zone. This dependency is pronounced when water retention is governed by capillary mechanism that depends mainly on particle and pore structure and pore-size distribution. Soil specimens subjected to a higher net normal stress exhibited lower initial gravimetric water content, clear decrease in the air-entry water content, slight increase in the air-entry suction, clear decrease in the water holding capacity, and reduction in desorption rate. Similar stress dependency to the wetting path with increasing the applied net normal stress was noticed.

(6) The reliability and accuracy of the newly modified stress controllable pressure plate device have been demonstrated through (i) the consistency of the SD-SWCCs test results of different sand-gypsum mixtures at various levels of net normal stress, (ii) the possibility of getting relatively identical results for identical specimens, and (iii) the applicability of many mathematical models to best-fit the experimental test results.

(7) The test results of SD-HCFs showed that the multistep and the one step transient outflow methods are inapplicable at matric suction values below the air-entry value because there is no flow of water. At residual zone, the flow of water is very little making the outflow methods inapplicable as well. Thus, the applicability of these methods is limited to the transition zone only. The SD-HCFs calculated by following Gardner (1956)'s multistep outflow method were always lower than the corresponding functions calculated according to Doering (1965)'s one step outflow method by one to one and a half order, for both the drying and the wetting paths of all sand-gypsum mixtures. This is due to the differences in assumptions, initial and boundary conditions which had been considered in these analytical solutions.

(8) There was clear increase in the drying/wetting $k(\psi)$ of the soil mixture with increasing gypsum content. This can be attributed to the increases in void ratio and water content of the specimen with increasing gypsum content. Smaller effect to the gypsum content was noticed on $k(w)$. There were clear hysteresis effects on $k(\psi)$ of the soil mixtures, with wetting function always lower than the corresponding drying one. Only minor hysteresis was noticed on $k(w)$, and that is because the water content hysteresis was eliminated in this representation.

(9) The influence of the net normal stress on HCFs of the compacted specimens tested was relatively small due to the initial conditions of the prepared specimens. The influence of net normal stress was more pronounced with soil mixtures of high gypsum contents, due to the increase in the compression index with increasing gypsum content. It was noticed that the increase of net normal stress to some extent causes the HCFs to have some increase due to the anticipated increase in the water phase continuity (squeezing action). Further increase in net normal stress causes decrease in HCFs due to substantial decrease in pore spaces and then in the water flow paths.

9.3. Conclusions from shear strength tests

The main conclusions regarding the effects of gypsum content, desaturation, and net normal stress level on the saturated and unsaturated shear strength parameters and deformation characteristics of the soil mixtures are shown below.

(1) Saturated soil specimens of low gypsum content exhibited ductile behaviour (non-peak stress-strain patterns), while those of high gypsum contents exhibited stiff behaviour with peak shear stress achieved at low shear strain, mostly below 1%. Gypsum content at which shearing behaviour is changed from ductile to stiff was around 30% for the sandy soil tested. At this percentage, maximum compaction improvement with minimum void ratio for the sandy soil was achieved.

(2) Shear displacement corresponding to maximum (Peak) shear stress showed clear decrease with increasing gypsum content in the soil mixture, whereas this displacement showed an increase with increasing the applied normal stress level. Accordingly, the initial shear stiffness of the soil mixture revealed clear increase with

increasing gypsum content and/or decreasing the applied normal stress level. Most of sand-gypsum mixtures, that compacted to 90% of the standard compaction, exhibited dilation behaviour with an amount increases with increasing gypsum content and decreases with increasing the applied net normal stress level.

(3) Saturated soil specimens exhibited clear increase in cohesion component and slight increase in friction component with increasing gypsum content up to 65% by weight. Further increase in gypsum content caused slight decrease in both shear components. The increase in shear strength was more pronounced at relatively small shear displacements when the peak shear stress is adopted. At relatively large shear displacements, specimens of different gypsum contents exhibited a tendency to come to nearly the same steady or critical shear stress value.

(4) The contribution of desaturation to the shear strength of the soil mixture exhibited clear decrease with increasing gypsum content, and moderate decrease with increasing the applied net normal stress level. Thus, the shear strength-water content function of the soil mixture becomes flatter showing low degree of curvature with increasing gypsum content. This function becomes more flat with increasing the net normal stress level as well.

(5) The shear stress-matric suction failure envelopes of the soil mixtures showed clear nonlinearity with a degree of curvature decreases with increasing gypsum content and/or increasing the level of net normal stress. The parameters ϕ^b and χ showed noticeable decrease at capillary stage with increasing gypsum content, while at residual stage these parameters exhibited an increase with increasing gypsum content, reaching maximum values at around 50% gypsum content and then clear decrease was noticed for further increase in gypsum content. The suction stress characteristic curve (SSCC) exhibited clear decrease with increasing gypsum content in the soil mixture and/or increasing the level of the applied net normal stress.

(6) Consistent shear stress-matric suction failure envelopes were found for various sand-gypsum mixtures by adopting the matric suction values estimated from SD-SWCC tests. This consistency confirms the reliability and the viability of the proposed approach of testing and analysing the shear strength parameters of unsaturated compacted specimens. The proposed procedure utilizes standard

laboratory direct shear equipment and takes a relatively short time to be completed. Thus, it offers an easy and convenient alternative way for the determination of the unsaturated shear strength parameters.

(7) The apparent cohesion of different sand-gypsum mixtures exhibited clear increase with decreasing water content, whereas the corresponding apparent friction angle showed some decrease with decreasing water content. This behaviour makes the effect of desaturation in increasing the shear strength is more pronounced at low levels of net normal stress.

(8) As with the saturated cohesion, the apparent cohesion-water content function revealed clear increase with increasing gypsum content in the soil mixture, reaching a highest level at 65% gypsum content. This behaviour can be attributed to that the cementation bonds between gypsum-gypsum particles are greater than the cementation bonds between gypsum-sand particles and these in turn are greater than the bonds between sand-sand particles.

(9) For any sand-gypsum mixture, representation of failure envelope in terms of intergranular effective stress results a unique line regardless the degree of saturation of soil specimens, i.e., both saturated and unsaturated specimens can be represented together. This representation makes the suction stress characteristic curves together with the saturated shear strength parameters can be considered to be completely defines the shear strength for any particular field problem.

(10) Good agreement was observed between the measured matric suction-shear stress envelopes and the predicted envelopes using Rassam and Cook (2002)'s semi-empirical predictive model for the sandy soil without gypsum or that of low gypsum content. With increasing gypsum content in the soil mixture, clear deviations between the measured and the corresponding predicted envelopes were observed making Rassam and Cook (2002)'s model inappropriate in shear strength prediction of highly gypsiferous soils.

9.4. Recommendations for future works

This study provided significant information regarding the impact of gypsum content and stress state on the classification parameters, volume changes, water flow

and retention characteristics, shear strength and deformation characteristics of unsaturated sandy soils. Furthermore, this study highlighted the need for additional works and future researches. Some of the recommendations of this study are:

(1) It is recommended to use the newly modified stress controllable pressure plate device with the developed procedures in measuring the main hydraulic functions of unsaturated soils. The precision, reliability, and simplicity of the device were demonstrated through an extensive laboratory programme. However, some optional attachments can be used with the device to extend its features and usage. Among these attachments are:

- (i) A small tensiometer can be inserted at the upper half of the soil specimen to measure the pore water pressure and then the unsaturated hydraulic conductivity can be calculated directly by applying Darcy's law, as described by the multistep direct method (Eching et al., 1994).
- (ii) A simple vertical shaft can be inserted through the top cap. Then, the vertical volume change of the specimens can be measured using an attached vertical deformation dial gauge.
- (iii) Hanging column accessory which enables the application of low suctions to soil specimens.
- (iv) Use of interchangeable high air-entry ceramic discs, mounted on stainless steel rings, and installed in the recess of the base plate by means of double "O" rings. Thus, ceramic discs of different air-entry values can be used depending on the soil type being tested, and this greatly reduces the time needed for equalization. This option also facilitates the cleaning of the spiral groove of the base plate from any anticipated depositions.

(2) Direct shear testing of unsaturated soils under controlling water content is desirable since less time is required for test as compared to tests under matric suction controlling where the time needed for equalization is relatively too long. However, further tests should be performed on different soil types to assess the general applicability of the proposed procedure.

(3) The influence of matric suction on the stress-deformation characteristics of the gypsiferous soils is recommended to be investigated. While the increase of net

normal stress causes sand-gypsum specimens exhibit more ductility, pilot shearing tests under controlling water content conditions revealed that the increase of matric suction reduces the specimen ductility and causes the specimen to exhibit more stiff behaviour.

(4) The contribution of matric suction to the soil shear strength of sand-gypsum mixtures was well pronounced when the peak shear stress was adopted as a failure criterion. It is recommended to examine the contribution of matric suction to the steady shear strength of sand-gypsum mixtures. Some pilot tests carried out in this study showed that the contribution of matric suction to the shear strength was mobilized at small shear displacements and gradually reduced with the progress of shear displacement.

REFERENCES

- Aitchison, G.D., 1961. Relationship of moisture and effective stress function in unsaturated soils, Conf. of Pore pressure and suction in soils, organized by British Nat. Soc. of Int. Soc. Soil Mech. Found. Eng., Inst. Of Civil Eng., London: Butterworths, pp. 47-52.
- Al-Aithawi, A.H., 1990. Time-dependent deformation of a gypseous silty soil, M.Sc. thesis, Civil Engineering Department, University of Baghdad, Iraq.
- Al-Dilaimy, F.K., 1989. The effect of gypsum content on the strength and deformation of remolded clay, M.Sc. thesis, Civil Engineering Department, University of Salah Al-Deen, Iraq, (in Arabic).
- Al-Heeti, A.A.H., 1990. The engineering properties of compacted gypsified soil, M.Sc. thesis, Civil Engineering Department, University of Baghdad, Iraq.
- Al-Janabi, A. S., 1990. Using of ammonium phosphate and carbonate as gypsiferous soil conditioners and their effect on growth and productivity of corn, Ph.D. thesis, College of Agriculture, University of Baghdad, Baghdad, Iraq. (In Arabic).
- Al-Kaissy, A. A., and Naji, T., 1985. Influence of barium chloride addition on plant growth and some properties of gypsiferous soil, Agri. Water Resources Res., Vol. 4, No. 3, pp. 107-119.
- Al-Mufti, A.A., 1997. Effect of gypsum dissolution on the mechanical behavior of gypseous soils, Ph.D. thesis, Civil Engineering Department, University of Baghdad, Iraq.
- Al-Nouri, I., and Saleam, S., 1994. Compressibility characteristics of gypseous sandy soils, Geotechnical Testing Journal, Vol. 17, Issue 4.
- Alonso, E.E., Gens, A., Hight, D.W., 1987. Special problem soils, general report, Proc. 9th ECSMFE Vol. 3. Balkema, Dublin, pp. 1087–1146.
- Al-Qaissy, F.F., 1989. Effect of gypsum content and its migration on compressibility and shear strength of the soil, M.Sc. thesis, Building and Construction Department, University of Technology, Baghdad, Iraq.
- Al-Saoudi, N.K.S., AL-Nouri, I.M.A., and Sheikha, A.A.H, 2001. The collapsible behaviour of gypseous soils, the 7th Jordanian Geological Conference, Jordanian Geologists Association, Amman, Jordan.
- American Society for Testing and Materials (ASTM), 1990. Standard test method for direct shear tests of soils under consolidated drained conditions. Designation ASTM D 3080-90.
- American Society for Testing and Materials (ASTM), 2002. Standard test methods for determination of the soil-water characteristic curve for desorption using a hanging column, pressure extractor, chilled mirror hygrometer, and/or centrifuge. Designation ASTM D 6836-02.
- American Society for Testing and Materials (ASTM), 2003. Standard test method for measurement of collapse potential of soils. Designation ASTM D 5333.

- American Society for Testing and Materials (ASTM), 2006. Standard practice for classification of soils for engineering purposes (Unified Soil Classification System).
- American Society for Testing and Materials (ASTM), 2008. Standard test methods for shrinkage factors of soils by the wax method. Designation ASTM D 4943-08.
- Azam, S., Abduljawad, S. N., Al-Shayea, N. A., and Al-Amoudi, O. S. B., 1998. Expansive characteristics of gypsiferous/ anhydritic soil formation, *Engineering Geology*, Vol. 51, pp. 89-107.
- Azzouz, A. S., Krizek, R. J., and Corotis, R. B., 1976. Regression analysis of soil compressibility, *Soils and Foundations*, Vol. 16, No. 2, pp. 19–29.
- Barazanji, A.F., 1973. Gypsiferous soils of Iraq, Ph.D. thesis, University of Ghent, Belgium.
- Barzanji, K.K.H., 1984. Infiltration rate characteristics of gypsiferous soils in northern Iraq (Jazirah-Area), M.Sc. thesis, Irrigation and Drainage Engineering Department, University of Mosul, Iraq.
- Bear, J., 1972. Dynamics of fluids in porous media, American Elsevier Publishing Company, Inc., New York.
- Bensallam, S., Bahi, L., Ejjaouani, H., Shakhirev, V., 2012. A new shrinkage curve model, applied to Moroccan clayey soil, *International Journal of Geosciences*, Vol. 3, pp. 507-514, doi:10.4236/ijg.2012.33053.
- Benson, C. H., and Gribb, M., 1997. Measuring unsaturated hydraulic conductivity in the laboratory and field. ASCE, Special Technical Publication No. 68, Reston, VA, pp. 113-168.
- Bishop, A. W. (1955, 1959). The principle of effective stress, Lecture delivered in Oslo, Norway, printed in *Teknisk Ukeblad*, Vol. 106, No. 39, pp. 859-863.
- Bishop, A. W., 1960. The measurement of pore pressure in triaxial test, proceedings, conference on pore pressure and suction in soils, London: Butterworths, pp. 38-46.
- Bishop, A. W., and Blight, G. E., 1963. Some aspects of effective stress in saturated and unsaturated soils, *Geotechnique*, Vol. 13, No. 3, pp. 177-197.
- Bittelli, M., Flury, M., 2009. Errors in water retention curves determined with pressure plates, *Soil Physics, Soil Science Society of America Journal*, Vol. 73, No. 5.
- Blight, G. E., 1965. A study of effective stresses for volume change, Symposium in moisture equilibria and moisture changes in the soils beneath covered areas, pp. 259-269, Australia: Butterworths.
- Blight, G.E., 1976. Migration of subgrade salts damages thin pavements. Proceeding of the American Society of Civil Engineers, ASCE, *Transportation Engineering Journal*, 102(TE4), pp. 779–791.
- Blyth, F.G.H., 1971. *A Geology for Engineers*, Fifth Edition, Edward Arnold Ltd., London.

- Bock, K. A., and Fredlund, D. G., 1980. Limitation of the axis translation technique, proceedings of the 4th International Conference on Expansive Soils, Denver, CO, pp. 117-135.
- Bolt, G. H., 1956. Physicochemical analysis of the compressibility of pure clays. *Geotechnique*, Vol. 6, pp. 86–93.
- Bolton, M. D., 1986. The strength and dilatancy of sands, *Geotechnique*, Vol. 36, No. 1, pp. 65-78.
- Bonder, B. H., and Miguel, M. G., 2011. Hysteresis phenomenon of a tropical soil profile observed by means of soil-water characteristic curves obtained in laboratory and field, Pan-Am CGS Geotechnical Conference.
- Borcher, C., Skopp, J., and Schepers, J., 1987. Unsaturated hydraulic conductivity determination by one-step outflow for fine-textured soils, *Trans. Amer. Assoc. of Agr. Engr.*, Vol. 30, No. 4, pp. 1038-1042.
- Brasher, B. R., Franzmier, D. P., Valassis, V., and Davidson, S. E., 1966. Use of Saran resin to coat natural soil clods for bulk density and water-retention measurements. *Soil Science*, 101(2): 108.
- Bridgwater, J., 1980. On the Width of Failure Zones, *Geotechnique*, Vol. 30, No. 4, pp. 533–536.
- Brooks, R. H., and Corey, A. T., 1964. Hydraulic properties of porous media, *Colorado State University Hydrology Paper*, Vol. 3, pp. 27.
- Brune, G., 1965. Anhydrite and gypsum problems in engineering geology, *Engineering Geology*, Vol. 2, No. 1, pp. 26–38.
- BS 1377-2, 1990. Soils for civil engineering purposes, Part 2: Classification tests, British Standards Institution.
- Buckingham, E., 1907. Studies of the movement of soil moisture, U.S.D.A. Bureau of soils, No. 38.
- Burland, J. B., 1965. Some aspects of the mechanical behaviour of partly saturated soils, Symposium in moisture equilibria and moisture changes in the soils beneath covered areas, pp. 270-278, Australia: Butterworths.
- Casini, F., Minder, P., Springman, S. M., 2001. Shear strength of unsaturated silty sand, Taylor & Francis Group, London, ISBN 978-0-415-60428-4.
- Chen, L., Miller and Kibbey, T. C. G., 2007. Rapid pseudo-static measurements of hysteretic capillary pressure-saturation relationship in unconsolidated porous media, *Geotechnical Testing Journal*, Vol. 30, No. 6.
- Clayton, C.R.I., Priest, J.A, and Rees, E.V.L, 2010. The effects of hydrate cement on the stiffness of some sands, *Geotechnique*, Vol. 60, No. 6, pp. 435–445, doi: 10.1680/geot.2010.60.6.435
- Clayton, C.R.I., 2011. Stiffness at small strain: research and practice. *Geotechnique*, Vol. 61, No.1, pp. 5-37, doi:10.1680/geot.2011.61.1.5.
- Clayton, C.R.I., Steinhagin, H.M., Powrie, W., 1995. Terzaghi's theory of consolidation and the discovery of effective stress. (Compiled from the work of

- K. Terzaghi and A.W. Skempton). Proceedings of the ICE - Geotechnical Engineering, Vol. 113, No. 4, pp. 191-205, doi:10.1680/igeng.1995.28015.
- Coleman, J. D., 1962. Stress/strain relations for partly saturated soils, *Geotechnique*, Vol. 12, No. 4, pp. 348-350.
- Collis-George, N., and Rosenthal, M., 1966. Proposed outflow method for the determination of the hydraulic conductivity of unsaturated porous materials, *Aust. J. Soil Res.*, Vol. 4, No. 1, pp. 165-180.
- Corey, A.T., and Kemper, W.D., 1961. Concept of total potential in water and its limitations, *Soil Sci.*, Vol. 91, No. 5, pp. 299-305.
- Corey, A.T., and Klute, A., 1985. Application of the potential concept to soil water equilibrium and transport, *Soil Science Society of America Journal*, Vol. 49, pp. 3-11.
- Croney, D., Coleman, J. D., and Lewis, W. A., 1950. Calculation of the moisture distribution beneath structures, *Cov. Eng. L.*, Vol. 45, pp. 524.
- Croney, D., Coleman, J.D., and Black, W.P.M., 1958. Movement and distribution of water in soil in relation to the highway design and performance, *Highway Res. Board*, Washington, DC, No. 40, pp. 226-252.
- Cui, Y. J., and Delage, P., 1996. Yielding and plastic behavior of unsaturated compacted silt, *Geotechnique*, Vol. 46, pp. 291-311.
- Cui, Y., Ta, A. N., Tang, A. M., and Lu, Y., 2010. Investigation of the hydro-mechanical behaviour of compacted expansive clay, *Frontiers of Architecture and Civil Engineering in China*, Vol. 4, No. 2, pp. 154-164, doi: 10.1007/S11709-010-0019-0.
- Dirksen, C., 1991. Unsaturated hydraulic conductivity, *Soil Analysis, Physical methods*, K. Smith and C. Mullins, eds., Marcel Dekker, New York, 209-269.
- Doering, E., 1965. Soil-water diffusivity by the one-step method, *Soil Sci.*, Vol. 99, No. 5, pp. 322-326.
- Drumright, E. E., 1989. The contribution of matric suction to the shear strength of unsaturated soils, PhD thesis, Colorado State University, Colorado.
- Ebrahimi-Birang, N., Fredlund, D. G., and Samarasekera, L., 2007. Hysteresis of the soil-water characteristic curve in the high suction range, *Ottawa Geo*.
- Eching, S., Hopmans, J., and Wendroth, O., 1994. Unsaturated hydraulic conductivity from transient multi-step outflow and soil water pressure data, *Soil Science Society of America Journal*, Vol. 58, pp. 687-695.
- Escario, V., 1980. Suction controlled penetration and shear tests, *Proceedings of the Fourth International Conference on Expansive*, ASCE, Vol. 2, pp. 781-797.
- Escario, V., and Saez, J., 1986. The shear strength of partly saturated soils, *Geotechnique*, Vol. 36, pp. 453 – 456.
- Escario, V., Juca, J., and Coppe, M. S., 1989. Strength and deformation of partly saturated soils, *Proceedings of the 12th international conference on soil mechanics and foundation engineering*, Rio de Janeiro, Vol. 3, pp. 43-46.

- Escario, V., Juca, J., and Coppe, M. S., 1989. Strength and deformation of partly saturated soils, *Proceedings of the 12th international conference on soil mechanics and foundation engineering*, Rio de Janeiro, Vol. 3, pp. 43–46.
- FAO, 1990. *Management of gypsiferous soils*, Food and Agricultural Organization of the United Nations, Rome.
- Fattah, M., Y., Al-Shakarchi, Y., J., and Al-Numani, H., N., 2008. Long-term deformation of some gypseous soils, *Eng. & Tech.* Vol. 26, No. 12.
- Feuerharmel, C., Pereira, A., Gehling, W. Y. Y., and Bica, A. V. D., 2006. Determination of the shear strength parameters of two unsaturated colluvium soils using the direct shear test, *ASCE Conference Proceedings, Unsaturated Soils*, pp. 1181-1190, doi: 10.1061/40802(189)96.
- Fookes, P.C., 1976. Road geotechnics in hot deserts, *Journal of the Institution of Highway Engineers*, Vol. 23, No. 10, pp. 11–23.
- Fookes, P.C., 1978. Middle East-inherent ground problems, *Quarterly Journal of Engineering Geology*, Vol. 11, No. 1, pp. 33–49.
- Fookes, P.C., and French, W.J., 1977. Soluble salt damage to surfaced roads in the Middle East, *Journal of the Institution of Highway Engineers*, Vol. 24, No. 11, pp. 10–20.
- Fourie, A., and Papageorgiou, G., 1995. A technique for the rapid determination of the moisture retention relationship and hydraulic conductivity of unsaturated soils, *Proc. Of the first Int. Conf. on Unsaturated Soils*, Balkema, Rotterdam, pp. 485-490.
- Fredlund, D. G., 1989. Soil suction monitoring for roads and airfields. *Symposium on the State-of the-Art of Pavement Response Monitoring Systems for Roads and Airfields*, Sponsored by the U.S. Army Corps of Engineers (Hanover, NH), March 6–9.
- Fredlund, D. G., and Morgenstern, N.R., 1977. Stress state variables for unsaturated soils, *ASCE J. Geotech. Eng. Div. GT5*, Vol. 103, pp. 447-466.
- Fredlund, D. G., Morgenstern, N. R., and Wider, R. A., 1978. Shear strength of unsaturated soils, *Canadian Geotechnical Journal*, Vol. 15, No. 3, pp. 313-321.
- Fredlund, D. G., and Rahardjo, H., 1993. *Soil mechanics for unsaturated soils*, John-Wiley & Sons Inc, New York.
- Fredlund, D. G., Rahardjo, H., and Gan, J. K-M., 1987. Nonlinearity of strength envelope for unsaturated soils, *Proceedings 6th international conference on expansive soils*, New Delhi, pp. 49-54.
- Fredlund, D. G., Sheng, D., and Zhao, J., 2011. Estimation of soil suction from the soil-water characteristic curve, *Canadian Geotechnical Journal*, Vol. 48, pp. 186–198, doi: 10.1139/T10-060.
- Fredlund, D. G., Xing, A., Fredlund, M. D., and Barbour, S. L., 1996. The relationship of the unsaturated soil shear strength to the soil–water characteristic curve, *Canadian Geotechnical Journal*, Vol. 33, pp. 440–448.

- Fredlund, D. G., Xing, A., and Huang, S., 1994. Predicting the permeability for unsaturated soils using the soil-water characteristic curve, *Canadian Geotechnical Journal*, Vol. 31, pp. 533-546.
- Fredlund, D.G., and Xing, A., 1994. Equations for the soil-water characteristic curve, *Canadian Geotechnical Journal*, Vol. 31, No. 4, pp. 521-532, doi:10.1139/t94-061.
- Fredlund, M. D., Wilson, G. W., and Fredlund, D. G., 2002. Representation and estimation of the shrinkage curve, *Third International Conference on Unsaturated Soils*, Recife, Brazil, pp. 145-149.
- Gan, J. K., Fredlund, D. G., and Rahardjo, H., 1988. Determination of the shear strength parameters of an unsaturated soil using the direct shear test, *Canadian Geotechnical Journal*, Vol. 25, No. 3, pp. 500-510.
- Gardner, W., 1956. Calculation of capillary conductivity from pressure plate outflow data, *Soil Sci. Amer. Proc.*, Vol. 20, pp. 317-320.
- Gardner, W., 1962. Note on the separation and solution of diffusion equations, *Soil Sci. Amer. Proc.*, 26:404.
- Gardner, W., and Widtsoe, J. A., 1921. The movement of soil moisture, *Soil Science*, Vol. 11, pp. 215-232.
- GCTS Testing Systems. Commercial Publication, Tempe, AZ, USA.
- Gee, G., Campbell, M., Campbell, G., and Campbell, J., 1992. Rapid measurement of low soil potentials using a water activity meter, *Soil Science Society of America Journal*, Vol. 56, pp. 1068-1070.
- Gens, A., Alonso, E. E., and Lloret, A., 1995. Effect of structure on the volumetric behaviour of a compacted soil. *Proceedings of the 1st International Conference on Unsaturated Soils*, E. E. Alonso and P. Delage, Eds., Paris, September 6-8, Balkema, Rotterdam, The Netherlands, Vol. 1, pp. 83-88.
- Graecen, E. L., 1960. Water content and soil strength, *Jornal of Soil Science*, Vol. 11, No. 2, pp. 313-333.
- Green, T.W., Paydar, Z., Cresswell, H.P., and Drinkwater, R.j., 1998. Laboratory outflow technique for measurement of soil water diffusivity and hydraulic conductivity, CSIRO, Australia, Technical report No. 12/98.
- Gribb, M., 1996. Parameter estimation for determining hydraulic properties of a fine sand from transient flow measurements, *Water Res. Res.*, Vol. 32, No. 7, 1965-1974.
- Guan, Y., and Fredlund, D. G., 1997. Use of Tensile Strength of Water for the Direct Measurement of High Soil Suction, *Canadian Geotechnical Journal*, Vol. 34, No. 4, pp. 604-614.
- Guan, Y., 1996. The measurement of soil suction, a PhD thesis, Dept. of Civil Engineering, University of Saskatchewan, Saskatoon, Canada.
- Gupta, S.C., Farrell, D.A., and Larson, W.E., 1974. Determining effective soil water diffusivities from one-step outflow experiments. *Soil Science Society of America Proceedings*, Vol. 38, pp. 701-716.

- Haines, W. B., 1923. The volume-changes associated with variations of water content in soil, *Journal of Agricultural Science*, Vol. 13, pp. 296-310.
- Haines, W. B., 1930. The hysteresis effect in capillary properties and the modes of moisture distribution associated therewith, *Journal of Agriculture Science*, Vol. 20, pp. 96-105.
- Harrison, B. A., and Blight, G. E., 2000. A comparison of in situ soil suction measurements. *Unsaturated soils for Asia*, Singapore, H. Rahardo, D. Toll, and E. Leong, eds., Balkema, Rotterdam, The Netherlands, 281–285.
- Hilf, J.W., 1956. Soil investigation of pore-water pressure in compacted cohesive soils, PhD thesis, Technical Memorandum No. 654, United States Department of the Interior, Bureau of Reclamation, Design and Construction Division, Denver, CO.
- Hillel, D. and Gardner, W., 1970. Measurement of unsaturated conductivity and diffusivity by infiltration through an impeding layer, *Soil Sci.*, Vol. 109, No. 3, pp. 149-153.
- Hillel, D., Krentos, V., and Stylianou, Y., 1972. Procedure and test of an internal drainage method for measuring soil hydraulic characteristics in situ, *Soil Sci.*, Vol. 114, No. 5, pp. 395-400.
- Ho, D.Y.F., and Fredlund, D.G., 1982. Increase in shear strength due to suction for two Hong Kong soils, *Proceedings of the ASCE Geotechnical Conference, Engineering and Construction on Tropical and Residual Soils*, Honolulu, Hawaii., U.S.A., January 11-15, pp. 263-295.
- Hough, B.K., 1957. *Basic soils engineering*, The Ronald Press Company, New York, pp. 114-115.
- Jennings, J. E., 1961. A revised effective stress law for use in the prediction of the behaviour of unsaturated soils, *Conf. of Pore pressure and suction in soils*, organized by British Nat. Soc. of Int. Soc. Soil Mech. Found. Eng., Inst. Of Civil Eng., London: Butterworths, pp. 26-30.
- Jotisankasa, A., 2005. Collapse behaviour of a compacted silty clay. PhD thesis, Imperial College, London.
- Kattab, S.A., 1986. Effect of gypsum on the strength of granular soil treated and untreated with cement, M.Sc. thesis, Civil Engineering Department, University of Baghdad, Iraq.
- Kawai, K., Karube, D., and Kato, S., 2000. The model of water retention curve considering effects of void ratio. In: Rahardjo, H., Toll, D.G., and Leong, E.C. (Eds.), *Unsaturated Soils for Asia*: 329–334. Rotterdam: Balkema.
- Khalili, N., and Khabbaz, M. H., 1998. A unique relationship for χ for the determination of shear strength of unsaturated soils, *Geotechnique*, Vol. 48, pp. 681-688, doi:10.1680/geot.1998.48.5.681.
- Khalili, N., and Khabbaz, M. H., 1998. A unique relationship for the determination of the shear strength of unsaturated soils, *Geotechnique*, Vol. 48, No. 5, pp. 681–687.

- Khalili, N., Geiser, F., and Blight, G. E., 2004. Effective stress in unsaturated soils: review with new evidence, *Int. J. Geomech. ASCE*, Vol. 4, No. 2, pp. 115-126.
- Klein C., and Hurlbut, C. S., 1985. *Manual of Mineralogy*, 20th ed., Wiley, New York.
- Klute, A., 1972. The determination of the hydraulic conductivity and diffusivity of unsaturated soils, *Soil Sci.*, Vol. 113, No. 4, pp. 264-276.
- Klute, A., and Dirksen, C., 1986. Hydraulic conductivity and diffusivity: Laboratory methods, *Methods of Soil Analysis, Part 1, Physical and Mineralogical Methods*, 2nd Ed., Soil Science Society of America, Madison, WI, 687-729.
- Lambe, T. W., 1960. A mechanistic picture of the shear strength of clay, *Proc., Research Conf. on the shear strength of cohesive soils*, ASCE, New York, 437.
- Lambe, T.W., 1951. *Soil testing for engineers*, New York: Wiley.
- Lambe, T.W., and Whitman, R.V., 1979. *Soil mechanics*, New York: Wiley.
- Lamborn, M. J., 1986. A micromechanical approach to modeling partly saturated soils, M.Sc. thesis, Texas A&M University, Texas.
- Lane, J.J., Law, T.L., and Station, K.D., 2001. Determination of the shear strength of an unsaturated clay till using conventional direct shear testing equipment. Undergraduate Thesis, Department of Civil Engineering, Lakehead University.
- Leonard, M., Singleton, J., and Gribb, M., 1996. Hydraulic conductivity measurement in unsaturated soils with a modified cone penetrometer, *Proc. Third International Symposium and Exhibition on Environmental Contamination in Central and Eastern Europe*, Sept. 1996, Warsaw, Poland.
- Leong, E. C., Lee, C. C., and Low, K. S., 2009. An active control system for matric suction measurement, *Soils and Foundations*, Vol. 49, No. 5, pp 807-811.
- Leong, E. C., Lee, C. C., and Low, K. S., 2011. Discussion of "Modified null pressure plate apparatus for measurement of matric suction" by Power, K. C. and Vanapalli, S. K., *Geotechnical Testing Journal*, Vol. 33, No. 4, Paper ID GTJ102478, *Geotechnical Testing Journal*, Vol. 34, No. 3, Paper ID GTJ103362.
- Likos, W. J., and Lu, N., 2003. Automated humidity system for measuring total suction characteristics of clay, *ASTM, Geotechnical Testing Journal*, Vol. 26, No.2.
- Lins, Y., 2009. Hydro-mechanical properties of partially saturated sand, PhD thesis, University Bochum.
- Lins, Y., Schanz, T., and Fredlund, D. G., 2009. Modified pressure plate apparatus and column testing device for measuring SWCC of sand, *Geotechnical Testing Journal*, Vol. 32, No.5.
- Lu, N., 2008. Is matric suction a stress variable?, *Journal of geotechnical and Geoenvironmental Engineering*, ASCE, Vol. 134, No. 7, pp. 899-905.

- Lu, N., Godt, J. W., and Wu, D. T., 2010. A closed-form equation for effective stress in unsaturated soil, *Water Resource Research*, Vol. 46, W05515, doi: 10.1029/2009WR008646.
- Lu, N., Likos, W. J., 2006. Suction stress characteristic curve for unsaturated soil, *Journal of geotechnical and Geoenvironmental Engineering*, ASCE, Vol. 132, No. 2, pp. 131-142.
- Lu, N., and Likos, W., 2004. *Unsaturated soil mechanics*, John Wiley & Sons Inc., New Jersey, USA.
- Lun, M. C. H., 2005. Behaviour of unsaturated soils under direct shear and triaxial compression, M.Sc. thesis, Civil Engineering Department, University of Calgary, Alberta, Canada.
- Mabirizi, D., and Bulut, R., 2011. Hysteresis between wetting and drying diffusivity parameters, *Unsaturated soils*, Alonso & Gens (eds), Taylor & Francis Group, London, ISBN 978-0-415-60428-4.
- Maqsood, A., Bussiere, B., Mbonimpa, M., and Aubertin, M., 2004. Hysteresis effects on the water retention curve: a comparison between laboratory results and predictive models, 57th Canadian Geotechnical Conference, 3A, 8 – 15, Quebec, Canada.
- Mason, J. B., 1992. Preparation of soil sampling protocols: Sampling techniques and strategies, Environmental Research Centre, University of Nevada-Las Vegas, Las Vegas, Nevada 89154.
- Matyas E.L. and Radhakrishna H.S., 1968. Volume change characteristics of partially saturated soil, *Geotechnique*, Vol. 18, pp. 432-448.
- McGarry, D., and Malafant, K.W., 1987. The analysis of volume change in unconfined units of soil, *Soil Science Society of America Journal*, Vol. 51, pp. 290-297.
- McKeen, R. G., 1981. Design of airport pavements for expansive soils, U. S. Dept. of Transportation, Federal Aviation Administration, Rep. No. DOT/FAA/RD-81/25.
- McKeen, R. G., and Hamberg, D. J., 1981. Characterization of expansive soils, *Transportation Research Record* 790, pp. 73–78.
- McQueen, I. S., and Miller, R. F., 1974. Approximating soil moisture characteristics from limited data: Empirical evidence and tentative model, *Water Resources Research*, Vol. 10, No. 3, pp. 521–527.
- Md. Noor, M.J., Mat. Jidin, R., and Hafez, M.A., 2008. Effective stress and complex soil settlement behaviour, *Universiti Teknologi MARA, EJGE*, Malaysia.
- Miller, E., and Miller, R., 1988. Physical theory for capillary flow phenomena, *Transport in porous media*, 3, pp. 324-332.
- Mofiz, S. A., Taha, M. R., Sharker, D. C., 2004. Mechanical stress-strain characteristics and model behaviour of geosynthetic reinforced soil composites, 17th ASCE Engineering Mechanics Conference, University of Delaware, Newark, DE.

- Morgenstern, N. R., 1979. Properties of compacted soils, Proc. of the 6th pan-american Conf. Soil Mech. Found. Eng., Vol. 3, pp. 349-354, Lima, Peru.
- Mualem, Y., 1976. A new model for predicting the hydraulic conductivity of unsaturated porous media, Water Resources Research, Vol. 12, pp. 593-622.
- Mualem, Y., 1984b. Prediction of the soil boundary wetting curve, Soil Science Vol. 137, No. 6, pp. 379-390.
- Murray, E., and Sivakumar, V., 2010. Unsaturated soils - fundamental approach to interpretation of soil behaviour. Wiley-Interscience Publications.
- Nelson, J. D., Miller, D. J., 1992. Expansive soils, John Wiley & Sons, Inc.
- Ng, C.W.W., and Pang, Y.W., 2000b. Influence of stress state on soil-water characteristics and slope stability, Journal of geotechnical and Geoenvironmental Engineering, ASCE, Vol. 26, No. 2, pp. 157-166.
- Ng, C.W.W., and Leung, A. K., 2012. Measurements of drying and wetting permeability functions using a new stress-controllable soil column, Journal of Geotechnical and Geoenvironmental Engineering, ASCE, Vol. 138, No. 1, ISSN 1090-0241.
- Ng, C.W.W., and Menzies, B., 2007. Advanced unsaturated soil mechanics and engineering, Taylor and Francis, London and New York.
- Ng, C.W.W., and Pang, Y.W., 2000a. Experimental investigation of soil-water characteristics of a volcanic soil. Canadian Geotechnical Journal, Vol. 37, No. 6, pp. 1252-1264.
- Oh, S., Lu, N., Kim, Y., Lee, S., and Lee, S., 2012. Relationship between the soil-water characteristic curve and the suction stress characteristic curve: Experimental evidence from residual soils, Journal of geotechnical and Geoenvironmental Engineering, ASCE, Vol. 138, No. 1, pp. 47-57.
- Padilla, J.M., Perera, Y. Y., Houston, W. N., and Fredlund, D.G., 2005. A new soil-water characteristic curve device, Proceedings of Advanced Experimental Unsaturated Soil Mechanics- an International Symposium, EXPERUS 2005, Trento, Italy, pp. 15-22.
- Palmeira, E. M., and Milligan, G. W. E., 1989. Scale effects in direct shear tests on sand, Proceedings of the 12th International Conference on Soil Mechanics and Foundation Engineering, Vol. 1, No. 1. pp. 739-742.
- Pan, H., Qing, Y., and Pei-yong, L., 2010. Direct and indirect measurement of soil suction in the laboratory, EJGE, Vol.15, Bund. A.
- Passioura, J.B., 1976. Determining soil water diffusivities from one-step outflow experiments, Australian Journal of Soil Research 15, 1-8.
- Paul Simms, 2003. A fundamental study of unsaturated flow in compacted clayey soil, a PhD thesis, University of Western Ontario, London, Ontario, Canada.
- Pavlakakis, G., and Barden, L., 1972. Hysteresis in the moisture characteristics of clay soil, Journal of Soil Science, Vol. 23, pp. 350-361.
- Pereira, J.H.F., and Fredlund, D.G., 2000. Volume change behavior of collapsible compacted gneiss soil, Journal of Geotechnical and Geoenvironmental

- Engineering, ASCE, Vol. 126, pp. 907–916, doi:10.1061/1090-0241(2000)126:10(907).
- Perez-Ruiz, D. D., 2009. A refined true triaxial apparatus for testing unsaturated soils under suction-controlled stress paths, a PhD thesis, University of Texas at Arlington, USA.
- Peterson, R. F. W., 1988. Interpretation of triaxial compression test results on partially saturated soils, *Advanced Triaxial Testing of Soil and Rock*, ASTM STP 977, American Society for Testing and Materials, Philadelphia, pp. 512-538.
- Peterson, R. W., 1990. The influence of soil suction on the shear strength of unsaturated soil, PhD thesis, Texas A&M University, Texas.
- Pham, H. Q., Fredlund, D. G., and Barbour, S. L., 2003. A practical hysteresis model for the soil-water characteristic curve for soils with negligible volume change, *Geotechnique*, Vol. 53, No. 2, pp. 293-298.
- Poulovassilis, A., 1970. Hysteresis of pore water in granular porous bodies, *Soil Science*, Vol. 109, No. 1, pp. 5-12.
- Power, K. C., and Vanapalli, S. K., 2009. Modified null pressure plate apparatus for measurement of matric suction, *Geotechnical Testing Journal*, Vol. 33, No. 4, Paper ID GTJ102478.
- Power, K. C., Vanapalli, S. K., Leong, E. C., Lee, C. C., and Low, K. S., 2011. Response to Discussion of "Modified null pressure plate apparatus for measurement of matric suction" by Power, K. C., and Vanapalli, S. K., *Geotechnical Testing Journal*, Vol. 33, No. 4, Paper ID GTJ102478, *Geotechnical Testing Journal*, Vol. 34, No. 3, Paper ID GTJ103764.
- Rahardjo, H., and Leong, E. C., 2006. Suction measurements, *ASCE Conf. Proceedings of the fourth international conference on unsaturated soils*, doi: 10.1061/40802(189)3.
- Rassam, D. W., and Cook, F., 2002. Predicting the shear strength envelope of unsaturated soils, *Geotechnical Testing Journal*, Vol. 25, No. 2, pp. 215–220.
- Rassam, D. W., Williams, D. J., 1999. A relationship describing the shear strength of unsaturated soils, *Canadian Geotechnical Journal*, Vol. 36, pp 363-368.
- Razouki, S. S., Al-Omeri, R.R., Nashat, I.H., Razouki, H.F., and Khalid, S., 1994. The problem of gypsiferous soils in Iraq. *Proceedings of the Symposium on Gypsiferous Soils and their Effect on Structures*. NCCL, Baghdad, 7–33.
- Razouki, S. S., and El-Janabi, O. A., 1999. Decrease in the CBR of a gypsiferous soil due to long term soaking, *Quarterly Journal of Engineering Geology and Hydrogeology*, Vol. 32, pp. 87-89.
- Razouki, S. S., and Ibrahim, A. N., 2007. Improves a gypsum sand roadbed soil by increased compaction, *Proceedings of the Institution of Civil Engineers, Transport* 160, pp. 27-31, Paper14742.
- Razouki, S. S., and Kuttah, D. K., 2004. Effect of soaking period and surcharge load on resilient modulus and California bearing ratio of gypsiferous soils,

- Quarterly Journal of Engineering Geology and Hydrogeology , Vol. 37, pp. 155-164, doi:10.1144/1470-9236/04-002.
- Razouki, S. S., and Kuttah, D. K., 2006. Predicting long-term soaked CBR of gypsiferous subgrade soils, Proceedings of the Institution of Civil Engineers, Transport 159, pp. 135-140, Paper14256.
- Razouki, S. S., Kuttah, D. K., Al-Damlugi, O. A., and Nashat, I. H., 2007. Strength erosion of a fine-grained gypsiferous soil during soaking, The Arabian Journal for Science and Engineering, Volume 32, Number 1B.
- Razouki, S. S., Kuttah, D. K., Al-Damlugi, O. A., and Nashat, I. H., 2008. Using gypsiferous soil for embankments in hot desert areas, Proceedings of the Institution of Civil Engineers, Transport 161, pp. 63-71, Paper 700042.
- Richards, B. G., 1965. Measurement of the free energy of soil moisture by the psychrometric technique using thermistors, in Moisture Equilibria and Moisture Change in Soils Beneath Covered Areas, A symposium, Australia: Butterworths, pp. 39-46.
- Richards, B. G., 1966. The significance of moisture flow and equilibrium in unsaturated soils in relation to the design of engineering structures built on shallow foundations in Australia, Symposium on permeability and capillary, Amer. Soc. Testing Materials, Atlantic City, New Jersey.
- Richards, L. A., 1928. The usefulness of capillary potential to soil moisture and plant investigators, J. Agric. Res., Vol. 37, pp. 719-742.
- Richards, L. A., 1931. Capillary conduction of liquids through porous medium, Journal of Physics, 318-333.
- Ridley, A. M. and Burland, J. B. 1993. A new instrument for the measurement of soil moisture suction. Geotechnique, Vol. 43, No. 2, pp. 321-324.
- Ridley, A. M., and Wray, W. K. 1995. Suction measurements: A review of current theory and practices, in E. E. Alonso and P. Delage (Eds.), Unsaturated Soils: Proceedings of the First International Conference on Unsaturated Soils, Paris, Balkema, Rotterdam, Presse des Ponts et Chaussees, pp. 1293-1322.
- Rijtema, P., 1959. Calculation of capillary conductivity from pressure plate outflow data with non-negligible membrane impedance, Netherlands J. Agr. Sci., Vol. 7, pp. 209-215.
- Roscoe, K. H., 1970. Tenth Rankine Lecture: The influence of strains in soil mechanics, Geotechnique, Vol. 20, No. 2, pp. 129-170.
- Scotter, D., and Clothier, B., 1983. A transient method for measuring soil water diffusivity and hydraulic conductivity, Soil Science Society of America Journal, Vol. 47, pp. 1068-1072.
- Seleam, S.N.M., 1988. Geotechnical characteristics of a gypseous sandy soil including the effect of contamination with some oil products, M.Sc. thesis, Building and Construction Department, University of Technology, Baghdad, Iraq.
- Sharma, R. S., 1998. Mechanical behaviour of unsaturated highly expansive clays. <http://ora.ox.ac.uk/objects/uuid:6ee59b08-357a-4d2d-96f1-c5987465f437>.

- Sheng, D., Fredlund, D. G., and Gens, A., 2008. A new modelling approach for unsaturated soils using independent stress variables, *Canadian Geotechnical Journal*, Vol. 45, pp. 511–534.
- Shihab, R. M., Al-Ani, A. N., and Fahad, A. A., 2002. Dissolution and transport of gypsum in gypsiferous soil treated with fuel oil and bentonite, *Emir. J. Agric. Sci.*, Vol. 14, pp. 01 – 07.
- Simunek, J., Kodesova, R., Gribb, M. M., and Genuchten, M. T., 1999. Estimating hysteresis in the soil water retention function from cone permeameter experiments, *Water Resources Research*, Vol. 35, No. 5, pp. 1329-1345.
- Sivakumar, R., 2005. Effects of Anisotropy on the Behaviour of Unsaturated Compacted Clay, PhD thesis submitted to the Queen's University of Belfast.
- Sivakumar, V., Tan, W.C., Murray, E.J., and McKinley, J.D., 2006. Wetting, drying and compression characteristics of compacted clay, *Geotechnique*, Vol. 56, No. 1, pp. 57–62.
- Soilmoisture Equipment Corporation, 2008. Commercial Publications, Santa Barbara, CA.
- Sowers, G.B., 1970. Introductory soil mechanics and foundations, The Macmillan Company, Collier- Macmillan Limited, London, 3rd Edition, pp.102.
- Stephens, D., 1989. A comparison of estimated and measured unsaturated hydraulic conductivity of two uniform soils in New Mexico, *Agricultural Res. Service*, Riverside, CA, pp. 249-261.
- Stephens, D., 1994. Hydraulic conductivity assessment of unsaturated soil, *Hydraulic Conductivity and Waste Contaminant Transport in Soil*, STP 1142, ASTM, Philadelphia, D. Daniel and S. Trautwein, eds., pp. 169-181.
- Stormont, J.C., Henry, K.S., and Evans, T.M., 1997. Water retention functions of four nonwoven polypropylene geotextiles, *Geosynthetics International*, Vol. 4, No. 6, pp. 661-672.
- Subhi, H.M., 1987. Properties of salt contaminated soils and their influence on the performance of roads in Iraq, Ph.D. thesis, Queen Mary College, University of London.
- Sun, D. A., Matsuoka, H., Yao, Y. P., and Ichihara, W., 2000. An elastoplastic model for unsaturated soil in three-dimensional stresses, *Soils Found.*, Vol. 40, No. 3, pp.17–28.
- Tadza, M. Y. M., 2011. Soil-water characteristic curves and shrinkage behaviour of highly plastic clays: An experimental investigation, PhD thesis, Geoenvironmental Research centre, Cardiff University, UK.
- Tami, D., Rahardjo, H., and Leong, E. C., 2004. Effects of hysteresis on steady-state infiltration in unsaturated slopes, *Journal of Geotechnical and Geoenvironmental Engineering*, ASCE, Vol. 130, No. 9, pp. 956 – 967.
- Tarantino, A. and Mongiovì, L., 2003. Calibration of tensiometer for direct measurement of matric suction. *Geotechnique*, Vol. 53, No. 1, pp. 137-14.
- Tarantino, A., 2007. A possible critical state framework for unsaturated compacted soils, *Geotechnique*, Vol. 57, No. 4, pp. 385–389.

- Tarantino, A., and Tombolato, S., 2005. Coupling of hydraulic and mechanical behaviour in unsaturated compacted clay. *Geotechnique*, Vol. 55, No. 4, pp. 307-317.
- Terzaghi, K., 1943. *Theoretical soil mechanics*, New York: Wiley.
- Terzaghi, K., and Peck, R. B., 1960. *Soil mechanics in engineering practice*, Wiley & Sons Inc. New Jersey.
- Thiel, R., 2001. Peak vs. residual shear strength for landfill bottom liner stability analyses, *Proceedings of the 15th Annual GRI Conference Hot Topics in Geosynthetics*, Geosynthetics Institute, Folsom, PA, pp. 40-70.
- Thu, T. M., Rahardjo, H., and Leong, E., 2007. Soil-water characteristic curve and consolidation behavior for a compacted silt, *Canadian Geotechnical Journal*, Vol. 44, pp. 266-275.
- Toker, N., 2002. Improvements and reliability of MIT tensiometers and studies on soil moisture characteristic curves, PhD Thesis, Massachusetts Institute of Technology.
- Toll, D. G., and Ong, B. H., 2003. Critical state parameters for an unsaturated residual sandy clay, *Geotechnique*, Vol. 53, No. 1, pp. 93-103.
- Tomlinson, M.J., 1978. Middle East highway and airfield pavements, *Quarterly Journal of Engineering Geology*, Vol. 11, No. 1, pp. 65-73.
- Topp, G. C., and Miller, E. E., 1966. Hysteresis moisture characteristics and hydraulic conductivities for glass-bead media, *Soil Science Society of America Journal*, Vol. 30, pp. 156-162.
- Topp, G. C., 1969. Soil water hysteresis measured in a sandy loam compared with the hysteresis domain model, *Soil Science Society of America Journal*, Vol. 33, pp. 645-651.
- Topp, G. C., 1971a. Soil water hysteresis on silt loam and clay loam soils, *Water Resources Research*, Vol. 7, No. 4, pp. 914-920.
- Tripathy, S., Elgabu, H., and Thomas, HR., 2012. Matric suction measurement of unsaturated soils with null-type axis-translation technique. *Geotechnical Testing Journal*, Vol. 35, No. 1, pp. 1-12.
- Tripathy, S., Leong, E. C., and Raharadjo, H., 2005. Suction of compacted residual soils. *Proceedings of International Conference "From Experimental Evidence Towards Numerical Modelling of Unsaturated Soils"*, September 18-19, 2003, Germany, Vol. 1, pp. 111-122.
- Tripathy, S., Subba Rao, K.S., and Fredlund, D.G., 2002. Water content-void ratio swell-shrink paths of compacted expansive soils, *Canadian Geotechnical Journal*, Vol. 39, pp. 938-959.
- Tse, M. K., 2007. Influence of stress states on soil-water characteristics, conjunctive surface-subsurface flow modelling and stability analysis, M.Phil. thesis, Hong Kong University of Science and Technology.
- Uchaipichat, A., 2010. Hydraulic hysteresis effect on compressibility of unsaturated soils, *Arpn Journal of Engineering and Applied Sciences*, Vol. 5, No. 10, pp. 92-97.

- Valiantzas, J., 1989. A simple approximate equation to calculate diffusivity from one-step outflow experiments, *Soil Science Society of America Journal*, Vol. 53, pp. 342-349.
- Valiantzas, J.D., Kerkides, P.G., and Poulouvassilis, A., 1988. An improvement to the one-step outflow method for determination of soil water diffusivities. *Water Resources Research*, Vol. 24, pp. 1911-1920.
- Van Genuchten, M. T., 1980. A closed form equation for predicting the hydraulic conductivity of unsaturated soils, *Soil Science Society of America Journal*, Vol. 44, pp. 892-898.
- Van Genuchten, M.T., 1980. A closed form equation for predicting the hydraulic conductivity of unsaturated soils, *Soil Science Society of America Journal*, Vol. 44, No. 5, pp. 892–898.
- Vanapalli, S. K., 1994. Simple test procedures and their interpretation in evaluating the shear strength of an unsaturated soil, PhD thesis, University of Saskatchewan, Canada.
- Vanapalli, S. K., and Fredlund, D. G., 2000. Comparison of empirical procedures to predict the shear strength of unsaturated soils using the soil-water characteristic curve, in *Advances in Unsaturated Geotechnics*, Shackelford, C. D., Houston, S. L., and Chang, N. Y., eds., GSP No. 99, ASCE, Reston, VA, pp. 195–209.
- Vanapalli, S. K., and Lane, J., 2002. A simple technique for determining the shear strength of unsaturated soils using the conventional direct shear apparatus, *Proceedings of the Second Canadian Specialty Conference on Computer Applications in Geotechnique*, April, 2002, Winnipeg, pp. 245-253
- Vanapalli, S. K., Fredlund, D. G., Pufahl, D. E., and Clifton, A. W., 1996. Model for the prediction of shear strength with respect to soil suction, *Canadian Geotechnical Journal*, Vol. 33, pp. 379–392.
- Vanapalli, S. K., Fredlund, D. G., Pufahl, D. E., and Clifton, A. W., 1996. Model for the prediction of shear strength with respect to soil suction, *Canadian Geotechnical Journal*, Vol. 33, pp. 379–392.
- Vanapalli, S. K., Garga, V. K., and Brisson, P., 2007. A modified permeameter for determination of unsaturated coefficient of permeability, *Geotech. Geol. Eng.*, Vol. 25, pp. 191-202.
- Vanapalli, S. K., Pufahl, D. E., and Fredlund, D. G., 1998. The effect of stress state on the soil-water characteristic behavior of a compacted sandy-clay till, *Proc. of 51st Canadian Geotechnical Conf.*, pp. 81–86.
- Vanapalli, S. K., Sharma, R. S., and Nicotera, M. V., 2008. Axis-translation and negative water column techniques for suction control, *Geotech. Geologic. Eng.*, Vol. 26, pp. 645-660.
- Vanapalli, S.K., Fredlund, D.G., and Pufahl, D.E., and Clifton, A.W., 1996. Model for the prediction of shear strength with respect to soil suction. *Canadian Geotechnical Journal*, Vol. 33, No. 3, pp. 379-392.
- Vanapalli, S.K., Fredlund, D.G., and Pufahl, D.E., 1999. The influence of soil structure and stress history on the soil-water characteristics of a compacted till, *Geotechnique*, Vol. 49, No. 2, pp. 143 – 159.

- Vanapalli, S.K., Pufahl, D.E., and Fredlund, D.G., 1999. Interpretation of the shear strength of unsaturated soils in undrained loading conditions. Proceedings of the 52nd Canadian Geotechnical Conference, Regina, October 25-27, pp. 643-650.
- Vassallo, R., Mancuso, C., and Vinale, F., 2007. Modelling the influence of stress-strain history on the initial shear stiffness of an unsaturated compacted silt, *Canadian Geotechnical Journal*, Vol. 44, pp. 463-472.
- Verheye, W. H., and Boyadgiev, T. G., 1997. Evaluating the land use potential of gypsiferous soils from field pedogenic characteristics, *Soil Use and Management*, Vol. 13, pp. 97-103.
- Wildenschild, D., Hopmans, J. W., and Simunek, J., 2001. Flow rate dependence of soil hydraulic characteristics, *Soil Science Society of America Journal*, Vol. 65, pp. 35-48.
- Wood, D.M., 1990. Soil behaviour and critical state soil mechanics, Cambridge, England, Cambridge University Press.
- Yang, H., Rahardjo, H., Leong, E. C., and Fredlund, D.G., 2004. Factors affecting drying and wetting soil-water characteristic curves of sandy soils, *Canadian Geotechnical Journal*, Vol. 41, pp. 908-920, doi: 10.1139/T04-042.
- Yankee Environmental Systems, 2006. Hygrometer: principle of operation chilled mirror hygrometers, Airport Industrial park, 101 Industrial Blvd., Turners Falls, MA 01376 USA.
- Younan, T. F., 1986. Effect of potassium oxalate, ammonium carbonate and oxalate, and barium chloride addition on solubility of gypsum in soil, M.Sc. thesis, College of Agriculture, University of Baghdad, Baghdad, Iraq. (In Arabic).
- Zanbak, C., Arthur, R.C., 1986. Geochemical and engineering aspects of anhydrite/gypsum phase transitions, *Bulletin of the Association of Engineering Geologists*, Vol. 23, No. 4, pp. 419-433.
- Zhou, J., 2008. A study of applied pressure on the soil-water characteristic curve, Proceedings of the 1st European Conference, E-UNSAT 2008, Durham, United Kingdom, doi: 10.1201/9780203884430.ch93.

APPENDIX: A

Table A.1. Fitting parameters and statistical indices of different SWCCs found by using the commercial pressure plate (using the same specimens throughout the whole tests).

Gypsum content%	Fitting parameters			W_s^*	Statistical parameters		
	a	n	m		SSr [*]	SSt [*]	R ^{2*}
0	2.41	1.36	0.31	15.22	0.0330	42.51	0.9992
10	2.42	1.34	0.45	18.18	0.3830	100.04	0.9962
20	5.19	0.82	0.67	19.00	0.7390	98.80	0.9925
30	2.10	1.23	0.45	20.93	1.4940	123.26	0.9879
40	15.10	0.59	1.26	22.44	4.1290	155.88	0.9735
50	1.88	1.51	0.46	26.49	2.9110	243.84	0.9881
*SSr : Sum of squares of residuals							
*SSt : Sum of squares							
*R ² : Coefficient of determination							
*W _s : Saturated water content							

Table A. 2. Fitting parameters and statistical indices of different combined SWCCs after the joining of the dew point potentiometer results with that of the modified stress controllable pressure plate device for specimens tested under 0 kPa net normal stress.

Gypsum content%	Fitting parameters			W_s^*	Statistical parameters		
	a	n	m		SSr [*]	SSt [*]	R ^{2*}
0	4.45	7.28	0.20	17.70	0.615	242.88	0.9975
20	13.18	2.47	0.38	17.60	0.813	313.85	0.9974
40	44.61	11.24	0.29	18.64	0.736	395.75	0.9981
65	65.12	10.50	0.40	22.40	0.211	677.27	0.9997
80	49.79	21.29	0.29	27.79	1.769	993.96	0.9982

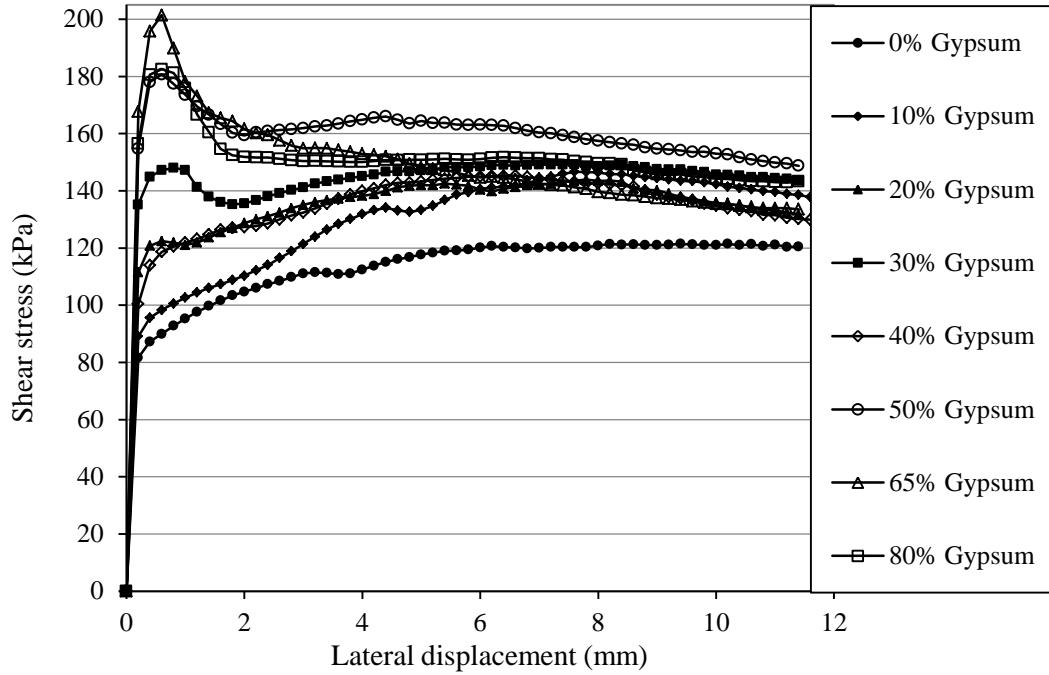
*SSr : Sum of squares of residuals

*SSt : Sum of squares

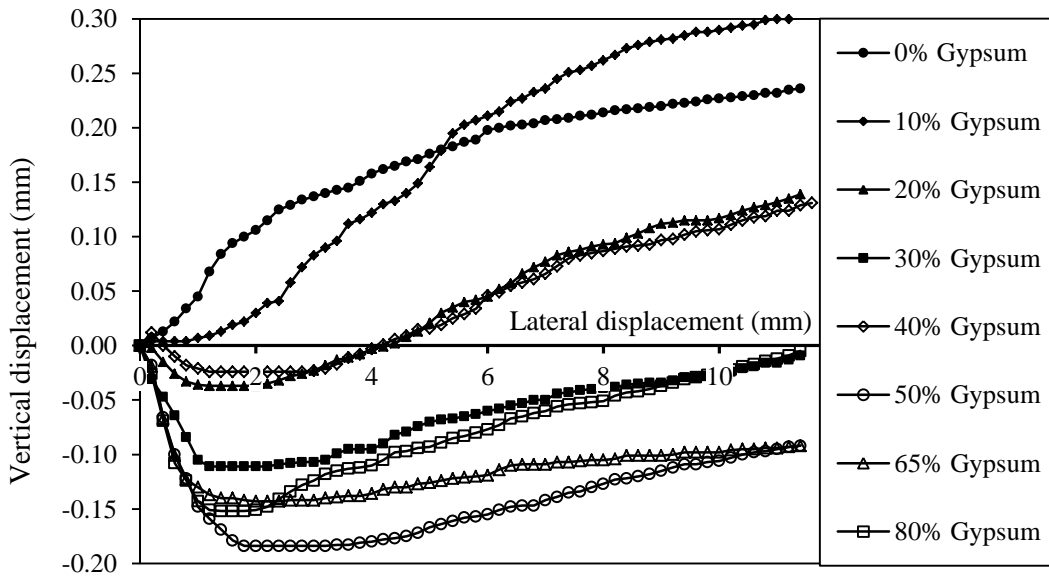
*R² : Coefficient of determination

*W_s : Saturated water content

APPENDIX: B

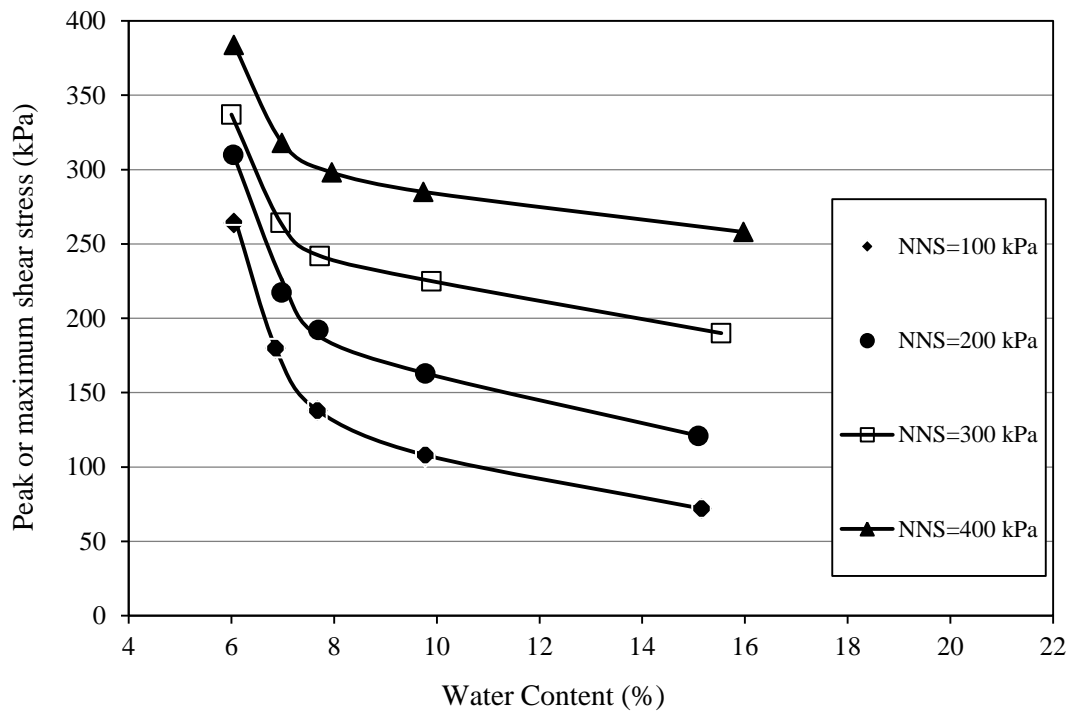


(A) Lateral displacement-shear stress curves .

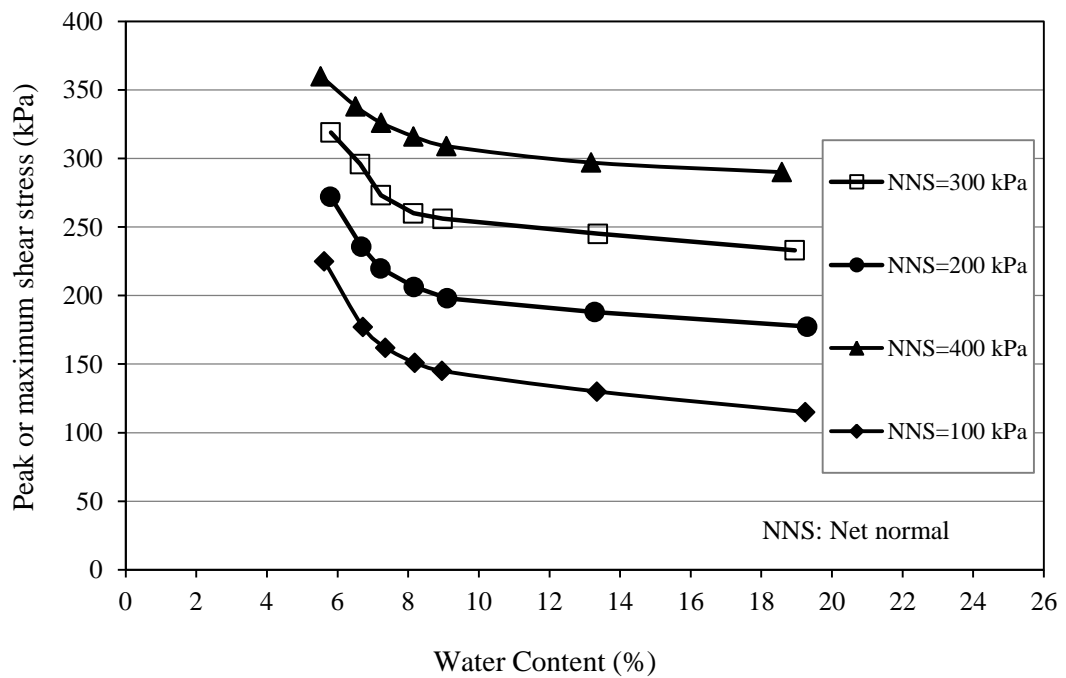


(B) Lateral displacement-Vertical deformation curves .

Figure B.1. Stress-deformation characteristic curves for different sand-gypsum mixtures tested under normal stress of 200 kPa, (A) Shear stress versus lateral displacement, (B) Vertical deformation versus lateral displacement.

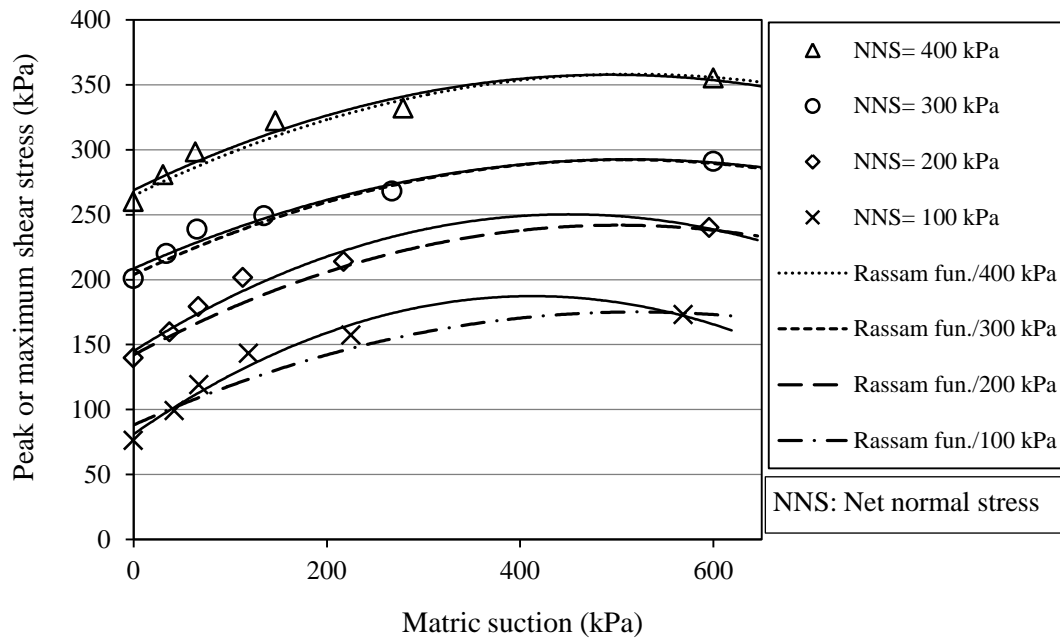


(A) 0% Gypsum content

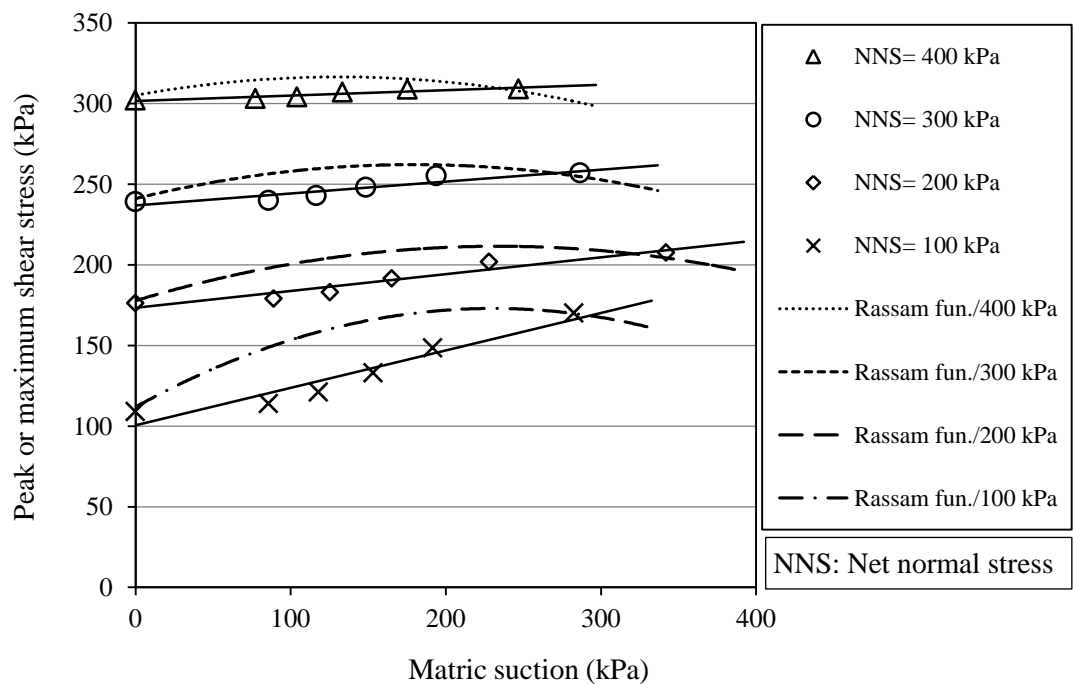


(B) 65% Gypsum content

Figure B.2. Peak or maximum shear stress vs. water content under four levels of net normal stress for sand-gypsum mixtures having (A) 0%, and (B) 65% gypsum content by weight.

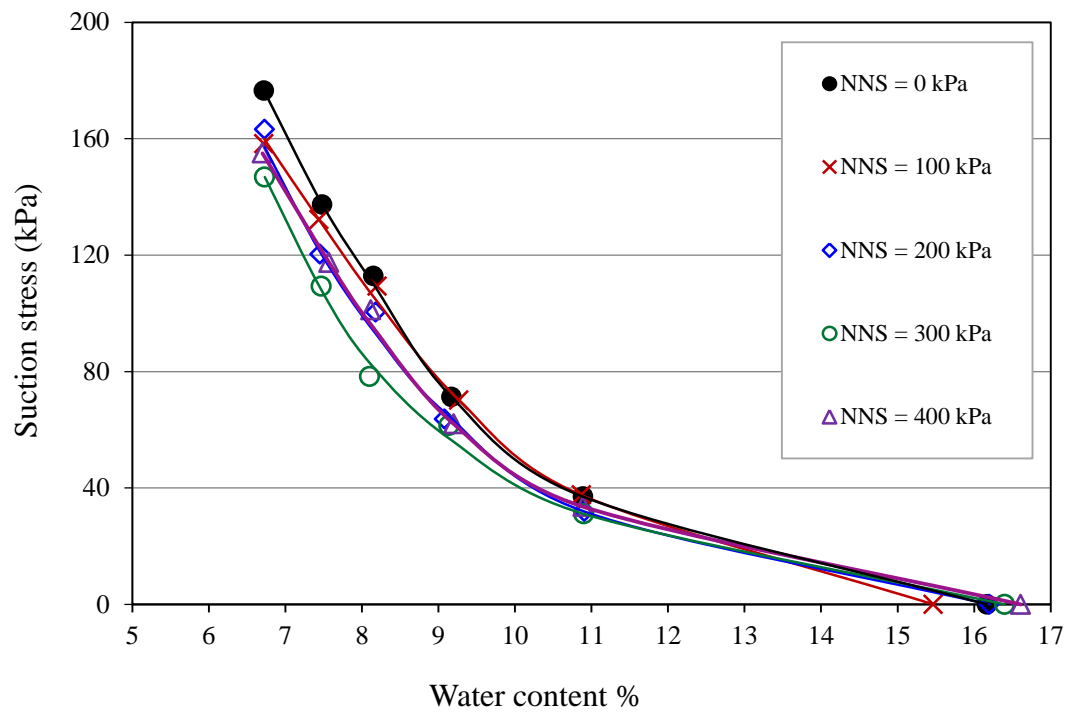


(A) 20% Gypsum content

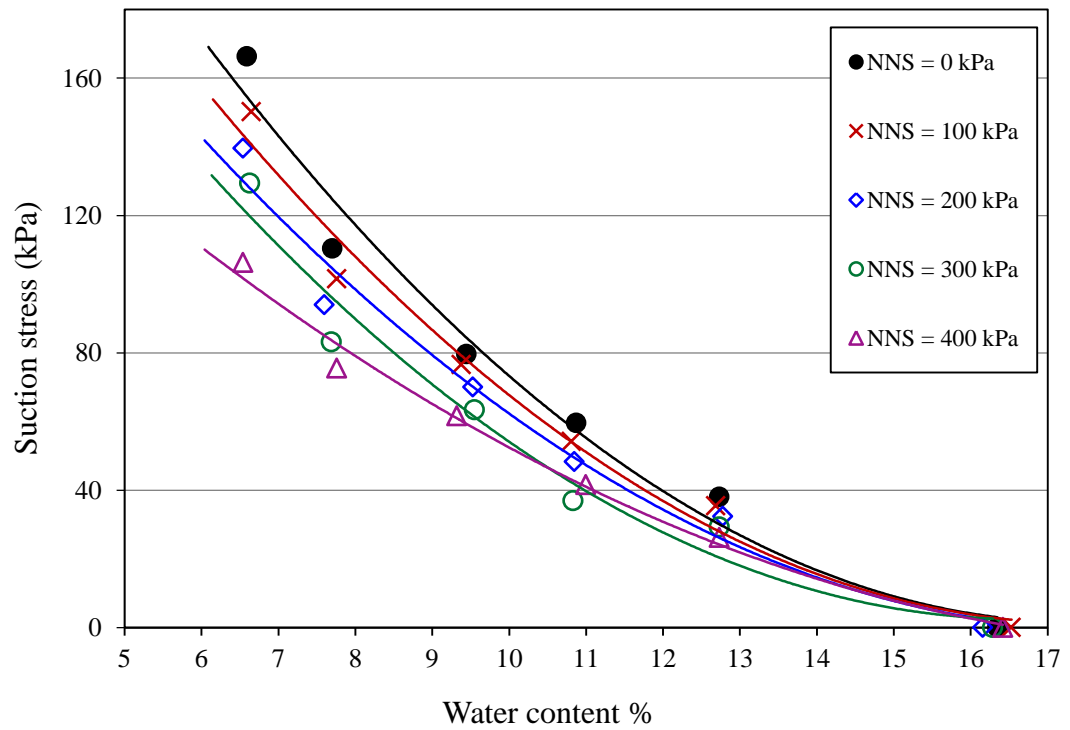


(B) 80% Gypsum content

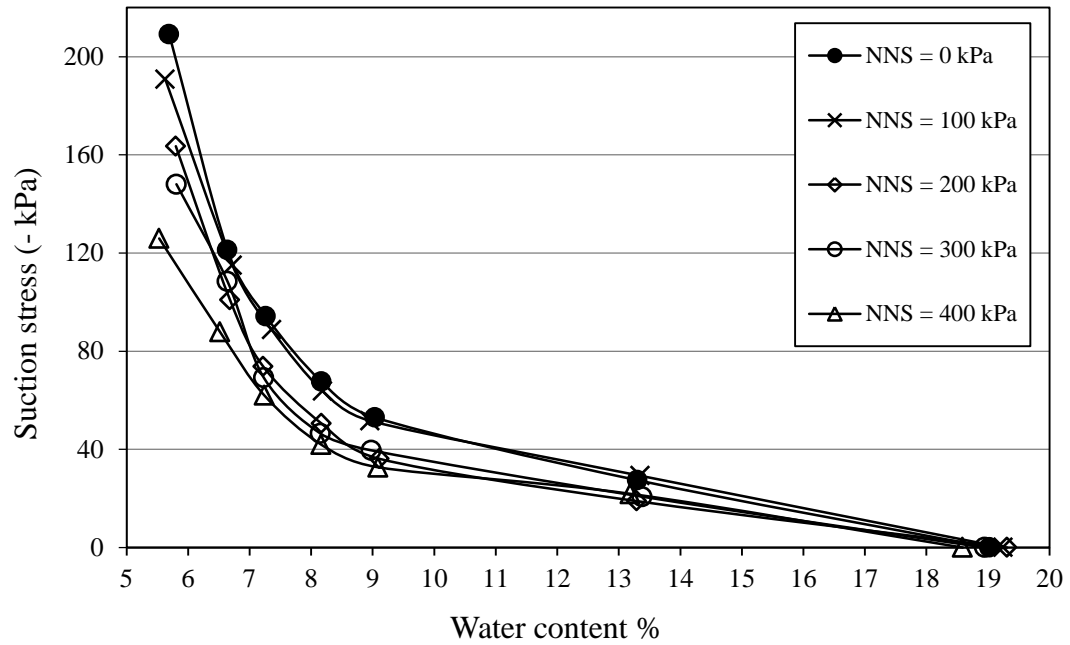
Figure B.3. Comparison of Rassam and Cook (2002)'s predictive function with the experimental shear strength envelopes, at different levels of net normal stress, for unsaturated sand-gypsum specimens having (A) 20%, and (B) 80% gypsum content by weight.



(A) 20% Gypsum content

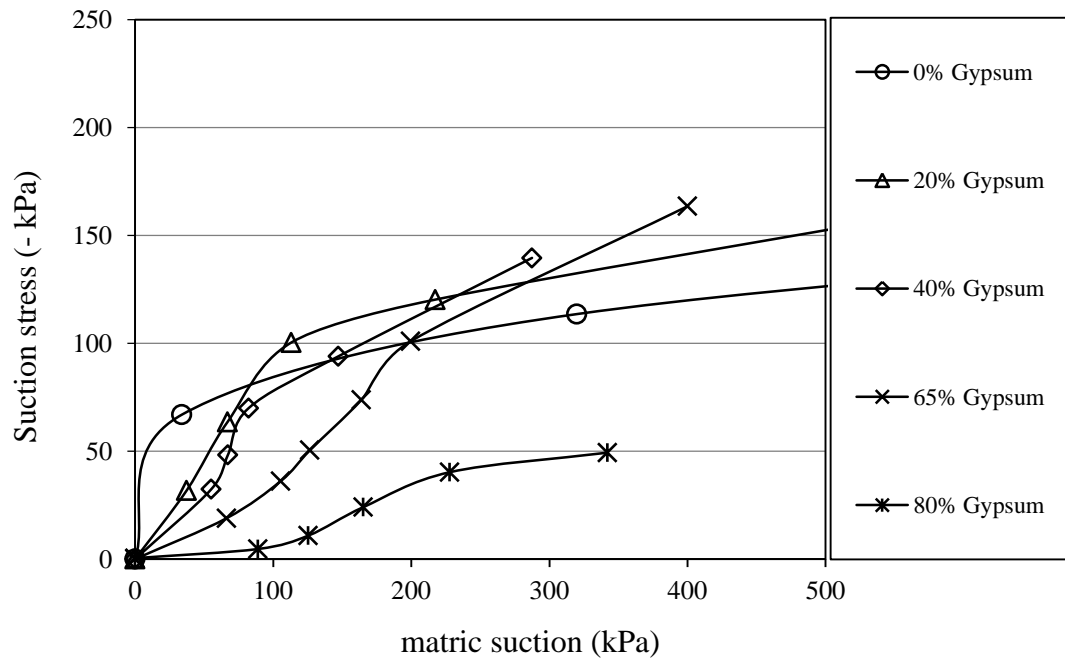


(B) 40% Gypsum content

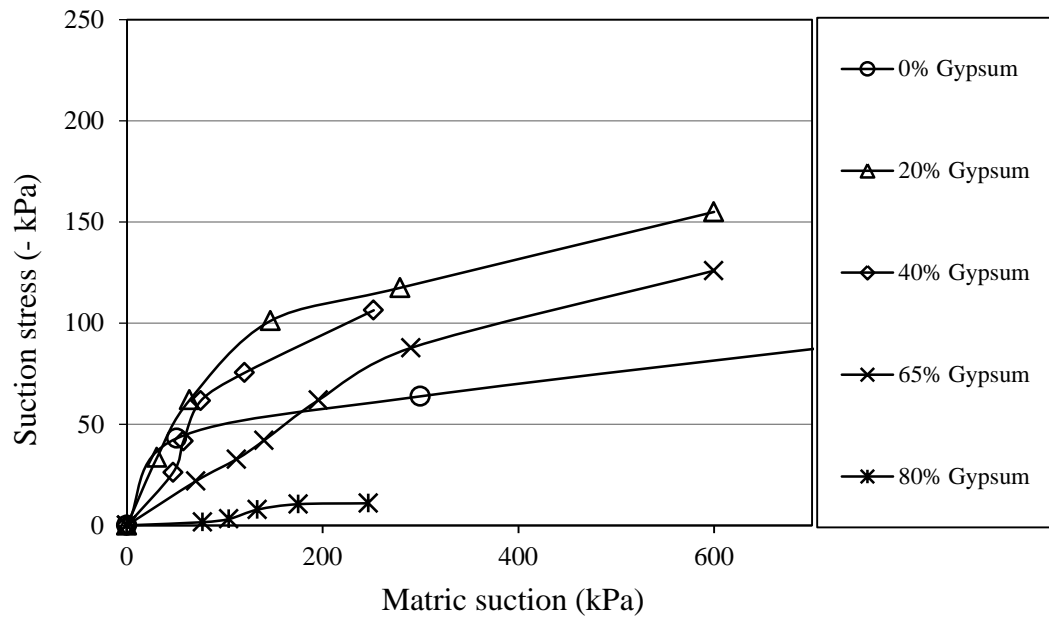


(C) 65% Gypsum content

Figure B.4. SSCCs in terms of water content (According to the approach of Lu and Likos, 2006) for sand-gypsum mixtures having (A) 20%, (B) 40%, and (C) 65% gypsum content by weight, at different levels of net normal stress.



(A) At 200 kPa net normal stress



(B) At 400 kPa net normal stress

Figure B.5. SSCCs in terms of matric suction (According to the approach of Ning Lu, 2006) for different sand-gypsum mixtures at net normal stress level of (A) 200 kPa, and (B) 400 kPa.

Table B.1. Peak shear strength of saturated sand-gypsum mixtures having different gypsum contents by weight.

Normal stress (kPa)	Peak shear strength (kPa)							
	Gypsum content %							
	0	10	20	30	40	50	65	80
100	72	75	76	92	98	115	124	113
200	121	126	140	149	156	181	193	177
400	254	238	260	290	289	314	329	304

Table B.2. Peak shear strength parameters of saturated sand-gypsum mixtures having different gypsum contents by weight.

Gypsum content %	0	10	20	30	40	50	65	80
ϕ (Deg.)	32.1	30.2	31.4	33.8	33.0	33.6	34.7	32.5
c (kPa)	3	5	18	21	26	48	55	49